UNIVERSITÀ DEGLI STUDI DI PALERMO
Dottorato di Ricerca in Energia e Tecnologie dell'Informazione
Dipartimento di Energia, Ingegneria dell'informazione e Modelli matematici (DEIM)
Settore Scientifico Disciplinare ING/IND 19

# NUMERICAL THERMO-MECHANICAL ANALYSIS OF THE DEMO WATER-COOLED LITHIUM LEAD BREEDING BLANKET CONCEPTUAL DESIGN

IL DOTTORE
**ING. GAETANO BONGIOVÌ**

IL COORDINATORE
**CHIAR.MA PROF.SSA MARIA STELLA MONGIOVÌ**

IL TUTOR
**CHIAR.MO PROF. PIETRO ALESSANDRO DI MAIO**

IL CO TUTOR
**PH.D. PIERLUIGI CHIOVARO**

CICLO XXIX
ANNO CONSEGUIMENTO TITOLO 2017

# Index

# List of acronyms

| | |
|---|---|
| BB | Breeding Blanket |
| BC | Bottom Cap |
| BP | Back-Plate |
| BSS | Back Supporting Structure |
| BZ | Breeder Zone |
| CEA | Commissariat à l'Energie Atomique |
| CIEMAT | Centro de Investigaciones Energéticas, Medioambientales y Tecnológicas |
| DB | Dittus & Bölter |
| DCLL | Dual-Coolant Lithium Lead |
| D-D | Deuterium-Deuterium |
| DEMO | Demonstration Fusion Reactor |
| D-T | Deuterium-Tritium |
| DPA | Displacement per Atom |
| DWT | Double Wall Tube |
| ENEA | Agenzia nazionale per le nuove tecnologie, l'energia e lo sviluppo economico sostenibile |
| EU | European Union |
| FEM | Finite Element Method |
| FPR | Fusion Power Reactor |
| FW | First Wall |
| HCLL | Helium-Cooled Lithium Lead |
| HCPB | Helium-Cooled Pebble Bed |
| HTC | Heat Transfer Coefficient |
| IB | Inboard Blanket segment |
| IO | ITER Organization |
| JET | Joint European Torus |
| KIT | Karlsruhe Institute of Technology |
| LOCA | Loss Of Coolant Accident |
| MMS | Multi Module Segment |

| | |
|---|---|
| NO | Normal Operation |
| NWL | Neutron Wall Loading |
| OB | Outboard Blanket segment |
| OP | Over-Pressurization |
| PF | Poloidal Field |
| PPCS-A | Power Plant Conceptual Study - Type A |
| PWR | Pressurized Water Reactor |
| RAFM | Reduced-Activation Ferritic Martensitic |
| R&D | Research and Development |
| RH | Remote Handling |
| RP | Radial-Poloidal |
| RΘ | Radial-Toroidal |
| SB | Segment Box |
| SDC-IC | Structural Design Code for ITER In-vessel Components |
| SP | Stiffening Plate |
| SW | Side Wall |
| TC | Top Cap |
| TBM | Test Blanket Module |
| TBR | Tritium Breeding ratio |
| TF | Toroidal Field |
| VV | Vacuum Vessel |
| WCLL | Water-Cooled Lithium Lead |
| WP | Work Package |
| WPBB | Work Package Breeding Blanket |

# List of symbols

| | |
|---|---|
| $\alpha$ | Volumetric expansion coefficient |
| $\Delta T$ | Thermal rise |
| $\underline{\underline{\varepsilon}}$ | Strain tensor |
| $\varepsilon_{ij}$ | Strain tensor component |
| $\Phi$ | Heat flux |
| $\Phi t_m$ | Neutron fluence |
| $\gamma_{ij}$ | Shear strain |
| $\lambda$ | Thermal conductivity |
| $\nu$ | Kinematic viscosity |
| $\underline{\underline{\sigma}}$ | Stress tensor |
| $\sigma_{ij}$ | Stress tensor component |
| $\sigma_{lim}$ | Stress limit |
| $\rho$ | Density |
| $\tau_{ij}$ | Shear stress |
| a | Cooling channel thickness on plasma side |
| $c_p$ | Specific heat |
| D | FW thickness |
| $d_c$ | Cooling channels with |
| E | Young's Modulus |
| F | Peak stress |
| G | Mass flow rate |
| H | Convective heat transfer coefficient |
| L | FW poloidal height |
| $N_{rp\ SPs}$ | Number of radial-poloidal SPs |
| $N_{r\theta\ SPs}$ | Number of radial-toroidal SPs |
| $N_{r\theta\ p\ SPs}$ | Number of pierced radial-toroidal SPs |

| | |
|---|---|
| $P$ | Primary stress (Chapter 1) / Cooling channels pitch (Chapter 2) |
| $P_b$ | Primary bending stress tensor |
| $\overline{P_b}$ | Primary bending stress intensity |
| $P_L$ | Local primary membrane stress tensor |
| $\overline{P_L}$ | Local primary membrane stress intensity |
| $P_m$ | General primary membrane stress tensor |
| $\overline{P_m}$ | General primary membrane stress intensity |
| Pb-Li | Lithium Lead |
| Pr | Prandtl's number |
| $Q$ | Secondary stress |
| $Q_{tot}$ | Total thermal power |
| $Q_b$ | Secondary bending stress tensor |
| $\overline{Q_b}$ | Secondary bending stress intensity |
| $Q_L$ | Local secondary membrane stress tensor |
| $\overline{Q_L}$ | Local secondary membrane stress intensity |
| $Q_m$ | General secondary membrane stress tensor |
| $\overline{Q_m}$ | General secondary membrane stress intensity |
| $K_{eff}$ | Effective bending shape factor |
| $K_t$ | Creep bending shape factor |
| Re | Reynold's number |
| $S_d$ | Allowable stress limit for the criteria against exhaustion of ductility |
| $S_e$ | Allowable stress limit for the criteria against immediate plastic flow localisation |
| $S_m$ | Allowable stress limit for the criteria against M type damages |
| $S_{rp\ SPs}$ | Radial-poloidal SPs thickness |
| $S_{r\theta\ SPs}$ | Radial-toroidal SPs thickness |
| $S_{r\theta\ p\ SPs}$ | Pierced radial-toroidal SPs thickness |
| $S_t$ | Allowable stress limit for the criteria against thermal-activated phenomena |
| $S_{u,min}$ | Minimum tensile ultimate strength |
| $S_{y,min}$ | Minimum tensile yield strength |
| $T$ | Thermal field |
| $T_m$ | Thickness averaged temperature |
| $T_{r,k}$ | Maximum allowable time |
| $\underline{u}$ | Displacement vector |
| $u$ | Water velocity |

| | |
|---|---|
| $U_p$ | Poloidal displacement |
| $U_r$ | Radial displacement |
| $U_t$ | Creep usage fraction |
| W | Tungsten armour thickness |
| $W_t$ | Cumulative creep rupture usage fraction |

# Introduction

The exploitation of the energy arising from nuclear fusion reactions as a source for the production of electricity represents one of the most difficult, and at the same time fascinating, challenges that the international scientific community is nowadays called to face. In fact, among the so-called “carbon-free” energy sources, the nuclear fusion is, without any doubt, the best option to replace, in the next future, the fossil fuels (coal, oil, natural gas, uranium) in the power plants devoted to produce electricity in a continuous and controllable way. Moreover, the intrinsic safety of a nuclear fusion power plant and the absence of long-lived radioactive waste produced during its operational phase, except for eventual activated structural materials, make the nuclear fusion as the most valuable option for the development of a worldwide energy scenario able to lead the mankind towards the achievement of a whole wellness. To this purpose, the nuclear fusion could play a pivotal role in the definition of a mixed strategy for the electricity production, aimed to supply the electric power necessary to continuously improve our standard of living and ensure, at the same time, a safety and continuous electricity supplying process for both domestic and industrial uses, realized paying attention to the concern for the environment.

Unfortunately, a grand-scale exploitation of the energy coming from the nuclear fusion reactions, namely the construction of a nuclear fusion power plant able to produce hundreds of MW of electrical power, is slowed down by several physical and technological issues. The latter are basically originated by the extremely severe operating conditions to be realized in a fusion power plant in order to allow that a sufficiently high nuclear fusion reactions ratio takes place to produce a considerable thermal power amount destined for the conversion in electricity. For example, one of the most important issues is represented by the necessity to have, in a space of a couple of meters, a region where temperature is equal to some hundred thousands of K very close to a component which must be maintained at ~4 K. It is clear that, in this case, the design of the wall devoted to separate the hottest region from the coldest component becomes a very challenging issue. For these reasons, the worldwide research projects devoted to study the potential exploitation of the nuclear fusion reaction in a large power plant are requiring the greatest effort, in terms of financial and human resources, that the international scientific community has ever made in order to go beyond the afore

mentioned technological issues.

To this purpose, the international scientific community involved in the Research and Development (R&D) activities on the nuclear fusion power plants established a roadmap aimed to realize, by the end of this century, the first Fusion Power Reactor (FPR). In this roadmap, the development of the nuclear fusion reactors based on a closed magnetic confinement system (TOKAMAK concept) is envisaged, due to the favourable intrinsic characteristics of this kind of reactors. In particular, several nuclear fusion machines based on the TOKAMAK concept have been built in order to attain the three main milestones that, due to their importance in the path towards the complete exploitation of the nuclear fusion energy, were established within the framework of the above said roadmap.

The first milestone regarded the demonstration of the scientific feasibility of the nuclear fusion energy and it culminated with the construction of the Joint European Torus (JET) machine, funded by the European Commission. The JET obtained its first plasma in 1983 and attained, in 1997, its main goal to produce 16 MW of fusion power, using a Deuterium-Tritium (D-T) plasma, from an input power of 24 MW.

On the basis of results obtained from JET experimental campaigns, the second milestone of the nuclear fusion energy roadmap has consisted in the construction of the ITER machine, aimed to demonstrate the engineering feasibility of nuclear fusion energy. This means that the ITER machine, nowadays under construction, will have to demonstrate that it is possible to build and run a large fusion machine able to produce much more energy than that it needs. This project is presently developed under the umbrella of an international organization, the ITER Organization (IO), composed by seven partners (European Union, USA, Russia, Japan, China, India, Republic of Korea). Although the ITER construction is currently ongoing, its first Deuterium-Deuterium (D-D) plasma is expected in 2025, while in 2035 the exploitation of the D-T reaction is foreseen. In order to accomplish its mission, the ITER machine has been designed with the aim of operating, during its full power operational phases, as an energy multiplier giving a ten-fold return on energy, namely producing 500 MW of fusion power from 50 MW of input power. No electric power will be generated in ITER.

The third milestone characterizing the fusion roadmap concerns the construction, after the 2050, of a DEMOnstration fusion reactor (DEMO) able to show off the economic feasibility of the electric kWh produced by a large size nuclear fusion power plant, which should be competitive in comparison to the kWh generated by fossil energy sources. In particular, the exploitation of the D-T nuclear fusion reaction is foreseen for DEMO since this is the most promising reaction, among those studied, in order to obtain a profitable energy production. After that, the first FPR should see the light by the end of the 21$^{st}$ century.

In this framework, the construction of ITER is flanked by the development of a conceptual design of DEMO in order to transfer the expertise and the know-how gained from the ITER project towards the further step of the nuclear fusion roadmap. In particular, each IO partner is

currently developing an its own DEMO design, on the basis of its own experience gained from the different phases of the ITER research, design and construction activities.

As far as European Union is concerned, the R&D activities connected to the development of the European DEMO are funded by the European Commission within the framework of the research programme Horizon 2020. In particular, in order to coordinate and develop these R&D activities, the EUROfusion consortium has been created. It promotes and develops the European researches aimed to realize the nuclear fusion roadmap, thanks to the joint effort of European research centres, universities and enterprises which are members of the consortium. In this context, Italy is at the forefront since ENEA is one of the members of the EUROfusion consortium and, furthermore, the most important Italian universities, such as University of Palermo, and enterprises, indicated by ENEA as linked third parties, are deeply involved in the EUROfusion action.

In this context, EUROfusion pays particular attention to the R&D activities concerning the DEMO plasma facing components, which are particularly critical since they have to withstand extremely severe operating conditions being directly faced to the plasma radiation. Among the DEMO plasma facing components, the Breeding Blanket (BB) plays an essential role in the machine design since it is mainly devoted to attain three crucial functions: shield the components located outside the plasma chamber, principally the coils, from the radiation arising from plasma, remove the thermal power deposited by neutron and photons by means of a proper cooling fluid in order to convert it in electrical power and, last but not least, provide the tritium necessary to the self-sustenance of the D-T nuclear fusion reactions, properly foreseeing a neutron multiplier to maximize the tritium production.

Nowadays, 4 BB concepts are under investigation in Europe in order to be chosen for the final DEMO design: the Helium-Cooled Lithium Lead (HCLL) BB which adopts gaseous helium as coolant and the Pb-Li eutectic alloy as breeder and neutron multiplier, the Helium-Cooled Pebble Bed (HCPB) BB which foresees gaseous helium as coolant too and pebble beds of lithium and beryllium ceramic compounds as breeder and neutron multiplier respectively, the Dual-Coolant Lithium Lead (DCLL) BB in which the Pb-Li eutectic alloy acts simultaneously as breeder-neutron multiplier and coolant together with gaseous helium and, finally, the Water-Cooled Lithium Lead (WCLL) BB in which subcooled pressurized water is used as coolant and the Pb-Li eutectic alloy is adopted as breeder and neutron multiplier.

The EUROfusion action is aimed to perform R&D activities on all these 4 BB concepts in order to select, by the 2027, the most promising one as basic concept for the DEMO design. To this purpose, all the 4 concepts have to be investigated under the neutronic, thermal-hydraulic and thermo-mechanical point of view in order to assess their performances and be able to compare them each other, allowing the selection of the best one for the definitive DEMO design. In particular, from the neutronic standpoint, the neutrons and gammas

interactions with materials and the tritium breeding reactions have to be mainly investigated in order to determine the thermal power deposited within the components, their shielding action and the tritium breeding capability of each BB concept. Furthermore, from the thermal-hydraulic point of view, the characterization of a proper cooling system, in terms of mass flow rates and pressure drops, and, as to the concept for which a liquid breeder is envisaged, the circulation of the Pb-Li are the fundamental issues to be addressed taking into account inputs coming from neutronics. Finally, from the thermo-mechanical standpoint, the determination of the temperature and stress spatial distributions, arising as a consequence of the appropriate thermo-mechanical loads and boundary conditions which basically come from the neutronic and thermo-hydraulic outcomes, is a key issue in order to ensure that the BB concept taken into account is able to fulfil the prescribed structural design criteria aimed to avoid the incipient structural crisis condition.

Within this international scientific framework, the research activity performed during the Ph.D. course in "Energia e Tecnologie dell'Informazione - curriculum fisica tecnica e ingegneria nucleare (XXIX ciclo)" ("*Energy and Information Technologies - nuclear engineering and applied physics curriculum, 29$^{th}$ cycle*"), held at the University of Palermo, has been part of the R&D activities promoted by EUROfusion and it has regarded the numerical thermo-mechanical analysis of the DEMO WCLL BB conceptual design, under selected steady-state loading scenarios, focussing attention on the outboard equatorial module.

The research activity has been mainly divided in two parts. In the first one, attention has been paid to the sizing of the First Wall and the Stiffening Plates in order to contribute to the conceptual design activities of the WCLL BB outboard equatorial module. In the second part, the so designed WCLL BB module has been assessed from the thermo-mechanical standpoint, under nominal and accidental steady-state loading conditions, in order to check the complete fulfilment of the prescribed structural criteria and suggest, in case of failing, proper design modifications. To this purpose, the study has been carried out in accordance with the Structural Design Code for ITER In-vessel Components (SDC-IC), purposely developed for the investigation of the thermo-mechanical behaviour of ITER in-vessel components and adopted also for the DEMO design.

The whole research activity has been performed following a theoretical-numerical approach based on the Finite Element Method (FEM) and adopting the quoted commercial ABAQUS FEM code, listed among the reference ones by the international scientific community involved in fusion relevant R&D activities.

The research activity performed and the methodologies adopted are herewith reported and discussed, paying particular attention to the obtained results and to the contribute given to the DEMO WCLL BB design, finally focussing attention on the open issues which will be further investigated in the next future.

# Chapter 1

# THE DEMO WATER-COOLED LITHIUM LEAD BREEDING BLANKET

## 1.1 Introduction

The realization, by 2050, of a Demonstration Fusion Power Reactor (DEMO) to follow ITER, with the capability of generating several hundreds of MW of net electricity, is viewed by European Union (EU) and many of the other partners involved in the construction of ITER as the remaining crucial step towards the grand-scale exploitation of fusion power [1].

The recently updated EU fusion roadmap, developed within the framework of Horizon 2020 research programme, advocates for a pragmatic approach and considers a pulsed “low extrapolation” DEMO. This should be based on mature technologies and reliable regimes of operation, as much as possible extrapolated from the ITER experience and on the use of materials and technologies adequate for the expected level of neutronic damage [1].

In order to promote and coordinate Research and Development (R&D) activities relevant to the DEMO development and funded by Horizon 2020 programme, the EUROfusion consortium has been created thanks to the joint effort of European universities, laboratories, industries and research centres. The main goal of the consortium is to achieve the milestones prescribed by the above mentioned roadmap.

To this purpose, in the EUROfusion consortium a DEMO conceptual design activity has now been launched [1] in parallel with the ITER construction phase. In fact, DEMO in Europe is considered to be the last step before a commercial Fusion Power Reactor (FPR) and capable of: (i) resolving all remaining physical and technical issues foreseen in the plant and demonstrating the necessary reactor relevant technologies; (ii) demonstrating production of several hundreds of MW of electricity; (iii) achieving tritium self-sufficiency, i.e. DEMO must make its own fuel; (iv) operating with adequate availability/reliability over a reasonable time span [2].

Presently, the DEMO reactor design has not been formally selected and detailed operational requirements are not yet available. In fact, two different nuclear fusion reactor concepts are currently candidate to be selected for the DEMO definitive design. The first option, based on the Stellarator machine concept, would allow to operate in steady-state conditions thanks to its intrinsic features, but it is characterized by a high geometric complexity which slows down its development on a large scale. The second option is based on the TOKAMAK concept, namely the same fusion reactors line selected for the JET and ITER machines. This kind of fusion reactors is more simple from the geometric point of view, but it is characterized by a pulsed operating phase.

In particular, where exactly DEMO should be located in between ITER and a commercial FPR depends on the resources, the gaps towards a commercial plant as well as the development risks that can be accepted, and the time scale to fusion deployment [2].

In this context, the research activity performed during the Ph.D. course has been developed in the framework of the R&D activities, promoted by EUROfusion, relevant to the DEMO reactor based on the TOKAMAK concept.

## 1.2 The DEMO reactor definition

The main goal of the DEMO nuclear fusion reactor is to demonstrate that a high availability of a fusion power plant, able to produce several 100s MW of net electricity, is achievable [1] with a competitive electric kWh price. In particular, a thermal power of 2000 MW is foreseen for DEMO, corresponding to a net electric power production of ~500 MW [2]. DEMO is therefore conceived for long plasma pulses (~2.5 h) and minimized dwell time between two pulses [1] as shown in Figure 1-1.

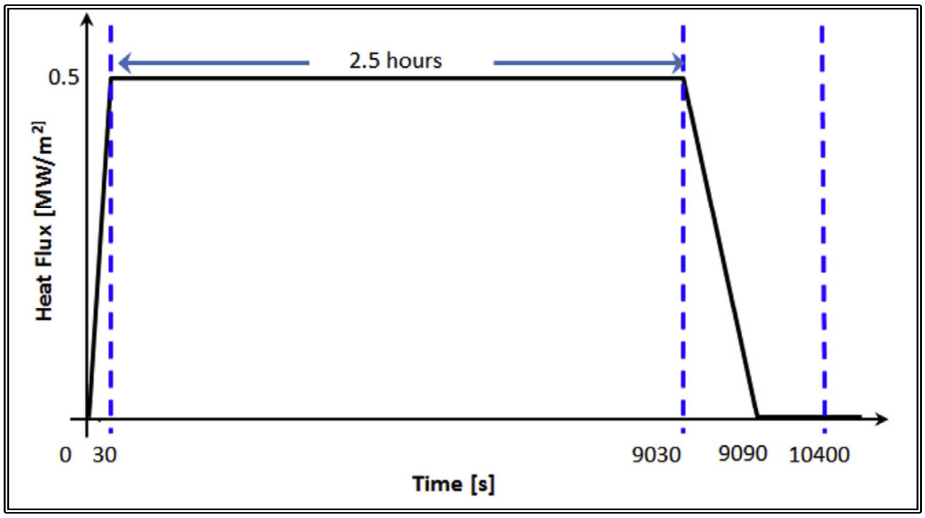


Figure 1-1.A typical DEMO pulsed operational period.

The DEMO architecture based on the TOKAMAK concept is that of a typical super conducting TOKAMAK machine. As to the major radius, a value of ~9 m is envisaged [1], with an aspect ratio ranging from 3 up to 4 [2].

An ITER-like single null plasma configuration is foreseen for DEMO, adopting a water-cooled divertor endowed with appropriate plasma facing components. In fact, inside the vessel the high heat flux targets of the divertor intersect the scrape-off layer, namely a narrow band collecting most of the particles that escape the plasma confinement.

DEMO will require tritium supply from external sources only for the plant start-up, while during its nominal operation phase it will be able to produce the tritium it needs thanks to its tritium breeding capability, ensuring the tritium self-sustenance of the system. This is possible thanks to the presence of the Breeding Blanket (BB), which is designed with the aim to accomplish three main goals: shield the Vacuum Vessel (VV) and the magnets from the radiation arising from plasma, supply the tritium necessary to the machine self-sustenance and remove the heat power deposited by neutrons, gammas and particles coming from plasma and both breeding and multiplication nuclear reactions. In DEMO, most of the plasma surface (∼85%) is surrounded by a BB containing large amounts of lithium to breed the tritium consumed in the plasma [1]. To compensate for the plasma-generated neutrons not interacting with lithium the BB also contain a neutron multiplier, either beryllium or lead.

The coolant, which is envisaged to exhaust about 85% of the power from the reactor [1], needs to be operated at high temperature to allow for efficient energy conversion (coolant inlet at ∼300◦C) [1]. The coolant is supplied to the BB by means of purposely dedicated feeding manifolds.

At the same time, in the DEMO design technologies and/or systems with high energy demand requiring recirculating power have been avoided or kept to a minimum; hence superconducting technology will be used for the magnets and the cooling scheme of the in-vessel components is being designed with attention to pressure drops. Also the total power of auxiliary heating and current drive systems has been minimized [1].

Reduced activation materials need to be used for some DEMO components to avoid the need for permanent waste repositories. Consequently, the Reduced-Activation Ferritic Martensitic (RAFM) EUROFER steel [1] has been chosen as structural material of the plasma facing components, like the BB, while AISI 316 steel has been chosen for the VV [2].

In order to thermally insulate the magnet coils the TOKAMAK is inside a large vacuum chamber, called cryostat. In addition thermal shields at ∼80 K protect the coils from radiation heat.

The port structures of a torus shaped water-cooled vacuum vessel penetrate the cage formed by the magnet system, currently based on 16 Toroidal Field (TF) and 6 Poloidal Field (PF) coils, providing access to the plasma, e.g. for systems heating the plasma or driving its current, for diagnostic devices or to maintain the in-vessel components.

The high neutronic damage envisaged for the in-vessel components (20 dpa for the starter blanket and 50 dpa for the second blanket [2] are predicted) and the consequent high dose rate expected for VV and cryostat cause the necessity of maintenance to be carried out remotely. Maintenance of in-vessel components will generally consist of the replacement of components by Remote Handling (RH) tools.

A schematic view of the DEMO TOKAMAK main systems is depicted in Figure 1-2.

However, establishing performance requirements and project development schedules linked to a target start of construction date is expected to be a strong driver in the selection of the technical features of the device, favouring more conservative technology choices for near term solutions [3]. A system engineering approach is viewed as essential from the early concept design stage: (i) to better understand the problems and evaluate the technical risks of foreseeable technical solutions; (ii) to identify design trade-offs and constraints to address the most urgent issues in physics, technology and design integration; and (iii) to prioritize the R&D needs. Ensuring that R&D is focussed on resolving critical uncertainties in a timely manner and that learning from R&D is used to responsively adapt the technology strategy is crucial to the success of the programme [3].

Involvement of industry and exploitation of international collaborations on a number of critical technical aspects is highly desirable, as already done in the EUROfusion consortium.

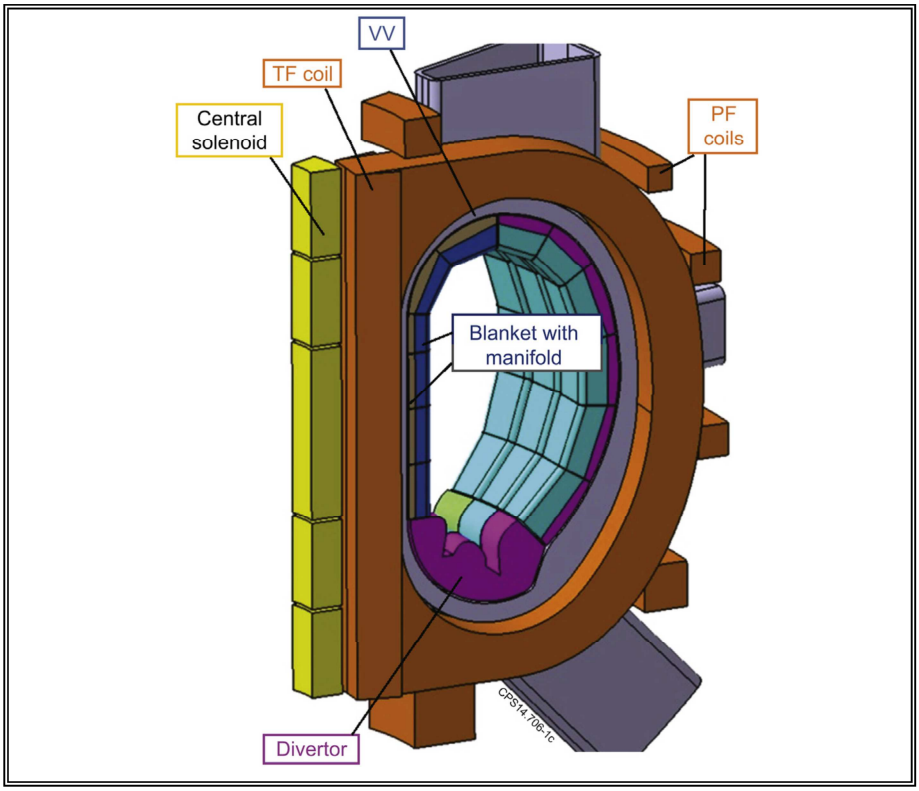


Figure 1-2. Configuration of the DEMO TOKAMAK main systems.

In order to clearly identify and resolve DEMO physical challenges beyond ITER, the physical basis of DEMO needs to be further developed, especially in areas with issues concerning the feasibility or the performance of the device.

To this purpose, a high number of studies that have strong implications on machine parameter selection and architectural layout have been initiated even though most of them are still in the pre-conceptual phase. They include [2]:

- the machine aspect ratio scan for a fixed electric power of 500 MW and a pulse duration of ~2.5 h (considered as a long pulse);
- the investigation of the impact of increasing plasma elongation constrained by vertical stability, through optimising, for example, PF coils geometric layouts and current distributions;
- the investigation of divertor configurations with a lower X-point height and larger flux expansion;
- the assessment of First Wall (FW) power handling design limits near the upper secondary null point and assessment of the technology and maintainability requirements of the proposed solutions;
- the investigation of the potential of a double null configuration: advantages (e.g., higher plasma performance with improved vertical position control, and reduced machine size) and disadvantages (e.g., tritium breeding, compatibility with proposed blanket vertical maintenance scheme, integration of upper divertor, etc.);
- the investigation of divertor strike-point sweeping, including technology issues such as thermal fatigue of the high heat flux components;
- the optimisation of the blanket shielding design in order to minimise vacuum vessel structural material activation;
- the detailed Tritium Breeding Ratio (TBR) sensitivity study in order to understand the tritium providing capability of the different BB options;
- the investigation of magnetic field ripple: trade-off between remote maintenance access, coil size and neutral beam injection access;
- the estimation of the minimum achievable dwell time and evaluate impact of trade-offs on central solenoid design, Balance of Plant, pumping, etc. .

For each of the above said areas, a proper research programme is currently ongoing within the framework of the EUROfusion consortium action in order to advance in the DEMO conceptual design activities and allow to fix some requirements and reasonable machine parameters. Each programme is coordinated and developed in the framework of a specific Work Package (WP) which ensures the achievement of the milestones prescribed by the EUROfusion Programme Management Unit.

Further details about the EUROfusion organization and the WPs actions have been reported in Appendix 1.

## 1.3 The Breeding Blanket design approach

Although EUROfusion consortium action has been organized according to several WPs, each one in charge of developing a specific aspect of the DEMO design, it has to be underlined that the BB can be considered as the key component of the machine since it is devoted to provide the tritium necessary to the self-sustenance of the nuclear fusion reactions. Within the framework of the EUROfusion consortium action, the R&D activities regarding the DEMO BB design have been organized in the pertinent WP, called WPBB. Details about the organisation of the WPBB action, with a list of all the research centres and laboratories involved in its activities, are reported in Appendix 1.

In this instance, it has to be remarked that WPBB R&D activities are focussed on the investigation of the 4 BB concepts presently candidate, in Europe, in order to be chosen for the final DEMO design. These BB concepts are:

- the Helium-Cooled Lithium Lead (HCLL) BB which adopts gaseous helium as coolant and the Pb-Li eutectic alloy as breeder and neutron multiplier;
- the Helium-Cooled Pebble Bed (HCPB) BB which foresees gaseous helium as coolant too and pebble beds of lithium and beryllium ceramic compounds as breeder and neutron multiplier respectively;
- the Dual Coolant Lithium Lead (DCLL) BB in which the Pb-Li eutectic alloy acts simultaneously as breeder-neutron multiplier and coolant together with helium;
- the Water-Cooled Lithium Lead (WCLL) BB in which subcooled pressurized water is used as coolant and the Pb-Li eutectic alloy is adopted as breeder and neutron multiplier;

The WPBB roadmap foresees that, by 2020, the number of concepts which will be further investigated will be reduced down to 3 and, by 2027, only one concept will be selected in order to be developed and integrated in the final DEMO design. To achieve this goal, several neutronic, thermal-hydraulic and thermo-mechanical requirements have been prescribed in order to investigate the BB concepts performances under both the operative and the accidental conditions envisaged for DEMO reactor and, moreover, a continuous updating of these requirements is ongoing by the WPBB leader.

Furthermore, different sets of additional requirements have been defined with the aim to take into account the limits coming from different scientific areas and be able to adopt a multi-disciplinary approach to the BB design

First of all, the BB shall be adapted to a reactor maintenance system based on a remote handling vertical replacement scheme through large upper ports [4]. According to this concept (Fig. 1-3) each blanket sector (toroidal portion between two TF coils) is vertically divided into 3 outboard (OB) and 2 inboard (IB) segments. For an 18-TF coils reactor this means 18 blanket sectors for a total of 90 individual segments [4].

At the present stage of design the architecture of each segment mainly follows the principle

of the Multi Module Segment (MMS) concept. A blanket segment is formed by a robust Back Supporting Structure (BSS) that support modules (boxes) that contain the Breeder Zone (BZ), the First Wall and the pertinent cooling fluids. The BSS includes also the main manifold system that feeds the modules and connects the primary heat transfer systems outside the Vacuum Vessel.

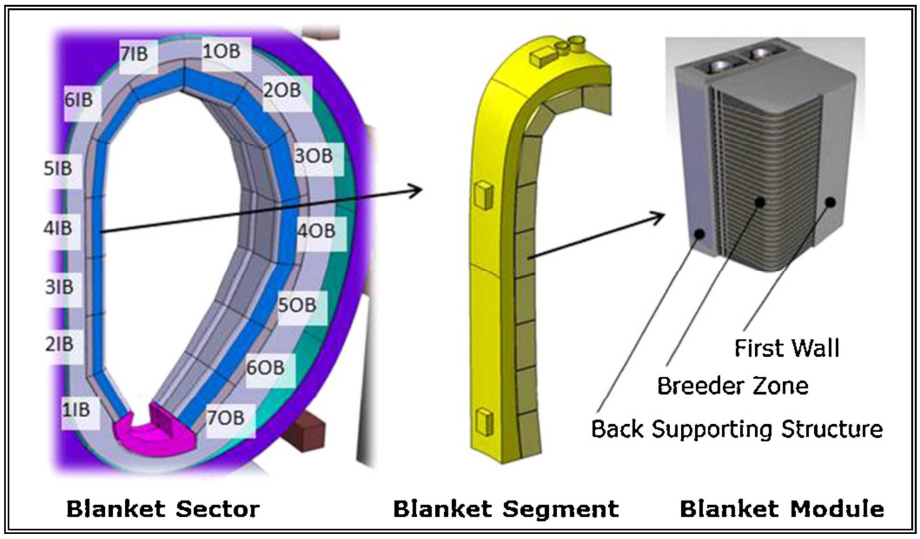


Figure 1-3. Typical blanket segmentation for a vertical maintenance system and MMS [4].

From the neutronic standpoint, main requirement for the DEMO reactor is to produce all the tritium necessary for the fusion reaction, not relying to any external sources (apart from some kilograms of tritium necessary to start the reactor operations).

As blankets are supposed to be the only components to breed tritium, the tritium self-sufficiency can be achieved only with an accurate nuclear design of this system. In particular breeder and neutron multiplier materials shall be located in proximity of the plasma flux and neutron absorption materials shall be minimized in the BZ. In particular the amount of steel that is used as structural material has to be reduced; amount of steel larger than 12 - 15% can degrade the TBR to unacceptable levels. Moreover, BB have to protect the VV against damages (dpa < 2.75), excessive heating and, depending on the materials, to reduce the activation of the VV structures [4].

From the thermal-hydraulic point of view, the design of the BB has to ensure an effective cooling of all the parts under surface and volumetric thermal loads to cope with temperature limits of the materials. EUROFER steel shall be kept under ~550 ° C, solid breeders under 920 ° C, beryllium under 650 ° C and Pb-Li under ~550◦C (at least at the interface with steel) [4]. Moreover, Pb-Li temperature has to be kept greater that 300 °C in order to avoid local solidification problems.

As to the FW design, three architecture options have been proposed [4], ranging from (i) a

fully thermal-hydraulically and mechanically integrated option (current reference design), through (ii) a thermal-hydraulically decoupled one, to (iii) a fully (also mechanically) decoupled option. The adoption of these different configurations will depend on the local loads acting on the blanket surface.

For relatively low surface loads (under 0.5 - 1.0 MW/m$^2$, depending on the used coolant) and uncertainties in the range of ±15% the solution (i) seems possible while for higher uncertainties the solution (ii) should be preferred. Solution (iii) could be adopted to reduce thermal and electro-megnetic loads or if the life-time of the FW components falls below the limits prescribed for the remaining blanket (e.g. for the use of other structural materials than EUROFER) requiring a local replacement [4].

From the thermo-mechanical standpoint, the BB structure have to withstand the thermo-mechanical loads it undergoes under selected loading conditions, such as the coolant pressure, the thermal-induced stresses and electro-magnetic loads. Characteristic of the BB designs is the presence of high pressure coolants (8 MPa for helium and 15.5 MPa for water) in small channels embedded in plates or in independent pipes. The structural assessment is performed following the reference structural design codes. Particularly critical for the thermo-mechanical design is the assessment of the box behaviour in case of in-box LOCA accident. In fact, during operation the box contains the breeder materials at low pressure (<0.2 MPa for helium purge in HCPB, ~1 MPa of hydrostatic load for Pb-Li) [4] being fully separated from the high pressure cooling system. In case of a rupture of a separating wall the box can be pressurized at the coolant pressure. The thermo-mechanical requirements have to cope with the neutronic requirements: reinforcements necessary to ensure the box stability are to be carefully implemented to avoid increasing the amount of steel in the BZ impacting the TBR. Moreover, electro-magnetic forces constitute another typical load challenge for the TOKAMAK-type reactor. They are caused by electrical currents induced by magnetic transients interacting with magnetic fields (Lorentz forces) or simply by the stationary interaction of magnetic fields with magnetic materials (Maxwell forces) [4]. These forces are in particular a challenge for the attachment system of the blankets to the VV, but also internal forces can affect the integrity of single boxes; therefore present efforts aim at assessing the performance of the MMS design.

## 1.4 Status of art of the 4 European Breeding Blanket concepts for DEMO

The 4 breeding blanket concepts candidate to be chosen for the DEMO design, already mentioned in § 1.3, are the HCPB, the HCLL, the WCLL and the DCLL BB. The WPBB, created in the framework of the EUROfusion consortium action, foresees the assessment of these 4 BB concepts under neutronic, thermal-hydraulics and thermo-mechanical point of

views in order to validate and develop their design.

Concerning HCPB BB, it is a solid breeder concept that uses a ternary Li-ceramics as breeder and beryllium as neutron multiplier material, while the cooling fluid is pressurized gaseous helium. The research activities on the DEMO HCPB BB have been based on the outcomes and the methodologies already developed for the ITER HCPB Test Blanket Module (TBM), performed under the coordination of the Karlsuhe Institute of Technology (KIT) [5-7]. The adaptation of the HCPB BB design to DEMO started in 2012, with a first version based on the robust "beer-box" architecture, used also for the ITER HCPB TBM, and with a segmentation in 10 boxes per segment. The results, however, were poor in term of TBR [4]. In fact, as the HCPB concept is characterized by a relatively moderated spectrum (due to the presence of large amount of beryllium), it is very sensitive to steel content [4].

Therefore, the adaptation of the design to the DEMO plant required a completely new architecture of the breeder zone. Opportunely modifying the "beer box" concept, it is possible to feed the different box structures directly from the BSS manifolds, reducing the intermediate level of box manifold. This new architecture (named "sandwich concept") has resulted in a steel amount reduction of about 11%in the BZ. In addition, this results in an increase of the radial thickness of the BZ, which has been used, in its turn, in order to increase the functional materials (breeder materials) amount in the BZ. Preliminary neutronic assessment reveals the possibility to reach TBR values higher than 1.20 [4]. Figure 1-4 shows the evolution of HCPB design from 2013 "beer box" concept up to 2015 "sandwich concept".

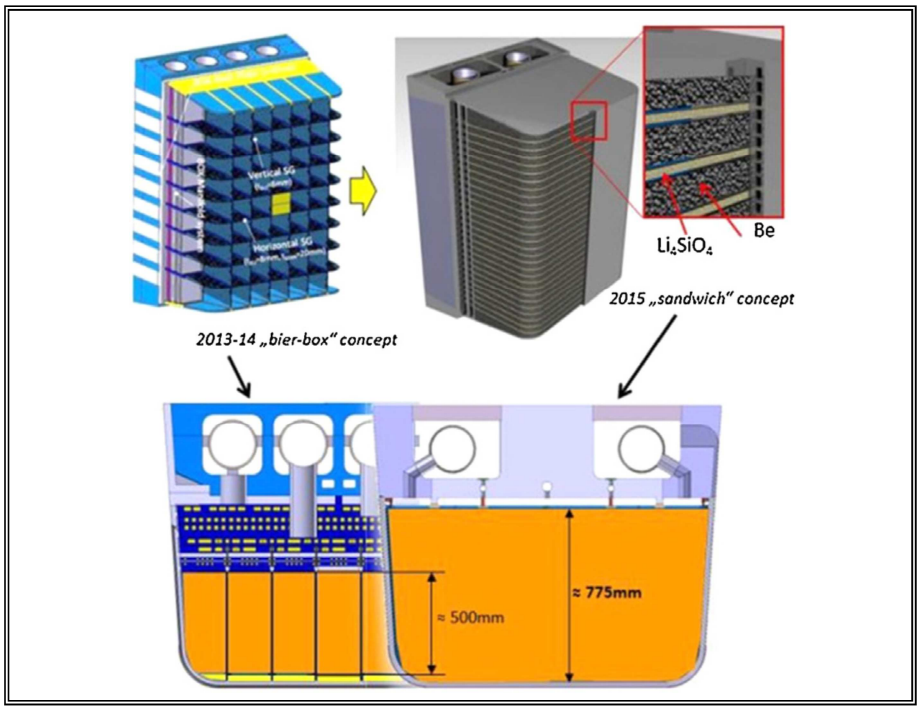


Figure 1-4. Evolution of the HCPB BB design.

Several campaigns of both transient and steady state thermal and thermo-mechanical analysis have been performed at KIT [8-9] adopting the “sandwich concept”, in order to consolidate the present knowledge on the performance of this new design proposed by the KIT HCPB team in 2015. In particular, the verification of the prescribed structural design criteria fulfilment under the assumed loading conditions has been performed. As an example, a typical Von Mises equivalent stress field, arising within the HCPB BB outboard equatorial module as a consequence of both thermal and mechanical loads, is depicted in Figure 1-5, together with the stress paths adopted for the criteria fulfilment verification [8]. The so obtained results will be used, among other studies, to establish a baseline design of the EU DEMO HCPB BB following the EUROfusion DEMO plant specifications [8].

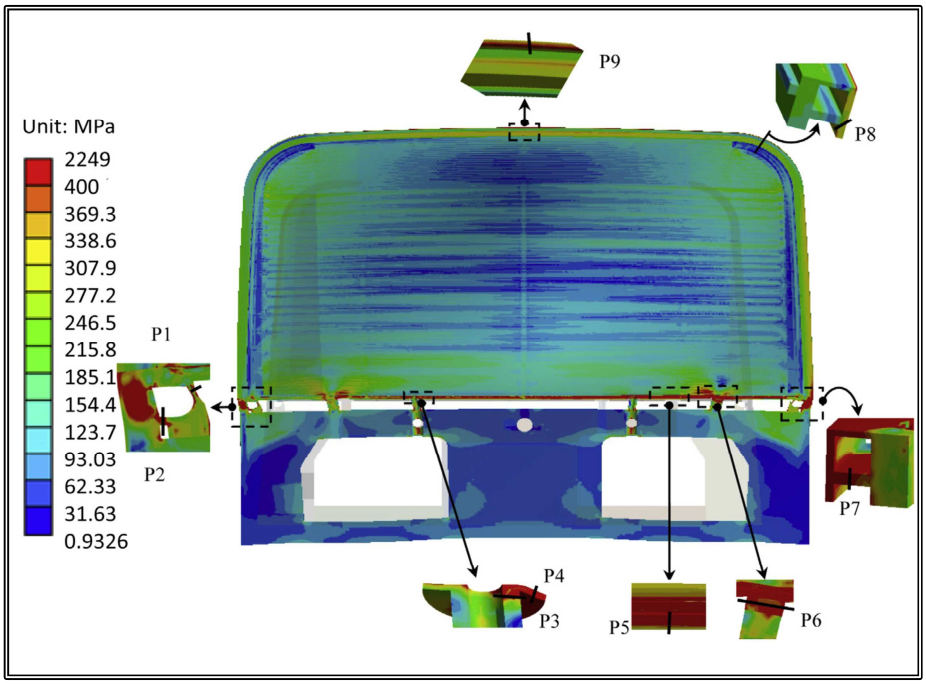


Figure 1-5. HCPB outboard equatorial module Von Mises equivalent stress field and paths.

As far as HCLL BB is concerned, this concept was proposed and deeply assessed since 2003 for the ITER TBM programme by the Commissariat à l’Energie Atomique (CEA) [10-13]. The HCLL BB foresees pressurized gaseous helium as coolant and the eutectic Pb15.8Li as breeder material. The Pb-Li circulates slowly in the blanket only to carry the breed tritium outside the reactor for extraction.

As already done by the HCPB BB research team, also for the HCLL the outcomes and methodologies set-up during the TBM research campaigns have been adopted for the design of DEMO HCLL BB. Nevertheless, design improvements are being implemented to adapt the design set-up for the ITER TBM to DEMO specifications and performance objectives [4].

The proposed design (Fig. 1-6), set-up in 2015, presents the typical “beer-box” architecture used in the TBM with modular Breeder Units. In particular the BSS has been designed following the tie rods concept used also in the TBM manifold region.

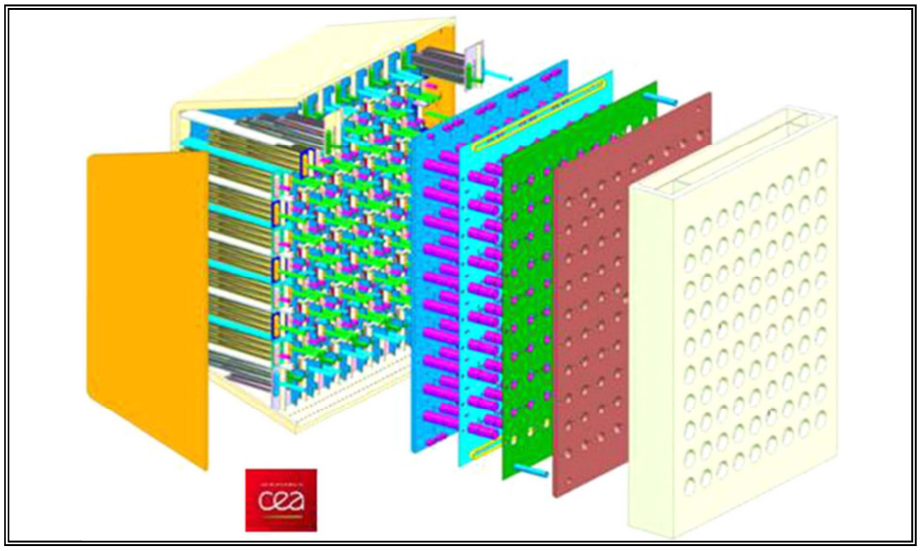

Figure 1-6. HCLL BB 2015 design.

Neutronic, thermal-hydraulic and thermo-mechanical analyses have been carried out in order to justify the design of the HCLL breeding blanket, showing attractive results for tie rods modules attachments system and relatively good behaviour of the box in case of LOCA [14-17]. As an example, some significant thermal and mechanical results for a typical HCLL BB Breeder Unit and for the tie rods attachment system are reported in Figures 1-7 and 1-8 respectively.

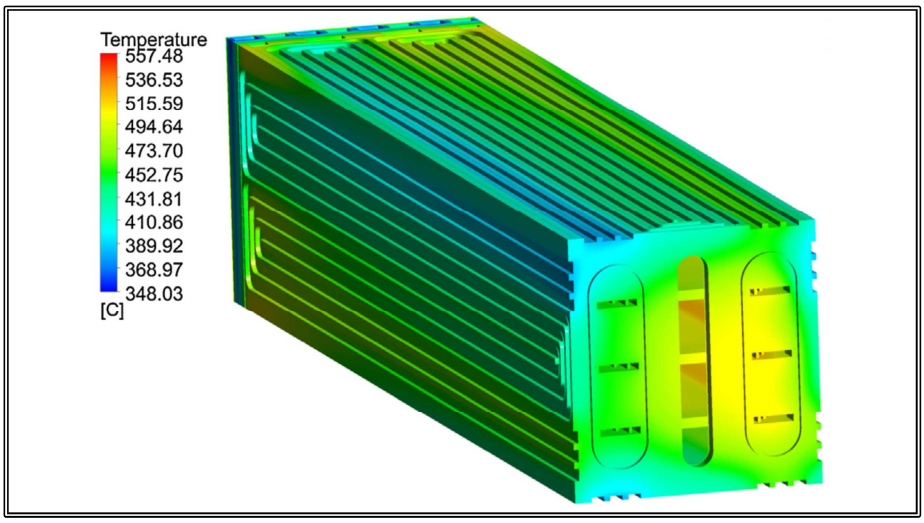


Figure 1-7. DEMO HCLL BB thermal results for a typical Breeder Unit.

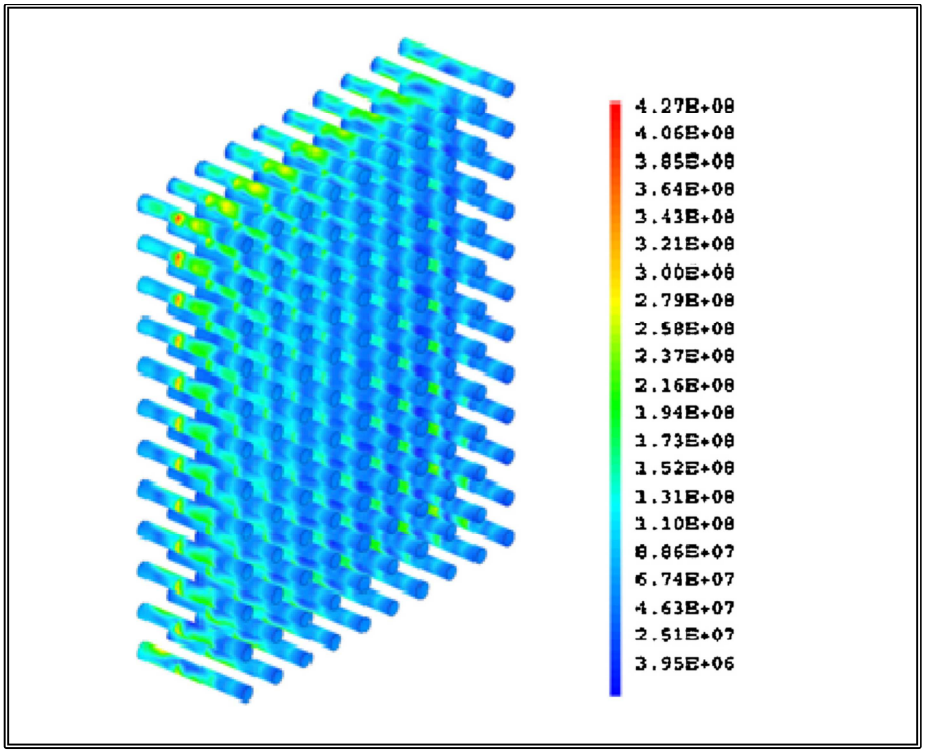


Figure 1-8. DEMO HCLL BB thermo-mechanical results for the tie rods attachment.

Moreover, from the thermal-hydraulic standpoint, analyses have confirmed outcomes obtained from TBM analyses [14-17]. As regards neutronics, the TBR predicted for the current design amount to 1.07 [4, 16], but the maximum theoretical TBR value that could be achieved by implementing design modifications, consisting in the increase of the inboard breeder zone thickness using an improved manifold scheme and a reduction of the number of both cooling plates and Stiffening Plates (SPs) in Breeding Units, is 1.19 [4].

Regarding the WCLL BB, this concept was developed in parallel with the HCPB in the framework of ITER TBM programme [18-20] by CEA, but it was abandoned in 2004 for the HCLL. The studies have been restarted in 2012 first by CEA [21-22], then by the ENEA team [4]. The concept is characterized by the use of water at PWR conditions (inlet at 285 ° C - outlet at 325 ° C at 15.5 MPa) as coolant and Pb-Li as liquid breeder.

The research activities on the DEMO WCLL BB performed by CEA have been based on the experience gained from the ITER TBM assessment, and they have been characterized by some preliminary analyses aimed at investigating, from the thermo-mechanical, thermal-hydraulic and neutronic standpoints, both the waved and flat FW geometric configurations. As an example, in Figure 1-9 the thermal field arising within the two investigated FW configurations, under preliminary nominal steady state conditions envisaged for the PPCS-A [21], is depicted. These results have been obtained by CEA preliminary thermal analyses on simplified 3D models [21].

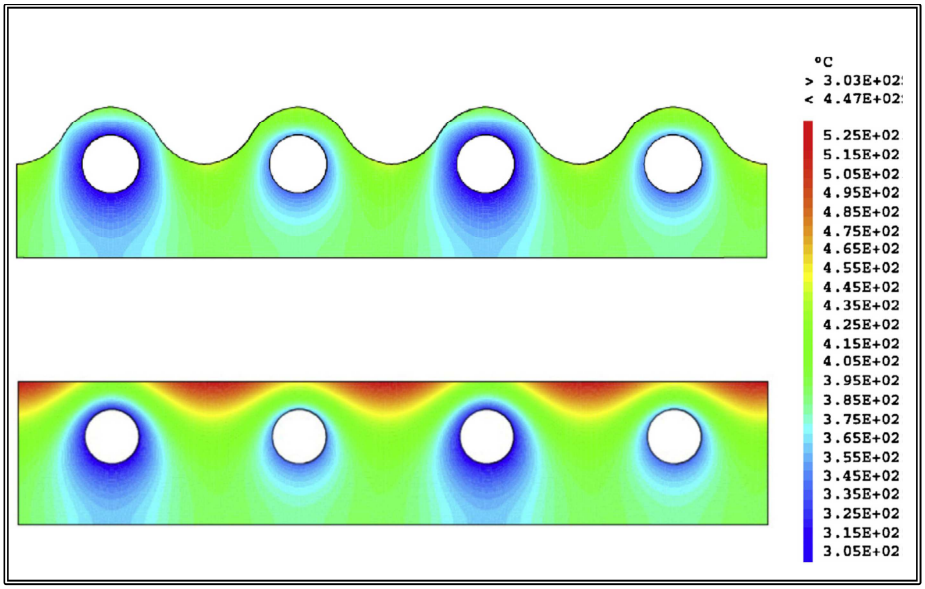


Figure 1-9. Thermal field within waved (on the top) and flat (on the bottom) WCLL BB FW.

Successively, a complete design of the DEMO WCLL BB outboard equatorial module have been proposed by CEA (Fig. 1-10). This design has been adopted as the starting point by ENEA when this organisation has become the responsible for the DEMO WCLL BB development, within the framework of EUROfusion WPBB action.

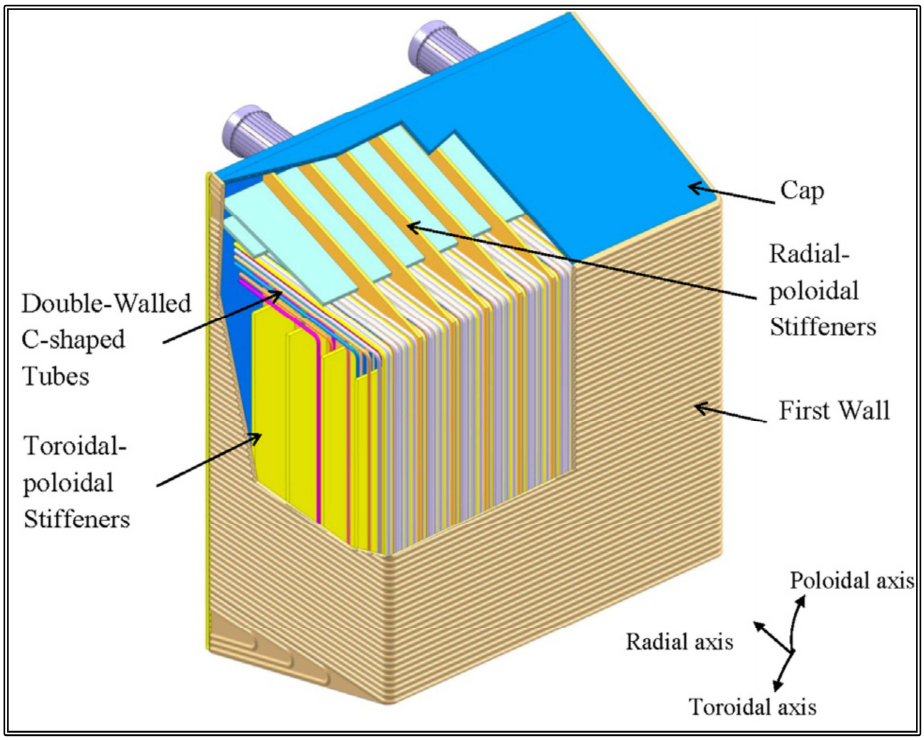


Figure 1-10. DEMO WCLL BB outboard equatorial module design proposed by CEA.

Figure 1-11 depicts a new DEMO WCLL BB design (first release in 2015) developed by ENEA, based on the rationale of having the same repeatable basic geometry (modularity of the breeding blanket) along the poloidal direction. Differently from CEA design, stiffeners are placed in the radial-toroidal plane and in the radial-poloidal plane. The cooling water flows through Double Wall Tubes (DWTs) with a C-shape and placed on a radial-toroidal plane. The computed velocity in the tubes is less than 2 m/s. The Pb-Li flow path in the breeding zone is "quasi" horizontal. Preliminary thermal analyses have been carried out to evaluate the temperature field in the module and within the breeder. It has to be remarked that the outcomes of this work have been fundamental to develop the 2015 WCLL BB design, as widely described in the following.

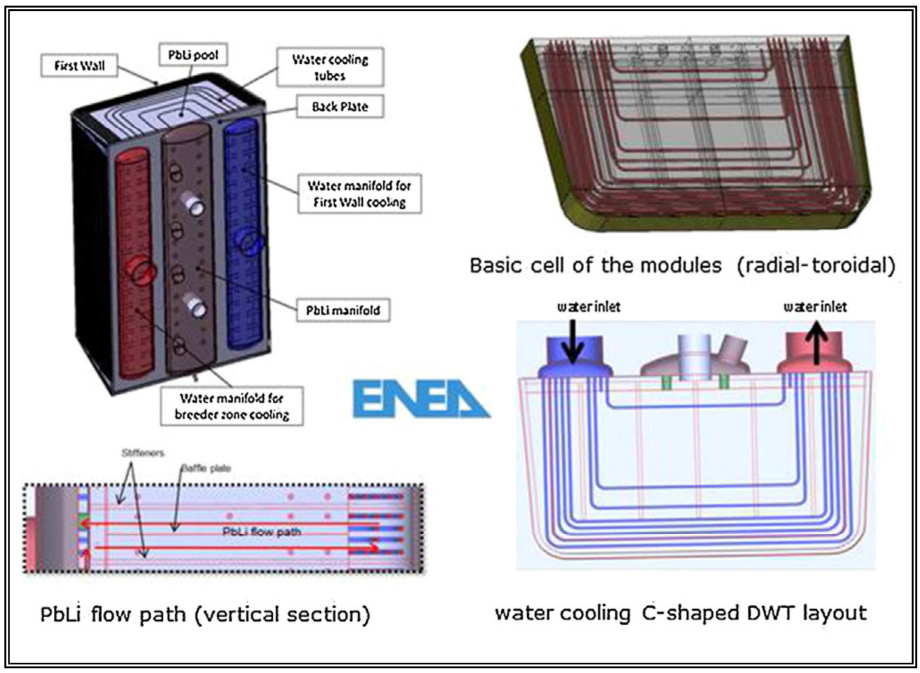


Figure 1-11. New WCLL BB 2015 design proposed by ENEA.

Concerning DCLL BB, also this concept can be found in the previous European studies and, like the WCLL BB, it was practically abandoned in the past R&D activities linked to ITER TBM programme [23]. Also for DCLL, studies have been restarted in 2014 thanks to the EUROfusion consortium action.

The concept is interesting for the potentiality to operate at high Pb-Li temperatures (up to 700°C) with consequently a high efficiency of the power conversion system. For DEMO a low temperature version (Pb-Li temperatures<500°C) was proposed and presently assessed, since it does not require the development of high temperature materials, making it possible for a near term application.

CIEMAT has been working on the new design since 2014 [24], according to the new

DEMO reactor specifications. The design is based on a multi-module segment, having 8 different modules attached to a common BSS. Each blanket module presents a poloidal circulation of Pb-Li in order to extract most of the reactor power, while the FW foresees He channels for cooling purposes [5]. The BZ consists of 4 parallel Pb-Li circuits, separated by radial stiffening grid. Thanks to the MMS design the Pb-Li velocity has been considerably reduced inside the modules (2 - 3 cm/s) resulting in relatively low MHD pressure losses (about 250 kPa in a preliminary estimation) [4].

A TBR of 1.13 has been estimated [25] and shielding performances have been assessed, demonstrating that the DCLL fulfils the current limit (together with the VV) in the TF coils established for DEMO (50 W/m$^3$) [4].

A schematic view of the currently investigated design is shown in Figure 1-12.

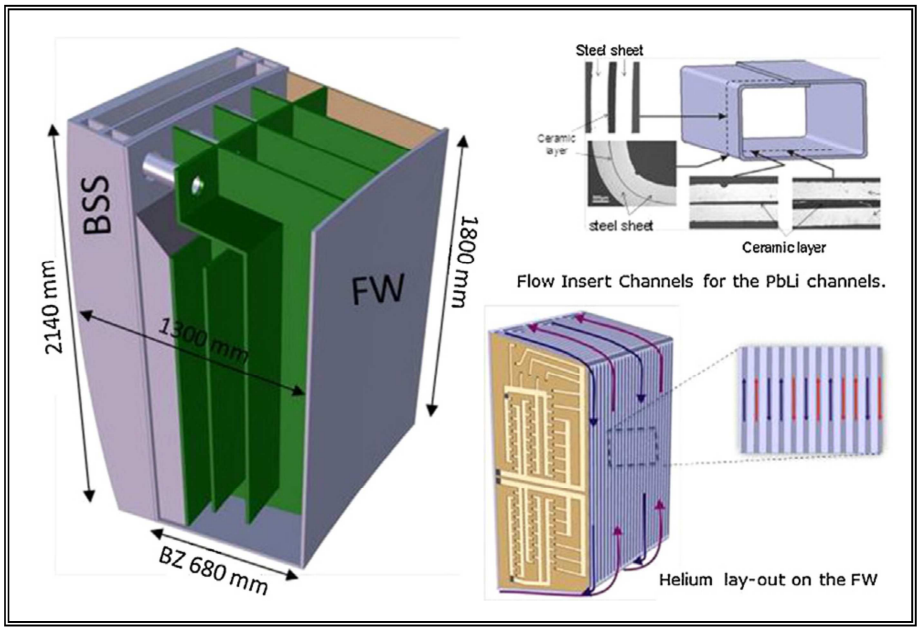


Figure 1-12. DCLL BB design proposed by CIEMAT.

## 1.5 Objective of the study and adopted methodology

As widely explained up to this point, the BB of the DEMO fusion reactor is the key components of the machine due to its main functions of shielding the out-vessel components from radiation arising from plasma, removing the heat power deposited by neutron and gammas within both structural materials and breeder and, last but not least, providing the tritium necessary to the fusion reactions.

For this reason, the research activity performed during the Ph.D. course has been specifically intended to design the DEMO WCLL BB and assess its thermo-mechanical

behaviour. In particular, in a first phase a preliminary geometric optimization of the FW and the SPs has been performed in order to select geometric configurations of these components able to withstand the severe loading conditions which they have to undergo during an in-box LOCA accident, simulated by the Over-Pressurization (OP) steady state loading scenario. This optimization study has allowed to attain the above mentioned 2015 WCLL BB design (Fig. 1-11) which has been assessed, in the second phase of the activity performed during the Ph.D course, under both the Normal Operation (NO) steady state loading scenario, namely the loading conditions which should be realized during the DEMO flat-top plasma operating phase, and the afore mentioned OP scenario.

The obtained results have been assessed in accordance with the Structural Design Criteria for ITER In-vessel Components (SDC-IC) code, in order to check the total fulfilment of the prescribed structural design criteria and, in case of failing, opportunely suggest design modifications to the WCLL BB project team.

Therefore, the research activity carried out has been fully developed within the framework of the WPBB of the EUROfusion consortium, since University of Palermo is a EUROfusion linked third party being indicated by ENEA.

The study herewith reported has been performed following a theoretical-numerical approach based on the Finite Element Method (FEM) and adopting the quoted commercial ABAQUS Finite Element code, listed among the reference ones by the international scientific community involved in R&D activities on nuclear fusion reactors engineering.

## 1.6 The thermo-mechanical problem for the DEMO breeding blanket

The object of the thermo-mechanical problem for a given 3D system, such as the DEMO breeding blanket, consists in the determination of the thermal, stress, strain and displacement spatial fields which arise within the investigated body, whose geometric and physical characteristics are known, as a consequence of the imposed thermal and mechanical loads and boundary conditions aimed to simulate the physical reality of the problem.

Concerning the thermal field, it is a scalar function of the spatial and temporal variables, given by:

$$T = T(x, y, z, t) \tag{1-1}$$

This temperature distribution arises within a 3D body as a consequence of the applied external and internal thermal loads, according to the thermal balance equation reported in [26]. The knowledge of the thermal conductivity tensor is fundamental for the thermal field calculation, since it represents the aptitude of the body to conduct heat. In case of the body can be considered as uniform, homogeneous and isotropic, the thermal conductivity tensor

becomes a constant and it can depend, at most, only on the temperature like the other physical quantities. Anyway, assuming pertinent hypothesis it is possible to integrate the thermal balance equation in order to obtain the thermal field function $T(x,y,z,t)$. Actually, the analytical solution can be found only introducing simplifying hypothesis and/or for particular systems characterized by a high degree of regularity from both the geometric and physical point of views. Instead, for real 3D systems, characterized by a certain degree of geometric and physical complexity such as the DEMO BB, the analytical resolution is practically impossible and, therefore, approximate solutions can be obtained adopting pertinent numerical methods able to provide solutions with a high level of reliability.

Regarding the stress field, it is a second order tensorial function of the spatial and temporal variables, given by:

$$\underline{\underline{\sigma}}(x,y,z,t)=\begin{vmatrix}\sigma_{xx} & \sigma_{xy} & \sigma_{xz}\\ \sigma_{yx} & \sigma_{yy} & \sigma_{yz}\\ \sigma_{zx} & \sigma_{zy} & \sigma_{zz}\end{vmatrix} \tag{1-2}$$

where $\sigma_{ij}=\sigma_{ij}(x,y,z,t)$, being i and j variable among x, y and z, represents the component along the j direction of the stress relevant to the plane having i as normal direction. In particular, the $\sigma_{ii}=\sigma_{ii}(x,y,z,t)$ are defined as normal stresses while the $\sigma_{ij}=\sigma_{ij}(x,y,z,t)$, with $i\neq j$, are called as shear stresses and are usually indicated as $\tau_{ij}=\tau_{ij}(x,y,z,t)$.

Concerning the strain field, it is a second order tensorial function of the spatial and temporal variables, given by:

$$\underline{\underline{\varepsilon}}(x,y,z,t)=\begin{vmatrix}\varepsilon_{xx} & \varepsilon_{xy} & \varepsilon_{xz}\\ \varepsilon_{yx} & \varepsilon_{yy} & \varepsilon_{yz}\\ \varepsilon_{zx} & \varepsilon_{zy} & \varepsilon_{zz}\end{vmatrix} \tag{1-3}$$

where $\varepsilon_{ij}=\varepsilon_{ij}(x,y,z,t)$, being i and j variable among x, y and z, represents the component along the j direction of the strain relevant to the plane having i as normal direction. In particular, the $\varepsilon_{ii}=\varepsilon_{ii}(x,y,z,t)$ are defined as normal strains while the $\varepsilon_{ij}=\varepsilon_{ij}(x,y,z,t)$, with $i\neq j$, are called as shear strains and are usually indicated as $\gamma_{ij}=\gamma_{ij}(x,y,z,t)$.

As to the displacement field, it is a three-components vectorial function of the spatial and temporal variables, given by:

$$\underline{u}(x,y,z,t)=\begin{vmatrix}u_x\\ u_y\\ u_z\end{vmatrix} \tag{1-4}$$

From the Theory of Elasticity it is known that [27], under the hypothesis of small strains, the solution of the thermo-mechanical problem for a 3D body can be obtained solving the system of equations composed of the three fundamental types of equations which govern the structural phenomena. These are the indefinite equilibrium equations, the strain-displacement equations and the constitutive equations.

The indefinite equilibrium equations state the equilibrium condition, as to both translation and rotation, for an elemental volume of a continuum 3D elastic body under steady-state conditions. They are arranged as a system of 6 partial differential equations in which the unknowns are the 9 functions composing the stress field [27].

The strain-displacement equations state the functional dependence which have to exist between the components of the strain function and those of the displacement function in order that the body undergoes deformations coherently with the continuity constraint, namely without undergo separations or self-penetrations. They are arranged as a system of 9 partial differential equations. The unknowns of this system are the 9 functions composing the strain field and the 3 functions composing the displacement field [27].

Lastly, the constitutive equations state the functional dependence existing between the stress field components and the strain field ones. They describe the reaction modalities of a given body when it has to withstand the applied thermo-mechanical loads, on the basis of the body internal constitution. These equations, under the hypothesis of homogeneous, isotropic and linear-elastic body, are arranged in a system of 6 algebraic equations where the unknowns are the functions composing the stress and strain fields [27].

The system composed of indefinite equilibrium, strain-displacement and constitutive equations is hence a system of 21 linearly independent algebraic-partial differential equations in the 21 unknowns given by the 9 functions composing the stress field, the 9 functions composing the strain field and the 3 functions composing the displacement field.

Opportunely handling this system of equations, it can be reduced to a system of 3 partial differential equations, of the second order, with non-constant coefficients, complete and coupled, where the unknowns are the 3 functions composing the displacement field. From the integration of this system with the pertinent boundary conditions, the three functions composing the displacement field can be obtained.

Once calculated the displacement field, it is possible to use this outcome in order to determine the strain field by means of the strain-displacement equations and, after this, the stress field function can be calculated on the basis of the strain field function by the constitutive equations.

In this way, it is possible to finally carry out the solution of the thermo-mechanical problem of a 3D body. Actually it has to be noted that an analytical solution can be found only for bodies which present extremely regular geometric and physic features.

It can be concluded that, for real 3D systems such as the DEMO BB, characterized by a

certain geometric and physic complexity, theoretical-numerical methods have to be adopted in order to obtain a solution for the thermo-mechanical problem.

## 1.7 The Finite Element Method

The exact solution of the system of equations which governs the thermo-mechanical behaviour of a given 3D system, having generic geometric and physic features, can be obtained with difficulty due to its analytic complexity.

For this reason, the resolution of thermo-mechanical problem for all that 3D systems characterized by a notable structural and physics complexity is possible only resorting to numerical resolving methods, which provide the approximate solution to the problem for some points of the integration domain. The employment of these methods widely spread thanks to the great development of the computational resources, which ensure the execution of the huge amount of operations connected to their application in a reasonable calculation time. The numerical methods are different on the basis of the approximation type implied by their adoption and on the basic hypothesis assumed for their development.

The most diffused numerical method is the Finite Element Method which have been developed during the second half of 1950s for structural calculation and, in the following years, has been perfected and applied also in other fields, such as thermal and fluid-dynamic calculations.

The FEM is based on the continuum body modelling as a set of regions having finite volume and simple shape which are juxtaposed each other, called Finite Elements. Each finite element is characterized by a finite number of vertexes, called Nodes and coincident with the points of the original body, devoted to connect it to the adjacent element. In this way the FEM is founded on the approximation of the continuum body in topologically simple domains, in order to attain a simplification of the governing equations which define their behaviour.

The FEM fundamental hypothesis foresees that the field functions values at a generic point, located within an element, functionally depend on nodal values by means of some particular functions, named shape functions, whose analytic expression is known and dependent on the element type.

Each node is characterized by a certain number of degrees of freedom, whose physical meaning is typical of the particular problem investigated (temperature, stress, displacement, pressure). The total number of degrees of freedom of a given element determines the approximation grade which has been selected in order to represent the field function trend at points located inside the element (linear, quadratic etc.). The number of degrees of freedom and the node number characterize the element behaviour.

The investigated problem is so connected, on the basis of the adopted spatial-temporal

discretization and the selected numerical approach (weighed residuals method or variational principle), to the resolution of a system of linear equations.

The FEM solving procedure is articulated in the following steps.

- *Calculation domain discretization.* The calculation domain is split, through a division in lines or planes, in a finite number of sub-domains called finite elements (FE). This procedure is known as *meshing*, since the term *mesh* is used to indicate the grid of nodes and elements in which the continuum body is divided. The adjacent FE are congruently juxtaposed and they are connected through nodes. One or more nodal variables are assigned to each node, in dependence on the investigated problem.
- *Governing equations of the single element.* Inside each element, the governing equations, in differential or variational form, expressed in terms of continuous variables, are transformed in algebraic equations, called FE equations, which are expressed in terms of the discrete nodal variables. A set of shape functions univocally defines the field function inside each element as a function of its nodal values.
- *FE equations assembly.* The mutually assembled elements, connected through their nodes, forms the model of the whole discretized system which corresponds to the real continuous one. In the same manner, the governing equations of each single element are assembled using element connection relationships between contact nodes. They constitute a set of algebraic equations, called global equations of the discretized and assembled system, which represent the analogous, in the discrete domain, of the differential equations in the original continuous domain. These equations define the answer of the discretized and assembled system.
- *Boundary conditions imposition.* The boundary conditions imposition, in terms of field functions, is performed modifying the structure of the original system of equations.
- *Solution of the global system of equations.* The global system of equations is solved through the adoption of proper numerical calculation techniques, developed before the FEM invention and purposely implemented in order to maximize their resolving an predictive power.
- *Study of the system answer*. The solution of the global system of equations is given in terms of independent nodal variables from which it is possible, on the basis of the shape functions, find the system answer in the whole continuous system. Other physical quantities of interest can be determined in this phase starting from the calculated solution. All the information relevant to the system answer can be shown in forms of numerical tables, graphs, diagrams or contour maps.

The first step is also known as pre-processing phase, steps from the second to the fifth constitute the processing phase while the sixth step represent the post-processing phase.

The formulation and the consequent resolution of a physical problem through the FEM

always follows the above described 6 steps, even if inside each of them the resolving procedure can be different coherently with the specific calculation algorithm taken into account. The advantages which favoured the FEM diffusion to the detriment of the other numerical methods are:

- excellent versatility in dealing with irregular geometries;
- possibility to locally change the discretization grade coherently with the specific needs;
- good accuracy and high approximation degree;
- good boundary conditions management;
- physical approach to the problem.

## 1.8 The Structural Design Criteria for ITER In-vessel Components code

The structural design of the DEMO WCLL BB has to take into account several rules, prescribed by purposely developed structural design codes, in order to assess whether the component may safely withstand the thermo-mechanical loads it undergoes without incurring in incipient structural crisis phenomena. To this purpose, the SDC-IC structural design code have been adopted in this study. The code foresees a stress classification on the basis of the type of load which has generated it. In particular, the stress categories defined by the SDC-IC structural design codes are:

- primary stress (P), which is that portion of the total stress which is required to satisfy equilibrium with the applied loading and which does not diminish after small scale permanent deformation [28];
- secondary stress (Q), which is that portion of the total stress which can be relaxed as a result of small scale permanent deformation. The basic characteristic of a secondary stress is that it is self-limiting. Local yielding and minor distortions can eliminate the conditions which cause the stress to occur [28].

Defining opportunely the thermo-mechanical loads and boundary conditions, it is possible to solve the thermo-mechanical problem (by hand or by a FEM code), so calculating primary and secondary stress tensors in each point of the geometric domain investigated. Observing the obtained solution, it is typically possible individuate the most stressed region of the investigated domain. There, purposely defining a linear path along the thickness of the region, a stress linearization procedure can be performed along the path abscissa in order to carry out, for each profile of the n-th stress tensor component function, the following characteristic functions:

- general membrane stress (indicated with the subscript m), which is the thickness-averaged value of the primary or secondary stress tensor [28];
- local membrane stress (indicated with the subscript L), which is the general membrane

stress calculated in proximity of a geometric discontinuity [28];

- bending stress (indicated with the subscript b), which is the stress distributed linearly through the thickness which has the same moment as the primary stress [28];
- peak stress (F), which is the increment of stress additive to the primary-plus-secondary stresses by reason of local discontinuities or local thermal stresses including the effects, if any, of stress concentrations [28].

Repeating the stress linearization procedure for all the components of the primary and secondary stress tensors, it can be obtained the general and local primary membrane stress tensors ($P_m$ and $P_L$, respectively), the primary bending stress tensor ($P_b$), the general and local secondary membrane stress tensor ($Q_m$ and $Q_L$, respectively), the secondary bending stress tensor ($Q_b$) and peak stress tensor (F).

Nevertheless, the results coming from the stress linearization procedure cannot be directly used. In fact, the tensorial nature of the so obtained functions makes them incomparable with the scalar stress limits prescribed by the SDC-IC code. For this reason, the definition of a scalar equivalent stress, representing the stress level of the point where it is defined, is needed. To this purpose, a resistance criterion (Von Mises, Tresca, etc.) is applicable in order to obtain the scalar values called as primary membrane stress intensity $\overline{P_m}$, the primary bending stress intensity $\overline{P_b}$ and so on. These scalar values are compared with the prescribed stress limits values in order to check the fulfilment of the structural design criteria.

Furthermore, another point to be addressed in order to perform the design of the DEMO WCLL BB concerns the classification of the loading scenarios. In fact, in order to consider the different operating conditions, it has to take into account the safety level of a component namely, with reference to the greater or lower probability of a certain event happens, it is necessary to define different levels of acceptability characterized by an increasing allowable stress intensity and, as a consequence, by a decreasing safety factor with respect to the structural integrity. On the basis of these considerations, different service levels are defined within structural design codes. With reference to the activity performed during the Ph.D. course, two levels have to be considered:

- Level A: nominal operating conditions or small deviations from normal exercise;
- Level D: accidental conditions with a small occurring probability, which entail the loss of the component.

Concerning SDC-IC, they are both the most conservative and comprehensive of all possible damage modes for Level A criteria [28].

In particular, in SDC-IC as in conventional codes, primary stresses are limited in order to guarantee the components against M (monotonic) type damages, while secondary stresses are limited to preserve them against C (cyclic) type damages, namely the progressive deformation and the time independent fatigue [29].

As to level A, in case thermal-activated phenomena (thermal creep e.g.) might be neglected, the following low temperature rules are imposed by SDC-IC code in order to protect components against M type damages [28]:

$$\overline{P_m} \le S_m(T_m, \Phi t_m) \tag{1-5}$$

$$\overline{P_L + P_b} \le K_{eff} S_m(T_m, \Phi t_m) \tag{1-6}$$

$$\overline{P_L} \le \min\left[1.5 S_m(T_m, \Phi t_m), S_{y,min}(T_m, \Phi t_m)\right] \text{ (in local non-overlapping areas)} \tag{1-7}$$

$$\overline{P_L} \le 1.1 S_m(T_m, \Phi t_m) \qquad \text{(in local overlapping areas)} \tag{1-8}$$

where $\overline{P_m}$ is the general primary membrane stress intensity, $\overline{P_L}$ is the local primary membrane stress intensity, $\overline{P_L + P_b}$ is the stress intensity of the sum of the aforementioned tensors $P_L$ and $P_b$, $K_{eff}$ is an effective bending shape factor depending on the resisting section, $S_m$ is the allowable stress limit depending on thickness averaged temperature $T_m$ and neutron fluence $\Phi t_m$ and $S_{y,min}$ is the minimum tensile yield strength depending on the thickness averaged temperature $T_m$ and neutron fluence $\Phi t_m$ too.

On the other hand, in case thermal-activated phenomena are not negligible, SDC-IC code imposes the following high temperature rules to be verified too [28]:

$$U_t\left(\overline{P_m}\right) \le 1 \tag{1-9}$$

$$U_t\left(\overline{P_L + \frac{P_b}{K_t}}\right) \le 1 \tag{1-10}$$

where $K_t$ is the so-called creep bending shape factor and $U_t$ is the creep usage fraction defined as follows:

$$U_t\left(\overline{\sigma_j}\right) = \sum_j \left(\frac{t_j}{t_{S,j}}\right) \tag{1-11}$$

that may be calculated adopting the following procedure based on the division of the component operating time t into N intervals chosen in such a way that the operating temperatures and stresses are approximately constant throughout the interval. In particular, for each interval j of duration tj, the highest operating temperature $T_j$ as well as the highest stress intensity $\overline{\sigma_j}$ reached are calculated. The maximum allowable time $t_{Sj}$ at any stress $\overline{\sigma_j}$ and temperature $T_j$ are obtained from the proper $S_t(T,t)$ curve, that gives the allowable stress limit depending on temperature T and on component operational time t [29]. In particular, $S_t(T,t)$

curve values have been drawn from [30].

As a first approximation, assuming that loads over the overall operating period are constant, it may be shown [29] that equs. (1-9) and (1-10) reduces to:

$$\overline{P_m} \le S_t(T,t) \tag{1-12}$$

$$\overline{P_L + \frac{P_b}{K_t}} \le S_t(T,t) \tag{1-13}$$

As it can be deduced from previous considerations, SDC-IC and conventional codes do not take into account secondary stresses when M type damages are verified since usually material ductility allows to accommodate thermal stresses. Anyway, since fusion relevant materials typically lose their ductility and become brittle when subjected to intense neutronic irradiation, some further rules have been included in SDC-IC structural safety code to properly take into account this phenomenon [29]. In particular, SDC-IC code defines two different modes of potential failure due to the limited ductility of the materials: immediate plastic flow localization and immediate local fracture due to exhaustion of ductility [31]. The relevant rules reported in SDC-IC structural safety code are [28]:

$$\overline{P_L + Q_L} \le S_e(T_m, \Phi t_m) \quad \text{immediate plastic flow localization} \tag{1-14}$$

$$\overline{P_L + P_b + Q + F} \le S_d(T, \Phi t, r_2) \quad \text{immediate local fracture due to exhaustion of ductility} \tag{1-15}$$

$$\overline{P_L + P_b + Q} \le S_d(T, \Phi t, r_3) \quad \text{immediate local fracture due to exhaustion of ductility} \tag{1-16}$$

where Se is the allowable stress intensity dependent on the thickness averaged temperature Tm and neutron fluence $\Phi t_m$ and $S_d$ is the allowable stress dependent on r-factors, temperature T and neutron fluence $\Phi t_m$ of the point under consideration where localized stress arises. Analytical definitions of r-factor, $S_e$ and $S_d$ functions are reported in [28, 29, 31]. It has to be underlined that, given that irradiated EUROFER retains considerable ductility after necking, the potential failure mode due to immediate plastic flow localisation is not an issue, while that induced by immediate plastic flow localisation may be a matter of serious concern [31].

Concerning level D, the same rules relevant to level A still hold, where different safety and loading factors are used [28]. In case thermal-activated phenomena might be neglected, the following low temperature rules are imposed by SDC-IC code to protect against M type damages [28]:

$$\overline{P}_m \le \min\begin{Bmatrix} 2.4S_m(T_m, \Phi t_m) \\ 0.7S_{u,min}(T_m, \Phi t_m) \end{Bmatrix} \tag{1-17}$$

$$\overline{P_L + P_b} \le K_{eff} \min\left\{\begin{matrix} 2.4S_m(T_m, \Phi t_m) \\ 0.7S_{u,min}(T_m, \Phi t_m) \end{matrix}\right\} \quad (1\text{-}18)$$

$$\overline{P_L} \le \min\left\{1.5\min\left\{\begin{matrix} 2.4S_m(T_m, \Phi t_m) \\ 0.7S_{u,min}(T_m, \Phi t_m) \end{matrix}\right\}, S_{y,min}(T_m, \Phi t_m)\right\} \quad \text{(in local non-overlapping areas)} \quad (1\text{-}19)$$

$$\overline{P_L} \le 1.11\min\left\{\begin{matrix} 2.4S_m(T_m, \Phi t_m) \\ 0.7S_{u,min}(T_m, \Phi t_m) \end{matrix}\right\} \quad \text{(in local overlapping areas)} \quad (1\text{-}20)$$

When thermal-activated phenomena are not negligible, SDC-IC code imposes the following high temperature rule to be verified too:

$$W_t\left[1.35 \cdot \left(\overline{P_m + \frac{P_b}{K_t}}\right)\right] \le 1 \quad (1\text{-}21)$$

where $W_t$ is the cumulative creep rupture usage fraction, defined as:

$$W_t = \sum_k \left(\frac{t_k}{t_{r,k}}\right) \quad (1\text{-}22)$$

where $t_k$ is the k-th application time, obtained dividing the operating time into N time intervals, and $t_{r,k}$ is the maximum allowable time deduced from the minimum isothermal creep rupture curves in correspondence to the highest operating temperature $T_k$ and stress intensity $\overline{\sigma_k}$ relevant to the k-th interval. In particular, maximum allowable time $t_{r,k}$ is obtained using following correlation:

$$\mathrm{Log}(t_r) = \left[\left(\frac{1000}{T}\right) \cdot \left(32.617 - 0.029856\sigma + 1.2561 \cdot 10^{-05}\sigma^2\right) - 30\right] \quad (1\text{-}23)$$

where T [K] is the operation temperature and σ [MPa] is the creep rupture stress. The material ductility loss for level D, due to the effect of the neutronic irradiation, is taken into account by SDC-IC code using the following rules [28]:

$$\overline{P_L + Q_L} \le 2S_e(T_m, \Phi t_m) \quad \text{immediate plastic flow localization} \quad (1\text{-}24)$$

$$\overline{P_L + P_b + Q + F} \le 1.35S_d(T, \Phi t, r_2) \quad \text{immediate local fracture due to exhaustion of ductility} \quad (1\text{-}25)$$

$$\overline{P_L + P_b + Q} \le 1.35S_d(T, \Phi t, r_3) \quad \text{immediate local fracture due to exhaustion of ductility} \quad (1\text{-}26)$$

## 1.9 Conclusion

The realization of the DEMO fusion reactor, aimed to follow ITER, is viewed by EU and many of the other partners involved in the construction of ITER as the remaining crucial step towards the grand-scale exploitation of fusion power. To this purpose, the EUROfusion consortium has been created thanks to the joint effort of the most important European universities, research centres and industries with the aim to coordinate and promote R&D activities concerning the DEMO design. In this framework, the development of a reliable BB design assumes a crucial role in the design of the whole DEMO machine, since it is the most critical component due to its peculiar function of providing tritium. Therefore, a specific WP regarding the BB R&D is foreseen by the EUROfusion action.

Within the framework of the activities promoted by the WPBB of the EUROfusion consortium, 4 different BB concepts are under investigation in order to be selected for the DEMO definitive design.

In this context, the research activity performed during the Ph.D. course has regarded the thermo-mechanical investigation of the WCLL BB performances in order to give a contribution to its design. A preliminary sizing of the FW and SPs has been carried out in order to attain a preliminary design for the WCLL BB outboard equatorial module, which has been investigated under both nominal and accidental thermo-mechanical steady state loading conditions. To this purpose, the SDC-IC code has been considered, checking the fulfilment of the prescribed structural criteria so that to avoid the incipient structural crisis conditions under both the nominal and accidental scenarios envisaged for the DEMO BB. The obtained results have been used in order to suggest design modifications to the WCLL BB project team, allowing the definition of a more detailed design of the outboard equatorial module. Therefore, the main goal of this work, fully developed in the framework of EUROfusion WPBB action, has been the contribution to the WCLL BB design in order to attain a reliable geometric configuration for the component.

# Chapter 2

# DESIGN OF THE DEMO WATER-COOLED LITHIUM LEAD BREEDING BLANKET OUTBOARD EQUATORIAL MODULE

## 2.1 Introduction

Within the framework of the DEMO R&D activities envisaged by the Breeding Blanket Work Package (WPBB) of the EUROfusion consortium action, an intense parametric research campaign has been carried out during the Ph.D. course in order to attain a conceptual design of the DEMO WCLL BB, paying attention to its outboard equatorial module. Attention has been mainly focussed on the First Wall and Stiffening Plates geometric optimization in order to select, for both the components, a geometric configuration able to safely withstand the thermo-mechanical loads it undergoes under the selected steady-state nominal and accidental loading scenarios, representing the DEMO flat-top plasma operational phase and a small in-box LOCA accident, respectively. To this purpose, the FW and SPs thermo-mechanical behaviour has been separately investigated adopting different approaches depending on the component features.

In particular, appropriate sets of geometric parameters have been selected and, for each of them, a proper range of variation has been determined. All the FW and SPs geometric configurations, resulting from the combination of the parameters values assumed, have been assessed from the thermal and mechanical standpoints in order to investigate their performances in accordance with the typical thermal-hydraulic design requirements and, from the mechanical point of view, with the structural criteria prescribed by the SDC-IC code. At the end of the study, it has been possible to select the most promising FW and SPs geometric configurations on the basis of the fulfilment of the above said thermal-hydraulic and structural design criteria. The models set-up, the loads and the boundary conditions assumed to perform the parametric study together with the main obtained results are described and critically discussed in this chapter, paying attention to the open issues.

## 2.2 The First Wall design activity

In order to attain a conceptual design of the DEMO WCLL BB outboard equatorial module an intense parametric research campaign, intended to perform the FW geometric optimization, has been carried out. To this purpose, the FW steady-state thermo-mechanical performances have been investigated taking into account the FW flat concept equipped with square cooling channels.

The research activity has been specifically intended to optimize the FW geometric configuration, maximizing the heat flux that it might safely withstand while fulfilling all the thermal-hydraulic and thermo-mechanical requirements prescribed by SDC-IC code. In particular, from the thermal-hydraulic standpoint it has been assumed that the structural material maximum allowable temperature, amounting to 550°C, cannot be exceeded and the velocity of FW channels cooling water has to be lower than the limit value of 8 m/s as indicated in [22]. Moreover, from the thermo-mechanical point of view, it has been assumed that the FW optimized configuration has to safely withstand the loads it undergoes under both steady state Normal Operation and Over-Pressurization loading scenarios, without incurring in yielding-induced structural crisis and ensuring the fulfilment of SDC-IC design criteria.

Regarding NO scenario, it represents the nominal thermo-mechanical loading conditions expected during the DEMO flat-top plasma operational state while, as to OP scenario, it is devoted to simulate the thermo-mechanical loads arising in case of a small in-box LOCA accident.

In order to perform this study, a set of 5929 different flat FW geometric configurations has been considered and the thermo-mechanical performances of each one of them have been investigated when subjected to 26 different heat flux values, for an overall number of 154154 parametric analyses.

The parametric analysis procedure has been totally automated by means of purposely set up Python script files, able to set up the simplified 3D FEM models of the FW configurations investigated, run the pertaining calculations together with the relevant stress linearization and check the fulfilment of thermal-hydraulic and thermo-mechanical requirements.

### 2.2.1 The geometric parameters

Within the framework of the research activity performed during the Ph.D. course, attention has been focussed on the FW flat concept endowed with square cooling channels and a 2 mm-thick (W) tungsten armour (Fig. 2-1). The FW characteristic geometric parameters potentially affecting its thermal-hydraulic and thermo-mechanical performances have been identified in the following ones (Fig. 2-1):

- cooling channels pitch (P);

- cooling channel width ($d_c$);
- cooling channel thickness on plasma side (a);
- FW thickness (D).

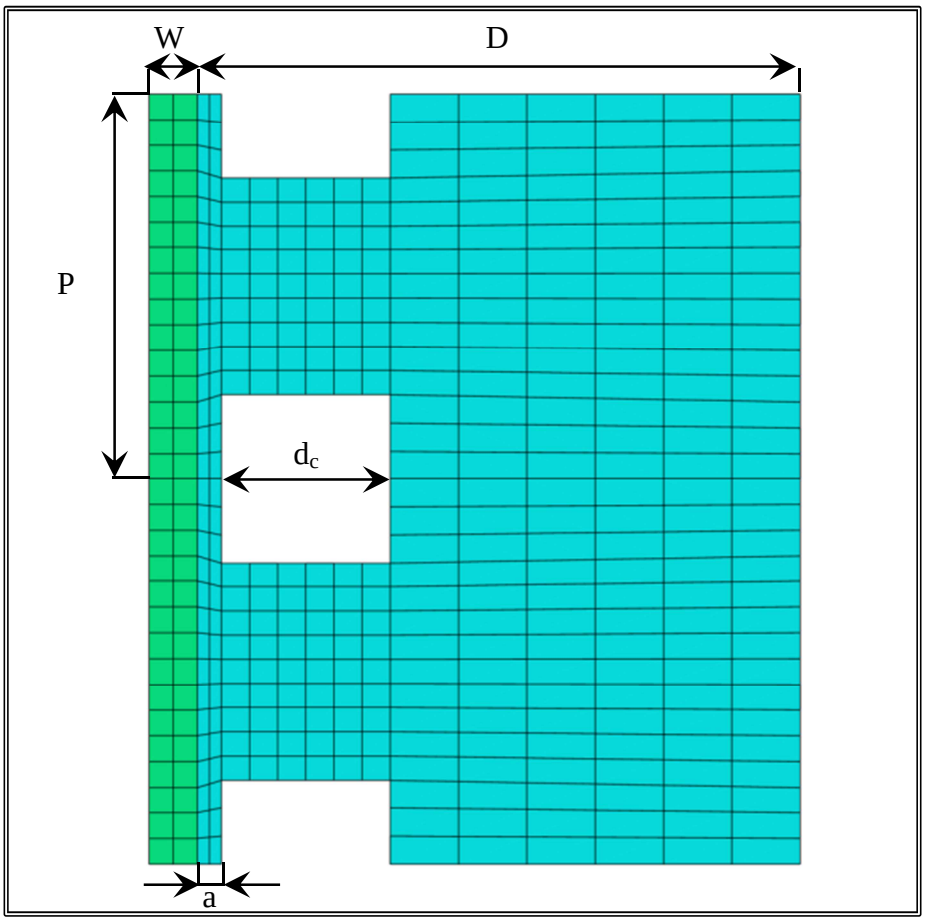


Figure 2-1. FW geometric parameters.

In order to assess the potential influence of the aforementioned parameters on the overall FW thermal-hydraulic and thermo-mechanical performances, allowing the optimization of its geometric configuration, a theoretical-numerical parametric study has been performed taking into account all the FW 3D geometric configurations resulting from the combination of the set of values of each single parameter selected to be investigated. To this purpose, according to the experience gained during the research campaign previously performed at the University of Palermo on the thermo-mechanical performances of the DEMO WCLL BB outboard equatorial module [32], each single parameter has been assumed to range potentially within the limits reported in Table 2-1. These ranges of values have been believed as physically acceptable in order to attain the goal of the research campaign originating, at the same time, realistic and feasible FW geometric configurations.

Table 2-1. Ranges of values for FW geometric parameters.

| Parameter | Range of values [mm] |
|---|---|
| $d_c$ | 6 - 12 |
| a | 1 - 3 |
| D | 19 - 25 |
| P | 16 - 26 |

Furthermore, for each single geometric parameter, the range of values reported in Table 2-1 has been equally subdivided in a fixed number of intervals to select a significant set of physically meaningful values to be investigated. In particular, concerning $d_c$ and D parameters 7 different values have been selected, subdividing their ranges of values in six intervals, while, as to a and P parameters 11 different values have been taken into account, subdividing their ranges of values in 10 intervals. A summary of all the values selected for the considered geometric parameters is reported in Table 2-2.

Table 2-2. Parameters values selected.

| $d_c$ [mm] | D [mm] | a [mm] | P [mm] |
|---|---|---|---|
| 6 | 19 | 1.0 | 16 |
| 7 | 20 | 1.2 | 17 |
| 8 | 21 | 1.4 | 18 |
| 9 | 22 | 1.6 | 19 |
| 10 | 23 | 1.8 | 20 |
| 11 | 24 | 2.0 | 21 |
| 12 | 25 | 2.2 | 22 |
| - | - | 2.4 | 23 |
| - | - | 2.6 | 24 |
| - | - | 2.8 | 25 |
| - | - | 3.0 | 26 |

As a consequence of the combination of all the values reported in the above shown Table 2-2, 5929 different 3D FW geometric configurations have been selected to be investigated by means of dedicated FEM analyses and a proper simplified 3D FEM model has been developed for each of them.

In order to assess the maximum heat flux arising from plasma ($\Phi$) each single FW geometric configuration is able to safely withstand under steady-state loading conditions without incurring in incipient structural crisis phenomenon, the thermo-mechanical behaviour of each of them has been numerically assessed when exposed to 26 different values of $\Phi$,

equally spaced in the range 0.5 - 3.0 MW/m$^2$.

Also for the definition of the heat flux variation range, reasonable values inferred from the past experience have been adopted. In particular, the lower limit (0.5 MW/m$^2$) has been inferred from the previous research campaign on the thermo-mechanical behaviour of the DEMO WCLL BB outboard equatorial module [32], being the typical value of the heat flux on the outboard equatorial module FW foreseen during the DEMO flat-top plasma operational state. On the other hand, the upper limit (3.0 MW/m$^2$) has been considered, according to the previous experience as a reasonable high heat flux value.

Therefore, for each one of the 5929 FW geometric configurations selected, 26 different thermal cases have been investigated for a total of 154154 thermo-mechanical analyses to be performed during the research campaign.

### 2.2.2 The FEM models

In order to obtain a realistic simulation of the FW thermo-mechanical behaviour, each 3D FEM model set-up reproduces a toroidal-radial slice of the DEMO WCLL BB outboard equatorial module, extending for two cooling channels pitch (2P) in the poloidal direction, for a breeder cell in the toroidal direction and for the whole module radial depth up to the Back-Plate (BP). Therefore, each model set-up includes all the five breeder cells, the proper portions of the poloidal-toroidal and toroidal-radial SPs as well as the pertaining segment of the BP.

Since the focus of the research campaign has been put on the optimization of the FW geometric configuration, in order to speed-up calculations, especially in the pre-processing and processing phases, it has been decided to avoid the modelling of eutectic Pb-Li breeder, DWTs and coolant flow domain, their thermo-mechanical effects being simulated adopting a proper set of loads, contact models and boundary conditions.

A mesh composed of linear hexahedral elements, contained within the ABAQUS code element library, which allows numerical simulations to be performed saving calculation time and ensuring accurate results, has been set-up for each FW geometric configuration selected in order to assess its thermo-mechanical behaviour.

A typical 3D FEM model, set-up for one of the 5929 different FW geometric configurations investigated, is depicted in Fig. 2-2. A proper Python script file has been set-up with the aim to automate the overall pre-processing phase of the parametric FEM analyses. In particular, it has allowed all the geometric parameters values to be combined in the 5929 different FW configurations to be studied, to set-up the proper 3D FEM model for each of them, performing the meshing procedure and the implementation of the proper set of loads and Boundary Conditions, and finally to run the analyses.

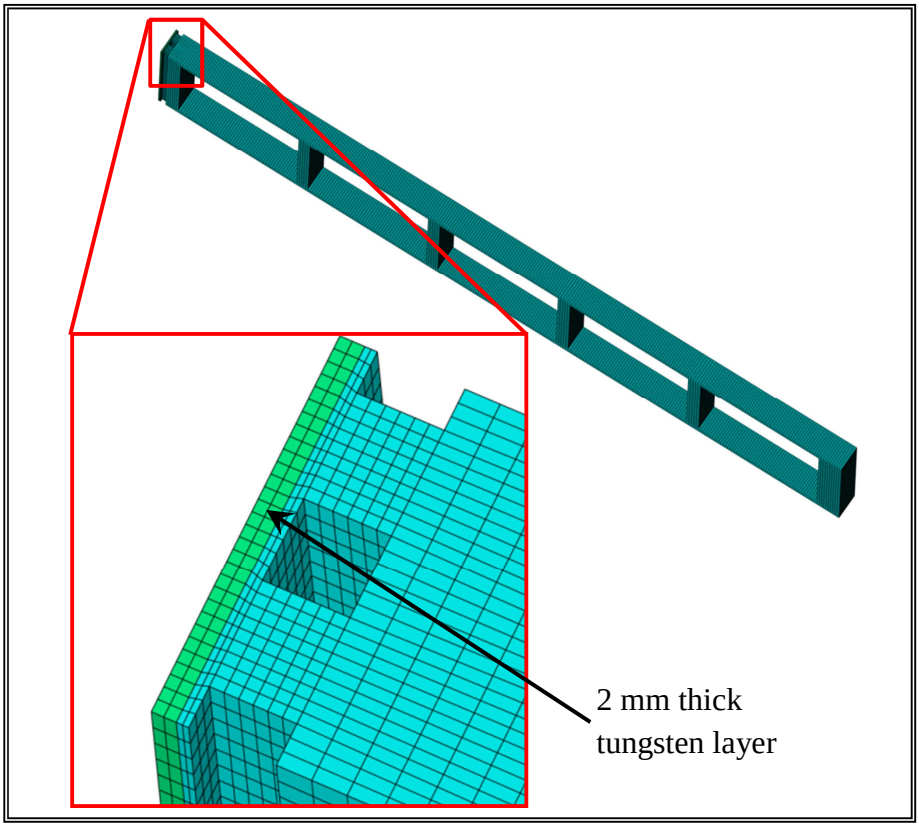


Figure 2-2. A typical 3D FEM model.

### 2.2.2.1 Materials

RAFM EUROFER steel has been assumed as the DEMO WCLL BB module structural material, except for the 2 mm thick FW armour that has been supposed made of tungsten. Materials have been considered homogeneous, uniform, isotropic and linear-elastic and their thermo-mechanical properties have been assumed to depend uniquely on temperature as indicated in [33-37], except for tungsten density that has been assumed to be constant and equal to 19300 kg/m$^3$ [34]. Thermo-mechanical properties at room temperature (20 °C) have been reported in Table 2-3, while their temperature-dependent behaviours can be deduced from Figures 2-3 and 2-4.

Table 2-3. Materials thermo-mechanical properties at 20 °C.

| Physical property | EUROFER | Tungsten |
|---|---|---|
| $\lambda_0$ | 28.30 W/(m·K) | 174.91 W/(m·K) |
| $c_{p0}$ | 448.0 J/(kg·K) | 132.33 J/(kg·K) |
| $\alpha_0$ | $1.04 \cdot 10^{-5}$ K$^{-1}$ | $5.25 \cdot 10^{-6}$ K$^{-1}$ |
| $E_0$ | $2.17 \cdot 10^{11}$ Pa | $4.08 \cdot 10^{11}$ Pa |

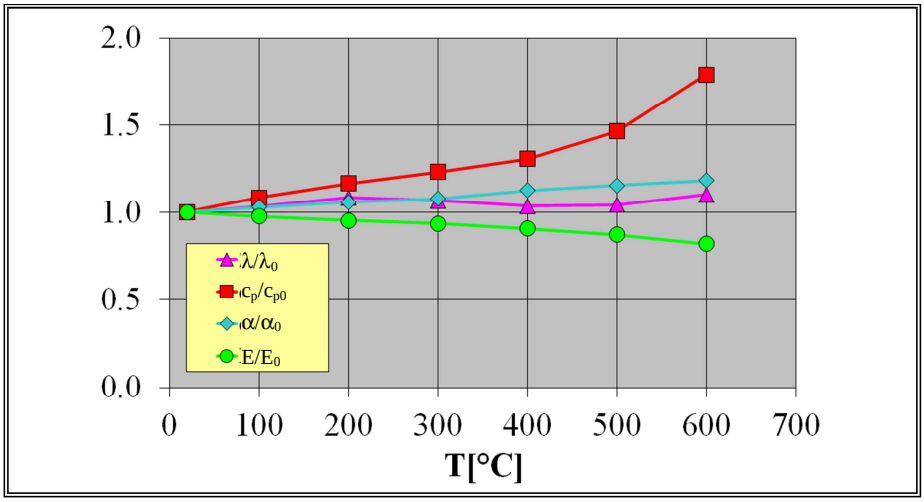


Figure 2-3. EUROFER thermo-mechanical properties vs. temperature.

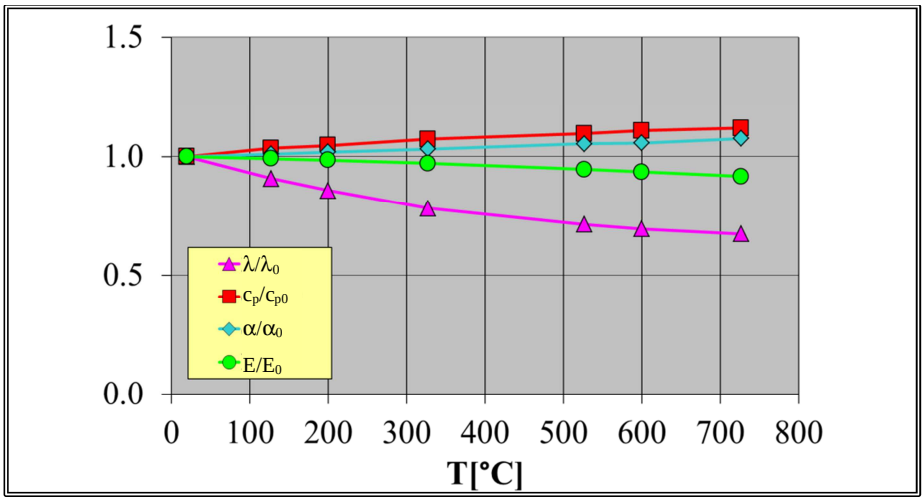


Figure 2-4. Tungsten thermo-mechanical properties vs. temperature.

#### 2.2.2.2 Thermal loads and boundary conditions

In order to assess the thermal behaviour of the 5929 different FW geometric configurations taken into account for each one of the 26 different thermal cases considered according to heat flux values investigated, the following thermal loads and boundary conditions have been imposed to the 3D FEM models:

- volumetric density of nuclear deposited heat power;
- heat flux on FW armour plasma facing surface;
- heat flux on Pb-Li wetted FW internal surface;
- forced convective heat transfer with water coolant at FW cooling channel surfaces;
- imposed temperatures to stiffening plates and back-plate.

Concerning the volumetric density of nuclear deposited heat power, an averaged value, calculated for the PPCS-A WCLL outboard breeding blanket equatorial module and properly scaled according to Neutron Wall Loadings (NWLs) of DEMO and PPCS-A reactors, has been imposed to the FW in order to simulate distributed heat power deposition due to the interactions between neutrons and gamma photons with structural material nuclei.

With regard to the heat flux on FW armour plasma facing surface, $\Phi$, devoted to simulate the heat power radiated by plasma towards the FW armour, it has been supposed to be uniformly distributed on the plasma facing surface of the tungsten armour highlighted in red in Figure 2-5. In particular, as already mentioned in § 2.2, for each FW geometric configuration investigated, 26 different $\Phi$ values, equally spaced in the range 0.5 - 3 MW/m$^2$, have been considered. The lower limit of this $\Phi$ values interval is the nominal average heat flux foreseen for the DEMO BB outboard equatorial module, while the upper limit has been assumed as a reasonably $\Phi$ maximum value. Therefore, for each of the 5929 FW geometric configuration considered, 26 different thermal cases have been investigated for a total of 154154 different thermal analyses performed.

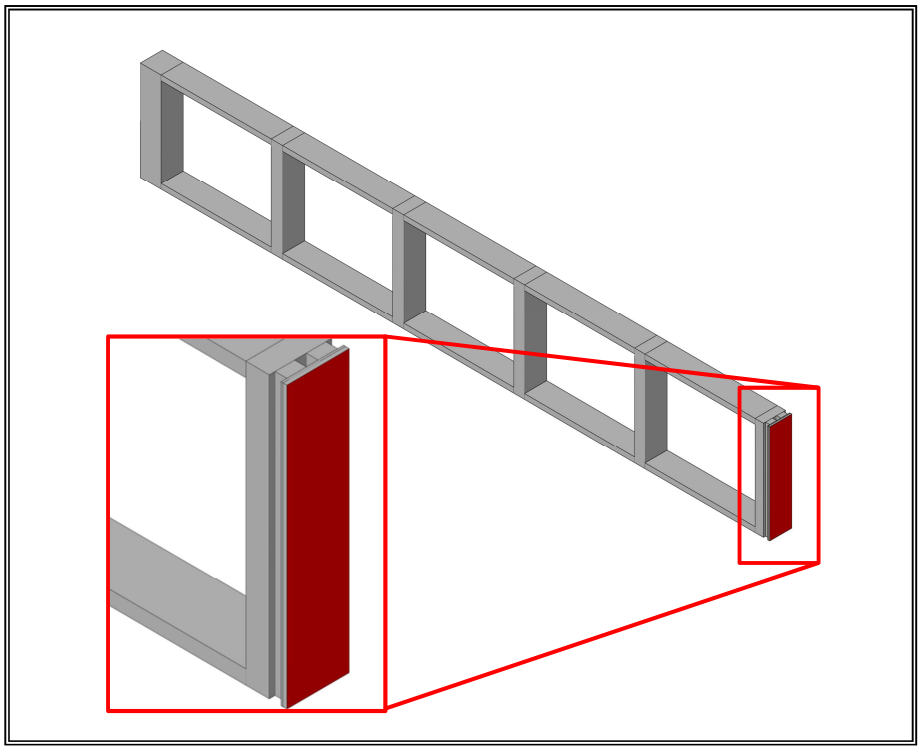

Figure 2-5. FW armour plasma facing surface.

As to the heat flux on Pb-Li wetted FW internal surface, intended to simulate the complex convective/diffusive heat transfer between the breeder and the FW internal surface without incurring in the heavy calculations needed whether breeder heat transfer is computed, a

uniformly distributed heat flux amounting to 0.074 MW/m$^2$ has been imposed at the FW/breeder interface, highlighted in red in Figure 2-6. This value has been inferred from the analysis of the thermo-mechanical behaviour of the DEMO WCLL outboard breeding blanket equatorial module reported in [32], resulting to be the average value of the normal heat flux at the FW/breeder interface calculated with reference to the FEM model reproducing the central poloidal-radial slice of the WCLL BB module. In fact, from analyses reported in [32], a heat transfer from breeder to FW internal surface has been observed.

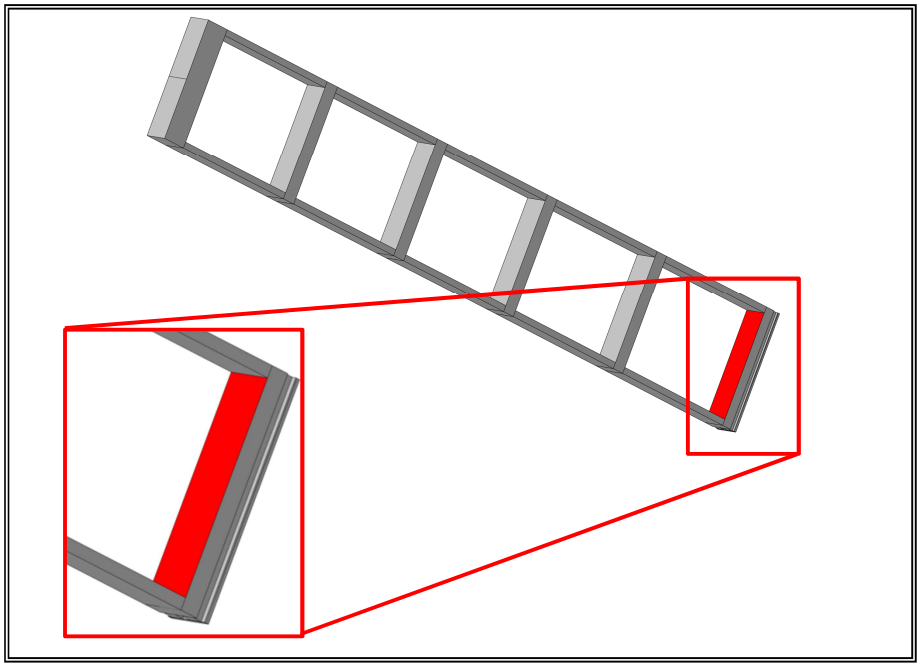

Figure 2-6. FW/breeder interface.

Forced convective heat transfer between water coolant and FW cooling channels has been simulated imposing, onto their surfaces (highlighted in red in Fig. 2-7), a convective boundary condition characterized by proper values of the convective heat transfer coefficient, h, and of the coolant bulk temperature, $T_w$, both the two potentially depending on the considered value of $\Phi$.

In order to evaluate h, it has been assumed that the heat power, $Q_{tot}(\Phi)$, deposited within First Wall - Side Walls (FW-SWs) according to the considered value of $\Phi$, is totally removed by water flowing through FW - SWs cooling channels.

Furthermore, water has been supposed to enter FW-SW cooling channels at the inlet temperature of 285 °C [4] and to experience a fixed thermal rise, $\Delta T$, of 40 °C [4] flowing through the SW - FW - SW cooling path. As a consequence of these assumptions, for each thermal case investigated, the total water mass flow rate $G_{tot}$ feeding FW-SWs cooling channels has been calculated as:

$$G_{tot}(\Phi) = \frac{Q_{tot}(\Phi)}{c_p \Delta T} \tag{2-1}$$

where $c_p$ is the water specific heat capacity, calculated, as all other coolant thermo-physical properties, at the average temperature of 305 °C and at the pressure of 15.5 MPa.

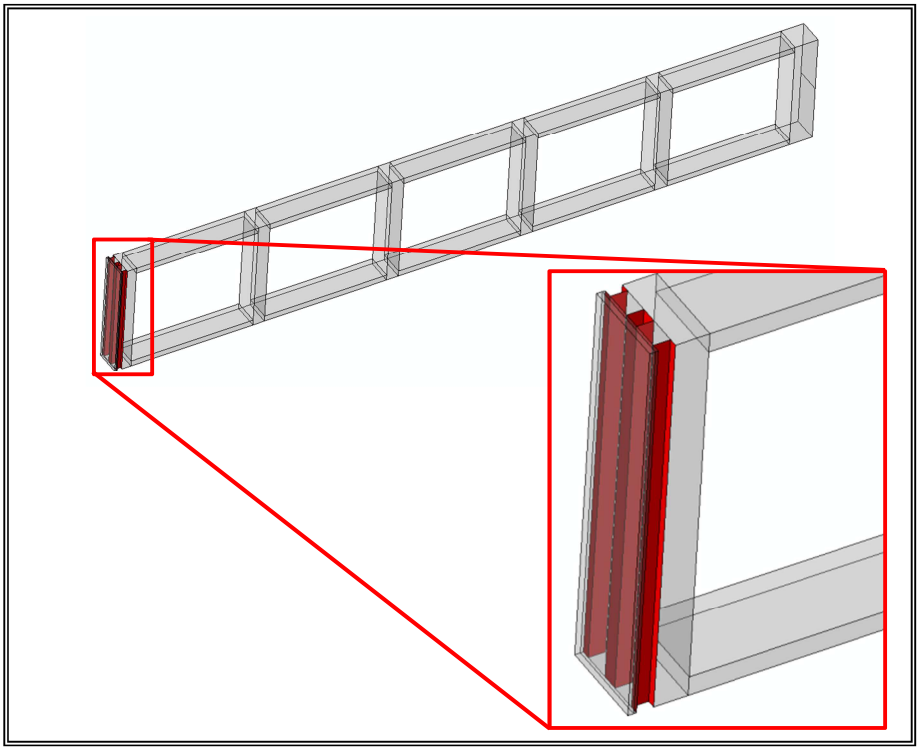

Figure 2-7. FW cooling channel surfaces.

Therefore, taking into account that the number of cooling channels depends uniquely on their poloidal pitch, P, and that their flow area amounts to $d_c^2$ it has been possible to easily derive the following functional dependence of the water flow velocity in a cooling channel, u(Φ,P,dc), on Φ, P and $d_c$

$$u(\Phi, P, d_c) = \frac{Q_{tot}(\Phi)}{c_p \Delta T}\left[\frac{P}{L d_c^2}\right] \tag{2-2}$$

where L is the FW poloidal height. Moreover, taking into account the definition of the Reynold's number it has been possible to derive the following analytical expression of its functional dependence, Re(Φ,P,$d_c$), on Φ, P and $d_c$:

$$Re(\Phi, P, d_c) = \frac{Q_{tot}(\Phi)}{\nu c_p \Delta T}\left[\frac{P}{L d_c}\right] \tag{2-3}$$

where ν is the water kinematic viscosity, calculated at the average temperature of 305°C and at the pressure of 15.5 MPa. Finally, adopting the widely accepted Dittus & Bölter correlation [35] for the assessment of h, the following analytical expression of its functional dependence h(Φ,P,dc) on Φ, P and dc has been derived and implemented in a FORTRAN routine, purposely set up for the analyses:

$$h\left(\Phi, P, d_c\right) = \frac{\Omega \lambda_w \, Pr^{0.33}}{\left(\nu c_p \Delta TL\right)^{0.8}} \left[Q_{tot}\left(\Phi\right)\right]^{0.8} \left[\frac{P^{0.8}}{d_c^{1.8}}\right] \tag{2-4}$$

where Ω is the numerical constant of the aforementioned correlation, $\lambda_w$ is the water thermal conductivity and Pr represent the water Prandtl dimensionless number, both the two calculated at the average temperature of 305°C, assumed for the coolant, and at the nominal pressure of 15.5 MPa. As far as the assessment of the water bulk temperature is concerned, since the FEM models set-up represent the central poloidal-radial slice of the module extending only for a cell in toroidal direction, it has been decided to neglect $T_w$ variation due to Φ along the small toroidal length of the simulated cooling channels and it has been assumed to be uniformly equal to 305 °C.

Finally, since the research campaign has been mainly focussed on the FW geometric optimization, in order to speed-up calculations avoiding the simulation of heat transfer within the stiffening plates and the back-plate, fixed temperature distributions have been imposed to the nodes of these regions of the 3D FEM models, inferring their values from the previously performed analysis of the thermo-mechanical behaviour of the central poloidal-radial slice of the DEMO WCLL outboard breeding blanket equatorial module [32].

#### 2.2.2.3 Mechanical loads and boundary conditions

In order to assess the mechanical behaviour of the 5929 different FW geometric configurations taken into account for each one of the 26 different thermal cases considered, according to FW heat flux values investigated, two different steady state loading scenarios, namely the Normal Operation and Over-Pressurization scenarios, have been investigated in this study. In particular, the Normal Operation scenario represents the loading conditions foreseen under the nominal operational phase, namely the flat-top plasma operational state, for the DEMO WCLL breeding blanket and it is mainly characterized by a coolant pressure of 15.5 MPa exerted on channels surfaces and a breeder pressure of 0.5 MPa acting onto internal module surfaces [22]. As far as the Over-Pressurization scenario is concerned, it represents the loading conditions immediately following that incidental sequence in which a coolant leak occurs in the Segment Box (SB) or in the DWTs and all the module internal surfaces experience a pressurization up to 15.5 MPa.

In order to simulate both the aforementioned steady-state loading scenarios, the following set of thermo-mechanical loads and boundary conditions has been imposed to the 3D FEM models:

- uniform pressure onto FW channel surfaces;
- uniform pressure onto SB internal surfaces;
- non-uniformly distributed thermal deformations;
- module constraints.

In order to simulate the mechanical action of water flowing through the FW cooling channels, a uniform pressure of 15.5 MPa has been applied to their internal surfaces in both loading scenarios investigated since it is the coolant pressure nominal value foreseen by the WCLL BB design parameters.

Concerning the simulation of the breeder mechanical action onto SB internal surfaces (highlighted in red in Fig. 2-8), a uniformly distributed pressure of 0.5 MPa has been adopted in the simulation of the Normal Operation loading scenario since it is the breeder nominal pressure inside the outboard equatorial module. This value has been increased up to the value of 15.5 MPa, equal to the coolant pressure, in the simulation of the Over-Pressurization loading scenario since it represents an in-box LOCA accidental condition.

The non-uniformly distributed thermal deformation field, arising within the module as a consequence of its thermal field and its isotropic thermal expansion tensor, has been taken into account by implementing, the proper spatial distribution of the thermal field previously obtained by the corresponding steady-state thermal analysis.

Finally, in order to reproduce, as more realistically as possible, the mechanical action of the module attachment system, the radial displacements of a set of nodes lying on BP external surface (nodes highlighted in red in Fig. 2-9) have been prevented in the FEM models.

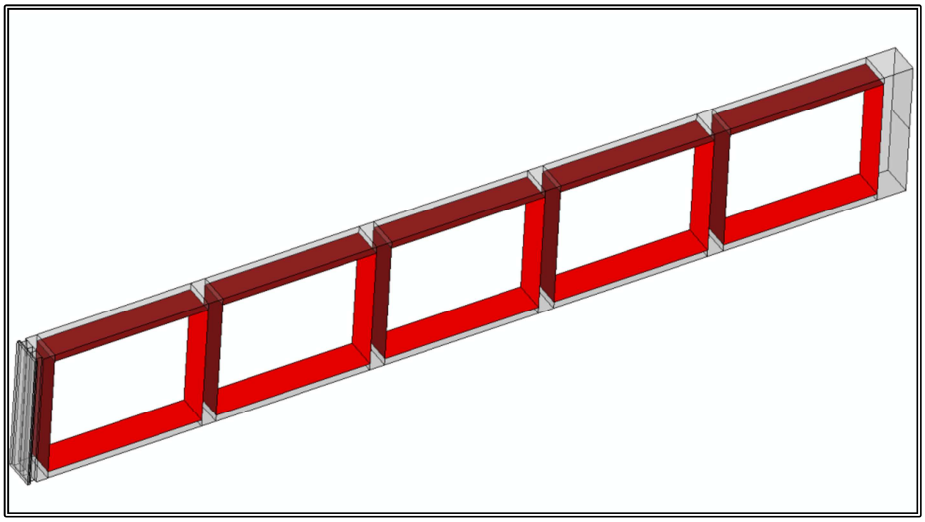

Figure 2-8. SB internal surfaces.

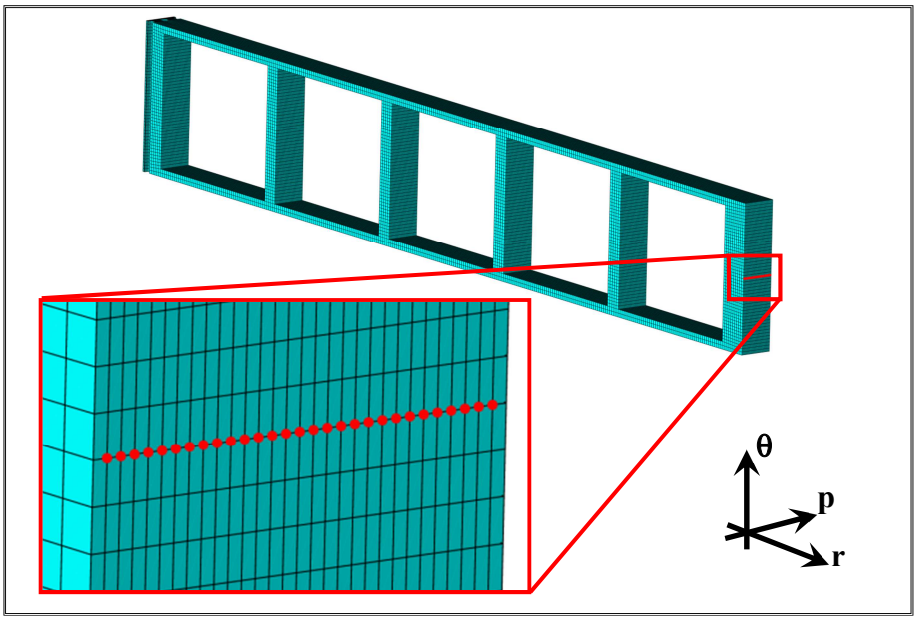


Figure 2-9. BP nodes constrained.

Moreover, symmetry and plane strain conditions have been imposed to the 3D FEM models, in toroidal and poloidal directions, as indicated in Figure 2-10, in order to realistically simulate the geometric continuity of the DEMO WCLL BB module. In particular, toroidal and poloidal symmetry conditions have been imposed to nodes lying onto surfaces having positive toroidal and poloidal normal versor respectively while the plain strain condition has been applied to nodes lying onto the opposite surfaces.

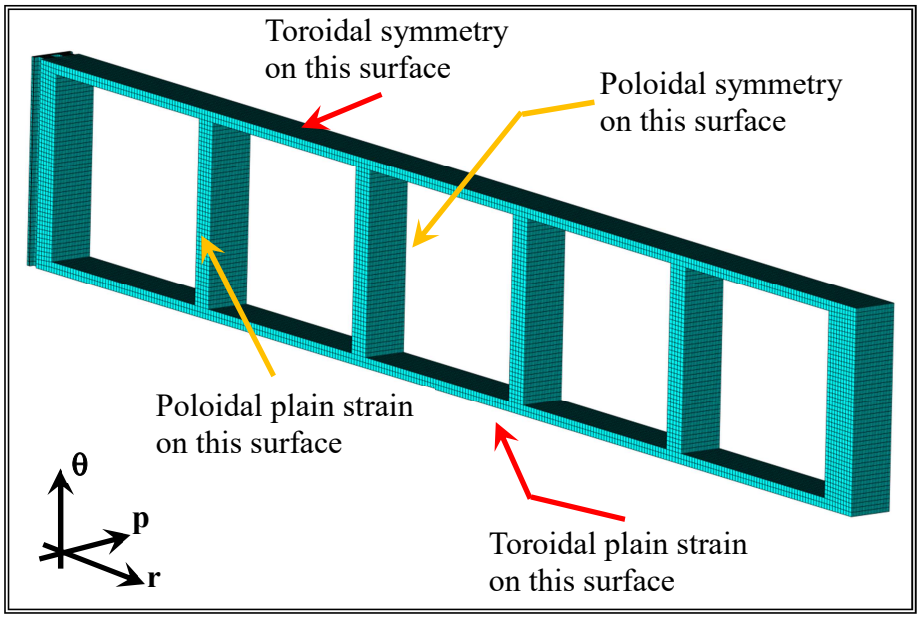


Figure 2-10. SB mechanical constraints.

### 2.2.3 The parametric campaign of analysis

In order to assess the potential influence of FW flat concept geometric parameters on its thermal-hydraulic and thermo-mechanical performances and to optimize its geometric configuration maximizing the heat flux that it might safely withstand, a theoretical-numerical parametric study has been performed taking into account the 5929 FW geometric selected configurations and investigating 26 different thermal cases for each one of them, for an overall set of 154154 un-coupled thermo-mechanical performed analyses.

Proper 3D FEM models have been set-up for the FW geometric investigated configurations and corresponding sets of thermal and mechanical loads and boundary conditions have been taken into account for the study.

Attention has been paid to the thermal field arising within the FW as to each of the 154154 numerically simulated thermal cases, as a consequence of the pertinent thermal scenario taken into account, in order to check the fulfilment of the FW thermal-hydraulic design requirements.

From the mechanical standpoint, the Von Mises equivalent stress field has been evaluated for each FW geometric and loading configurations investigated in order to check the verification of SDC-IC structural design rules.

In particular, it has to be underlined that the Nominal Operation loading scenario is classified as Level A scenario, since it represents the loading conditions expected during the nominal flat-top plasma operational phase of the DEMO reactor, while the Over-Pressurization scenario is classified as Level D scenario, since it is intended to simulate the accidental loading conditions in case of an in-box LOCA accident.

Therefore, in order to assess the thermo-mechanical behaviour of the 5929 FW configurations when subjected to the assumed 26 different heat flux values, the proper set of SDC-IC design criteria has been taken into account coherently with the type of each investigated loading scenario.

To this purpose, a stress linearization procedure has been carried out along the most significant FW paths with the aim to check the fulfilment of the SDC-IC safety criteria in both Level A and Level D operating conditions. Finally, the geometric configurations fulfilling the aforesaid requirements and structural design criteria and able, at the same time, to withstand the highest heat flux value have been proposed as the reference ones.

#### 2.2.3.1 Results

Results of the 154154 thermal analyses carried out have been processed in order to exclude all those thermal cases in which thermal and hydraulic requirements foreseen for the FW have not been fulfilled, excluding them from the study prosecution.

In particular, all those thermal cases in which the maximum allowable EUROFER steel temperature, fixed to 550 °C according to [4], has been exceeded within the FW have been considered as unacceptable.

Moreover, among the remaining assessed thermal cases, a further filter has been applied, based on the average velocity, u, of the cooling water flow. In particular, a value of 8 m/s has been imposed [22] as the coolant velocity upper limit, with the aim to avoid a considerable arising of corrosion and erosion phenomena on the cooling channel surfaces and, furthermore, limit the coolant pressure drop [38].

Therefore all thermal cases for which coolant velocity value, calculated according to Equation (2-2), overcomes the imposed upper limit have been excluded.

At the end of the thermal-hydraulic screening phase, only 66443 thermal cases have been found to fulfil the aforementioned requirements and, only for them, mechanical analyses have been performed under both Normal Operation and Over-Pressurization loading scenarios with the aim of assessing their aptitude to fulfil the prescribed structural design criteria.

The remaining cases have been excluded and no mechanical assessment has been performed for them.

To this purpose, in order to check that also mechanical requirements would be met and that each FW geometric configuration investigated would safely withstand the thermo-mechanical loads it undergoes in both considered loading scenarios, a stress linearization procedure has been performed according to SDC-IC code design rules in some significant paths located within the FW and reported in blue in Figures 2-11 and 2-12.

It has to be highlighted that Normal Operation scenario has been considered as a Level A scenario, since it represents the steady-state nominal operation phase of DEMO, while Over-Pressurization scenario has been classified as Level D since it concerns accidental conditions due to an in-box LOCA accident.

Therefore, SDC-IC design criteria taken into account for Level A and Level D loading conditions are listed in Table 2-4.

Table 2-4. Summary of SDC-IC design criteria considered.

| **Level A criteria** | **Level D criteria** |
|---|---|
| $P_m / S_m < 1$ | $P_m / \sigma_{lim} < 1$ |
| $(P_m + P_b) / K_{eff} * S_m < 1$ | $(P_m + P_b) / K_{eff} * \sigma_{lim} < 1$ |
| $(P_m + Q_m) / S_e < 1$ | $(P_m + Q_m) / 2 * S_e < 1$ |
| $P_m / S_t < 1$ (if $T_{Max\text{-}path} > 450$ °C) | $W_t$ $[1.35*(P_m+P_b/K)] < 1$ (if $T_{Max\text{-}path} > 450$ °C) |
| $(P_m + P_b/K) / S_t < 1$ (if $T_{Max\text{-}path} > 450$ °C) | |

The verification of the thermal-hydraulic requirements for each considered thermal case, the relevant stress linearization procedure, the identification of those configurations unable to meet the prescribed SDC-IC criteria as well as the assessment of those others able to safely withstand the highest investigated heat flux values have been totally automated by means of a purposely set up Python script file.

The development of this automated procedure has allowed to minimize the computational time and perform so an elevated number of result comparisons.

In particular, results of the mechanical analyses of the abovementioned 66443 cases have shown that only 4 configurations, summarized in Table 2-5, are able to fulfil the 9 SDC-IC safety criteria taken into account up to a maximum heat flux of 2.0 MW/m$^2$. These configurations have been selected as the most promising one among those investigated in this study and, for this reason, they are worth to be further assessed adopting more realistic FEM models. In fact, it has to be underlined that obtained results are influenced by the imposed boundary conditions and the assumptions made in this study.

Anyway, results relevant to these 4 cases, in terms of thermal field (Figs. 2-13 - 2-16), Von Mises equivalent stress spatial distribution (Figs. 2-17 - 2-24) and SDC-IC rules verifications (Tabs. 2-6 - 2-9) have been reported in the following.

Table 2-5. Summary of the 4 FW optimum configurations.

| | **Case 1** | **Case 2** | **Case 3** | **Case 4** |
|---|---|---|---|---|
| $\Phi$ [MW/m$^2$] | 2.0 | 2.0 | 2.0 | 2.0 |
| $d_c$ [mm] | 7 | 7 | 7 | 7 |
| P [mm] | 16 | 16 | 16 | 16 |
| a [mm] | 1.0 | 1.0 | 1.0 | 1.0 |
| D [mm] | 22 | 23 | 24 | 25 |
| Channels nr. | 93 | 93 | 93 | 93 |
| h [W/m$^2$ °C] | 49289.18 | 49289.18 | 49289.18 | 49289.18 |
| u [m/s] | 6.43 | 6.43 | 6.43 | 6.43 |
| G [kg/s] | 0.2244 | 0.2244 | 0.2244 | 0.2244 |
| $T_{Max\text{-}FW}$ [°C] | 496.8 | 497.0 | 496.9 | 497.0 |

As it can be deduced from results reported in Table 2-5, the maximum FW temperature achieved in the 4 selected cases is well below the maximum EUROFER allowable value of 550 °C, as well as the calculated maximum cooling water velocity, that is quite lower than the

prescribed limit of 8 m/s.

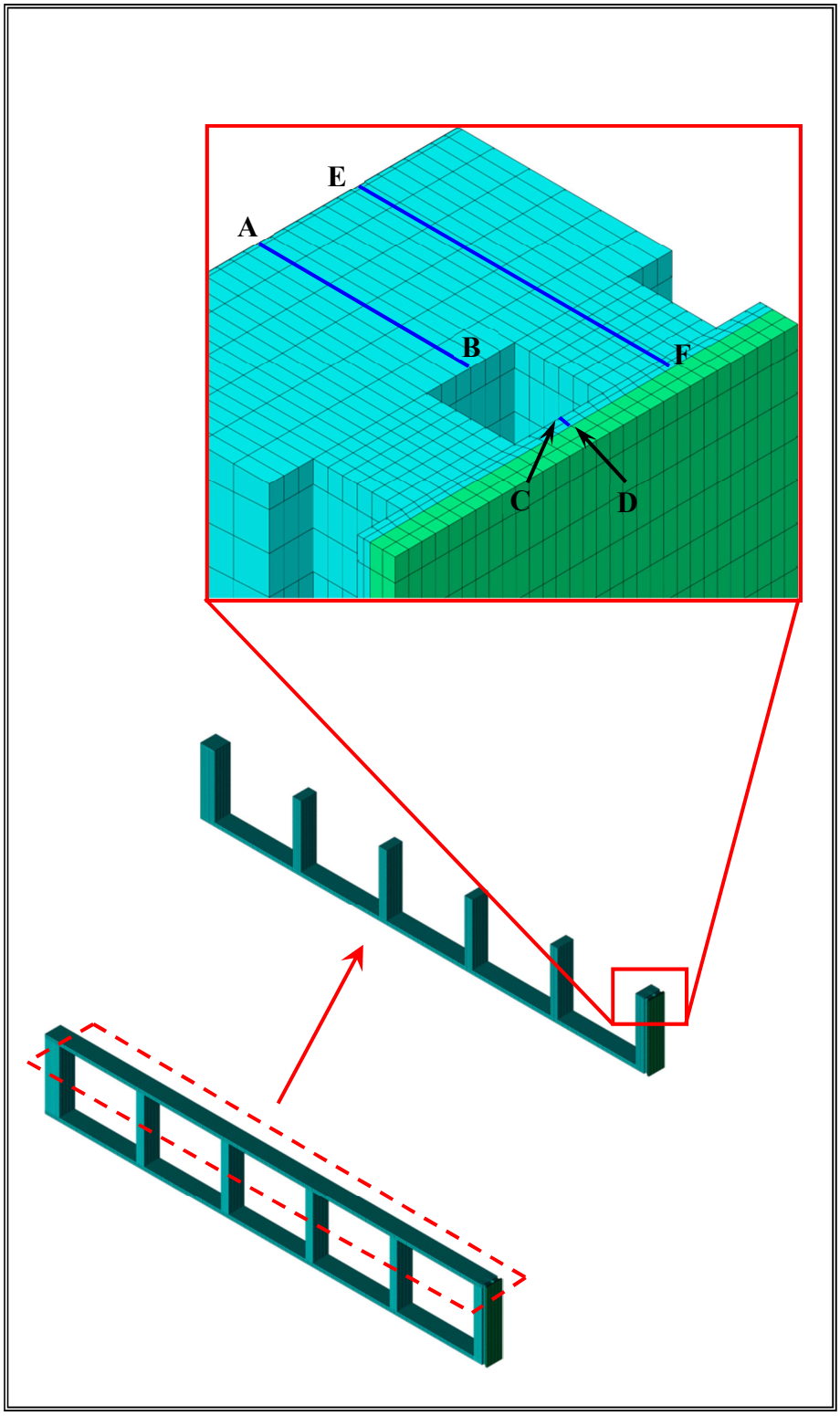


Figure 2-11. FW stress linearization paths.

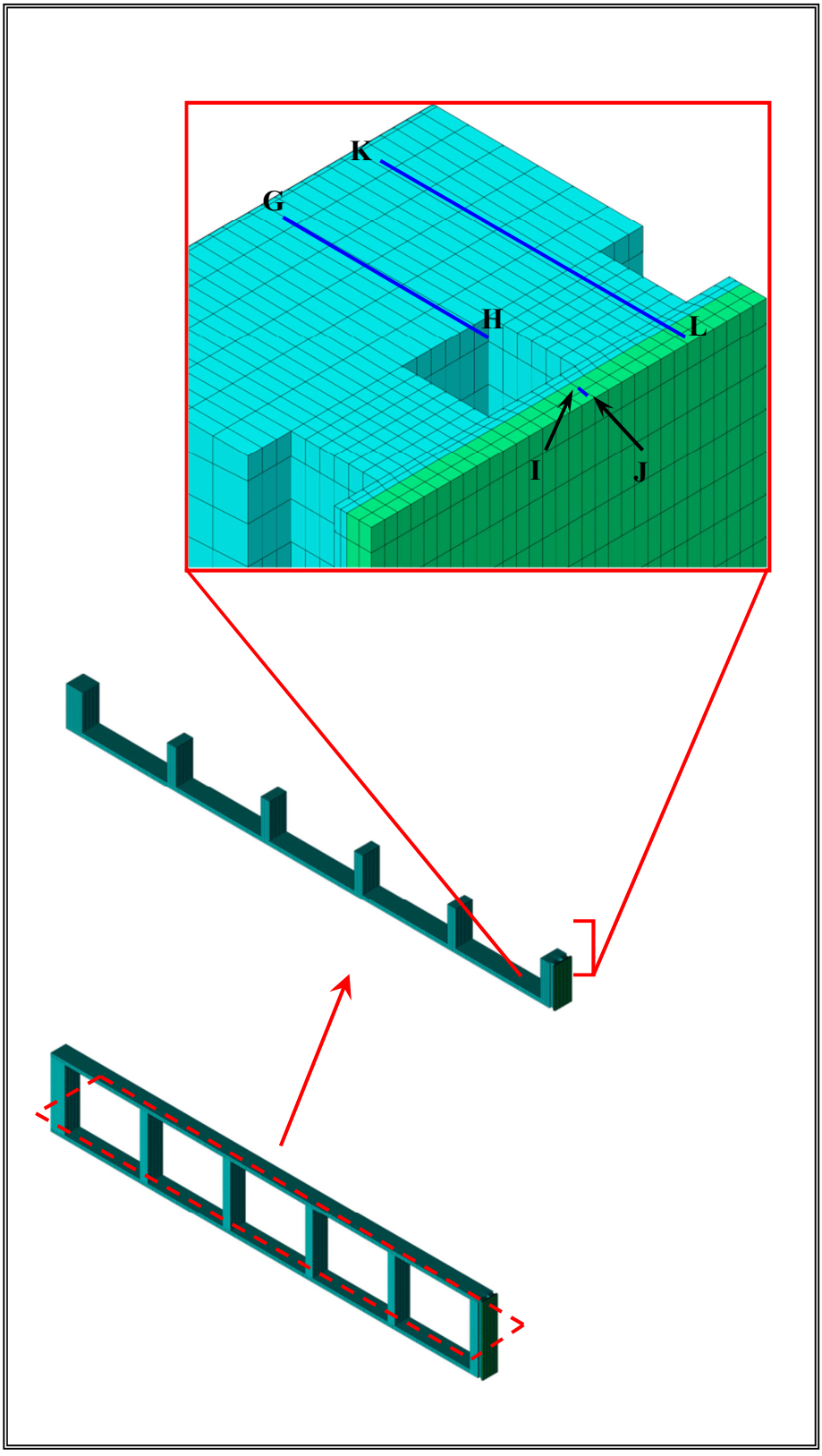


Figure 2-12. FW stress linearization paths.

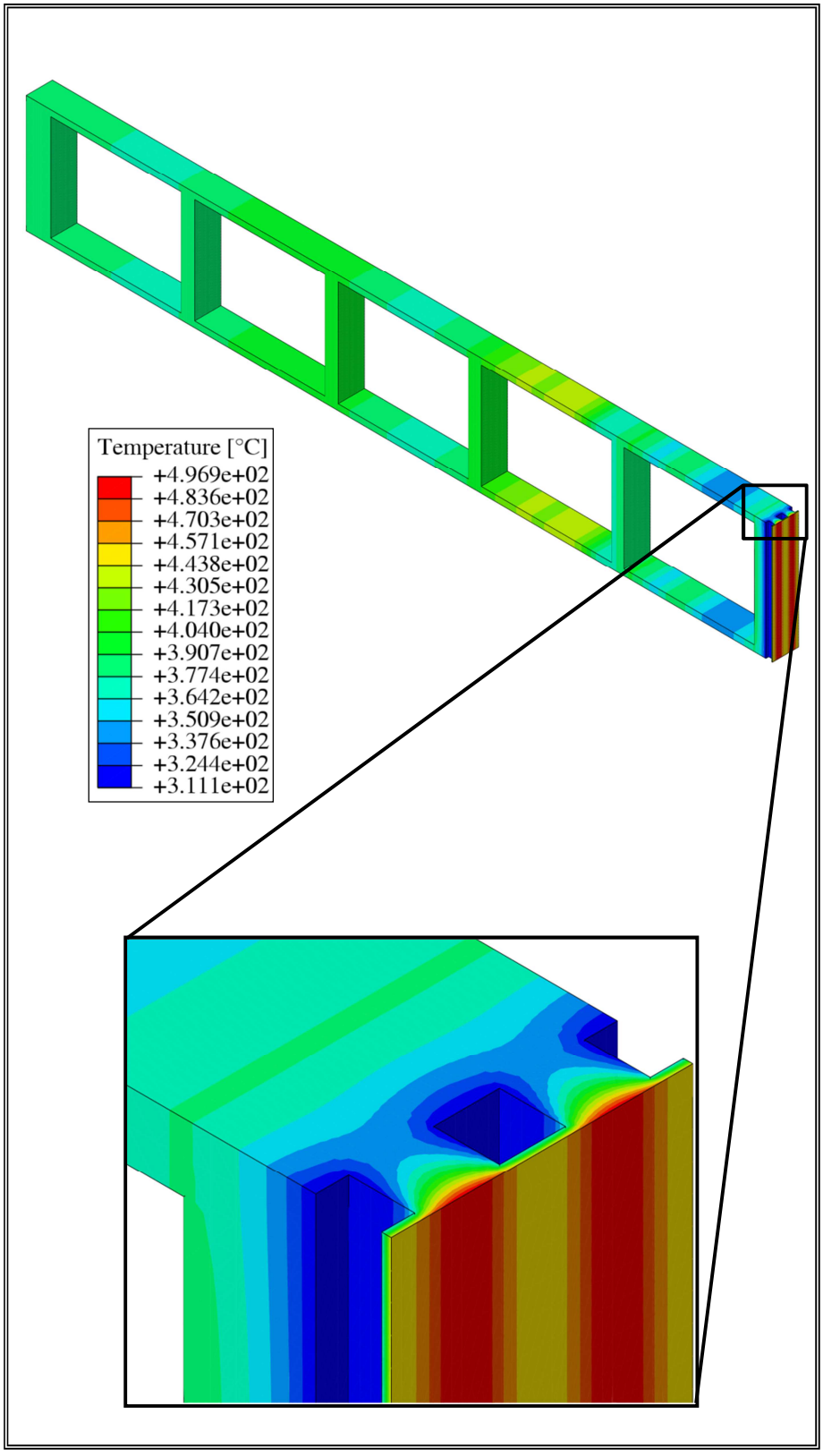


Figure 2-13. Case 1 - Thermal field.

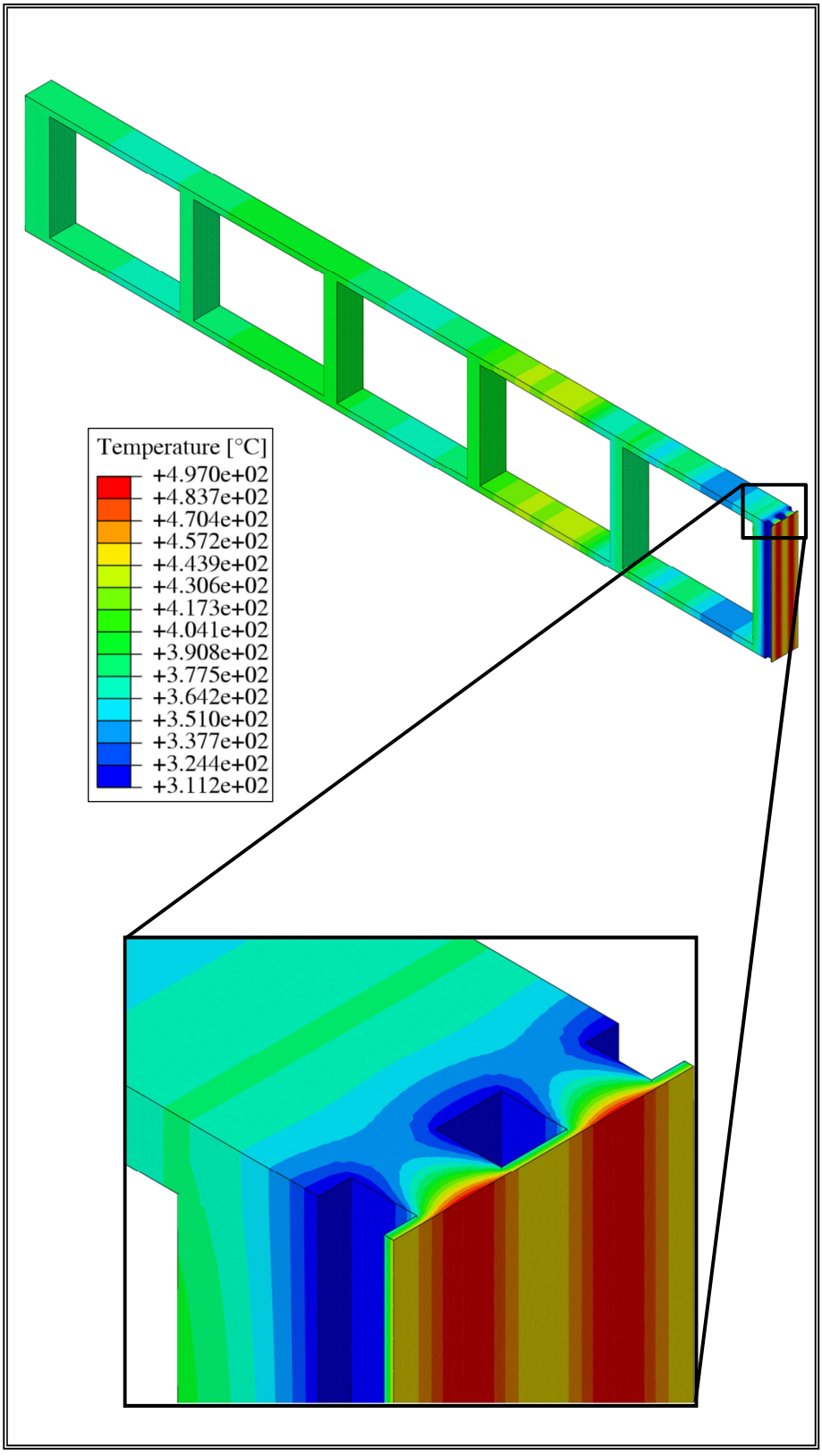


Figure 2-14. Case 2 - Thermal field.

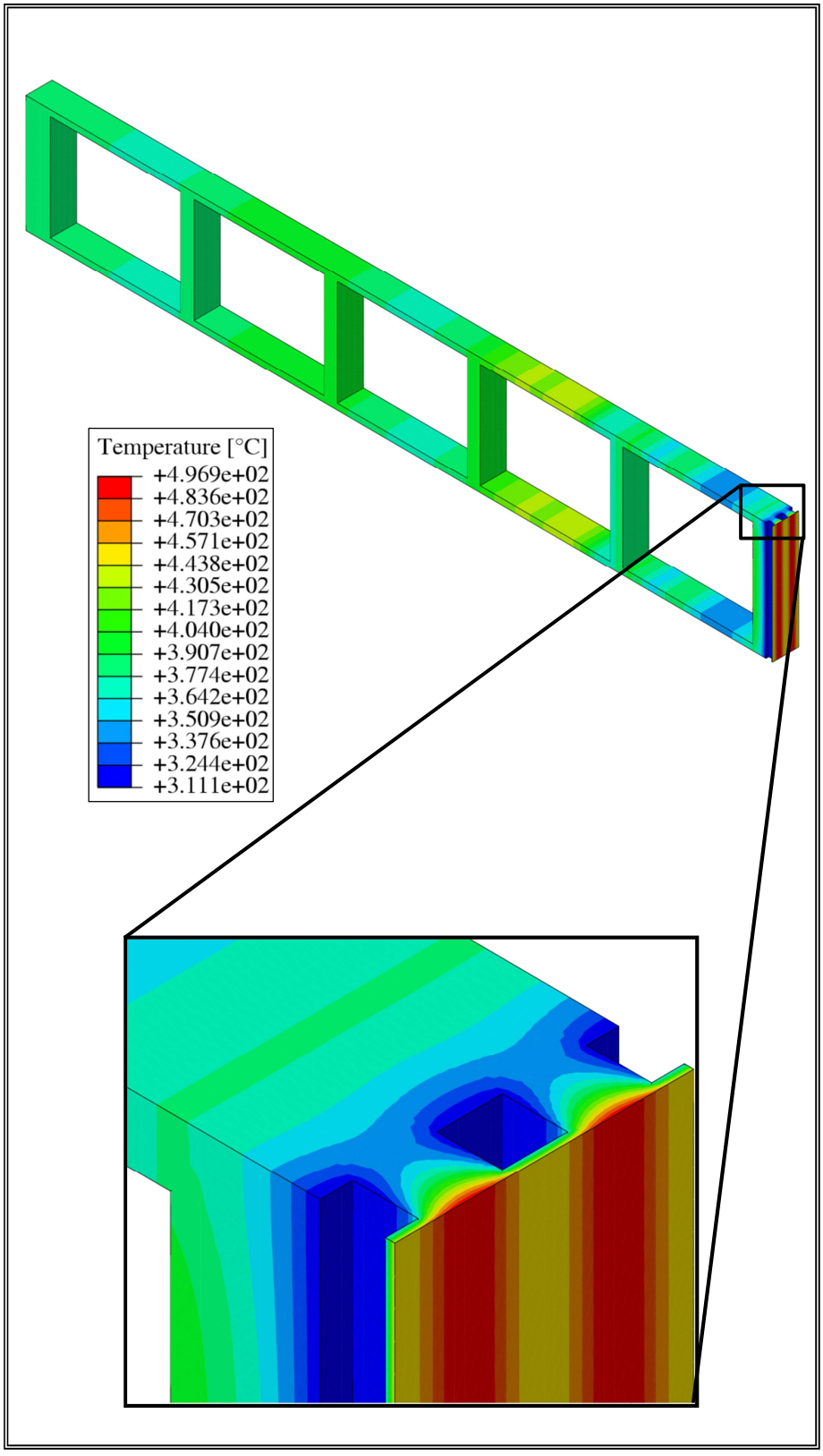


Figure 2-15. Case 3 - Thermal field.

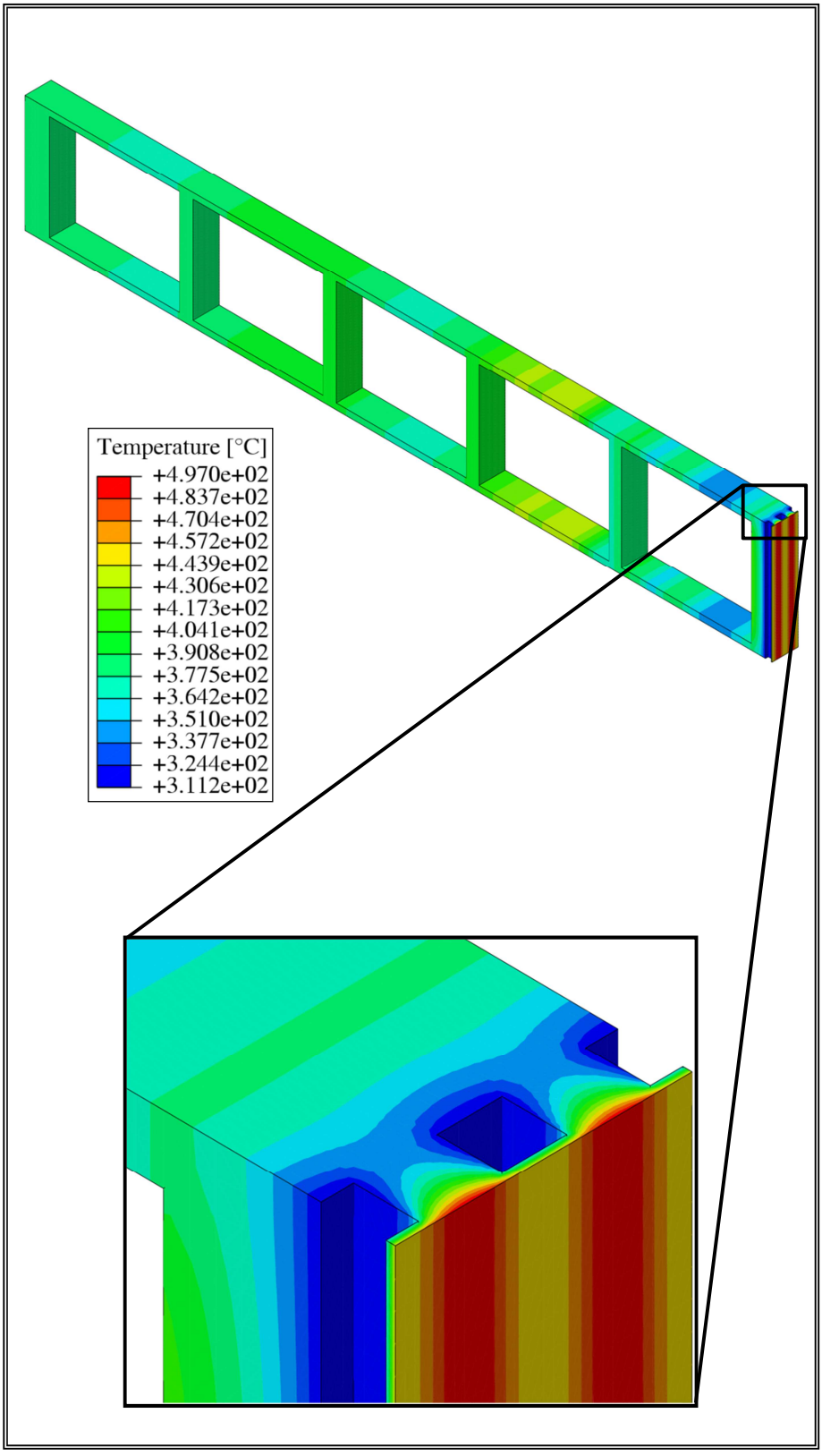


Figure 2-16. Case 4 - Thermal field.

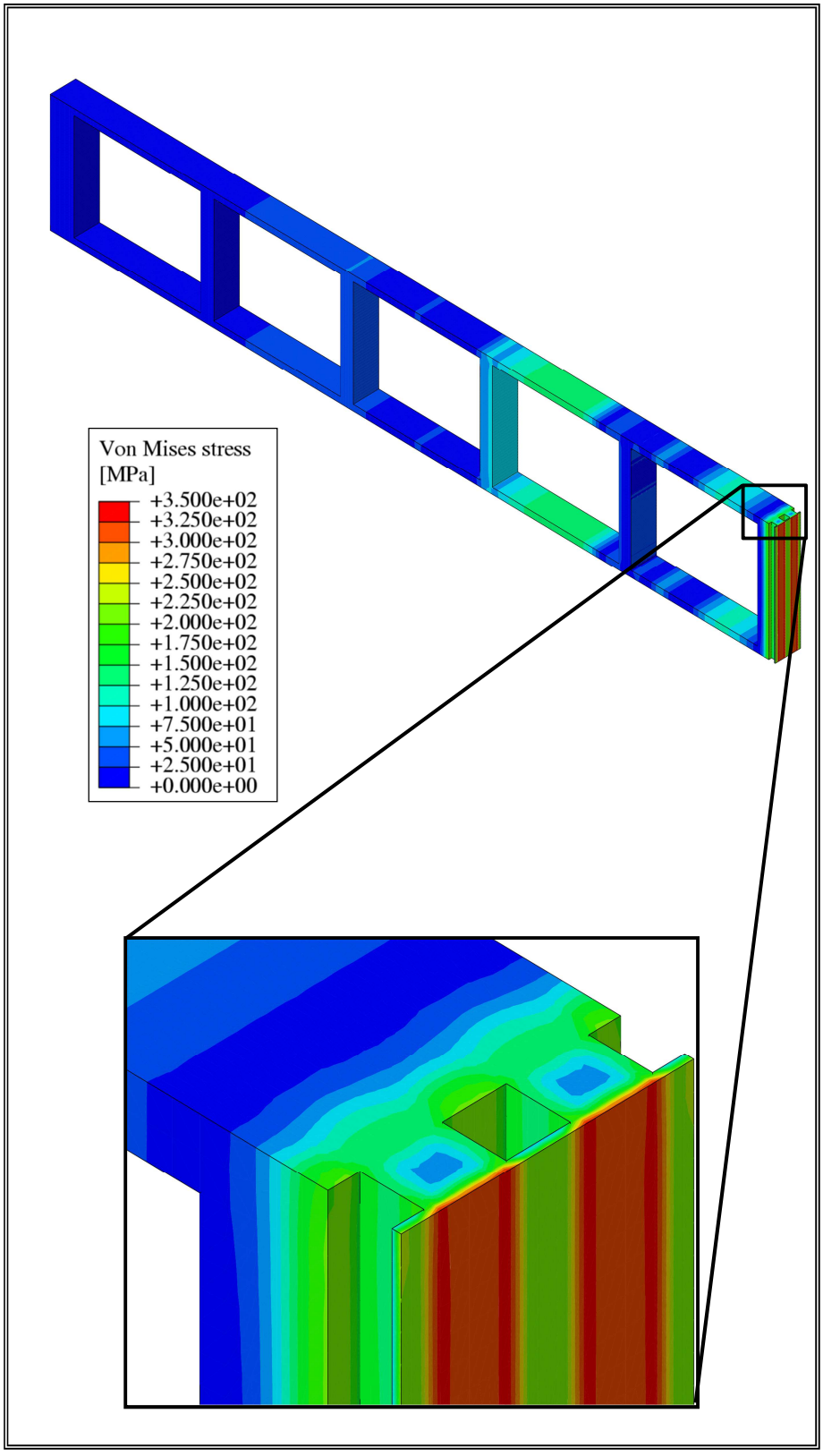


Figure 2-17. Case 1 - Von Mises equivalent stress field - Normal Operation scenario.

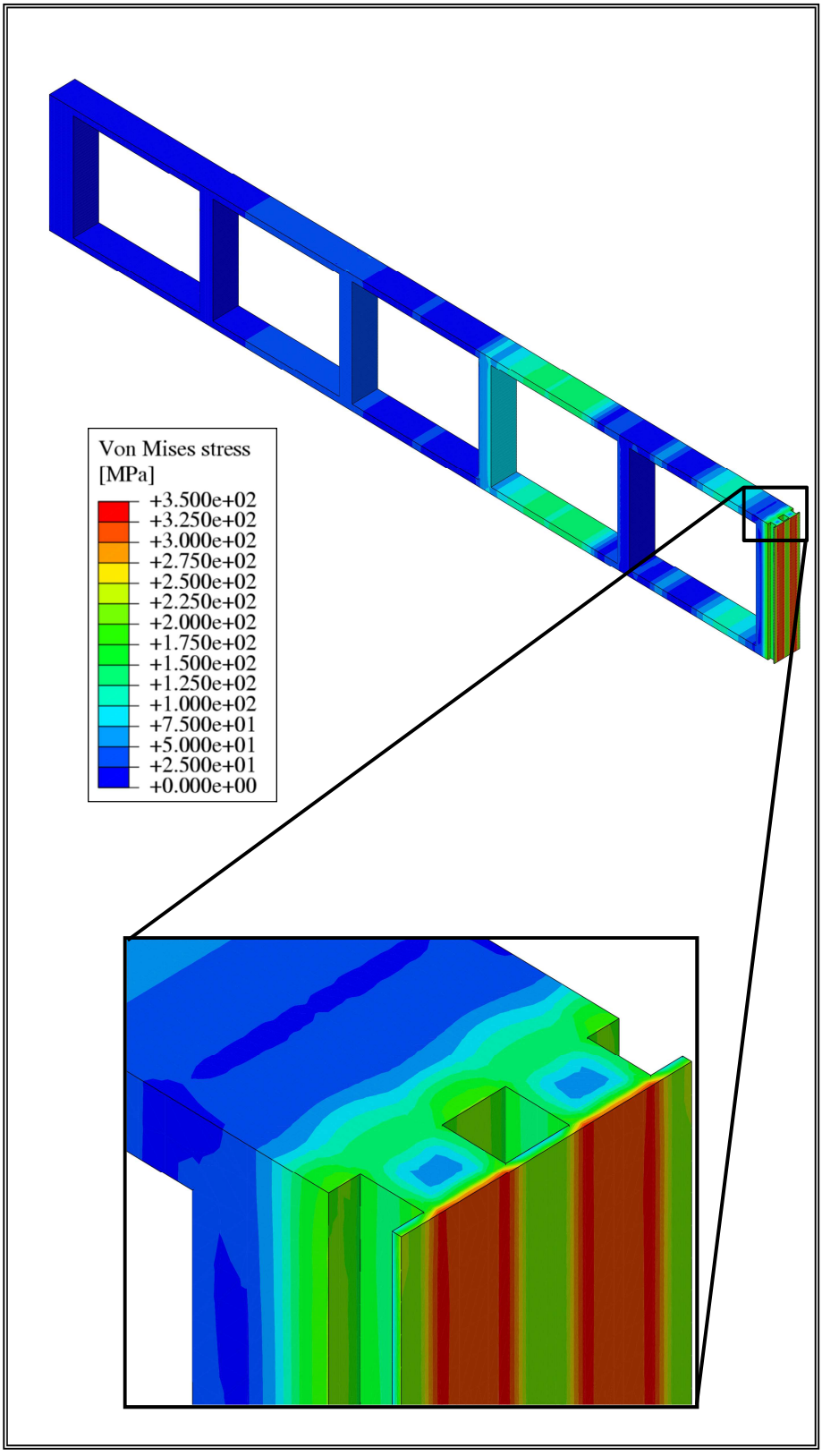


Figure 2-18. Case 2 - Von Mises equivalent stress field - Normal Operation scenario.

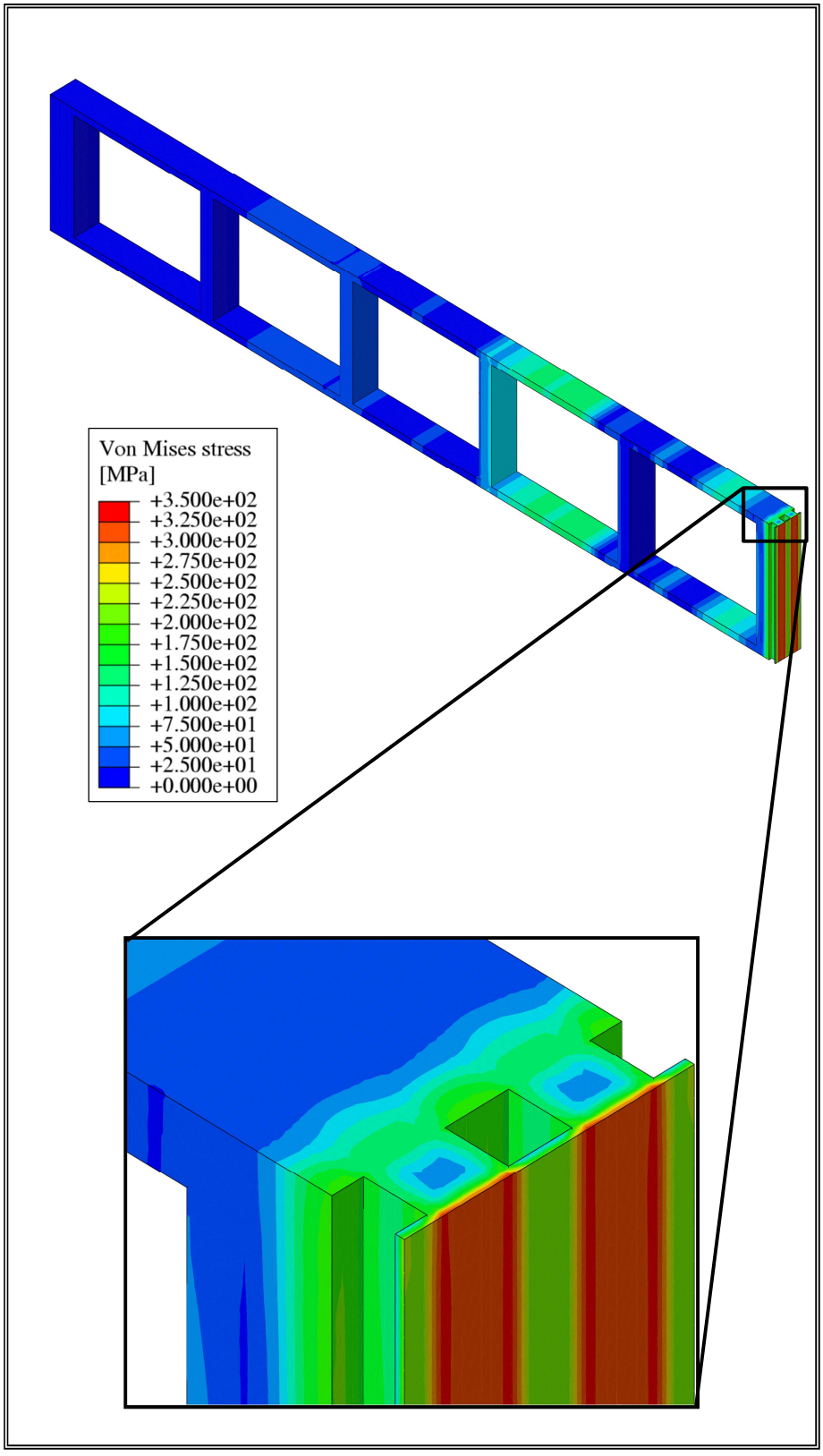


Figure 2-19. Case 3 - Von Mises equivalent stress field - Normal Operation scenario.

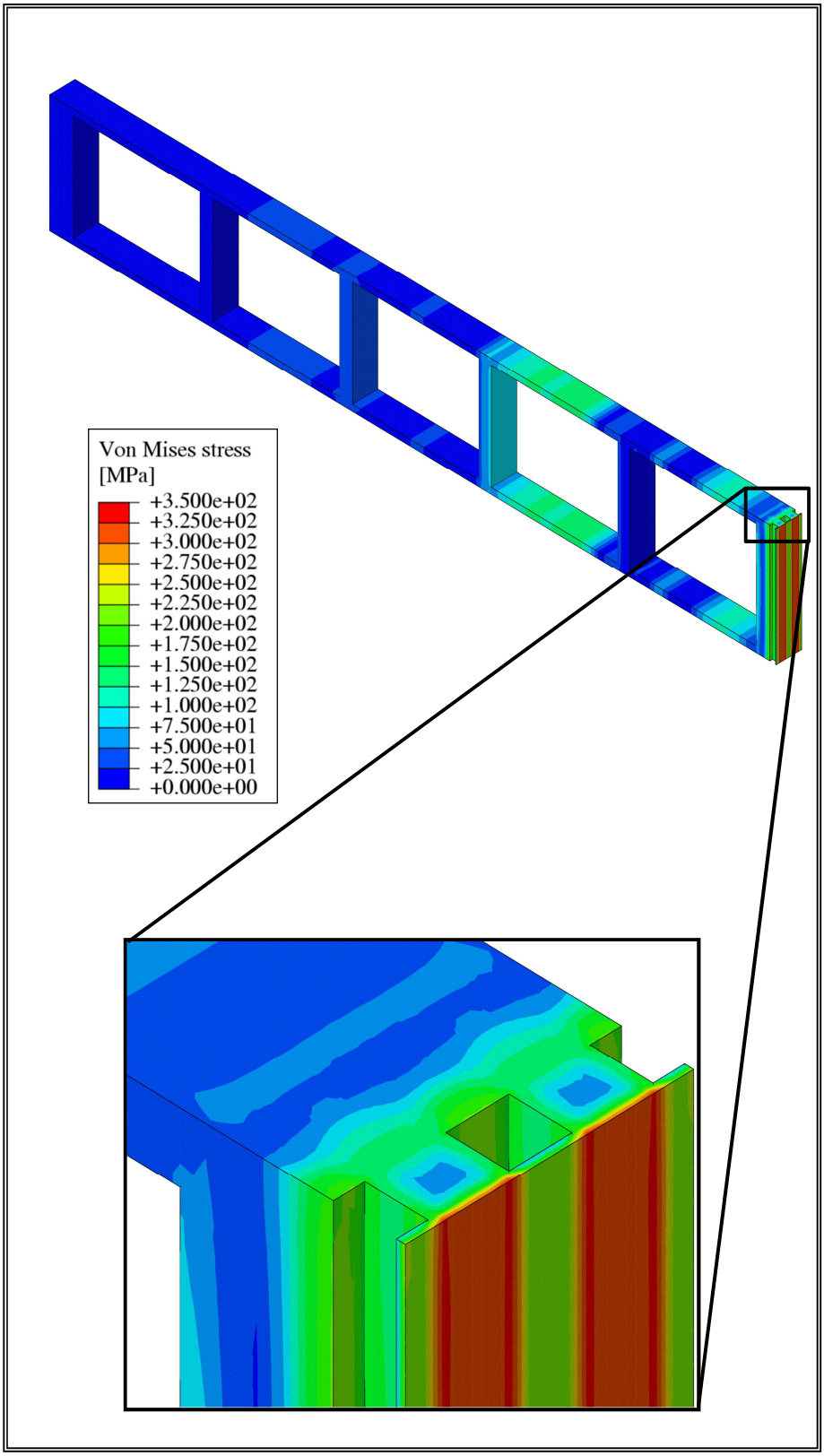


Figure 2-20. Case 4 - Von Mises equivalent stress field - Normal Operation scenario.

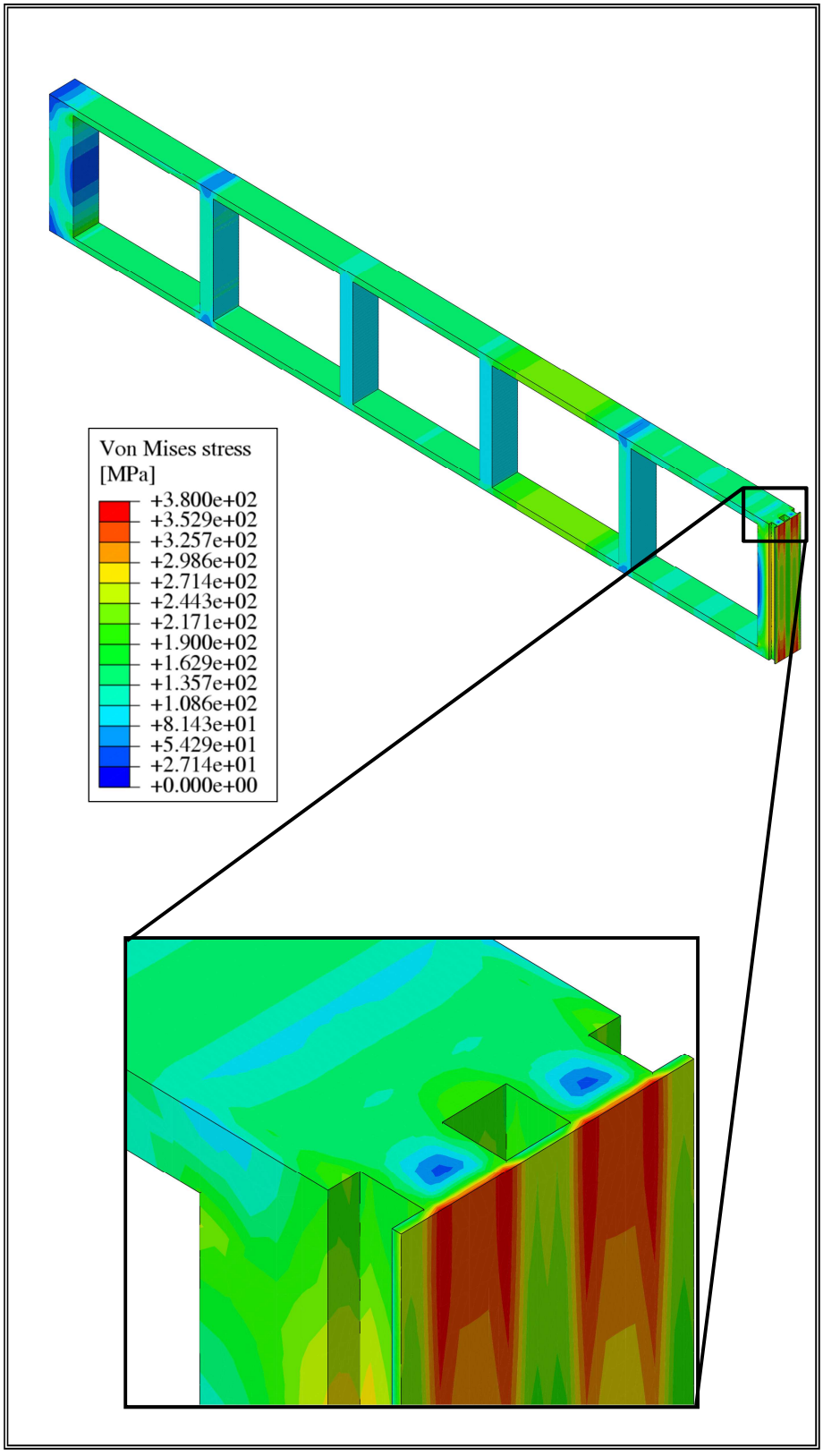


Figure 2-21. Case 1 - Von Mises equivalent stress field - Over-Pressurization scenario.

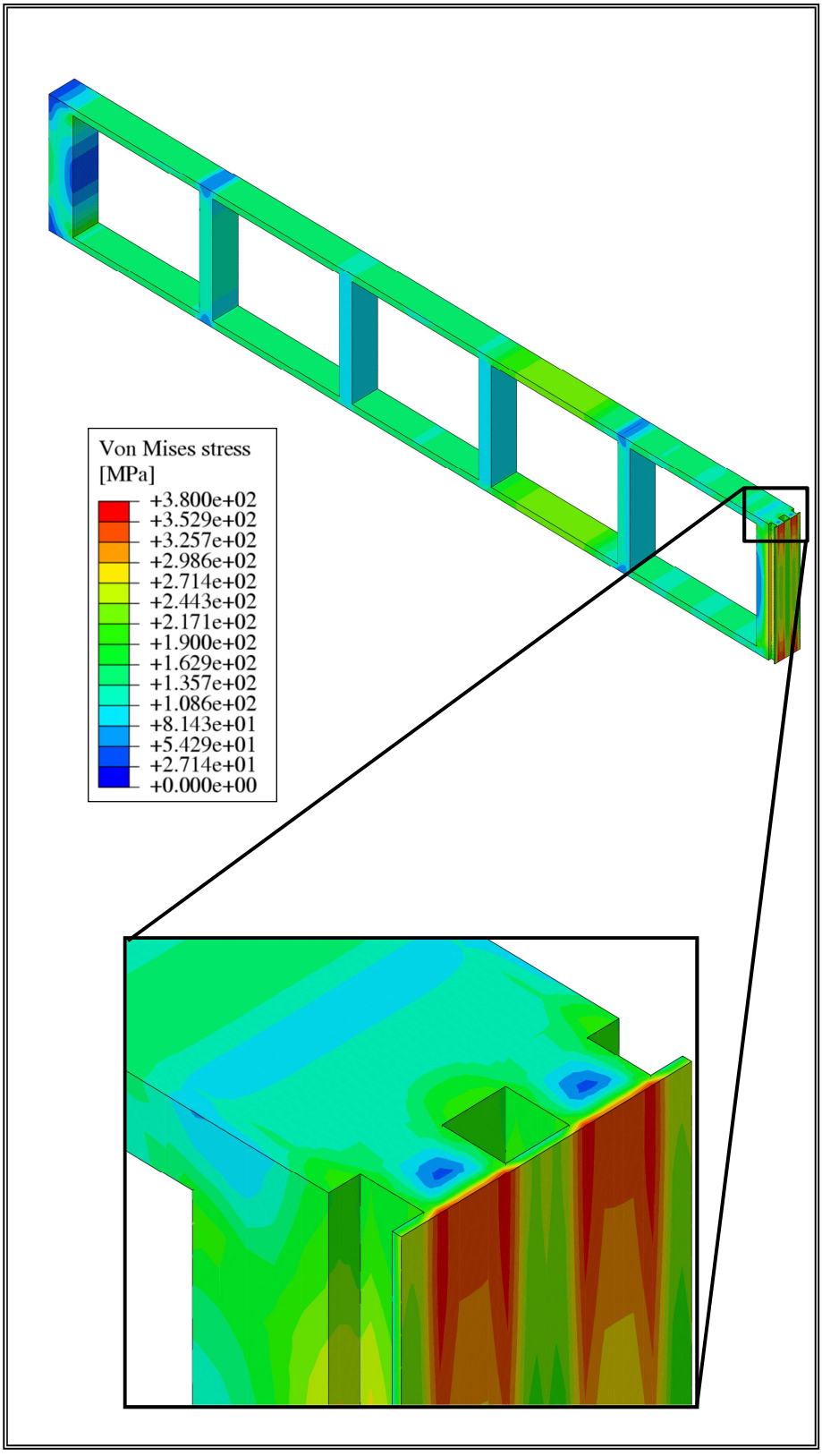


Figure 2-22. Case 2 - Von Mises equivalent stress field - Over-Pressurization scenario.

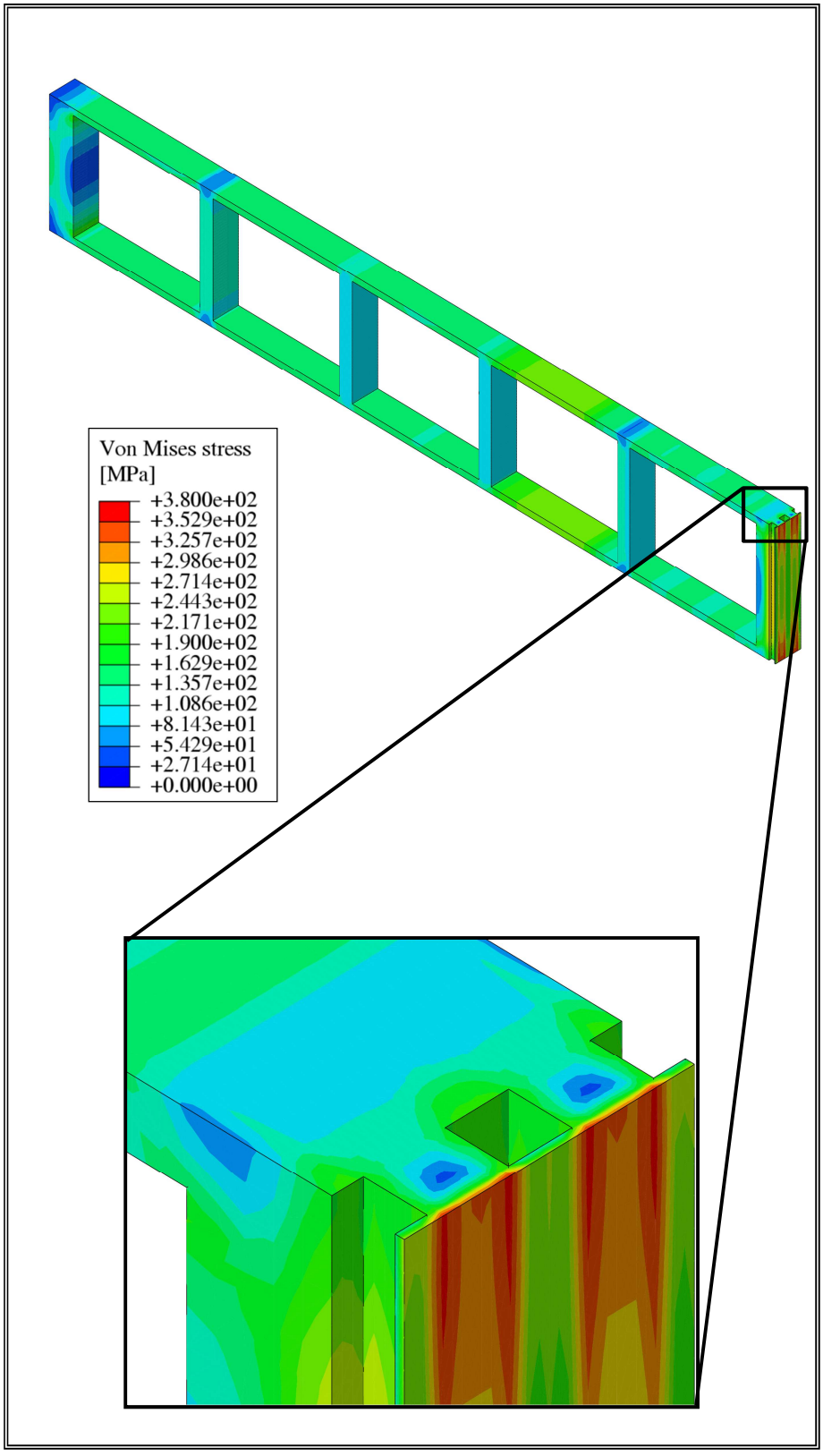


Figure 2-23. Case 3 - Von Mises equivalent stress field - Over-Pressurization scenario.

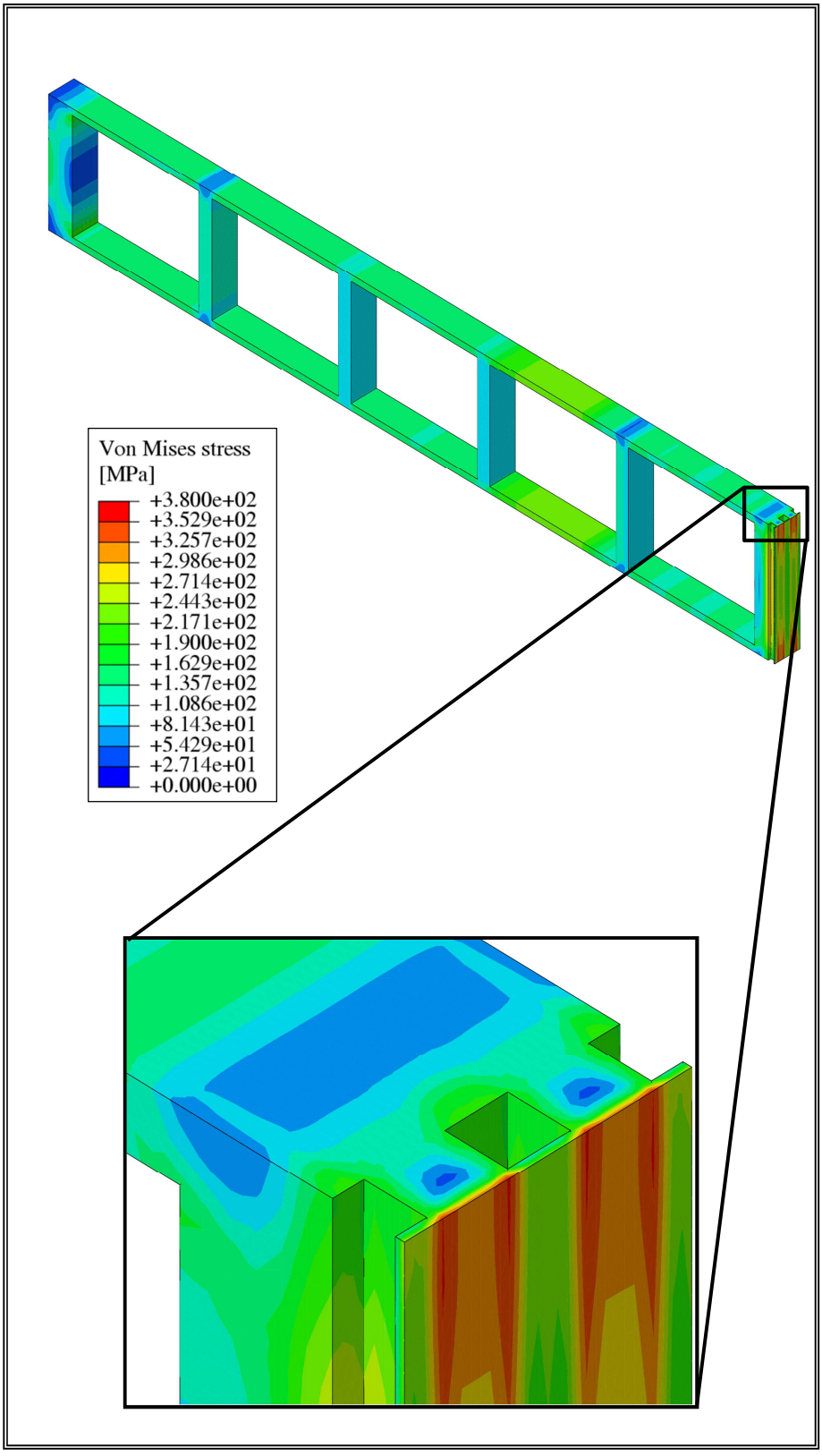


Figure 2-24. Case 4 - Von Mises equivalent stress field - Over-Pressurization scenario.

Table 2-6. Case 1 stress linearization.

| | **Stress linearization path** | | | | | |
|---|---|---|---|---|---|---|
| | **AB** | **CD** | **EF** | **GH** | **IJ** | **KL** |
| $T_{Max\text{-}Path}$ [°C] | 384.95 | 448.03 | 496.66 | 392.05 | 448.07 | 496.76 |
| **Level A criteria** | | | | | | |
| $P_m/S_m$ | 0.049 | 0.069 | 0.059 | 0.035 | 0.091 | 0.053 |
| $(P_m+P_b)/K_{eff}\ S_m$ | 0.046 | 0.057 | 0.068 | 0.054 | 0.068 | 0.065 |
| $(P_m+Q_m)/S_e$ | 0.439 | 0.956 | 0.356 | 0.401 | 0.939 | 0.313 |
| $P_m/S_t$ | - | - | 0.052 | - | - | 0.047 |
| $(P_m+P_b/K)/S_t$ | - | - | 0.081 | - | - | 0.0784 |
| **Level D criteria** | | | | | | |
| $P_m/\sigma_{lim}$ | 0.477 | 0.173 | 0.483 | 0.226 | 0.604 | 0.375 |
| $(P_m+P_b)/K_{eff}\ \sigma_{lim}$ | 0.523 | 0.126 | 0.577 | 0.271 | 0.405 | 0.455 |
| $(P_m+Q_m)/2\ S_e$ | 0.559 | 0.587 | 0.532 | 0.343 | 0.613 | 0.444 |
| $W_t[1.35\ (P_m+P_b/K)]$ | - | - | ~ 0 | - | - | 0.699 |

Table 2-7. Case 2 stress linearization.

| | **Stress linearization path** | | | | | |
|---|---|---|---|---|---|---|
| | **AB** | **CD** | **EF** | **GH** | **IJ** | **KL** |
| $T_{Max\text{-}Path}$ [°C] | 388.04 | 448.03 | 496.67 | 399.60 | 448.09 | 496.83 |
| **Level A criteria** | | | | | | |
| $P_m/S_m$ | 0.046 | 0.069 | 0.057 | 0.035 | 0.090 | 0.051 |
| $(P_m+P_b)/K_{eff}\ S_m$ | 0.044 | 0.057 | 0.067 | 0.053 | 0.068 | 0.065 |
| $(P_m+Q_m)/S_e$ | 0.382 | 0.947 | 0.326 | 0.323 | 0.933 | 0.250 |
| $P_m/S_t$ | - | - | 0.050 | - | - | 0.045 |
| $(P_m+P_b/K)/S_t$ | - | - | 0.080 | - | - | 0.078 |
| **Level D criteria** | | | | | | |
| $P_m/\sigma_{lim}$ | 0.458 | 0.176 | 0.467 | 0.239 | 0.587 | 0.376 |
| $(P_m+P_b)/K_{eff}\ \sigma_{lim}$ | 0.498 | 0.128 | 0.551 | 0.276 | 0.393 | 0.441 |
| $(P_m+Q_m)/2\ S_e$ | 0.515 | 0.577 | 0.500 | 0.331 | 0.604 | 0.428 |
| $W_t[1.35\ (P_m+P_b/K)]$ | - | - | ~ 0 | - | - | 0.445 |

Table 2-8. Case 3 stress linearization.

| | **Stress linearization path** | | | | | |
|---|---|---|---|---|---|---|
| | **AB** | **CD** | **EF** | **GH** | **IJ** | **KL** |
| $T_{Max\text{-}Path}$ [°C] | 391.06 | 448.04 | 496.98 | 407.43 | 448.12 | 496.89 |
| **Level A criteria** | | | | | | |
| $P_m/S_m$ | 0.044 | 0.070 | 0.055 | 0.034 | 0.089 | 0.050 |
| $(P_m+P_b)/K_{eff}\ S_m$ | 0.043 | 0.057 | 0.067 | 0.052 | 0.067 | 0.064 |
| $(P_m+Q_m)/S_e$ | 0.326 | 0.937 | 0.295 | 0.242 | 0.926 | 0.182 |
| $P_m/S_t$ | - | - | 0.049 | - | - | 0.044 |
| $(P_m+P_b/K)/S_t$ | - | - | 0.079 | - | - | 0.077 |
| **Level D criteria** | | | | | | |
| $P_m/\square_{lim}$ | 0.441 | 0.180 | 0.453 | 0.250 | 0.571 | 0.376 |
| $(P_m+P_b)/K_{eff}\ \square_{lim}$ | 0.475 | 0.131 | 0.526 | 0.279 | 0.382 | 0.428 |
| $(P_m+Q_m)/2\ S_e$ | 0.473 | 0.567 | 0.468 | 0.320 | 0.595 | 0.412 |
| $W_t[1.35\ (P_m+P_b/K)]$ | - | - | ~ 0 | - | - | 0.291 |

Table 2-9. Case 4 stress linearization.

| | **Stress linearization path** | | | | | |
|---|---|---|---|---|---|---|
| | **AB** | **CD** | **EF** | **GH** | **IJ** | **KL** |
| $T_{Max\text{-}Path}$ [°C] | 394.38 | 448.05 | 496.72 | 415.65 | 448.15 | 496.97 |
| **Level A criteria** | | | | | | |
| $P_m/S_m$ | 0.041 | 0.070 | 0.053 | 0.033 | 0.088 | 0.048 |
| $(P_m+P_b)/K_{eff}\ S_m$ | 0.044 | 0.057 | 0.066 | 0.054 | 0.067 | 0.064 |
| $(P_m+Q_m)/S_e$ | 0.266 | 0.925 | 0.266 | 0.155 | 0.917 | 0.106 |
| $P_m/S_t$ | - | - | 0.047 | - | - | 0.043 |
| $(P_m+P_b/K)/S_t$ | - | - | 0.078 | - | - | 0.076 |
| **Level D criteria** | | | | | | |
| $P_m/\sigma_{lim}$ | 0.427 | 0.185 | 0.440 | 0.260 | 0.556 | 0.375 |
| $(P_m+P_b)/K_{eff}\ \sigma_{lim}$ | 0.460 | 0.134 | 0.507 | 0.285 | 0.371 | 0.416 |
| $(P_m+Q_m)/2\ S_e$ | 0.431 | 0.557 | 0.435 | 0.310 | 0.586 | 0.394 |
| $W_t[1.35\ (P_m+P_b/K)]$ | - | - | ~ 0 | - | - | 0.200 |

## 2.3 Study of the thermo-mechanical behaviour of the First Wall potentially optimized configurations

The 4 potentially optimized FW configurations have been selected at the end of a parametric study carried out by adopting a simplified 3D FEM model of the DEMO WCLL BB outboard equatorial module, released by CEA in 2012 [21], properly endowed with the potentially optimized flat FW geometric configurations. Nevertheless, these outcomes have been obtained adopting a simplified 3D FEM models, in which the thermo-mechanical action of the Segment Box on the FW has not been realistically simulated. In fact, fixed temperature distribution have been imposed within SPs and back-plate without simulating the heat transfer phenomena occurring within breeder zone, which may affect the FW thermo-mechanical performances. Furthermore, also the mechanical action of the caps on the FW has not been taken into account in the parametric campaign of analysis, since the 3D FEM models set-up have been intended to simulate a central portion of the DEMO WCLL BB outboard equatorial module central radial-poloidal slice. For these reasons, the necessity of a more detailed analysis of the DEMO WCLL BB outboard equatorial module, endowed with these 4 FW configurations, arose in order to confirm results of the simplified parametric study. Consequently, the research campaign relevant to the FW geometric optimization has been followed by another thermo-mechanical analysis campaign, performed adopting more realistic 3D FEM models, in order to verify the outcomes of the parametric analysis.

### 2.3.1 The FEM models

In order to more realistically investigate the thermo-mechanical behaviour of the potentially optimized FW geometric configurations selected at the end of the previously performed parametric study, 4 different 3D FEM models have been set-up, realistically reproducing the central poloidal-radial slice of the 2012 DEMO-WCLL outboard breeding blanket equatorial module [21] equipped with the different flat FW potentially optimized configurations (Fig. 2-25). Each model includes one breeder cell in the toroidal direction and all the five breeder cells in the radial direction. Moreover, Pb-15.7Li breeder, Double Walled Tubes and cooling water flow domain have been included into the model too (Fig. 2-26). For each 3D geometric model a mesh independency procedure has been performed, obtaining a spatial discretization that ensures results accuracy saving calculation time. Since the 4 FEM models only differs in the total FW thickness value (Tab. 2-5), the 4 meshes set-up show very similar features. In particular, for each 3D FEM model, the mesh set-up has been characterized by a node number ranging from $\sim 2.33 \cdot 10^6$ (Configuration 1) to $\sim 2.36 \cdot 10^6$ (Configuration 4) and an element number ranging from $\sim 3.13 \cdot 10^6$ to $\sim 3.29 \cdot 10^6$ respectively.

Concerning the element type, both hexahedral and tetrahedral linear elements, foreseen by the ABAQUS FEM code elements library, have been adopted.

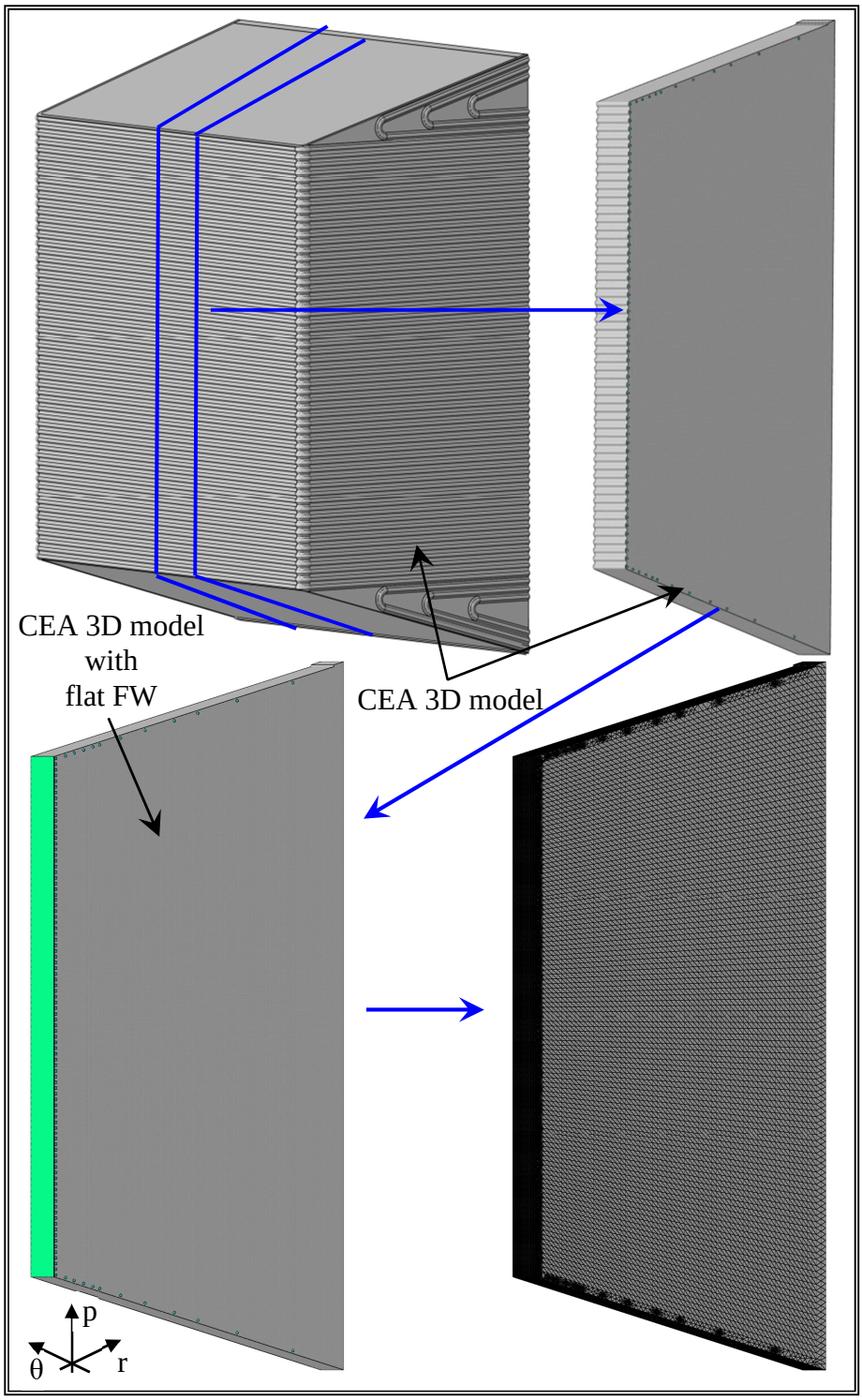


Figure 2-25. 3D FE model of the central poloidal-radial slice.

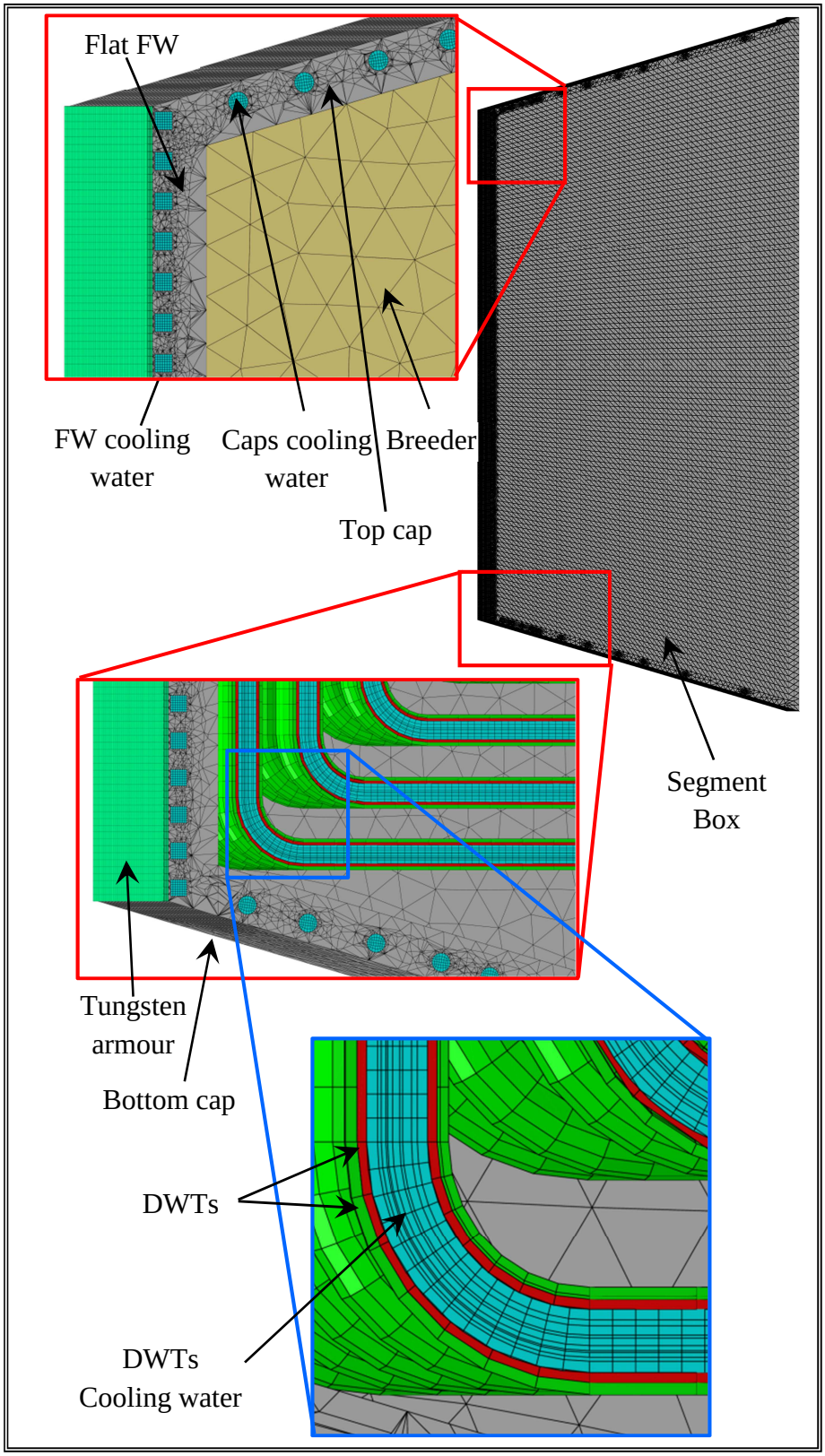


Figure 2-26. Internals of a 3D FE model of the central poloidal-radial slice.

### 2.3.1.1 Materials

RAFM EUROFER steel has been assumed as the structural material, except for the 2 mm-thick FW armour that has been supposed made of tungsten. Moreover, the Pb-15.7Li alloy has been assumed as breeder.

Materials have been considered homogeneous, uniform, isotropic and linear elastic and their thermo-physical properties have been assumed to depend uniquely on temperature as indicated in [33], except for tungsten density that has been assumed to be constant and equal to 19300 kg/m$^3$ [34 - 37].

Thermo-physical properties of the materials at 20 °C have been reported in Table 2-10 while their temperature-dependent behaviour have been shown in Figures 2-27 - 2-29.

Table 2-10. Thermo-physical properties at 20 °C [21] [33-34] [39].

| | **EUROFER** | **Tungsten** | **Pb-15.7Li** |
|---|---|---|---|
| $\rho_0$ [kg/m$^3$] | 7750 | 19300 | 10172 |
| $\lambda_0$ [W/(m·°C)] | 28.30 | 174.91 | 7.69 |
| $c_{p0}$ [J/(kg·°C)] | 448.0 | 132.33 | 192.0 |
| $\alpha_0$ [°C$^{-1}$] | $1.04 \cdot 10^{-5}$ | $5.25 \cdot 10^{-6}$ | $11.68 \cdot 10^{-5}$ |
| $E_0$ [Pa] | $2.17 \cdot 10^{11}$ | $4.08 \cdot 10^{11}$ | - |

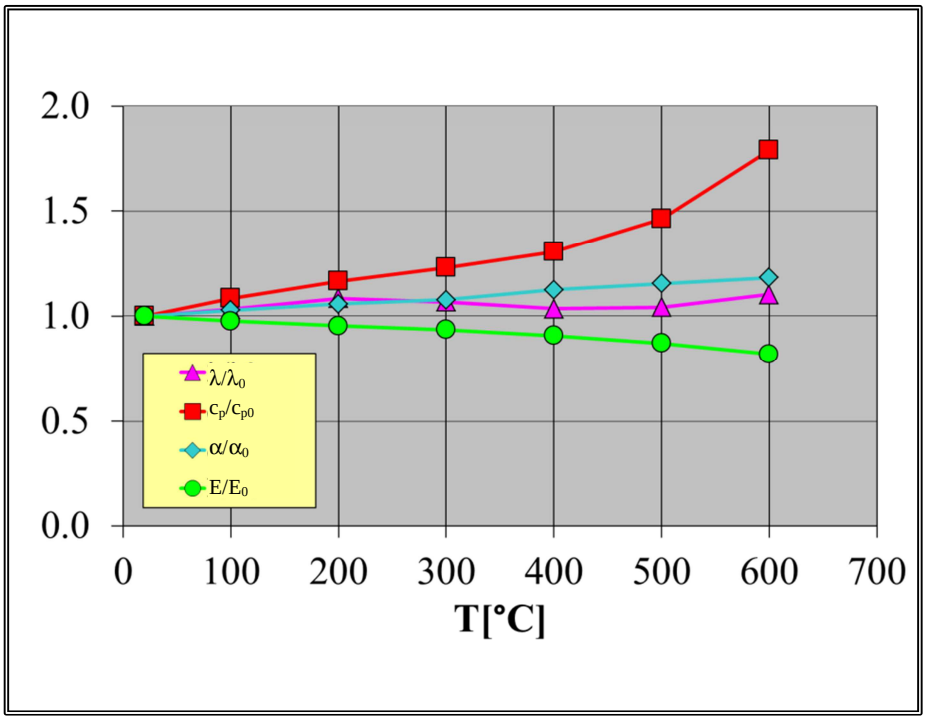


Figure 2-27. EUROFER thermo-physical properties temperature-dependent behaviour.

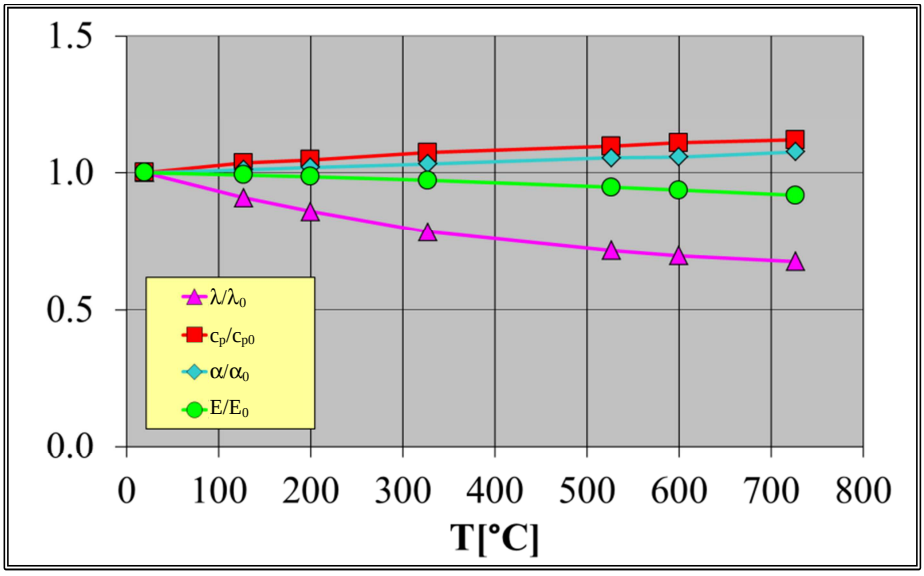


Figure 2-28. Tungsten thermo-physical properties temperature-dependent behaviour.

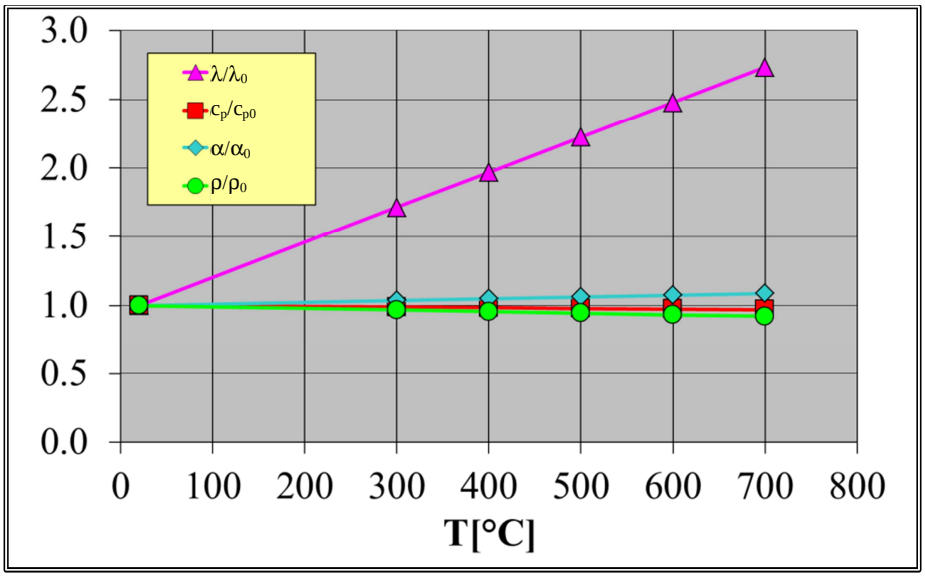


Figure 2-29. Pb-15.7Li thermo-physical properties temperature-dependent behaviour.

For each model, un-coupled steady-state thermo-mechanical analyses have been performed in order to assess the thermo-mechanical performances of the DEMO WCLL BB outboard equatorial module, endowed with 4 different flat FW geometric configurations, under both the NO and the OP loading scenarios. Attention has been paid to the FW, in order to verify the fulfilment of the SDC-IC safety criteria when the mechanical action of the Segment Box on the FW is more realistically simulated. To this purpose a proper set of thermo-mechanical loads and boundary conditions has been applied to the 4 FEM models taken into account, in order to realistically reproduce the loading conditions relevant to NO and OP scenarios.

### 2.3.1.2 Thermal loads and boundary conditions

From the thermal point of view, the following loads and boundary conditions have been applied for both NO and OP scenarios, since the difference between the two scenarios is given by the pressure exerted by the breeder onto the SB internal surfaces:

- normal heat flux (Φ) acting on the FW plasma facing surface;
- non-uniform spatial distribution of volumetric density of heat power;
- thermal interactions;
- forced convective heat transfer.

Concerning the normal heat flux (Φ) acting on the FW plasma facing surface, a uniform value of 2.0 MW/m$^2$ has been imposed to the red surface shown in Figure 2-30.

In order to simulate the non-uniform spatial distribution of volumetric density of nuclear heat power, deposited by neutrons and gammas interacting with nuclei of structural materials, water and breeder, a proper FORTRAN subroutine has been set-up for each model and integrated within the analysis procedure. In these subroutines, the spatial distribution of volumetric density of deposited nuclear heat power calculated for the PPCS-A outboard breeding blanket [40], properly scaled by the ratio between DEMO and PPCS-A Neutron Wall Loadings, has been adopted (Figs.2-31 - 2-34), except for the 2 mm thick tungsten armour in which a uniform value equal to 9.28 MW/m$^3$ has been imposed [40]. As a first approximation, the same spatial distribution of volumetric density of heat power has been adopted for all the 4 models set-up, even though they differ each other in the FW geometry.

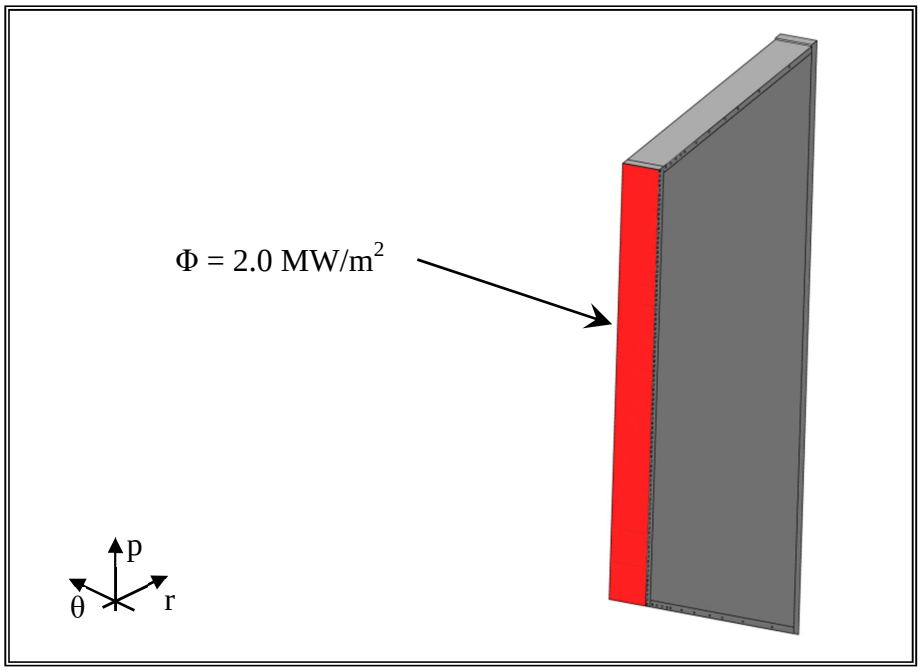


Figure 2-30. Plasma facing surface.

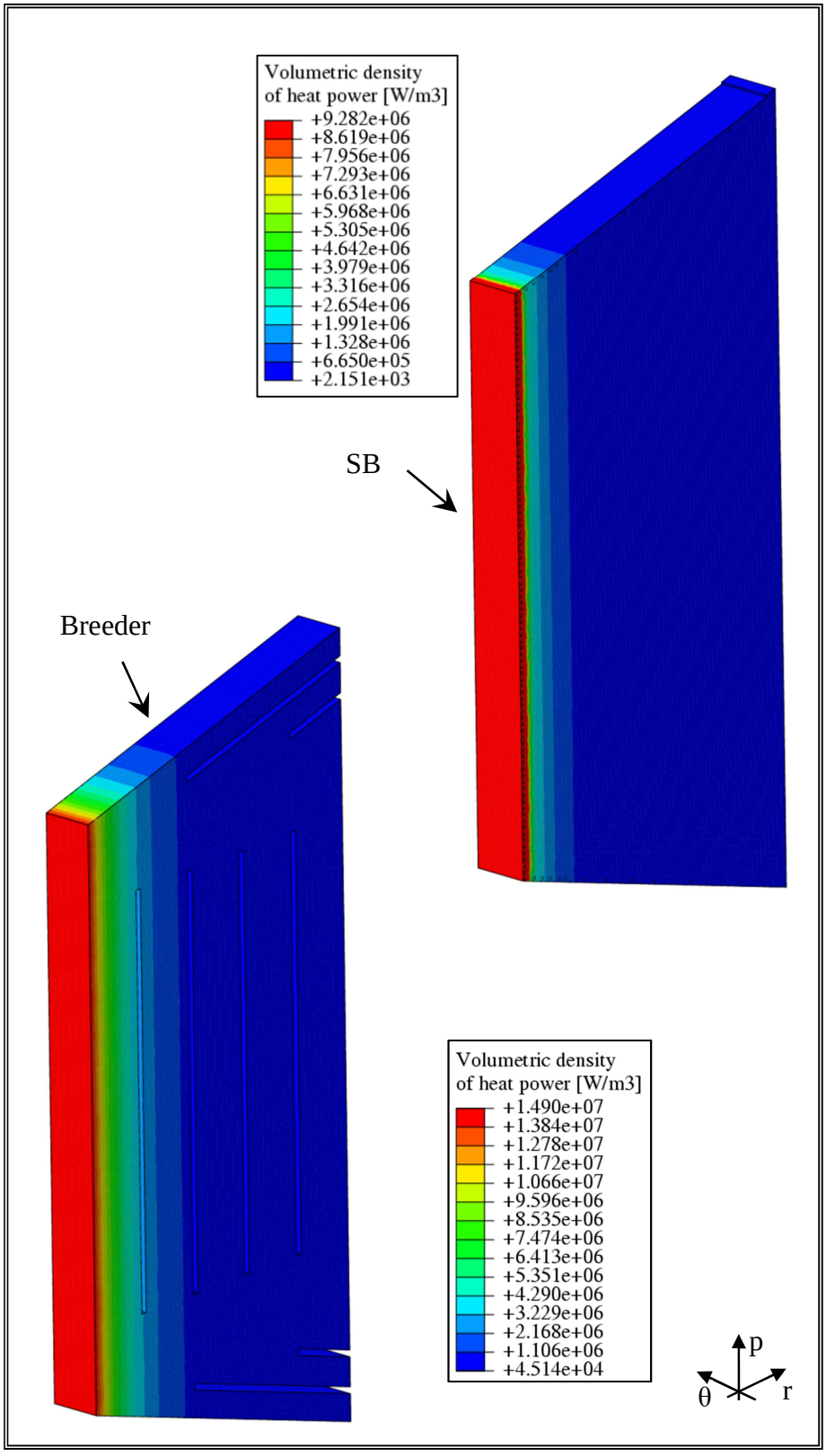


Figure 2-31. Volumetric density of nuclear heat power field: SB and breeder.

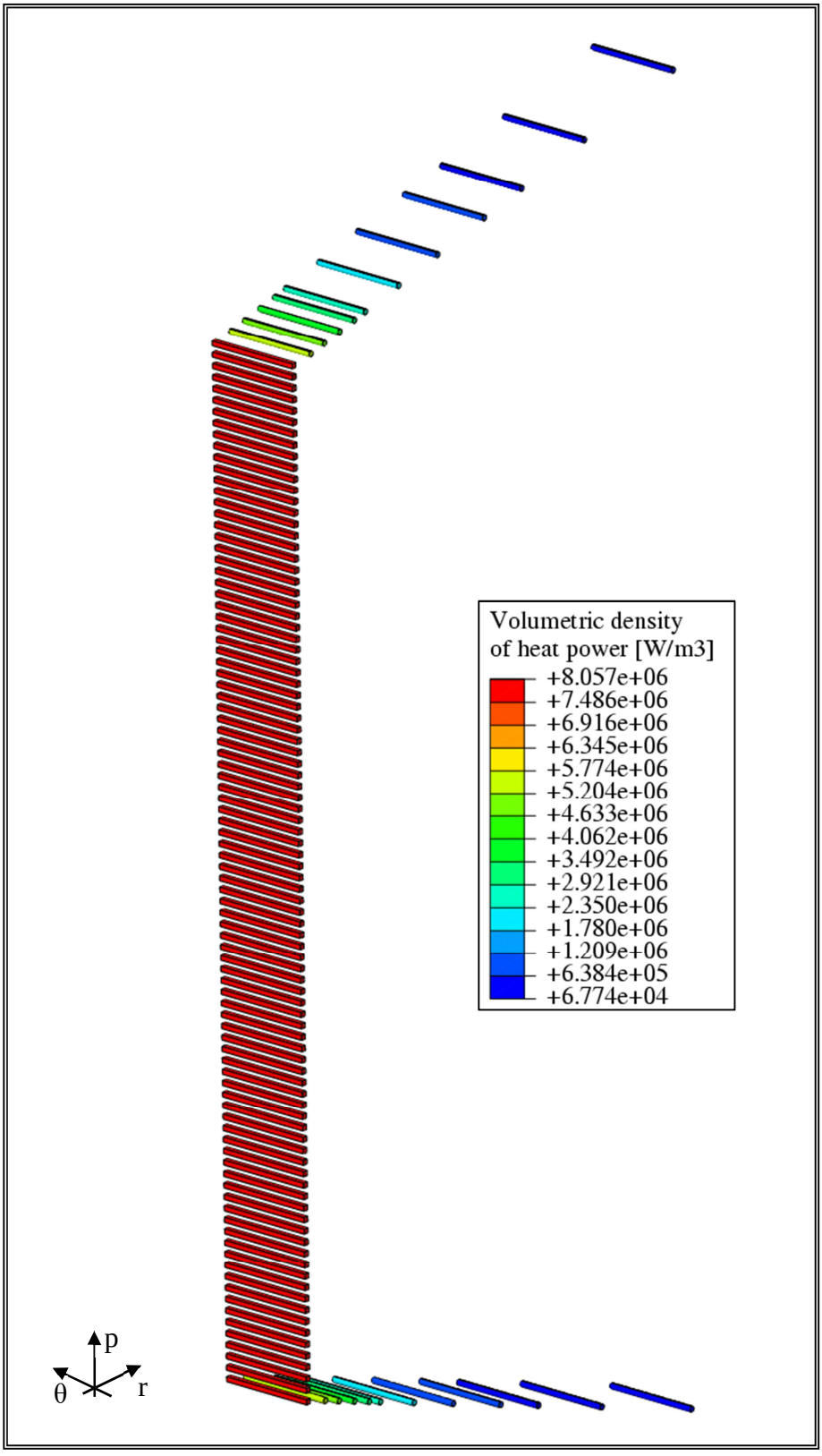


Figure 2-32. Volumetric density of nuclear heat power field: FW and caps cooling water.

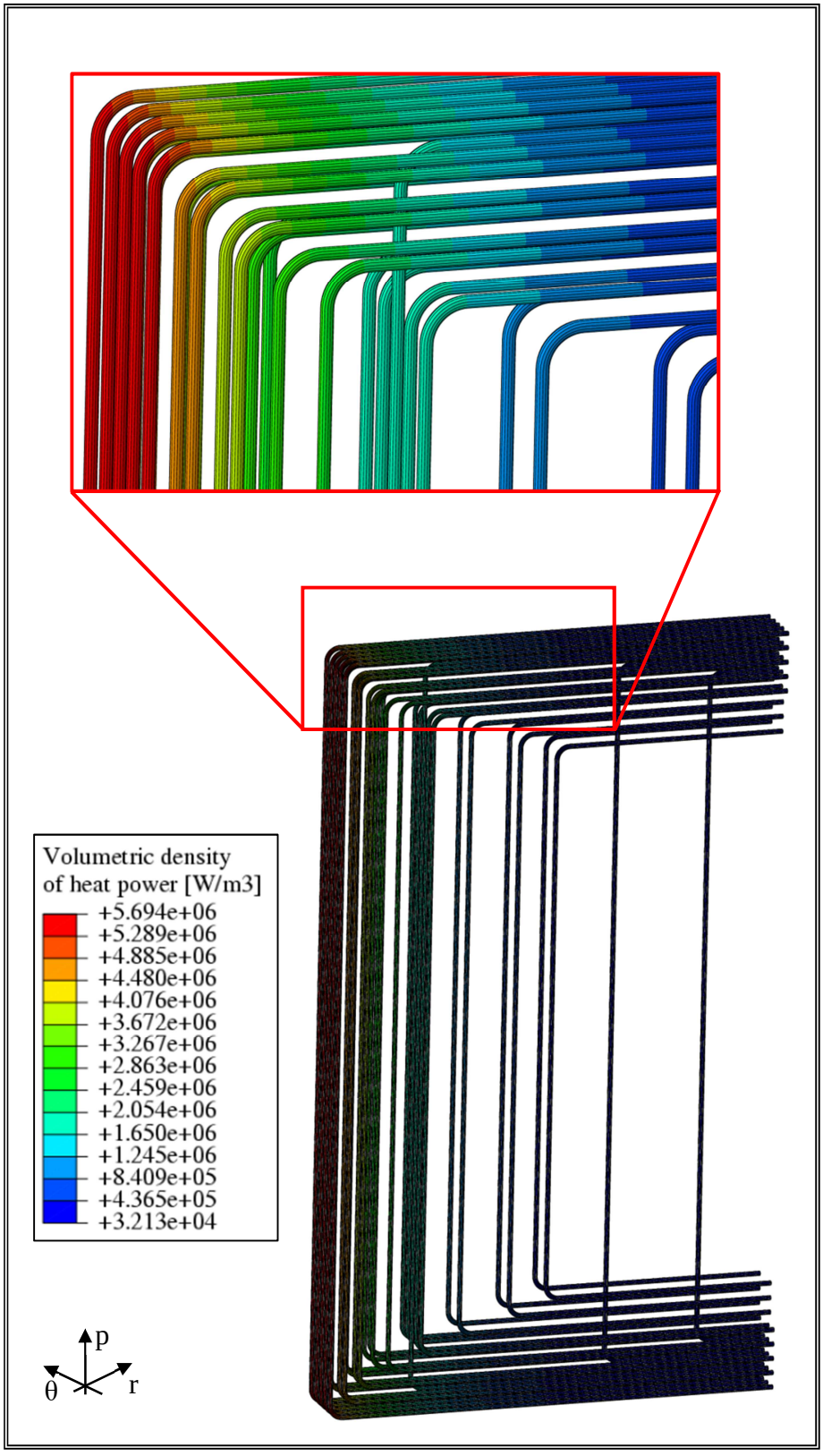


Figure 2-33. Volumetric density of nuclear heat power field: DWTs cooling water.

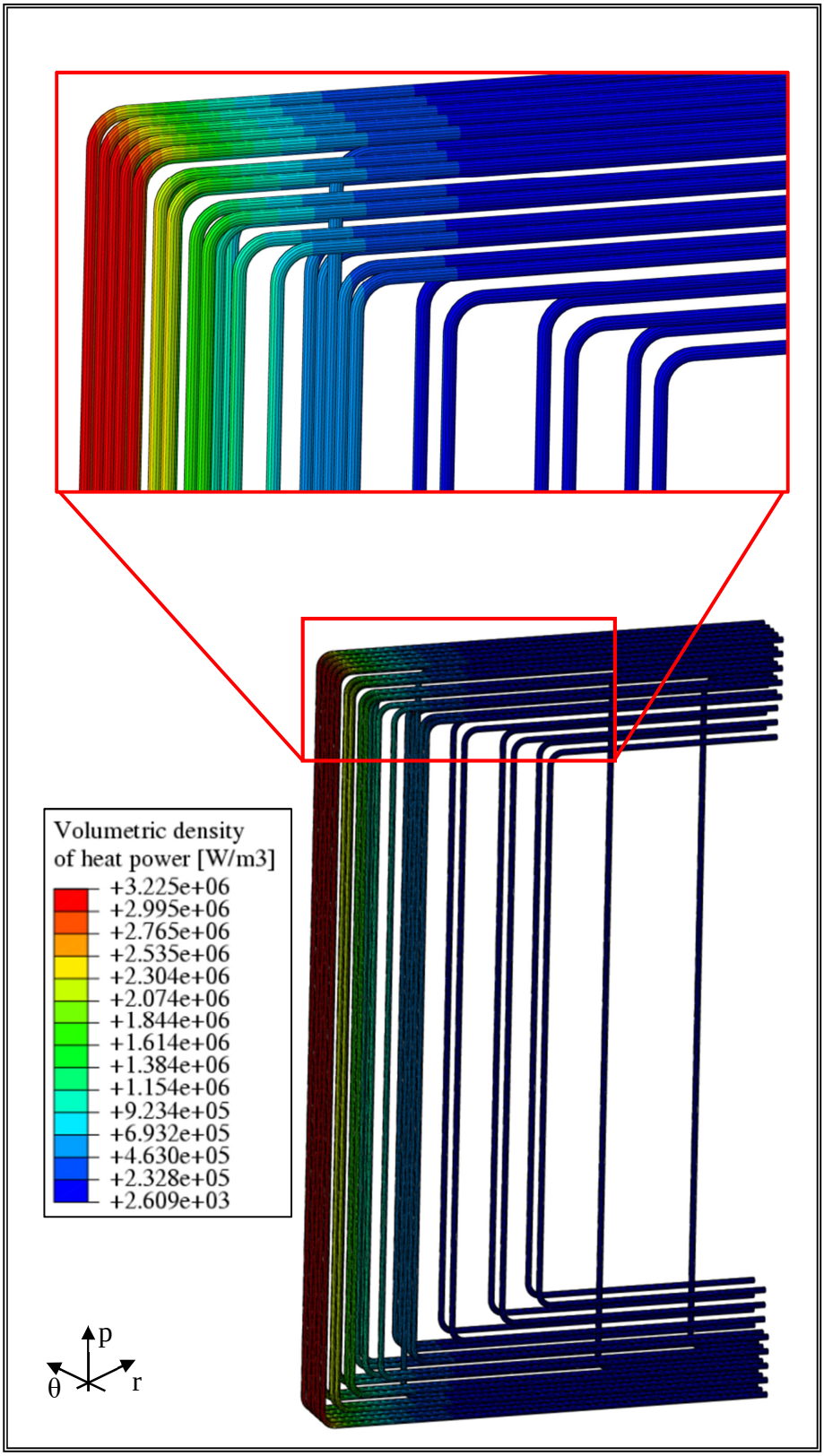


Figure 2-34. Volumetric density of nuclear heat power field: DWTs.

As to thermal interactions between breeder and both SB internals and DWTs external surface, a proper contact model, characterized by a thermal conductance of $10^5$ W/(m$^2$·°C), has been adopted. The same contact model has been taken into account in order to simulate the thermal effect of the copper layer interposed between internal and external tube of DWTs. This approach allows to simulate a "perfect" thermal contact among surfaces, neglecting the thermal resistance. Finally, DWTs and module Back-Plate have been considered as a continuum from the thermo-mechanical point of view.

Regarding forced convective heat transfer occurring between cooling water and both FW-caps channels and DWTs, the so-called "frozen" flow field approach has been adopted, assuming fixed mass flow rates (G) and heat transfer coefficients (h) within each channel or tube, calculated imposing a water temperature increase of 40 °C ($\Delta T_{Design}$) between the inlet (285 °C [40]) and the outlet headers of the module. This approach has allowed to calculate the coolant bulk temperature spatial distribution along the channel or tube current abscissa and, consequently, to more realistically simulate the convective heat transfer among cooling water and the corresponding wetted surfaces. In particular, heat transfer coefficients have been calculated using the Dittus & Bölter (DB) correlation [35]. In order to reproduce the cooling water path, the DWTs have been divided in two different groups. The first one includes the 17 tubes, devoted to remove heat power from the first radial cell (blue arrows in Figure 2-35), inside which water ($T_{inlet}$ = 285 °C) flows. The second group contains the remaining 13 DWTs, devoted to cool others 4 radial cells (yellow arrows in Figure 2-35), inside which water flows in counter-current in comparison with the first group. As to the $T_{inlet}$ of the cooling water flowing inside the second group of DWTs, it is equal to the mixing temperature ($T_{mixing}$) of the water exiting the first one [40]. The $T_{mixing}$ value is calculated during the analysis by means of a purposely set-up thermal coupling model.

Values of the mass flow rates and of the heat transfer coefficients calculated are reported in Table 2-11. It has to be observed that, since the number of FW cooling channels is the same for all the 4 configurations investigated, the same values of G and h have been adopted. Since coolant inside FW channels flows in counter-current, two different inlet temperatures (308.57 °C and 304.7 °C) have been imposed to the FW coolant domain since the inlet sections are located on both the FW toroidal sides. These inlet temperature values were calculated in the campaign of thermal analyses reported in [41], where a purposely set-up iterative procedure was followed in order to calculate the inlet temperature, on both the FW toroidal sides, of FW cooling water in the central-slice model, taking into account also a "peripheral slice" 3D FEM model and a purposely set-up thermal balance equation which stated that the total coolant thermal rise between module inlet and outlet was equal to $\Delta T_{Design}$ = 40 °C.

An analogous approach has been followed for the assumption of the caps coolant inlet temperature $T_{inlet}$, which has been drawn from outcomes of the research campaign reported in [41], obtained by the above mentioned iterative procedure.

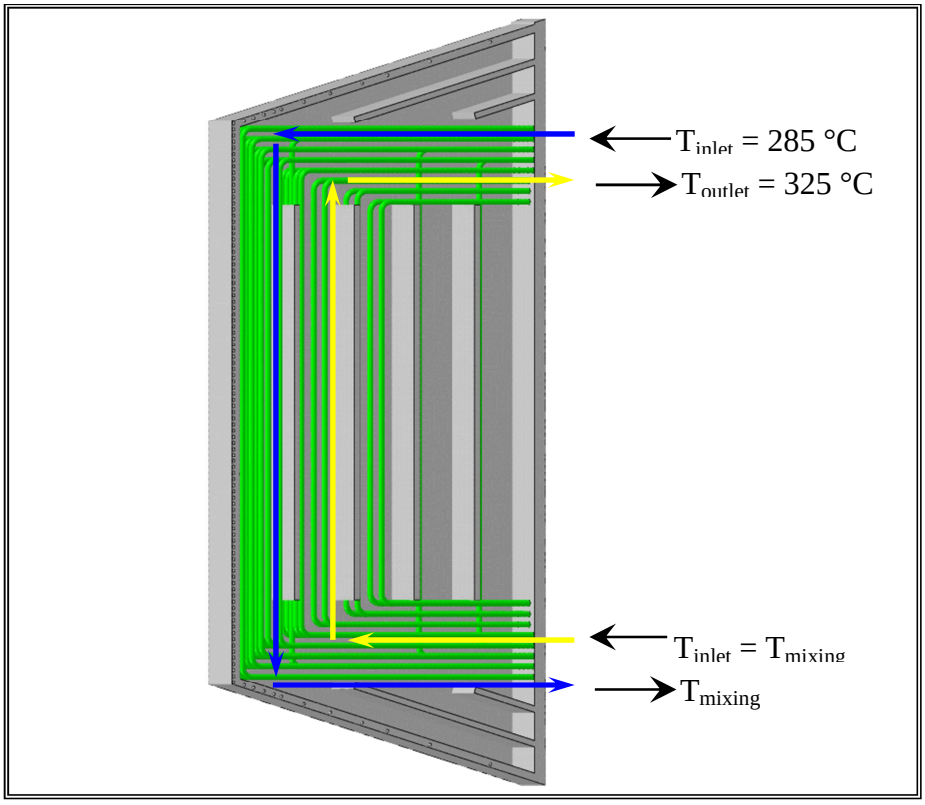


Figure 2-35. Cooling water flow path inside DWTs.

Table 2-11. Mass flow rates and heat transfer coefficients.

| **Component** | **G [kg/s]** | **h [W/(m$^2$·°C)]** |
|---|---|---|
| First Wall | 0.224 | 49289 |
| Top cap | 0.020 | 6836 |
| Bottom cap | 0.023 | 7479 |
| 1$^{st}$ radial cell DWTs | 0.075 | 19329 |
| 2$^{nd}$ - 5$^{th}$ radial cell DWTs | 0.098 | 24917 |

### 2.3.1.3 Mechanical loads and boundary conditions

From the mechanical point of view, the following loads and boundary conditions have been applied in order to properly set-up NO and OP loading scenarios, respectively classified, according to SDC-IC structural design code, as Level A and Level D:

- thermal deformation field;
- internal pressure;
- mechanical restraints.

The thermal deformation field, arising within the module as a consequence of its non-uniform thermal field and its thermal expansion tensor, has been properly imposed as thermal load in each calculation domain considered.

Regarding cooling water wetted surfaces, a uniform pressure of 15.5 MPa [40] has been imposed in both NO and OP loading scenarios in order to simulate the mechanical action of the cooling water flowing inside each tube and channel. As to SB internals and DWTs external surfaces, which are the breeder wetted surfaces, the uniform pressure of 0.5 MPa [40] has been imposed in NO loading scenario since this is the value envisaged for the breeder, within the WCLL BB outboard equatorial module, during the nominal operational phase of DEMO. Regarding OP scenario, since it represents accidental conditions originated by a cooling water leak inside the module (small in-box LOCA accident), a uniform pressure of 15.5 MPa, has been imposed onto all the breeder wetted surfaces.

In both loading scenarios investigated the set of same mechanical restraints has been set-up in order to reproduce, as more realistically as possible, the action of the module attachment system designed by CEA [21] and considered in the present study. To this purpose, displacement along the poloidal direction ($u_p$) of the nodes highlighted in blue in Figure 2-36 has been prevented. Moreover, a radial mechanical constraint ($u_r = 0$) has been imposed to nodes shown in red in Figure 2-36. Finally, a toroidal symmetry condition and a toroidal plane strain condition have been imposed to nodes lying on faces A and B (Fig. 2-36) respectively, in order to simulate the presence of the rest of the module.

The above said thermal and mechanical loads and boundary conditions have been summarized in Table 2-12.

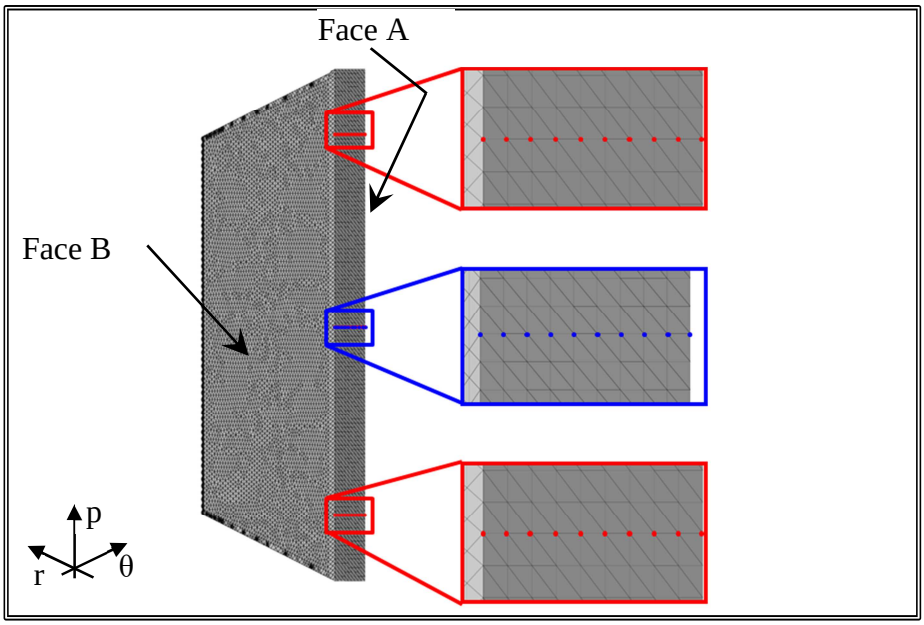


Figure 2-36. Mechanical boundary conditions.

Table 2-12. Mass flow rates and heat transfer coefficients.

| Load or boundary condition | NO scenario | OP scenario |
|---|---|---|
| Thermal analysis | | |
| Normal heat flux acting on FW | 2.0 MW/m$^2$ | 2.0 MW/m$^2$ |
| Non-uniform spatial distribution of volumetric density of heat power | PPCS-A data scaled with NWLs | PPCS-A data scaled with NWLs |
| Forced convective heat transfer | YES | YES |
| Thermal interactions | YES | YES |
| Mechanical analysis | | |
| Thermal deformation field | Depending on the configuration | Depending on the configuration |
| Internal pressure | 15.5 MPa water 0.5 MPa breeder | 15.5 MPa |
| Mechanical restraints | YES | YES |

### 2.3.2 The thermo-mechanical analysis

Un-coupled steady-state thermo-mechanical analysis have been performed in order to investigate the thermal behaviour of the 4 different 3D FEM models set-up, each reproducing the 2102 DEMO WCLL BB outboard equatorial module properly endowed with the 4 FW potentially optimized geometric configurations.

On the basis of thermal results, the corresponding mechanical analysis under NO and OP loading scenarios have been performed in order to determine the Von Mises equivalent stress field arising within the 4 considered FEM models.

At the end of each analysis, a stress linearization procedure has been performed in order to check, in the most critical paths located within the FW domain (Figs. 2-37 - 2-38), the fulfilment of the SDC-IC structural safety rules relevant to NO (Level A) and OP (Level D) loading scenarios, summarized in Table 2-13.

Table 2-13. Summary of SDC-IC design criteria considered.

| Level A criteria | Level D criteria |
|---|---|
| $P_m / S_m < 1$ | $P_m / \sigma_{lim} < 1$ |
| $(P_m + P_b) / K_{eff} * S_m < 1$ | $(P_m + P_b) / K_{eff} * \sigma_{lim} < 1$ |
| $(P_m + Q_m) / S_e < 1$ | $(P_m + Q_m) / 2 * S_e < 1$ |
| $P_m / S_t < 1$ (if $T_{Max\text{-}path} > 450$ °C) | $W_t$ [$1.35*(P_m+P_b/K)$] < 1 (if $T_{Max\text{-}path} > 450$ °C) |
| $(P_m + P_b/K) / S_t < 1$ (if $T_{Max\text{-}path} > 450$ °C) | |

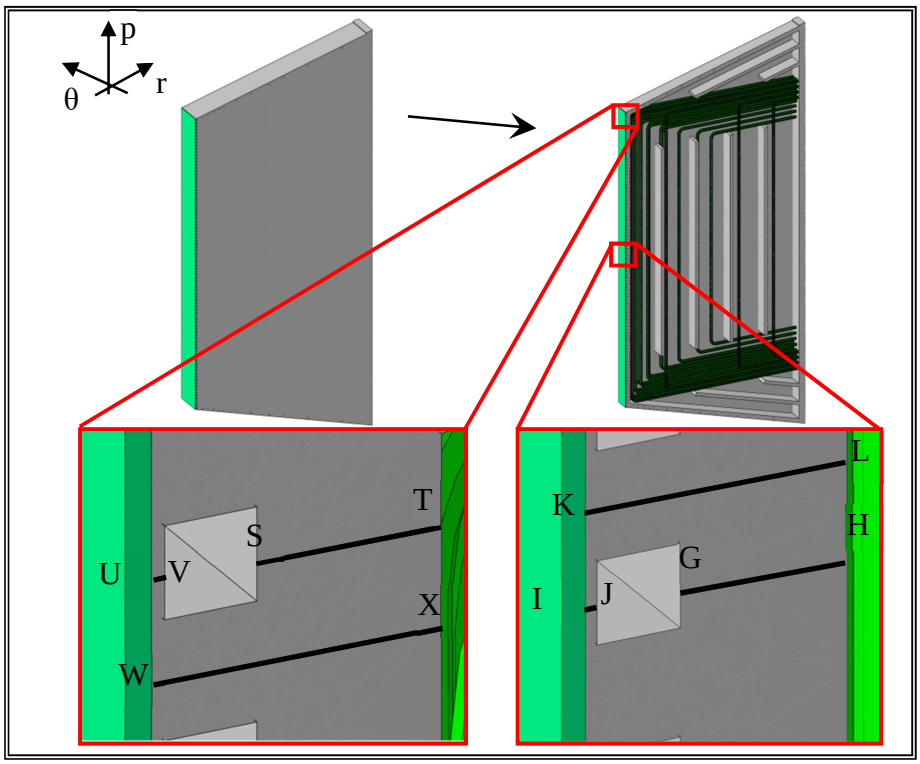


Figure 2-37. FW paths located at the toroidal mid plane section.

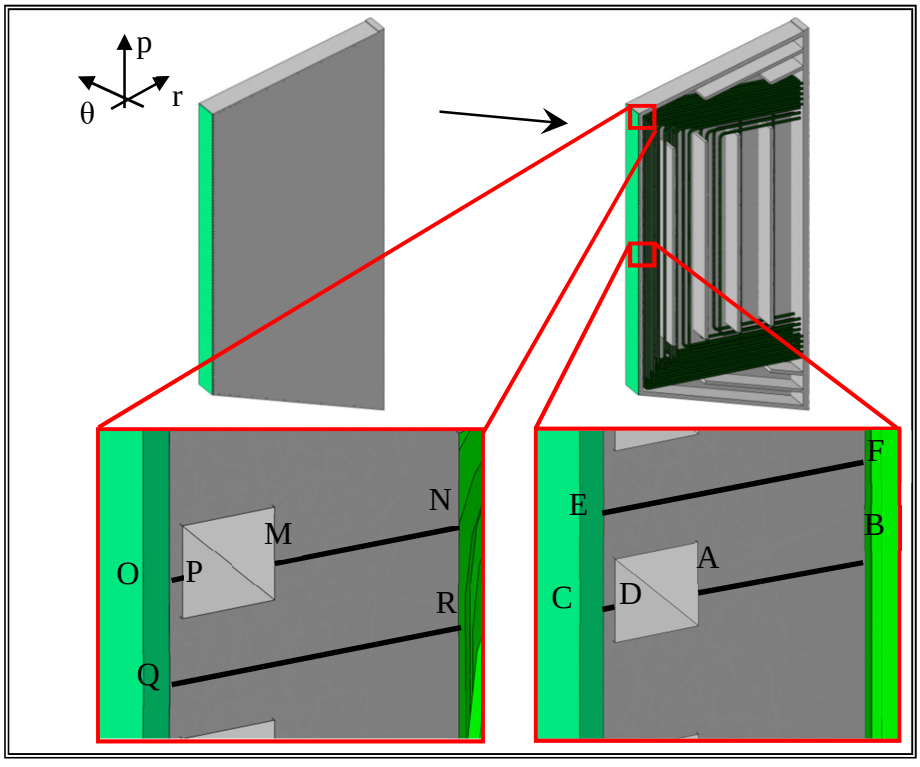


Figure 2-38. FW paths located close to a radial-poloidal SPs.

#### 2.3.2.1 Results

Results in terms of thermal field (Figs. 2-39 - 2-42) have shown that no significant differences are predicted among the 4 cases investigated. It is remarkable that the EUROFER maximum temperature calculated is well below the limit value of 550 °C in each geometric configuration assessed. These results lead to the conclusion that, from the thermal standpoint, the more realistic simulation of the SB thermal behaviour does not particularly affect the thermal performances of the 4 investigated potentially optimized FW geometric configurations.

From the mechanical standpoint, the Von Mises equivalent stress fields (Figs. 2-43 - 2-46) carried out suggest that Configuration 4 is the best case, since lowest maximum Von Mises stress values (486.7 MPa and 496.9 MPa for NO and OP loading scenarios respectively) are predicted for it. Moreover, it has to be noted that the FW most stressed regions are those located close to the caps. This suggests that the mechanical action of the SB, and of the caps in particular, has a strong impact on the FW thermo-mechanical performances in terms of Von Mises equivalent stress values.

Finally, a stress linearization procedure has been performed in order to check, in the most critical paths located within the FW of the 4 geometric configurations investigated, the fulfilment of the SDC-IC structural design criteria. These results (Tabs. 2-14 - 2-21) have shown that the most critical criterion is, for both NO and OP scenario, that concerning the immediate plastic flow localisation.

This criterion remains in fact un-satisfied along some paths located within the steel thickness interposed between the tungsten armour and the FW cooling channel side, in all the 4 configurations investigated. Nevertheless, stress linearization results indicate that the best case among those taken into account is still Configuration 4, since in this case the lowest values of both $(P_m+Q_m)/S_e$ and $(P_m+Q_m)/2S_e$ ratios are predicted.

In conclusion, a SB design review appears to be necessary since results of this more realistic study seem to indicate that, also for Configuration 4, the SB mechanical behaviour significantly affects the FW performances, being the main responsible of the SDC-IC criteria failure.

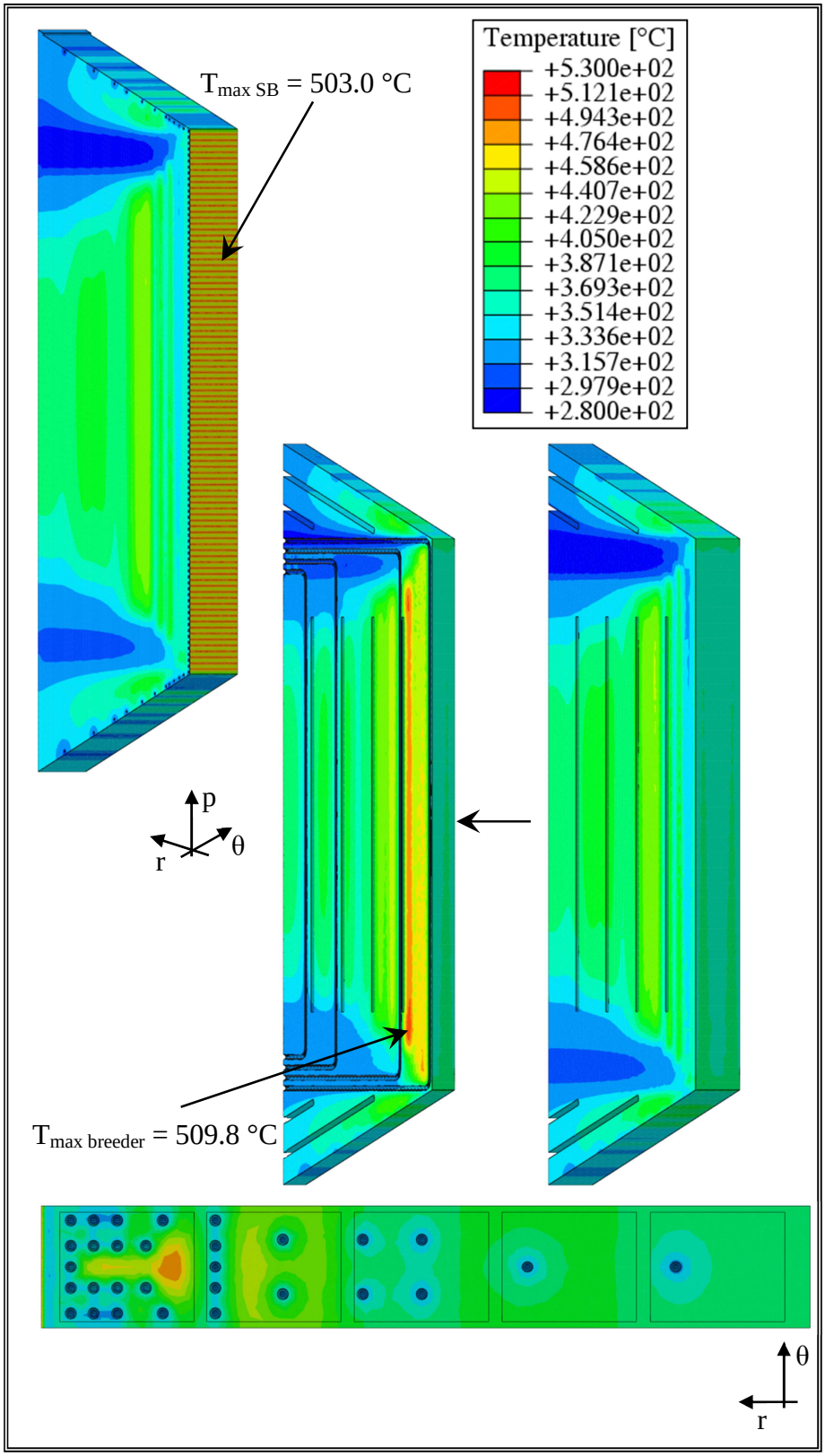


Figure 2-39 - Configuration 1 thermal field.

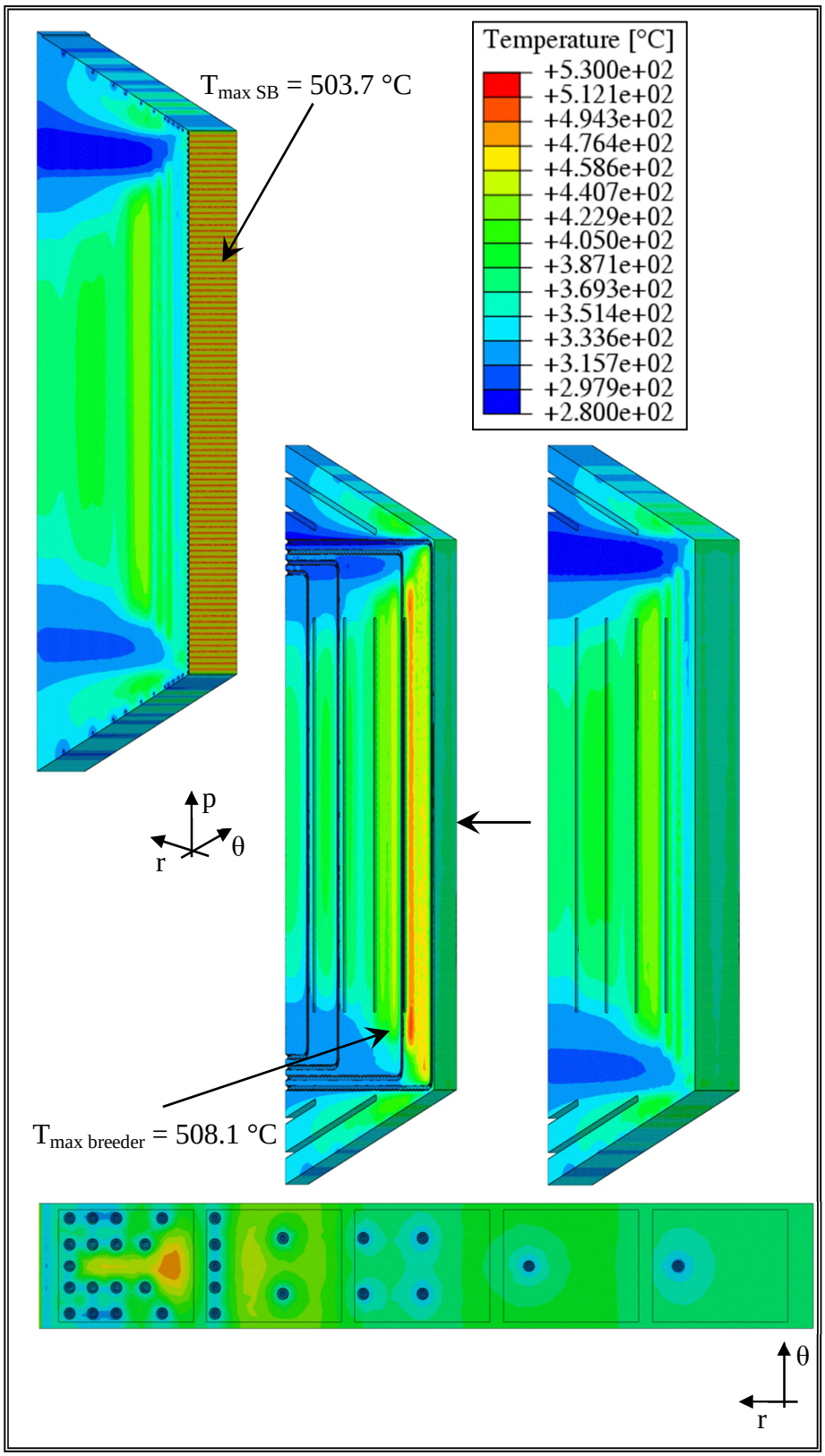


Figure 2-40 - Configuration 2 thermal field.

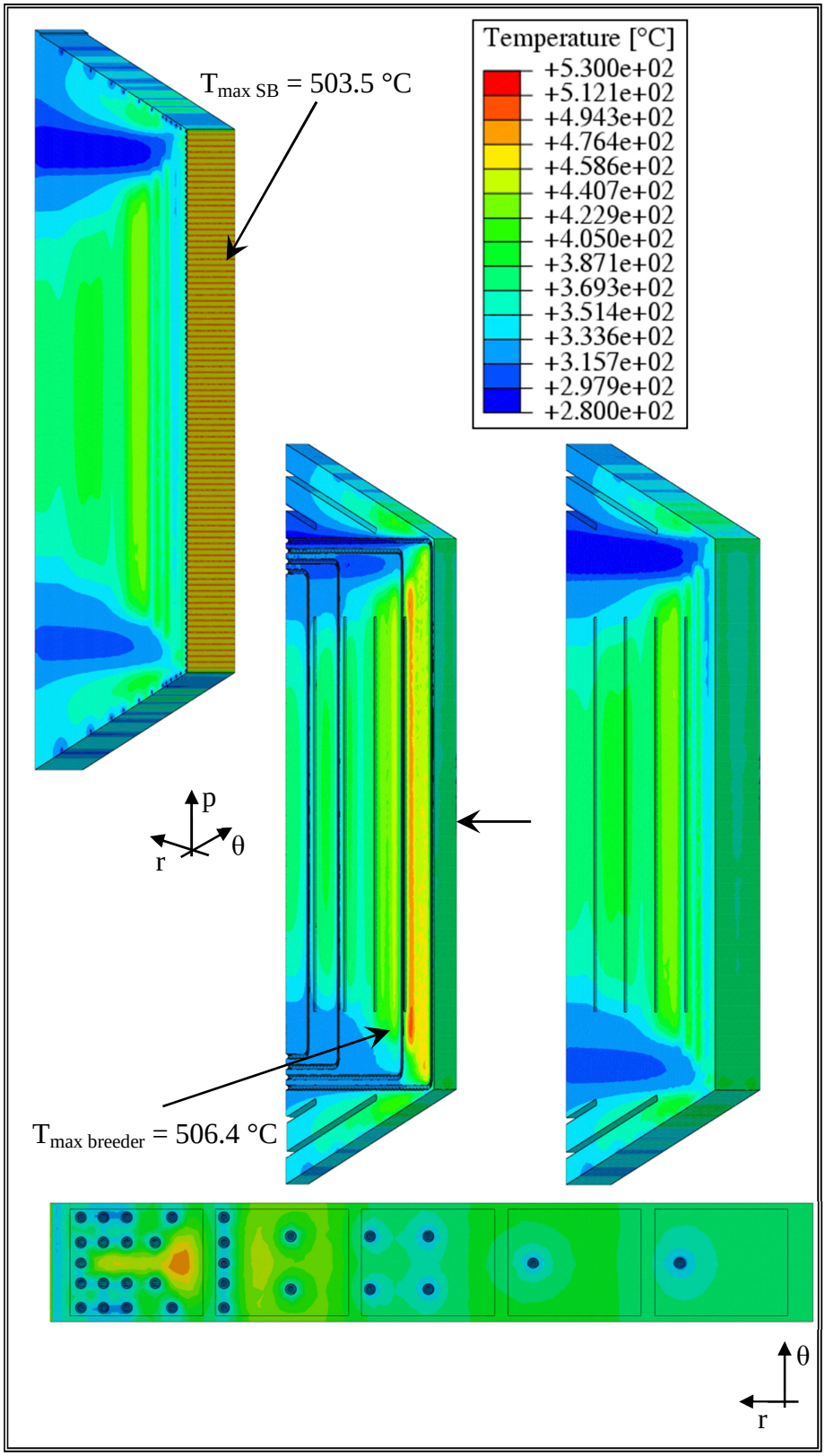


Figure 2-41 - Configuration 3 thermal field.

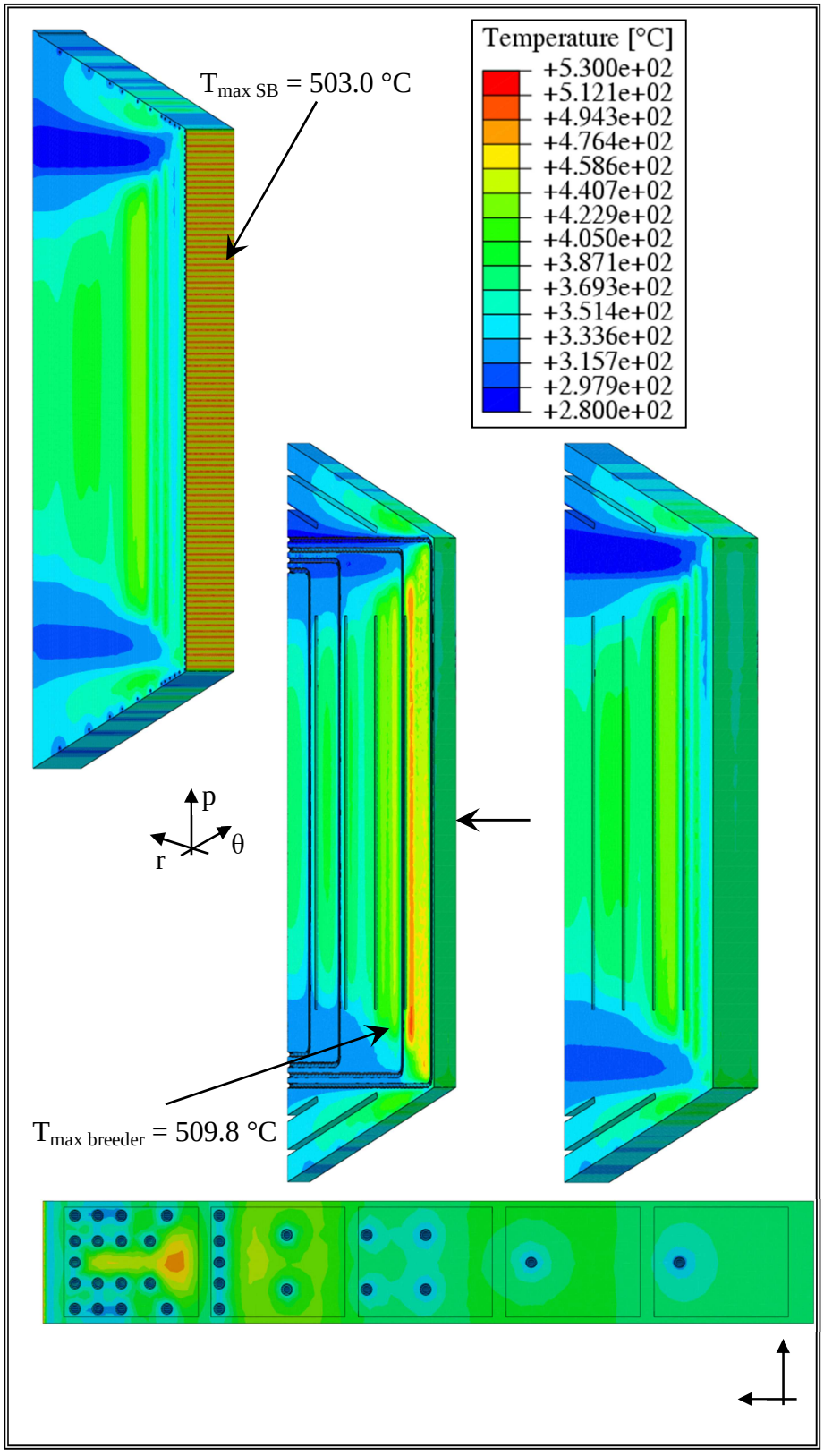


Figure 2-42 - Configuration 4 thermal field.

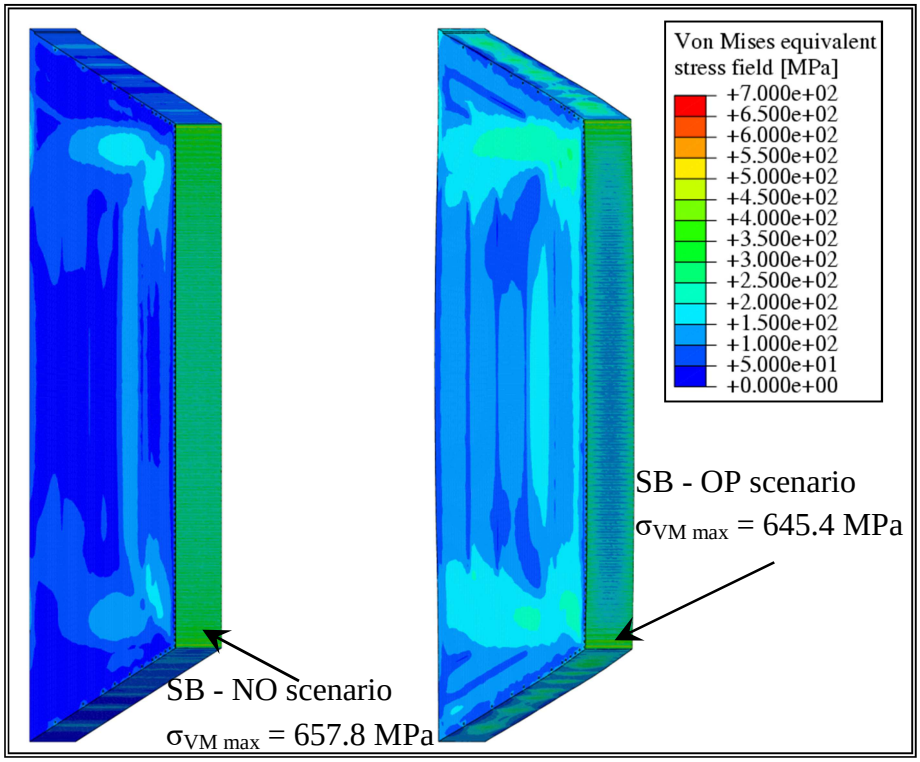


Figure 2-43 - Configuration 1 SB Von Mises equivalent stress field.

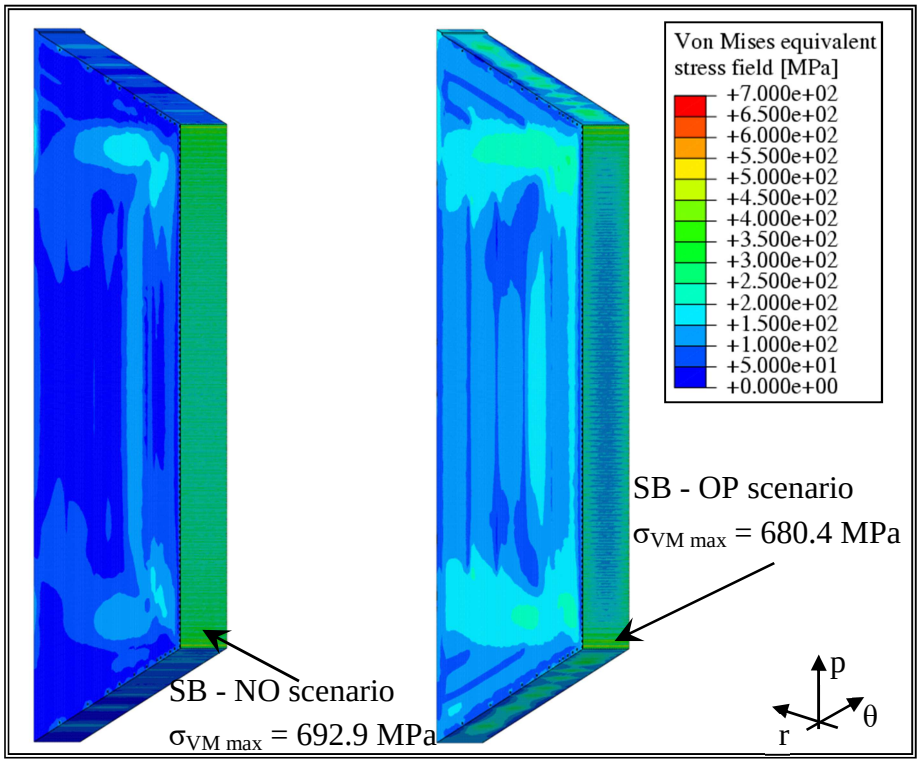


Figure 2-44 - Configuration 2 SB Von Mises equivalent stress field.

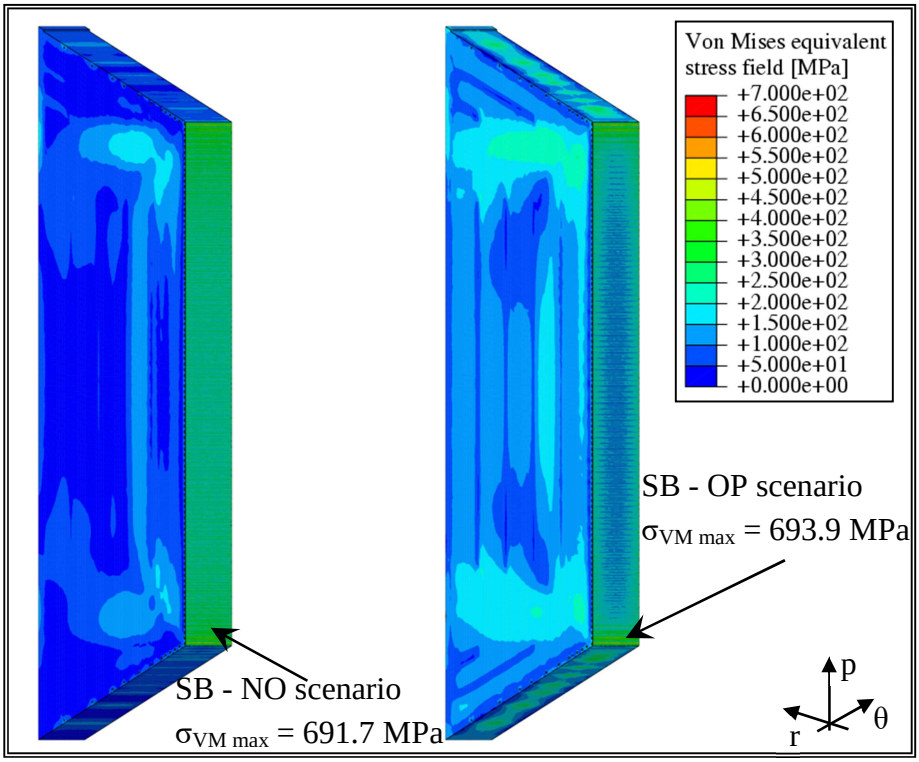


Figure 2-45 - Configuration 3 SB Von Mises equivalent stress field.

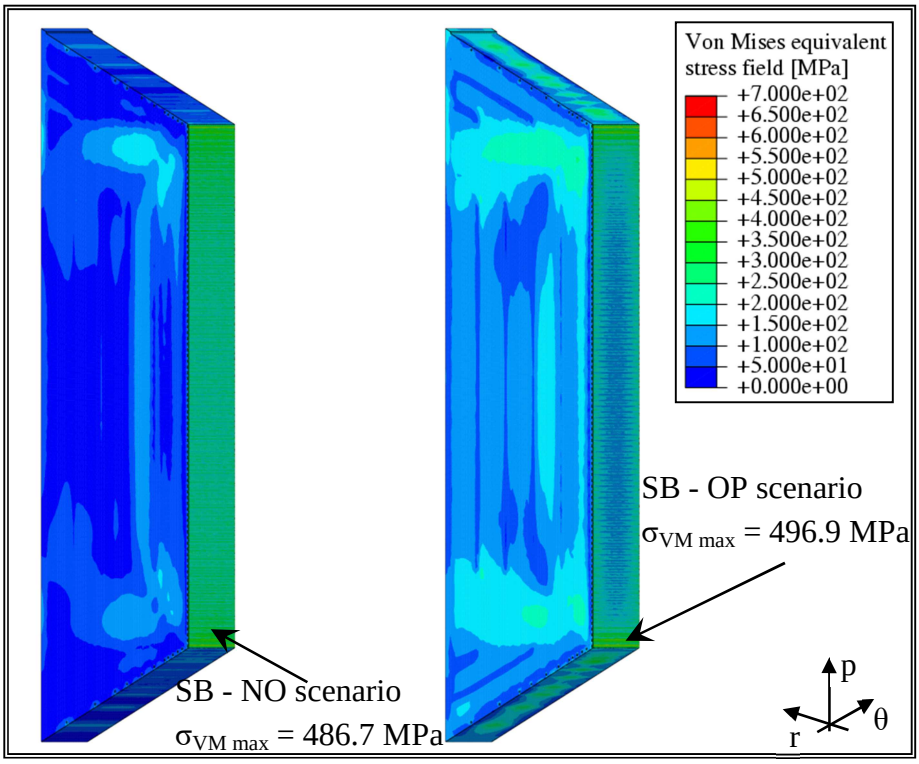


Figure 2-46 - Configuration 3 SB Von Mises equivalent stress field.

Table 2-14 - SDC-IC safety criteria - paths located close to a radial-poloidal SPs.

| **Configuration 1** | | | | | | |
|---|---|---|---|---|---|---|
| | **Stress linearization path** | | | | | |
| | **AB** | **CD** | **EF** | **MN** | **OP** | **QR** |
| $T_{Max\text{-}Path}$ [°C] | 362.6 | 447.9 | 494.0 | 354.7 | 430.5 | 491.7 |
| **Level A criteria** | | | | | | |
| $P_m/S_m$ | 0.037 | 0.062 | 0.040 | 0.035 | 0.074 | 0.034 |
| $(P_m+P_b)/K_{eff}$ Sm | 0.045 | 0.049 | 0.080 | 0.050 | 0.057 | 0.070 |
| $(P_m+Q_m)/S_e$ | 0.384 | 1.117 | 0.343 | 0.406 | 2.282 | 0.484 |
| $P_m/S_t$ | 0.020 | 0.045 | 0.035 | 0.019 | 0.050 | 0.030 |
| $(P_m+P_b/K)/S_t$ | 0.033 | 0.052 | 0.091 | 0.036 | 0.057 | 0.078 |
| **Level D criteria** | | | | | | |
| $P_m/\sigma_{lim}$ | 0.223 | 0.203 | 0.201 | 0.217 | 0.254 | 0.246 |
| $(P_m+P_b)/K_{eff}\ \sigma_{lim}$ | 0.209 | 0.138 | 0.220 | 0.173 | 0.171 | 0.206 |
| $(P_m+Q_m)/2\ S_e$ | 0.339 | 0.423 | 0.309 | 0.359 | 1.223 | 0.396 |
| $W_t[1.35\ (P_m+P_b/K)]$ | - | - | 5.6E-05 | - | - | 4.8E-06 |

Table 2-15 - SDC-IC safety criteria - paths located at the toroidal mid plane section.

| **Configuration 1** | | | | | | |
|---|---|---|---|---|---|---|
| | **Stress linearization path** | | | | | |
| | **AB** | **CD** | **EF** | **MN** | **OP** | **QR** |
| $T_{Max\text{-}Path}$ [°C] | 361.4 | 448.9 | 494.3 | 357.1 | 430.8 | 488.2 |
| **Level A criteria** | | | | | | |
| $P_m/S_m$ | 0.044 | 0.088 | 0.021 | 0.36 | 0.083 | 0.032 |
| $(P_m+P_b)/K_{eff}$ Sm | 0.051 | 0.064 | 0.065 | 0.047 | 0.063 | 0.072 |
| $(P_m+Q_m)/S_e$ | 0.542 | 1.180 | 0.440 | 0.244 | 2.349 | 0.291 |
| $P_m/S_t$ | 0.024 | 0.064 | 0.019 | 0.020 | 0.057 | 0.027 |
| $(P_m+P_b/K)/S_t$ | 0.038 | 0.069 | 0.072 | 0.035 | 0.063 | 0.079 |
| **Level D criteria** | | | | | | |
| $P_m/\sigma_{lim}$ | 0.274 | 0.534 | 0.333 | 0.202 | 0.278 | 0.246 |
| $(P_m+P_b)/K_{eff}\ \sigma_{lim}$ | 0.221 | 0.357 | 0.301 | 0.156 | 0.187 | 0.202 |
| $(P_m+Q_m)/2\ S_e$ | 0.483 | 0.217 | 0.479 | 0.269 | 1.238 | 0.314 |
| $W_t[1.35\ (P_m+P_b/K)]$ | - | - | 7.1E-05 | - | - | 3.0E-06 |

Table 2-16 - SDC-IC safety criteria - paths located close to a radial-poloidal SPs.

| **Configuration 2** | | | | | | |
|---|---|---|---|---|---|---|
| | **Stress linearization path** | | | | | |
| | **AB** | **CD** | **EF** | **MN** | **OP** | **QR** |
| $T_{Max\text{-}Path}$ [°C] | 366.8 | 448.2 | 496.5 | 354.7 | 430.4 | 490.4 |
| **Level A criteria** | | | | | | |
| $P_m/S_m$ | 0.038 | 0.071 | 0.031 | 0.041 | 0.091 | 0.039 |
| $(P_m+P_b)/K_{eff}$ Sm | 0.050 | 0.048 | 0.067 | 0.054 | 0.069 | 0.065 |
| $(P_m+Q_m)/S_e$ | 0.401 | 1.083 | 0.374 | 0.394 | 2.220 | 0.497 |
| $P_m/S_t$ | 0.021 | 0.05 | 0.27 | 0.022 | 0.062 | 0.034 |
| $(P_m+P_b/K)/S_t$ | 0.038 | 0.052 | 0.076 | 0.039 | 0.069 | 0.074 |
| **Level D criteria** | | | | | | |
| $P_m/\sigma_{lim}$ | 0.202 | 0.205 | 0.177 | 0.237 | 0.251 | 0.268 |
| $(P_m+P_b)/K_{eff}$ $\sigma_{lim}$ | 0.183 | 0.140 | 0.204 | 0.169 | 0.168 | 0.201 |
| $(P_m+Q_m)/2$ $S_e$ | 0.335 | 0.413 | 0.279 | 0.363 | 1.188 | 0.409 |
| $W_t$[1.35 $(P_m+P_b/K)$] | - | - | 3.4E-05 | - | - | 1.3E-05 |

Table 2-17 - SDC-IC safety criteria - paths located at the toroidal mid plane section.

| **Configuration 2** | | | | | | |
|---|---|---|---|---|---|---|
| | **Stress linearization path** | | | | | |
| | **AB** | **CD** | **EF** | **MN** | **OP** | **QR** |
| $T_{Max\text{-}Path}$ [°C] | 363.9 | 449.4 | 492.9 | 356.3 | 432.3 | 490.3 |
| **Level A criteria** | | | | | | |
| $P_m/S_m$ | 0.046 | 0.086 | 0.024 | 0.051 | 0.095 | 0.038 |
| $(P_m+P_b)/K_{eff}$ Sm | 0.060 | 0.63 | 0.067 | 0.066 | 0.069 | 0.071 |
| $(P_m+Q_m)/S_e$ | 0.459 | 1.073 | 0.374 | 0.226 | 2.308 | 0.307 |
| $P_m/S_t$ | 0.026 | 0.063 | 0.021 | 0.028 | 0.066 | 0.033 |
| $(P_m+P_b/K)/S_t$ | 0.045 | 0.068 | 0.074 | 0.048 | 0.070 | 0.080 |
| **Level D criteria** | | | | | | |
| $P_m/\sigma_{lim}$ | 0.259 | 0.526 | 0.307 | 0.227 | 0.286 | 0.243 |
| $(P_m+P_b)/K_{eff}$ $\sigma_{lim}$ | 0.252 | 0.355 | 0.323 | 0.192 | 0.192 | 0.223 |
| $(P_m+Q_m)/2$ $S_e$ | 0.424 | 0.203 | 0.391 | 0.265 | 1.227 | 0.254 |
| $W_t$[1.35 $(P_m+P_b/K)$] | - | - | 1.2E-05 | - | - | 2.9E-06 |

Table 2-18 - SDC-IC safety criteria - paths located close to a radial-poloidal SPs.

| Configuration 3 | | | | | | |
|---|---|---|---|---|---|---|
| | Stress linearization path | | | | | |
| | AB | CD | EF | MN | OP | QR |
| $T_{Max-Path}$ [°C] | 370.2 | 447.8 | 495.1 | 355.0 | 424.8 | 490.4 |
| **Level A criteria** | | | | | | |
| $P_m/S_m$ | 0.040 | 0.063 | 0.031 | 0.038 | 0.089 | 0.036 |
| $(P_m+P_b)/K_{eff}$ Sm | 0.051 | 0.052 | 0.069 | 0.056 | 0.063 | 0.064 |
| $(P_m+Q_m)/S_e$ | 0.334 | 1.008 | 0.359 | 0.408 | 2.068 | 0.500 |
| $P_m/S_t$ | 0.022 | 0.046 | 0.027 | 0.020 | 0.060 | 0.031 |
| $(P_m+P_b/K)/S_t$ | 0.039 | 0.055 | 0.078 | 0.040 | 0.063 | 0.072 |
| **Level D criteria** | | | | | | |
| $P_m/\sigma_{lim}$ | 0.199 | 0.205 | 0.183 | 0.231 | 0.252 | 0.263 |
| $(P_m+P_b)/K_{eff}$ $\sigma_{lim}$ | 0.165 | 0.143 | 0.197 | 0.169 | 0.169 | 0.205 |
| $(P_m+Q_m)/2$ $S_e$ | 0.296 | 0.353 | 0.282 | 0.360 | 1.123 | 0.411 |
| $W_t$[1.35 $(P_m+P_b/K)$] | - | - | 2.4E-05 | - | - | 1.0E-05 |

Table 2-19 - SDC-IC safety criteria - paths located at the toroidal mid plane section.

| Configuration 3 | | | | | | |
|---|---|---|---|---|---|---|
| | Stress linearization path | | | | | |
| | AB | CD | EF | MN | OP | QR |
| $T_{Max-Path}$ [°C] | 366.9 | 449.0 | 493.5 | 356.7 | 427.2 | 486.5 |
| **Level A criteria** | | | | | | |
| $P_m/S_m$ | 0.46 | 0.084 | 0.023 | 0.039 | 0.094 | 0.033 |
| $(P_m+P_b)/K_{eff}$ Sm | 0.58 | 0.061 | 0.066 | 0.057 | 0.064 | 0.068 |
| $(P_m+Q_m)/S_e$ | 0.413 | 1.100 | 0.369 | 0.210 | 2.203 | 0.309 |
| $P_m/S_t$ | 0.026 | 0.062 | 0.020 | 0.021 | 0.064 | 0.028 |
| $(P_m+P_b/K)/S_t$ | 0.044 | 0.066 | 0.073 | 0.041 | 0.065 | 0.074 |
| **Level D criteria** | | | | | | |
| $P_m/\sigma_{lim}$ | 0.260 | 0.512 | 0.311 | 0.208 | 0.283 | 0.232 |
| $(P_m+P_b)/K_{eff}$ $\sigma_{lim}$ | 0.242 | 0.344 | 0.310 | 0.191 | 0.190 | 0.224 |
| $(P_m+Q_m)/2$ $S_e$ | 0.400 | 0.213 | 0.380 | 0.254 | 1.192 | 0.262 |
| $W_t$[1.35 $(P_m+P_b/K)$] | - | - | 1.8E-05 | - | - | 2.1E-06 |

Table 2-20 - SDC-IC safety criteria - paths located close to a radial-poloidal SPs.

| **Configuration 4** | | | | | | |
|---|---|---|---|---|---|---|
| | **Stress linearization path** | | | | | |
| | **AB** | **CD** | **EF** | **MN** | **OP** | **QR** |
| $T_{Max-Path}$ [°C] | 373.2 | 447.9 | 496.5 | 357.5 | 423.2 | 490.3 |
| **Level A criteria** | | | | | | |
| $P_m/S_m$ | 0.037 | 0.066 | 0.028 | 0.039 | 0.093 | 0.036 |
| $(P_m+P_b)/K_{eff}$ Sm | 0.049 | 0.052 | 0.066 | 0.057 | 0.063 | 0.067 |
| $(P_m+Q_m)/S_e$ | 0.317 | 1.036 | 0.332 | 0.405 | 2.028 | 0.473 |
| $P_m/S_t$ | 0.021 | 0.048 | 0.024 | 0.021 | 0.062 | 0.031 |
| $(P_m+P_b/K)/S_t$ | 0.038 | 0.055 | 0.074 | 0.041 | 0.063 | 0.075 |
| **Level D criteria** | | | | | | |
| $P_m/\sigma_{lim}$ | 0.198 | 0.207 | 0.186 | 0.233 | 0.250 | 0.263 |
| $(P_m+P_b)/K_{eff}$ $\sigma_{lim}$ | 0.164 | 0.143 | 0.194 | 0.169 | 0.169 | 0.203 |
| $(P_m+Q_m)/2$ $S_e$ | 0.289 | 0.361 | 0.266 | 0.358 | 1.102 | 0.394 |
| $W_t$[1.35 $(P_m+P_b/K)$] | 1.9E-12 | 2.0E-08 | 2.6E-05 | 1.1E-13 | 4.2E-09 | 1.1E-05 |

Table 2-21 - SDC-IC safety criteria - paths located at the toroidal mid plane section.

| **Configuration 4** | | | | | | |
|---|---|---|---|---|---|---|
| | **Stress linearization path** | | | | | |
| | **AB** | **CD** | **EF** | **MN** | **OP** | **QR** |
| $T_{Max-Path}$ [°C] | 369.3 | 449.3 | 493.0 | 356.7 | 425.0 | 488.1 |
| **Level A criteria** | | | | | | |
| $P_m/S_m$ | 0.040 | 0.087 | 0.022 | 0.045 | 0.098 | 0.032 |
| $(P_m+P_b)/K_{eff}$ Sm | 0.050 | 0.064 | 0.064 | 0.061 | 0.66 | 0.062 |
| $(P_m+Q_m)/S_e$ | 0.345 | 1.059 | 0.350 | 0.267 | 2.140 | 0.320 |
| $P_m/S_t$ | 0.023 | 0.063 | 0.019 | 0.024 | 0.066 | 0.028 |
| $(P_m+P_b/K)/S_t$ | 0.038 | 0.069 | 0.070 | 0.045 | 0.066 | 0.069 |
| **Level D criteria** | | | | | | |
| $P_m/\sigma_{lim}$ | 0.251 | 0.501 | 0.309 | 0.227 | 0.277 | 0.235 |
| $(P_m+P_b)/K_{eff}$ $\sigma_{lim}$ | 0.237 | 0.337 | 0.297 | 0.183 | 0.186 | 0.218 |
| $(P_m+Q_m)/2$ $S_e$ | 0.354 | 0.194 | 0.362 | 0.269 | 1.158 | 0.251 |
| $W_t$[1.35 $(P_m+P_b/K)$] | 6.4E-14 | 4.3E-04 | 1.9E-05 | 2.8E-14 | 1.4E-08 | 1.7E-06 |

## 2.4 Summary of the First Wall design activity

Within the framework of the DEMO R&D activities envisaged by the EUROfusion WPBB action, a research campaign has been carried out during the Ph.D. course in order to investigate the steady state thermo-mechanical performances of the DEMO WCLL breeding blanket First Wall and optimize its geometric configuration, from both thermal and mechanical point of view.

In particular, attention has been paid to the FW flat concept, equipped with square cooling channels, of the DEMO WCLL outboard breeding blanket equatorial module. In the first phase, a parametric assessment has been launched, taking into account the four FW characteristic geometric parameters potentially affecting FW thermal-hydraulic and thermo-mechanical performances. To this purpose, a set of 5929 different flat FW geometric configurations have been considered, resulting from the combination of the selected values of these parameters. Moreover, in order to assess the maximum heat flux arising from plasma that each single configuration is able to safely withstand under steady state conditions, their thermo-mechanical behaviour has been numerically simulated when exposed to 26 different values of $\Phi$, equally spaced in the range 0.5 - 3 MW/m$^2$, for an overall set of 154154 cases investigated.

Thermal cases in which the predicted maximum temperature within the FW has exceeded the EUROFER maximum allowable value of 550 °C and the calculated cooling water velocity has resulted higher than the upper limit of 8 m/s, have been considered as unacceptable. In particular, thermal analyses have shown that 66443 cases fulfil the thermal-hydraulic restrictions imposed. For these cases mechanical analysis have been performed under both Normal Operation and Over-Pressurization steady state loading scenarios.

A stress linearization procedure has been performed along some significant FW paths in order to check the fulfilment of the SDC-IC criteria foreseen for Level A and Level D loading conditions. Mechanical results have shown that only 4 configurations are able to withstand a heat flux up to 2 MW/m$^2$ on the FW plasma facing surface.

These potentially optimized FW geometric configurations have been considered for the second phase of the FW design activity, where their thermo-mechanical performances under Normal Operation and Over-Pressurization loading scenarios have been investigated adopting more realistic 3D FEM models representing the DEMO WCLL outboard breeding blanket equatorial module, based on the layout released by CEA in 2012, properly endowed with the 4 FW potentially optimized configurations. Thermo-mechanical analyses have been properly carried out in order to more realistically assess, in accordance with SDC-IC structural design criteria, the potential influence of the Segment Box on the 4 selected FW configurations. These thermo-mechanical results have indicated that, when the mechanical action of the SB on the FW is more realistically represented and investigated, the FW regions near to the caps

are the most stressed ones and the SDC-IC safety criteria are not completely met. Consequently, it can be concluded that a deep DEMO WCLL BB outboard equatorial module design review is needed in order to reduce the stress intensity and ensure the total SDC-IC design criteria fulfilment within the FW. Anyway, Configuration 4 might be taken into account in order to update the DEMO WCLL BB outboard equatorial module geometric design since it is the most promising one among those investigated in this study. In fact, on the basis of the present study, the preliminary module design developed by ENEA, within the framework of EUROfusion WPBB activities, and shown in § 1.4 has been developed assuming a FW configuration very similar to Configuration 4. The unique difference between the obtained FW layout from the parametric study and that effectively assumed for the module design is represented by the steel thickness interposed between tungsten and cooling channels, increased up to 3 mm in order to meet manufacturing requirements.

Moreover, the automated procedure set-up in this work and devoted to optimize the FW geometric configuration might be exported for future similar applications, since the advancements in the DEMO design will implicate an update of the design requirements with a probable necessity to further optimize the blanket components, included FW.

## 2.5 The Stiffening Plates design activity

Results of the previous thermo-mechanical campaigns of analysis, regarding the FW geometric optimization, have suggested that a complete design review of the DEMO WCLL BB outboard equatorial module is needed in order to obtain a geometric configuration able to safely withstand thermo-mechanical loads it undergoes under the envisaged Normal Operations and Over-Pressurization steady-state loading conditions, totally fulfilling the SDC-IC structural design criteria. In particular, during the previously carried out studies, it has been observed that the Segment Box (composed of the Caps, Back-Plate and Stiffening Plates) thermo-mechanical behaviour affects, in a non-negligible manner, the stress values arising within FW. For this reason, modifications in the SPs design appear to be necessary in order to achieve a SP geometric configuration able to ensure the SB structural integrity under both nominal and accidental loading conditions reducing, at the same time, its influence on the FW thermo-mechanical performances. To this purpose, a research campaign devoted to perform the geometric optimization of the Stiffening Plates has been performed during the Ph.D. course, adopting the configuration of the SB of the DEMO WCLL BB outboard equatorial module released by CEA in 2012 and replacing the original SP grid (stiffening grid) with potentially optimized ones purposely set-up to perform the parametric campaign of thermo-mechanical analysis. In particular, the different SP geometric configurations taken into account differ each other in the number and thickness of the plates, since these two

geometric quantities have been selected as parameters. In the present study the spatial arrangement of the stiffening grid has been modified respect to the module designed by the CEA, on the basis of the DEMO WCLL BB baseline given by the EUROfusion lead engineers. In particular, the CEA SP design was characterized by a stiffening grid composed of radial-toroidal and poloidal-toroidal SPs (Fig. 2-47), while in this study the CEA poloidal-toroidal SPs have been replaced by radial-poloidal ones. This new assumption on the SP spatial arrangement leads to a strong modification of the breeder flow path inside the module, causing the appearance of radial-toroidal breeder cells in the module design and the consequent modification of the cooling DWT spatial arrangement. In fact, differently from the DWT layout shown in § 2.3.1.2 and designed by CEA in 2012, the replacement of the poloidal-toroidal SPs with radial poloidal ones makes the DWT layout radial-toroidal too. Nevertheless, in this parametric study the presence of the DWTs, which do not have structural function, has been neglected since the main purpose of the parametric campaign of analysis has been the investigation of the potential influence of the number and thickness of the SPs on the SB thermo-mechanical behaviour. Once adopted the aforesaid SP design option, the potential influence of the SP number and thickness on the SB of the 2012 DEMO WCLL BB outboard equatorial module has been investigated, in order to select a potentially optimized stiffening grid configuration able to allow the SB safely withstand the thermo-mechanical loads it undergoes under steady-state conservative loading conditions derived from the OP scenario.

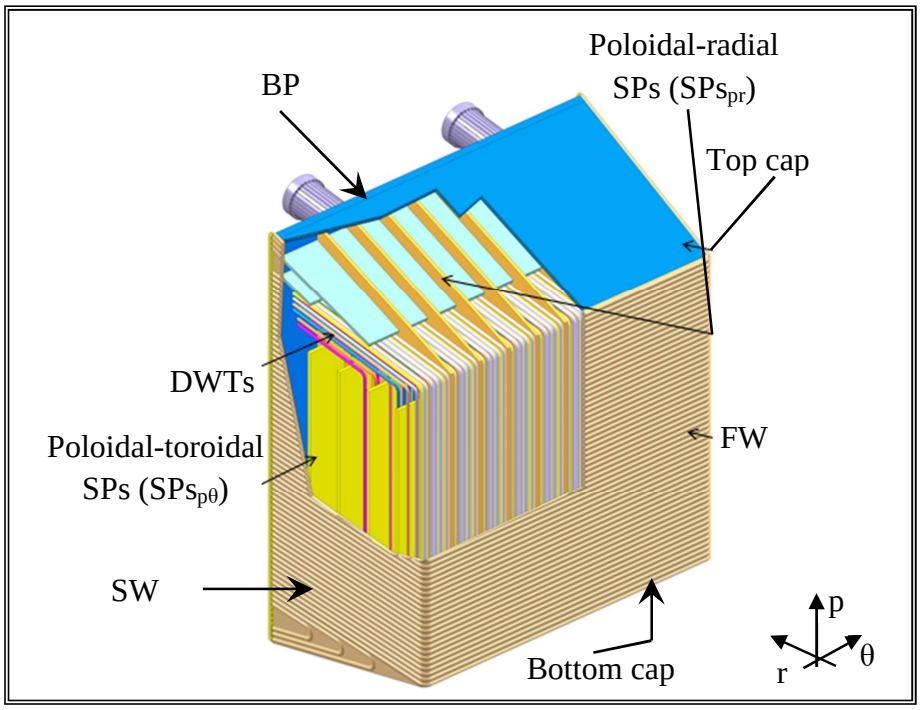


Figure 2-47 - DEMO WCLL BB outboard equatorial module designed by CEA in 2012.

### 2.5.1 The geometric parameters

In order to perform the geometric optimization of the SP design, a stiffening grid composed of radial-poloidal (rp) and radial-toroidal (rθ) plates has been considered in the present study, developed within the framework of the WPBB activities of the EUROfusion consortium action. As already said before, the assumed stiffening grid layout is alternative to that previously defined by CEA in the old design of the DEMO WCLL BB outboard equatorial module.

The so formed stiffening grid divides the SB internals in radial-toroidal elemental breeder cells, which are repeated in poloidal direction in order to form the DEMO WCLL BB outboard equatorial module layout. Inside each radial-toroidal cell, a radial-poloidal-radial breeder flow path is envisaged.

Moreover, inside each breeder cell, a further pierced radial-toroidal SP is foreseen, with the main function of addressing the lithium flow towards its path inside the cell. In fact, the pierced radial-toroidal SPs allow the breeder circulation inside the module along a radial-poloidal-radial flow path, while the filled radial-toroidal SPs delimitate the breeder cells inside the SB along the poloidal direction. This means that only the latter have a real structural function, while the former have been conceived for thermal-hydraulic function exclusively. On the other hand, also poloidal-radial SPs have an exclusively structural function without having a strong influence on the breeder circulation.

This SP layout has been considered for the parametric campaign of analysis devoted to geometrically optimize its design, assuming as geometric parameters the number of radial-poloidal ($N_{rp\ SPs}$), radial-toroidal ($N_{r\theta\ SPs}$) and pierced radial-toroidal ($N_{r\theta\ p\ SPs}$) SPs together with their thicknesses, which have been indicated with $S_{rp\ SPs}$, $S_{r\theta\ SPs}$ and $S_{r\theta\ p\ SPs}$ respectively.

For each parameter, a proper range of values has been reasonably defined in order to investigate realistic and manufacturable SPs configurations. Opportune combinations of these parameter values, assumed as physically reasonably and structurally feasible, have been selected and corresponding 3D FEM models, representing the SB designed by CEA endowed with the SPs configuration investigated, have been set-up. Each so obtained 3D FEM model has been assessed, from the thermo-mechanical point of view, under the conservative loading conditions derived from OP steady-state loading scenario in order to investigate its aptitude to make the SB stiffer avoiding the insurgence of excessive displacement, especially along radial and poloidal directions.

To this purpose, attention has been paid, for each SP geometric configuration taken into account, to the poloidal and radial SB displacement fields.

The parameter values relevant to the SP geometric configurations assessed in this study have been summarized in Table 2-22.

Table 2-22 - Summary of the characteristics of the SPs configurations investigated.

| Configuration | $N_{rp\ SPs}$ | $S_{rp\ SPs}$ [m] | $N_{r\theta\ p\ SPs}$ | $S_{r\theta\ p\ SPs}$ [m] | $N_{r\theta\ SPs}$ | $S_{r\theta\ SPs}$ [m] |
|---|---|---|---|---|---|---|
| 0 | 0 | - | 3 | 0.002-0.02 | 0 | - |
| 1 | 5 | 0.016 | 4 | 0.002 | 3 | 0.016 |
| 2 | 5 | 0.016 | 4 | 0.010 | 3 | 0.016 |
| 3 | 5 | 0.016 | 6 | 0.002 | 5 | 0.016 |
| 4 | 5 | 0.016 | 4 | 0.002 | 3 | 0.020 |
| 5 | 5 | 0.016 | 5 | 0.002 | 4 | 0.012 |
| 3 - Case 1 | 5 | 0.016 | 4 ribs | 0.010x0.010 | 5 | 0.016 |
| 3 - Case 2 | 5 | 0.016 | 4 ribs | 0.020x0.020 | 5 | 0.016 |
| 3 - Case3 | 5 | 0.016 | 4 + 8 ribs | 0.002 + 0.010x0.010 | 5 | 0.016 |
| 3 - Case4 | 5 | 0.016 | 4reinf+ 8 ribs | 0.002 + 0.010x0.010 | 5 | 0.016 |
| 3 - new pitch | 5 | 0.016 | 4 | 0.002 | 5 | 0.016 |
| 6 | 5 | 0.016 | 9 | 0.002 | 10 | 0.008 |
| 7 | 5 | 0.016 | 9 | 0.002 | 10 | 0.012 |
| 8 | 10 | 0.012 | 9 | 0.002 | 10 | 0.012 |

### 2.5.2 The FEM models

In order to perform the geometric optimization assessment of the SPs, a 3D FEM model of the DEMO WCLL BB outboard equatorial module SB, designed by CEA in 2012, has been set-up, properly integrated with the different SP geometric configurations investigated. The FEM models realistically reproduce the DEMO WCLL BB outboard equatorial module SB, composed of the FW, the SW, the Caps and the BP, inside which the original stiffening grid has been replaced by the potentially optimized ones, differing each other in the number and the thickness of the SPs.

Since the focus of the research campaign has been put on the optimization of the SP geometric configuration, in order to speed-up calculations, especially in the pre-processing and processing phases, it has been decided to avoid the modelling of eutectic Pb-Li breeder, Double Walled Tubes and coolant flow domain, their thermo-mechanical effects being simulated adopting a proper set of loads, contact models and boundary conditions.

In particular, the first step of the parametric campaign, has represented a preliminary phase

during which the thermo-mechanical performances of the SB of the 2012 DEMO WCLL BB outboard equatorial model properly endowed 6 different SP geometric configurations (from Configuration 0 up to Configuration 5 reported in Table 2-22) have been investigated.

Concerning Configuration 0, the 3D geometric model shown in Figure 2-48 has been realized. It represents the SB of the 2012 DEMO WCLL BB outboard equatorial module endowed only with 3 pierced radial-toroidal SPs. In particular, the central SP is 0.02 m thick while the thickness of the other two amounts to 0.002 m. This SP spatial arrangement originates a unique breeder cell inside the module, since no filled radial-toroidal SPs have been designed in Configuration 0. The geometric domain has been discretized adopting a mesh characterized by 601912 nodes connected in 2151483 linear tetrahedral elements.

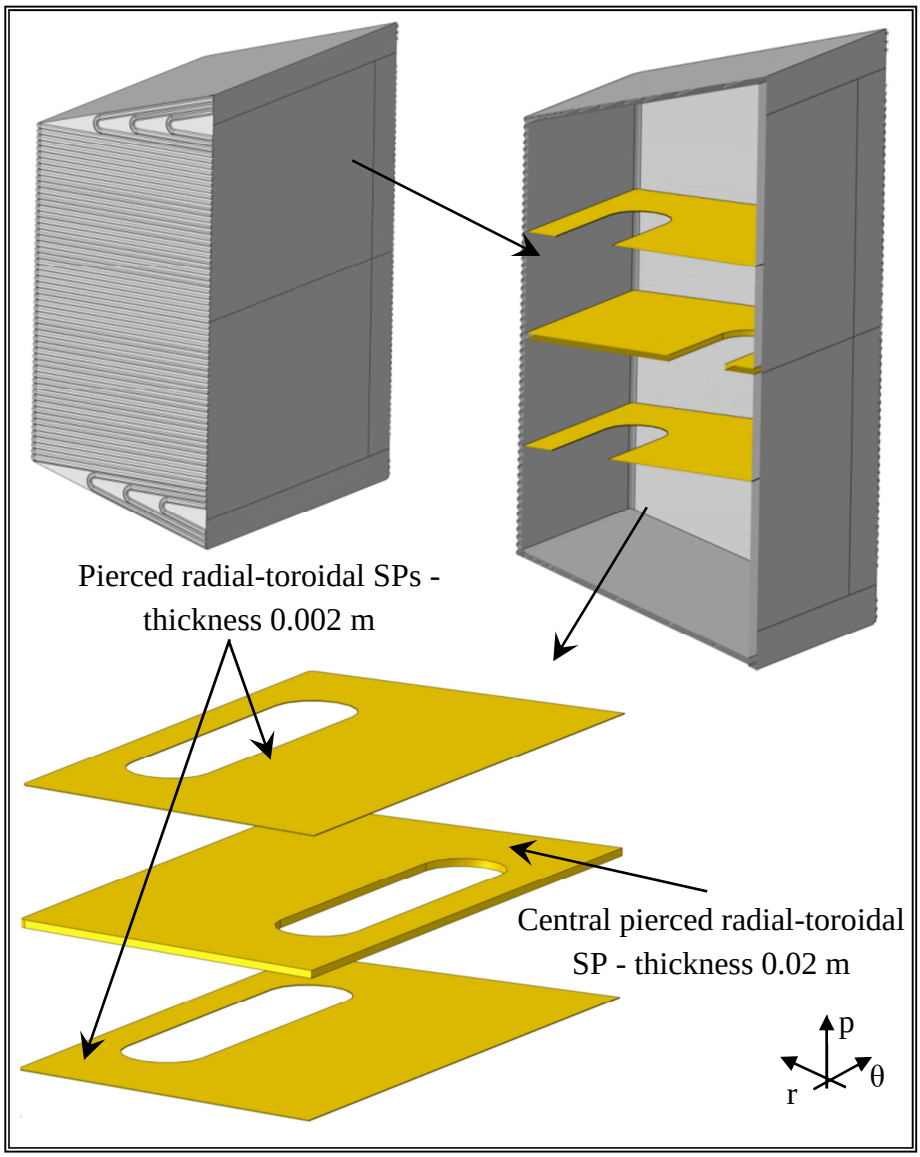


Figure 2-48 - Configuration 0 - 3D geometric model exploded view.

As far as Configuration 1 is concerned, the 3D geometric model shown in Figure 2-49 has been realized. It reproduces the SB of the 2012 DEMO WCLL BB outboard equatorial module, designed by CEA, properly endowed with 3 filled and 4 pierced radial-toroidal SPs. In particular, filled radial-toroidal SPs are 0.016 m thick while the thickness of the pierced ones amounts to 0.002 m. This SP geometric configuration foresees also 5 radial-poloidal SPs 0.016 m thick. The mesh set-up is characterized by 510181 nodes connected in 1841394 linear tetrahedral elements.

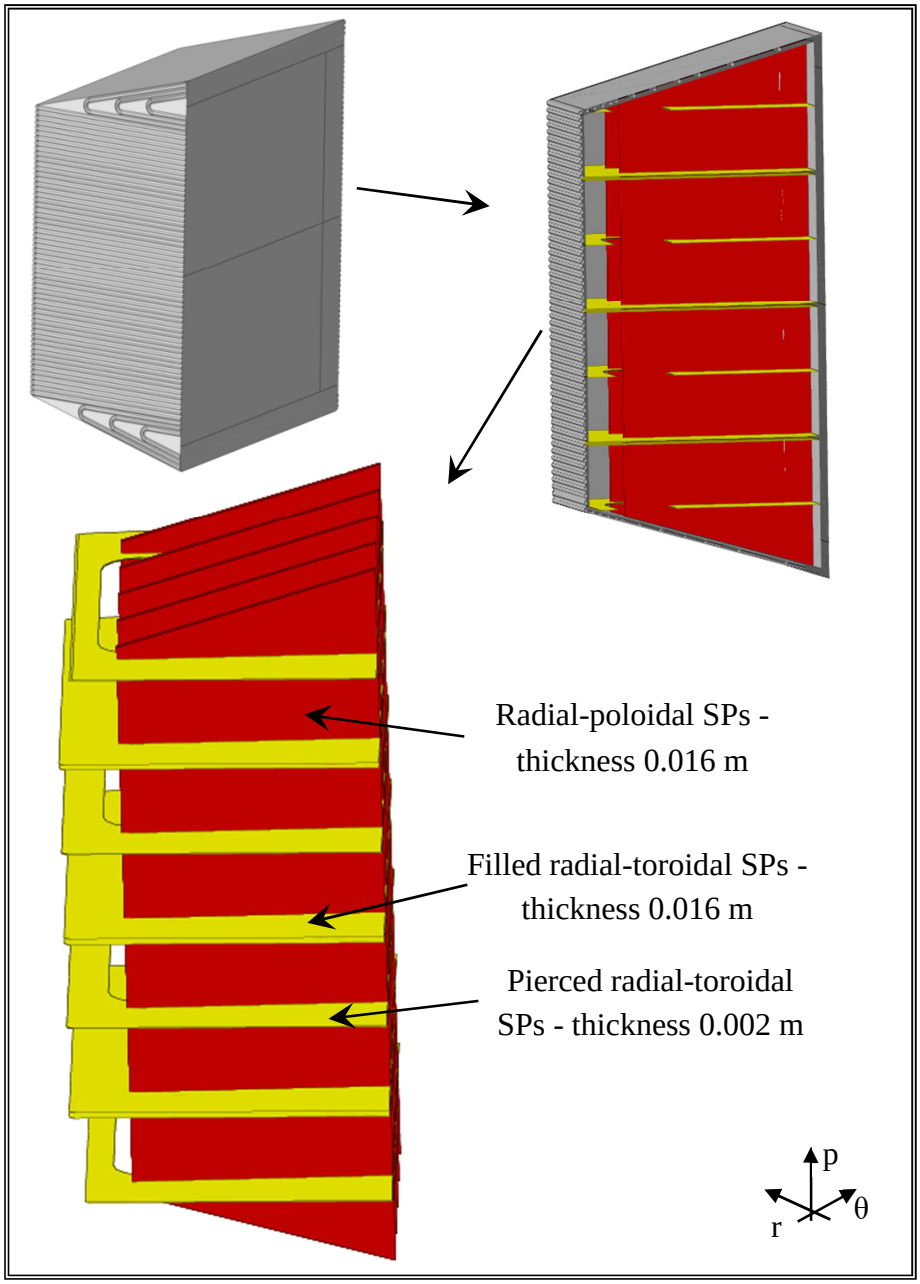


Figure 2-49 - Configuration 1 - 3D geometric model exploded view.

Regarding Configuration 2, the 3D geometric model shown in Figure 2-50 has been realized on the basis of results carried out from Configuration 1. The SB of the 2012 DEMO WCLL BB outboard equatorial module has been again endowed with 3 filled and 4 pierced radial-toroidal SPs, the former still 0.016 m thick while the thickness of the latter has been increased up to 0.010 m. The SP geometric configuration foresees also 5 radial-poloidal SPs 0.016 m thick. The mesh set-up is characterized by 482990 nodes connected in 1815356 linear tetrahedral elements.

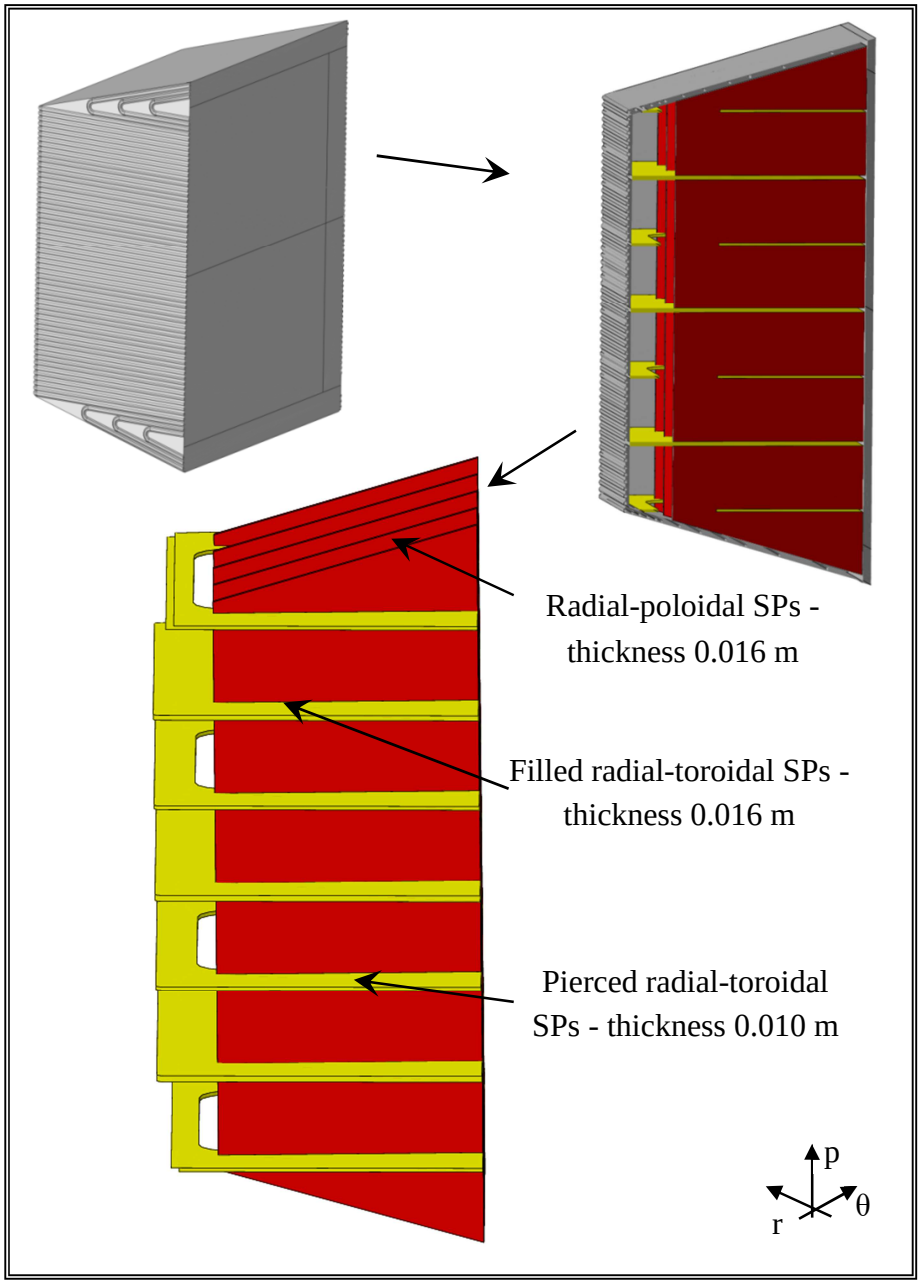


Figure 2-50 - Configuration 2 - 3D geometric model exploded view.

Concerning Configuration 3, the 3D geometric model shown in Figure 2-51 has been realized on the basis of results carried out from Configuration 2. The SB of the 2012 DEMO WCLL BB outboard equatorial module has been endowed with 5 filled and 6 pierced radial-toroidal SPs, the former still 0.016 m thick while the thickness of the latter has been reduced down to 0.002 m given that their number has been increased. The SP geometric configuration still foresees 5 radial-poloidal SPs 0.016 m thick. The mesh set-up is characterized by 517810 nodes connected in 1859187 linear tetrahedral elements.

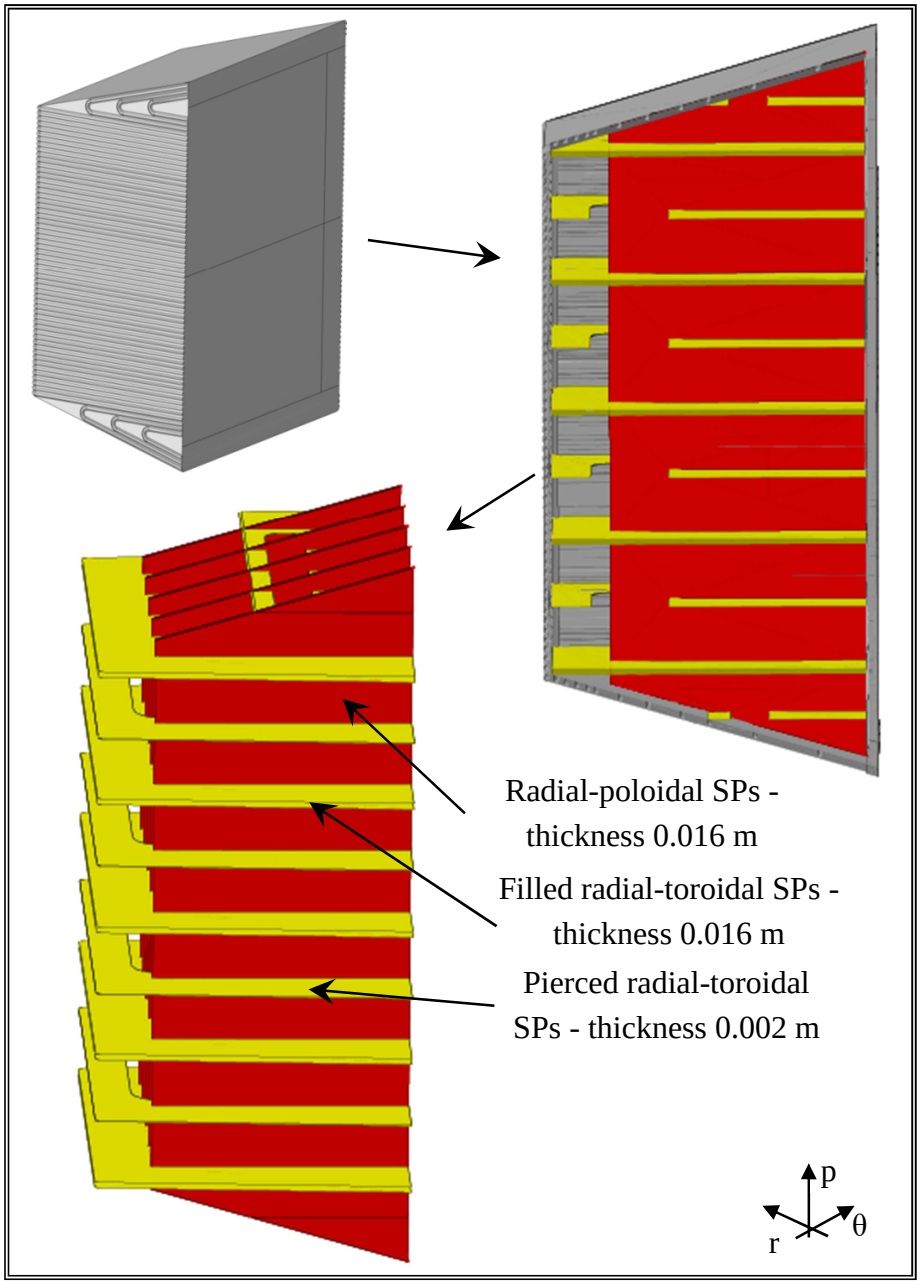


Figure 2-51 - Configuration 3 - 3D geometric model exploded view.

As to Configuration 4, the 3D geometric model shown in Figure 2-52 has been realized as a possible alternative. The SB of the 2012 DEMO WCLL BB outboard equatorial module has been endowed with 3 filled and 4 pierced radial-toroidal SPs, the former 0.020 m thick while the thickness of the latter has been maintained equal to 0.002 m. The SP geometric configuration still foresees 5 radial-poloidal SPs 0.016 m thick. The mesh set-up is characterized by 430863 nodes connected in 1628000 linear tetrahedral elements.

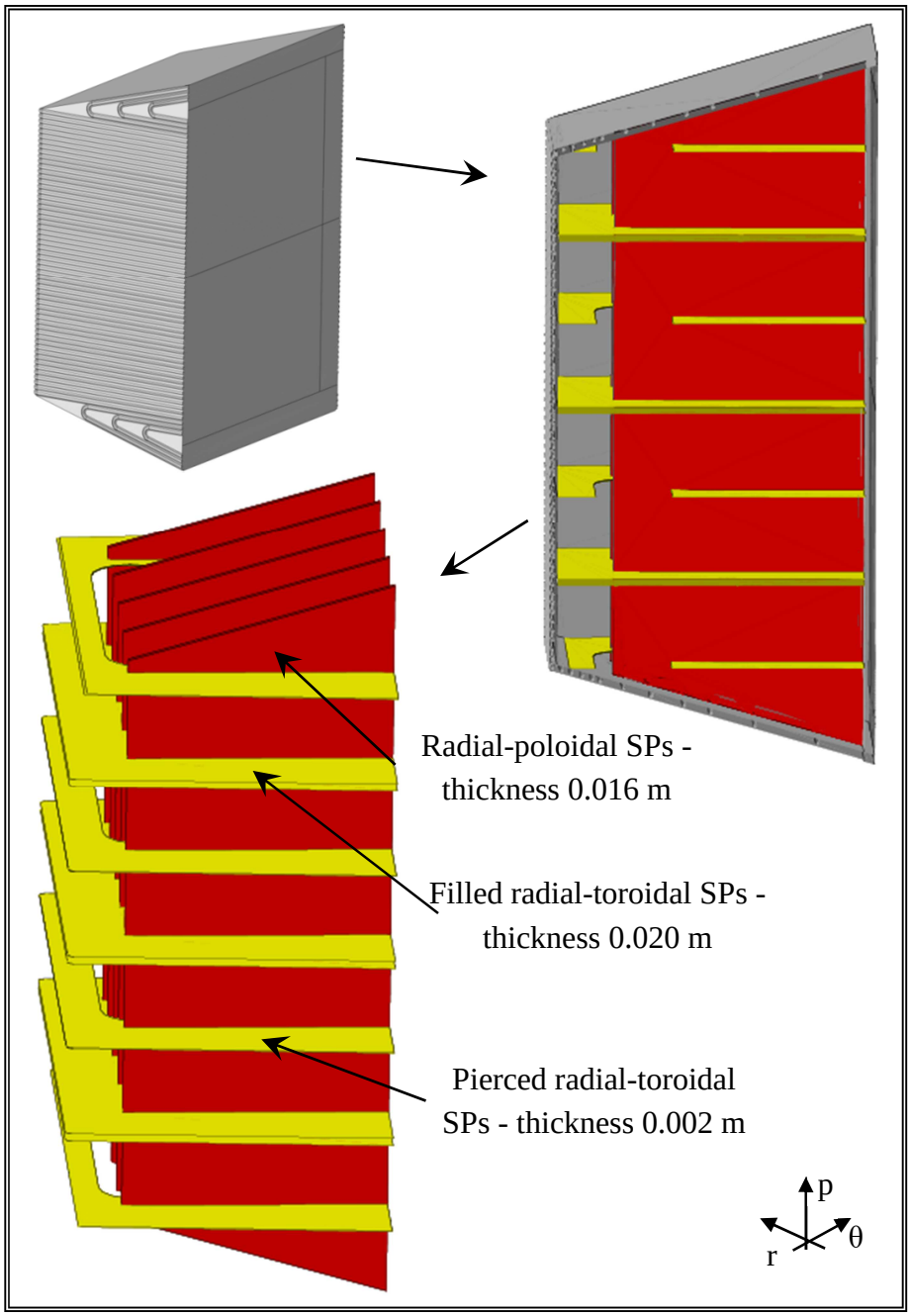


Figure 2-52 - Configuration 4 - 3D geometric model exploded view.

Regarding Configuration 5, the 3D geometric model shown in Figure 2-53 has been realized. The SB of the 2012 DEMO WCLL BB outboard equatorial module has been endowed with 4 filled and 5 pierced radial-toroidal SPs, the former 0.012 m thick while the thickness of the latter has been maintained equal to 0.002 m. The SP geometric configuration still foresees 5 radial-poloidal SPs 0.016 m thick. The mesh set-up is characterized by 469511 nodes connected in 1784410 linear tetrahedral elements.

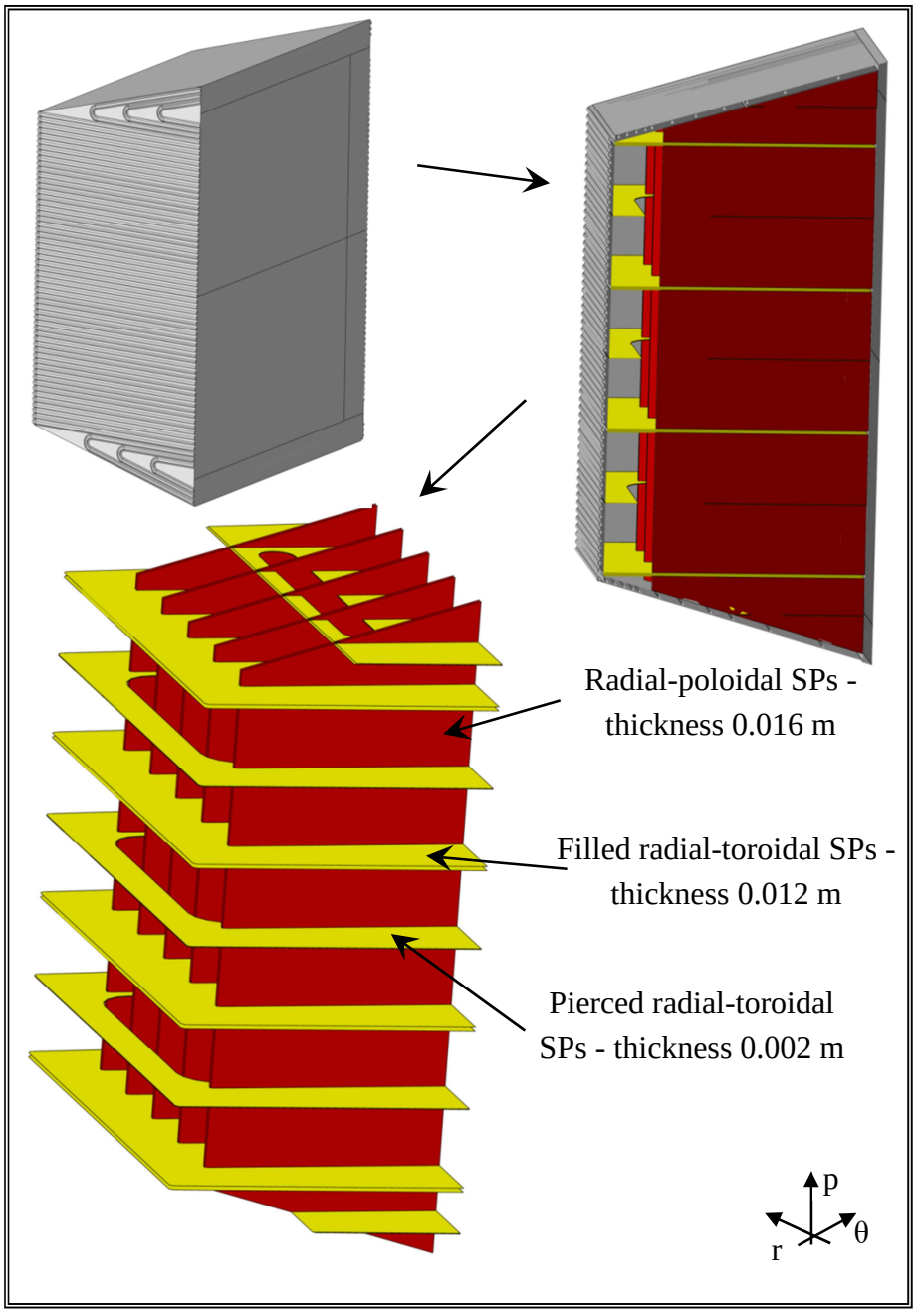


Figure 2-53 - Configuration 5 - 3D geometric model exploded view.

The second step of the SP optimization procedure has consisted in a further parametric campaign of analysis in which 3D FEM models of the 2012 DEMO WCLL BB outboard equatorial module properly endowed with SP configuration derived from Configuration 3 has been adopted. In this second parametric campaign of analysis, 4 different SP geometric configurations have been taken into account (Table 2-22). In particular, the number and the thickness of the poloidal-radial SPs have been maintained as those relevant to Configuration 3 (5 SPs 0.016 m thick), as well as done for the filled radial-toroidal SPs (5 SPs 0.016 m thick). As to pierced radial-toroidal SPs, in Case 1 and Case 2 they have been replaced by radial-toroidal ribs, while in Case 3 and 4 “mixed” configurations of ribs and “reinforced” SPs have been adopted. Concerning radial-toroidal ribs, they are characterized by a square cross section (0.01 m or 0.02 m side) while the “reinforced” pierced radial-toroidal SPs consist in the pierced SPs whose edges have been made thicker by the addiction of “kerbs” similar to the aforesaid radial-toroidal ribs.

Regarding Configuration 3 - Case 1, the 3D geometric model shown in Figure 2-54 has been realized. The filled radial-toroidal SPs and the radial-poloidal ones relevant to Configuration 3 have been maintained, while the 6 pierced radial-toroidal SPs have been replaced with 4 square section (0.01 m side) toroidal-radial ribs. The mesh set-up is characterized by 501826 nodes connected in 1800274 linear tetrahedral elements.

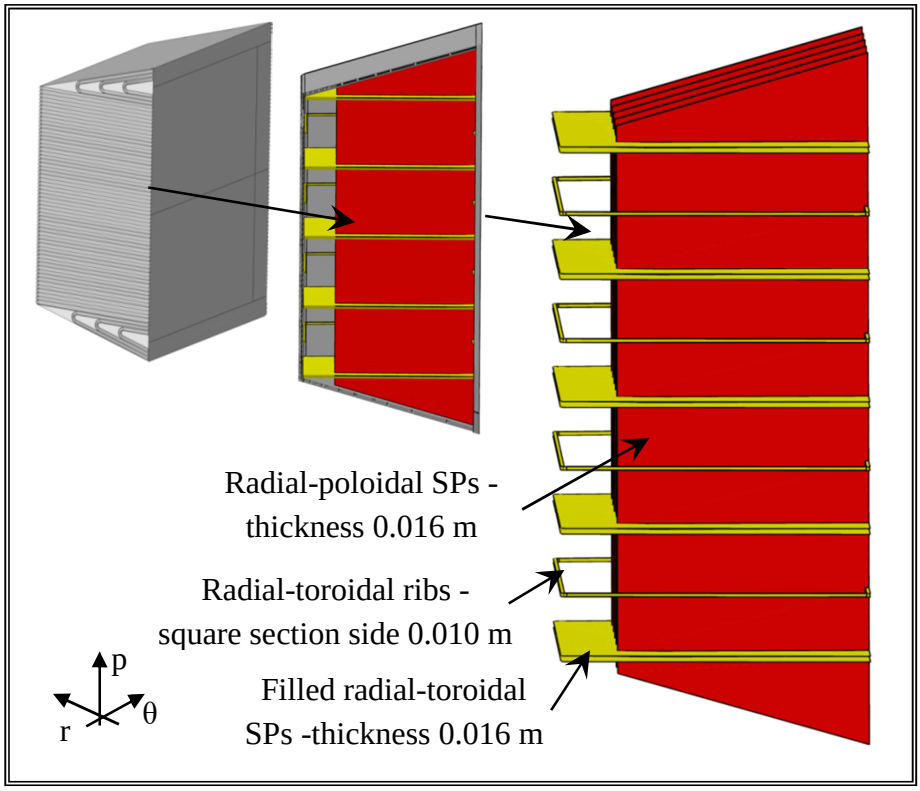


Figure 2-54 - Configuration 3 - Case 1 – 3D geometric model exploded view.

Regarding Configuration 3 - Case 2, the 3D geometric model shown in Figure 2-55 has been realized. The filled radial-toroidal SPs and the radial-poloidal ones relevant to Configuration 3 have been maintained, while the 6 pierced radial-toroidal SPs have been replaced with 4 square section (0.02 m side) ribs. The mesh set-up is characterized by 449557 nodes connected in 1715739 linear tetrahedral elements.

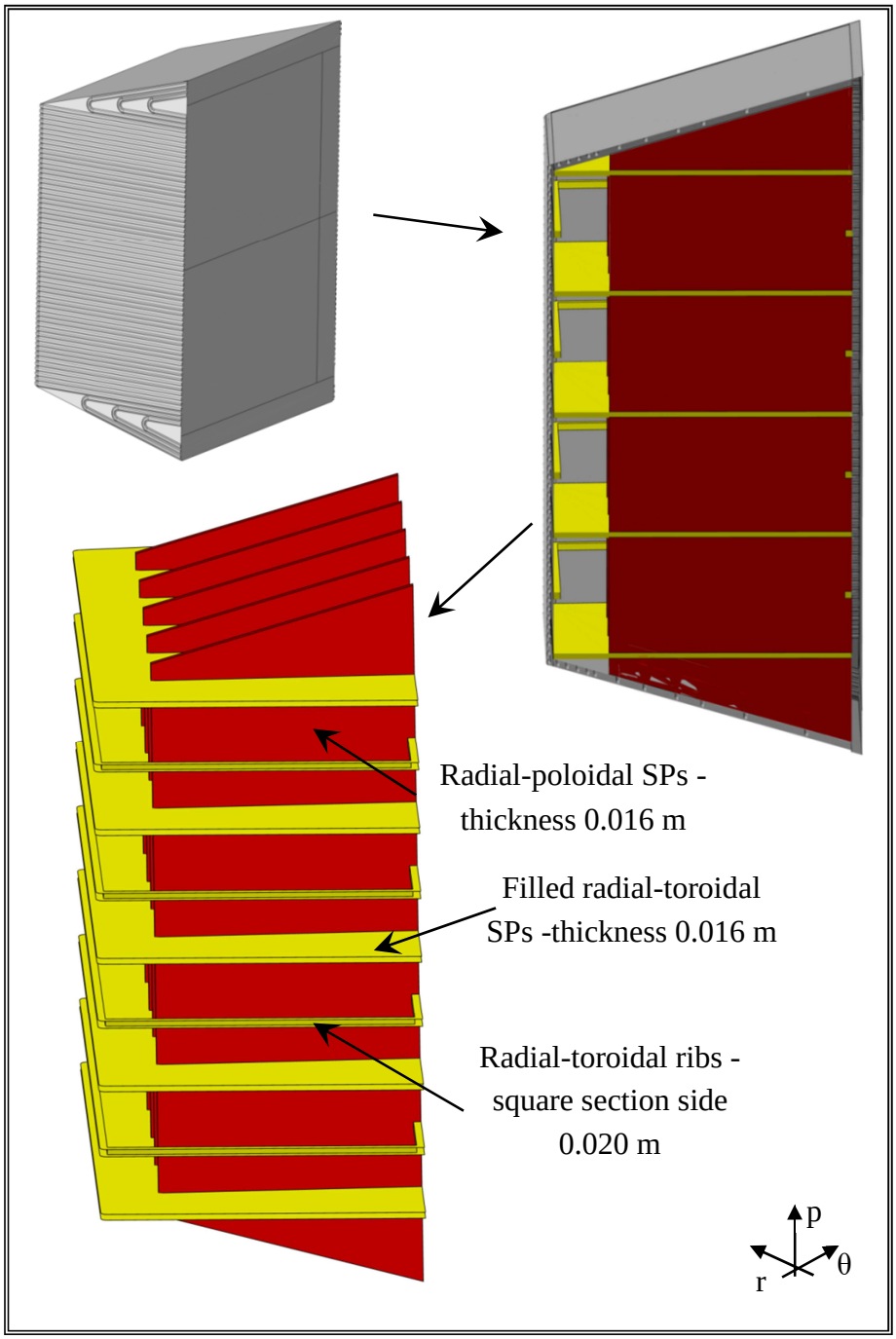


Figure 2-55 - Configuration 3 - Case 2 – 3D geometric model exploded view.

Regarding Configuration 3 - Case 3, the 3D geometric model shown in Figure 2-56 has been realized. The filled radial-toroidal SPs and the radial-poloidal ones relevant to Configuration 3 have been maintained and 4 pierced radial-toroidal SPs 0.002 m thick together with 8 ribs characterized by a square section of 0.01 m side have been inserted in order to achieve a geometric configuration able to limit the maximum value of the radial displacement. The mesh set-up is characterized by 482318 nodes connected in 1829463 linear tetrahedral elements.

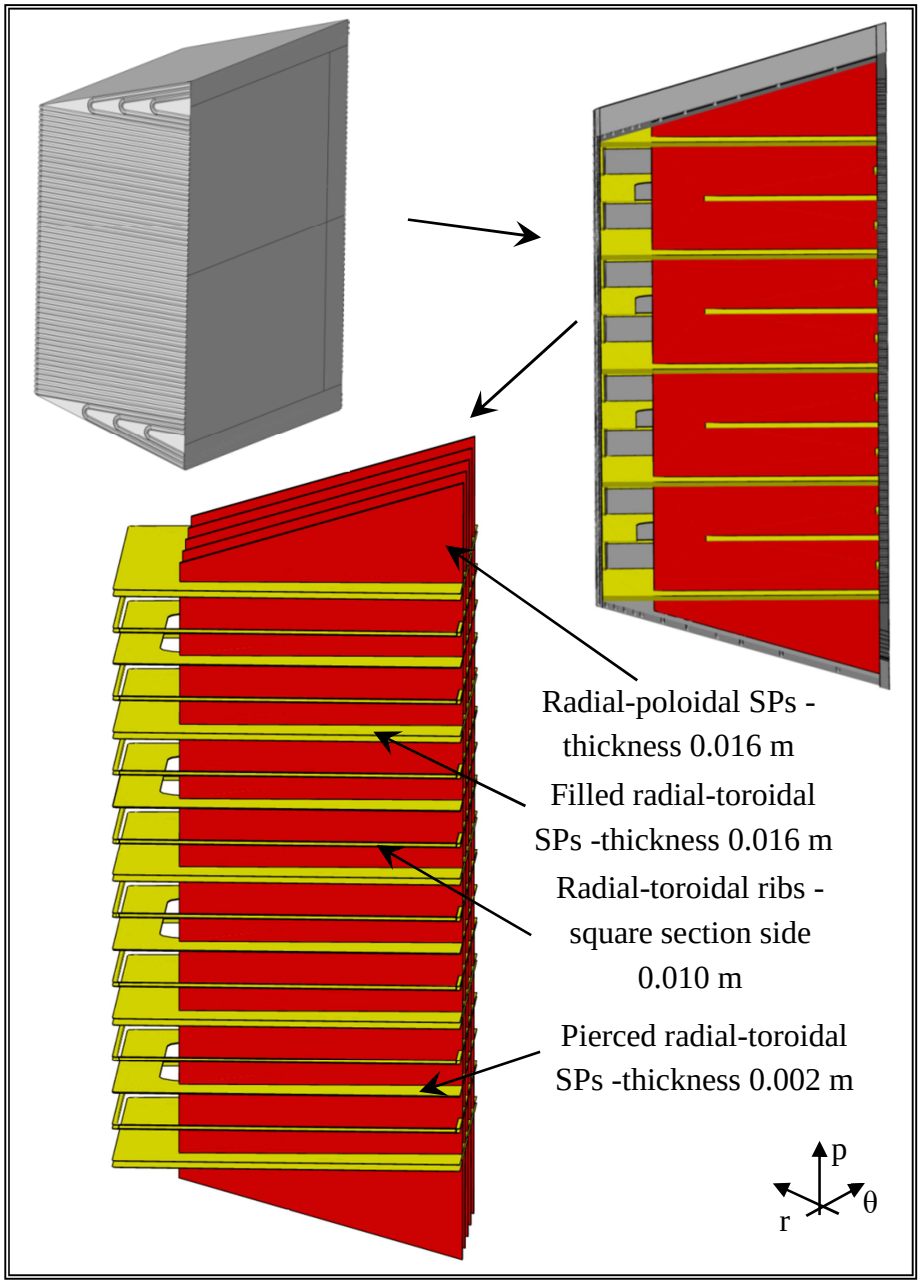


Figure 2-56 - Configuration 3 - Case 3 - 3D geometric model exploded view.

Regarding Configuration 3 - Case 4, the 3D geometric model shown in Figure 2-57 has been realized. The stiffening grid relevant to Configuration 3 - Case 3 has been maintained, replacing the 4 pierced radial-toroidal SPs 0.002 m thick with 4 “reinforced” ones, in which the edges have been made thicker by the addiction of “kerbs” similar to the ribs. Hence, in this configuration 4 “reinforced” pierced radial-toroidal SPs 0.002 m thick together with 8 square section ribs of 0.01 m side have been taken into account. The mesh set-up is characterized by 533633 nodes connected in 1904980 linear tetrahedral elements.

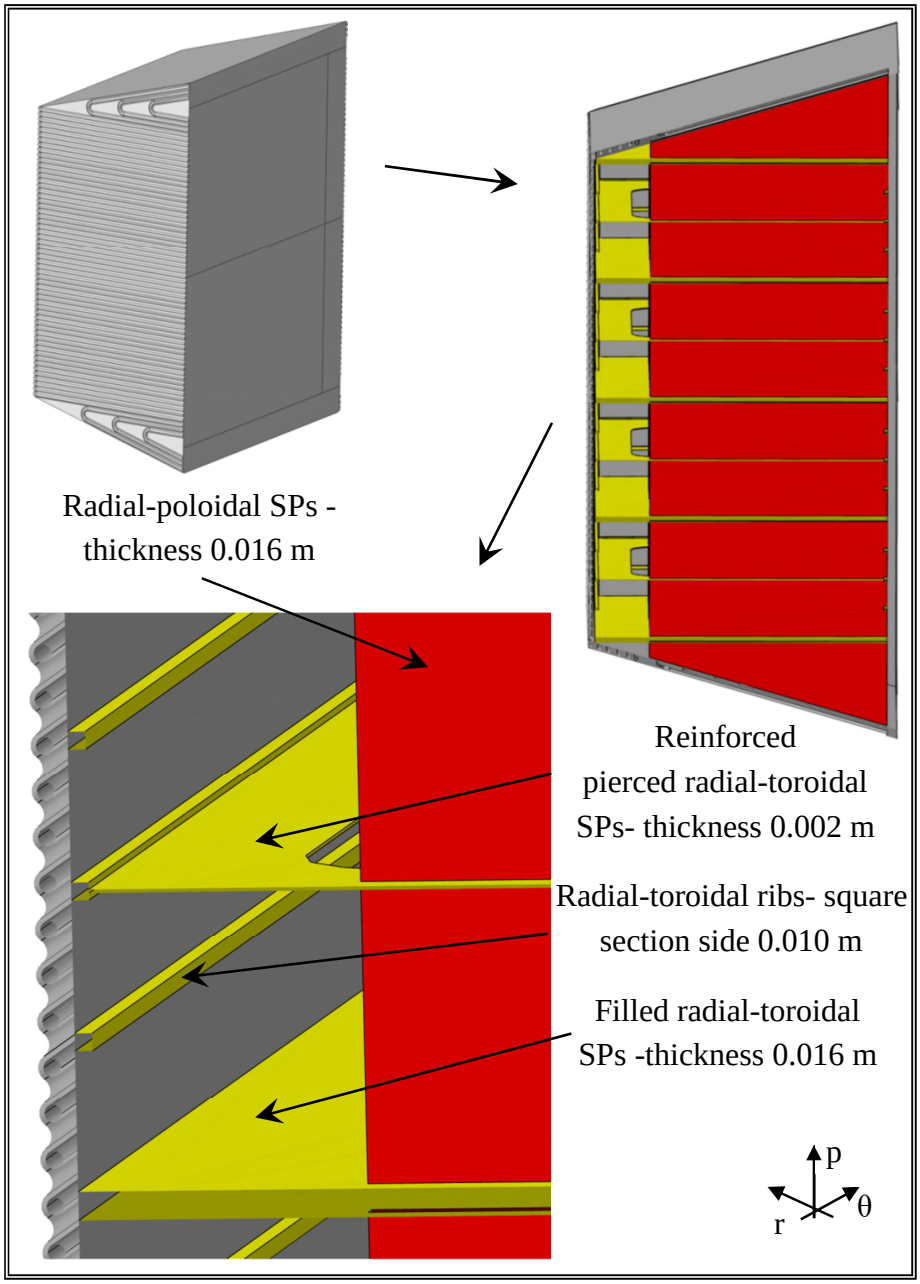


Figure 2-57 - Configuration 3 - Case 4 - 3D geometric model exploded view.

Furthermore, concerning Configuration 3 - New SP pitch, a spatial pitch of 0.250 m has been assumed for all the radial-toroidal SPs. As a consequence five 0.016 m thick filled SPs and four 0.002 m thick pierced radial-toroidal ones have been adopted in this configuration. Concerning this further case investigated, the 3D geometric model shown in Figure 2-58 has been realized and a mesh characterized by 529367 nodes connected in 1915756 linear tetrahedral elements has been set-up.

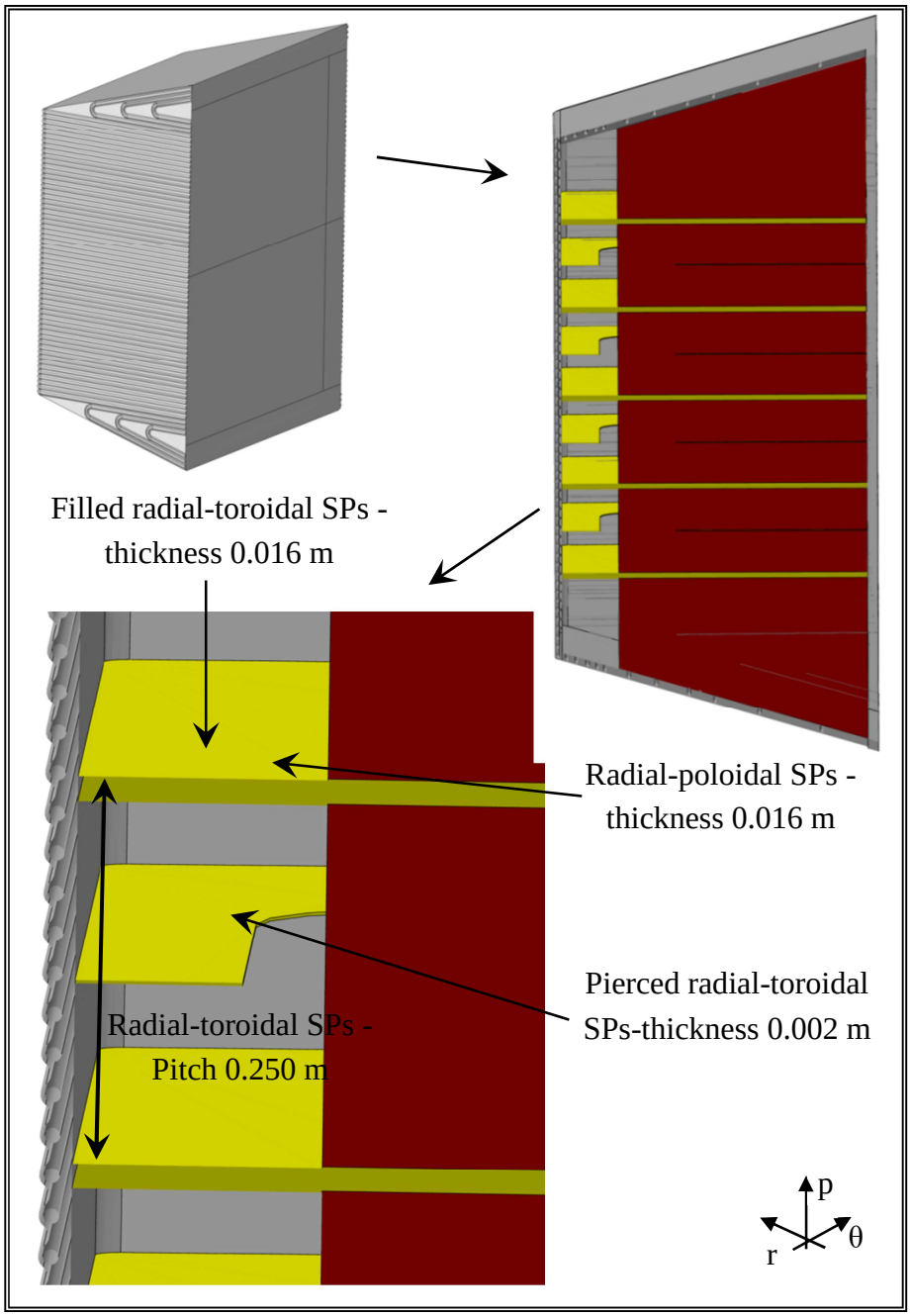


Figure 2-58 - Configuration 3 - New SP pitch – 3D geometric model exploded view.

As to Configuration 6, it is characterized by foreseeing 10 radial-toroidal SPs, whose thickness has been assumed to be equal to 0.008 m, spatially arranged with a poloidal pitch of 0.150 m. In addition, it includes 9 pierced radial-toroidal SPs 0.002 m thick, each dividing in two equal cells the region included between two 0.008 m thick SPs, and 5 poloidal-radial SPs of 0.016 m of thickness. Comparing Configurations 3 and 6, it can be observed that the steel volume of the not pierced radial-toroidal SPs has been conserved. Concerning Configuration 6, the 3D geometric model shown in Figure 2-59 has been realized and a mesh characterized by 575780 nodes connected in 2051156 linear tetrahedral elements has been set-up.

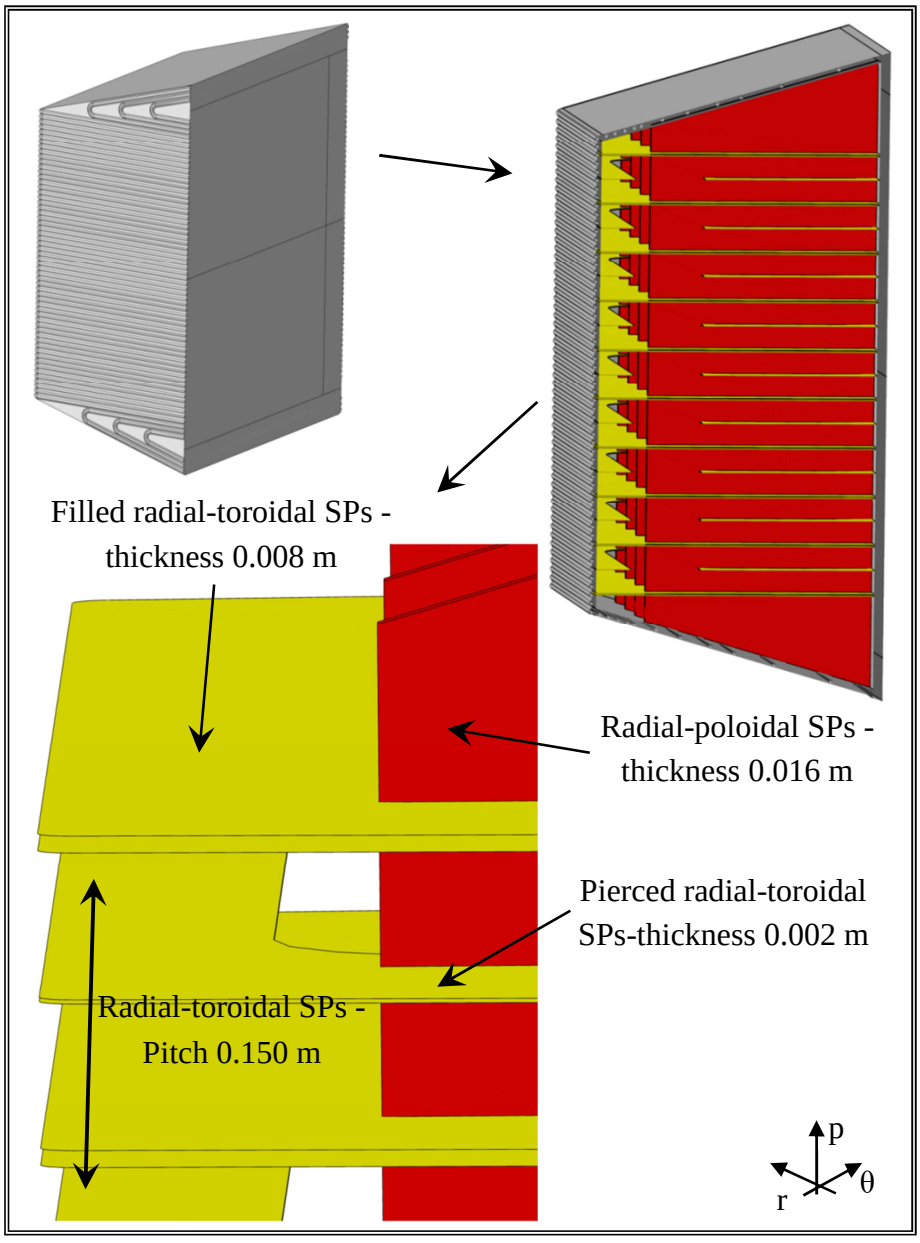


Figure 2-59 - Configuration 6 - 3D geometric model exploded view.

The last step of the SP optimization procedure has consisted in the investigation of two further SP geometric configurations, derived from Configuration 6.

The first configuration, named Configuration 7, foresees 10 radial-toroidal SPs, whose thickness has been increased respect to Configuration 6 up to 0.012 m, spatially arranged with the poloidal pitch, equal to 0.150 m, already adopted for Configuration 6. Configuration 7 (Figure 2-60) also includes the 9 pierced radial-toroidal SPs 0.002 m thick, each dividing in two equal cells the region included between two 0.012 m thick SPs and the 5 poloidal-radial SPs of 0.016 m of thickness.

The second SP configuration taken into account, named Configuration 8 (Figure 2-61), foresees the same radial-toroidal SPs spatial arrangement of the Configuration 7 while, concerning poloidal-radial SPs, 10 plates 0.012 m thick have been considered instead of the plates 0.016m thick taken into account in the previous SPs geometric configurations investigated.

As far as Configuration 7 is concerned, the 3D geometric model has been discretized using a mesh characterized by 583764 nodes connected in 2089939 linear tetrahedral elements while, as to Configuration 8, a mesh characterized by 609082 nodes connected in 2171907 linear tetrahedral elements has been realized.

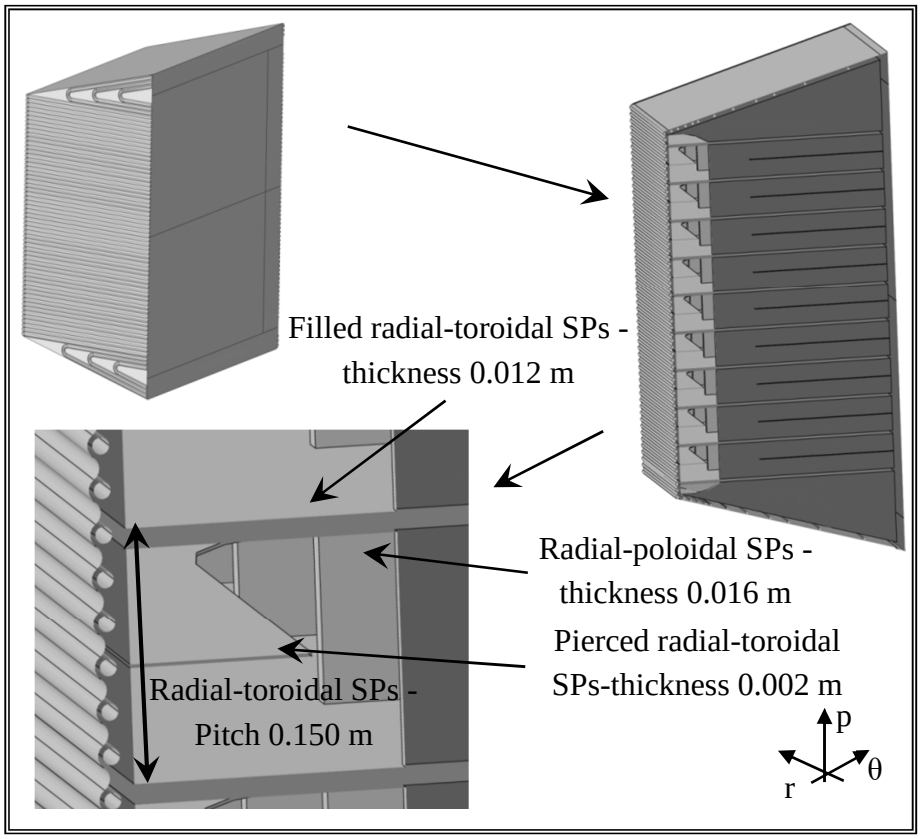


Figure 2-60 - Configuration 7 - 3D geometric model exploded view.

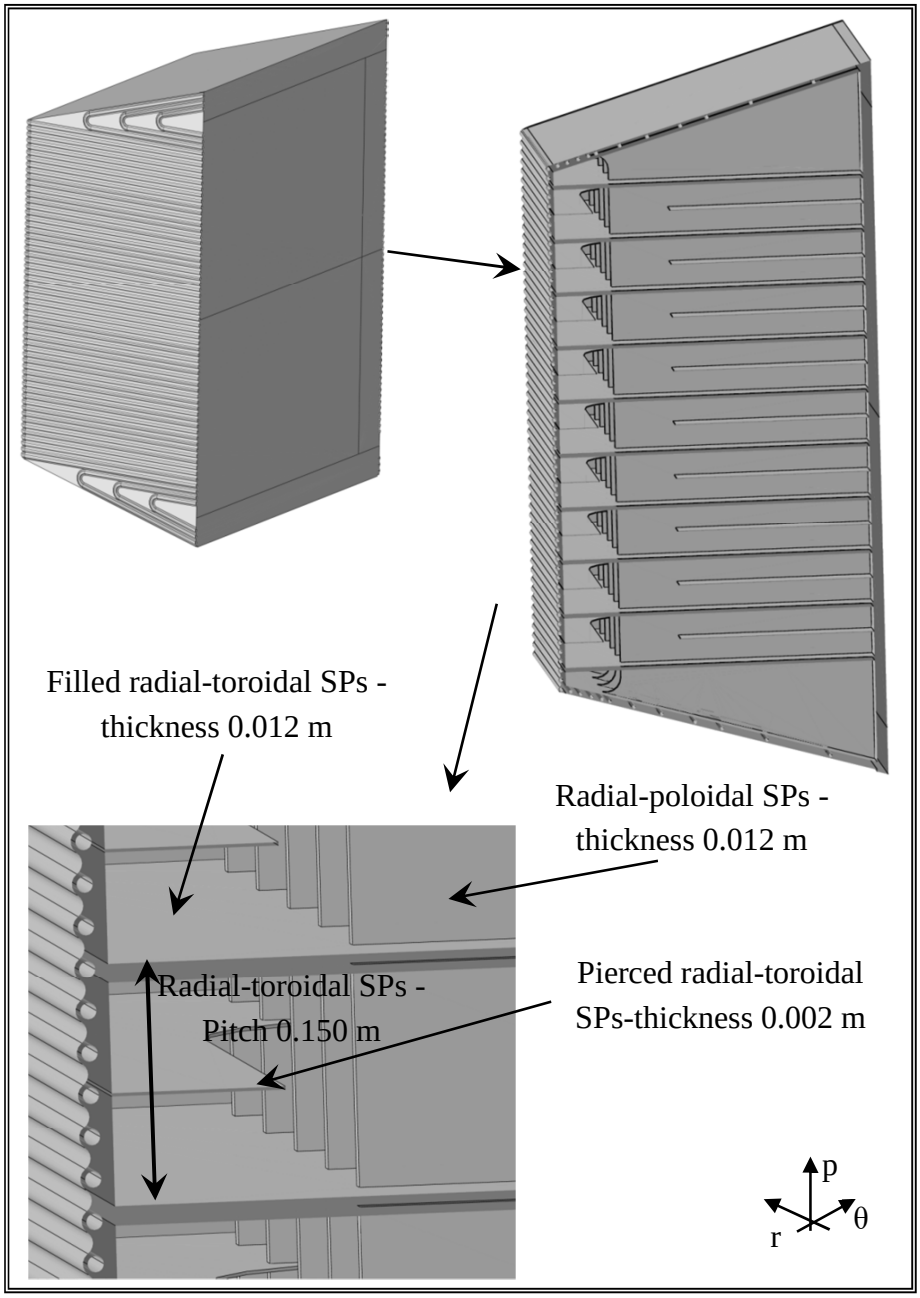


Figure 2-61 - Configuration 8 - 3D geometric model exploded view.

### 2.5.2.1 Materials

RAFM EUROFER steel has been considered as structural material for both SB and SPs. The thermo-physical properties and assumptions adopted in this parametric study are the same already reported in § 2.2.2.1 and in § 2.3.1.1. Hence, for sake of brevity, material data and assumptions adopted have not been further reported.

#### 2.5.2.2 Thermal loads and boundary conditions

From the thermal point of view it has been observed that the worst condition in which the module could operate is a scenario foreseeing the whole SB reaches EUROFER maximum allowable temperature of 550 °C. Under this assumption, the thermal deformation field considerably affects the module thermo-mechanical behaviour. Therefore, no thermal analyses have been performed since this uniform thermal field has been adopted in mechanical calculations.

#### 2.5.2.3 Mechanical loads and boundary conditions

From the mechanical standpoint, particularly conservative steady-state loading conditions, derived from the OP scenario, named in the following as conservative OP loading scenario. In this scenario, the following mechanical loads and boundary conditions have been imposed to the 3D FEM models set-up in this study:

- uniform thermal deformation field;
- internal pressure;
- mechanical restraints.

Since a uniform thermal field has been conservatively considered for all the geometric configurations taken into account, a uniform thermal deformation field, arising as a consequence of the thermal expansion tensor and the uniform temperature value of 550 °C, has been imposed to the whole domain of investigation.

Concerning internal pressure, a value of 15.5 MPa has been imposed on to the SW-FW-SW cooling channels internal surface in order to take into account the mechanical action of the cooling water. Moreover, the same pressure value has been also imposed to the breeder wetted surfaces, in order to simulate a loading scenario consisting in a loss of coolant inside the SB (small in-box LOCA accidental loading conditions), as well as already done for the OP scenario.

As fa as mechanical restraints are concerned, in order to realistically simulate the mechanical action of the attachment system, designed by CEA for the DEMO WCLL BB outboard equatorial module and devoted to connect the module to the vacuum vessel, on the module BP, the following set of boundary conditions has been assumed.

Concerning nodes lying on the red lines shown in Figure 2-62, displacement along the radial direction has been prevented in order to simulate the radial rods action.

Furthermore, regarding nodes lying along green and blue lines in Figure 2-62, poloidal and toroidal displacements have been prevented in order to simulate the mechanical action of the shear keys which are supposed to be part of the attachment system together with the aforementioned radial rods.

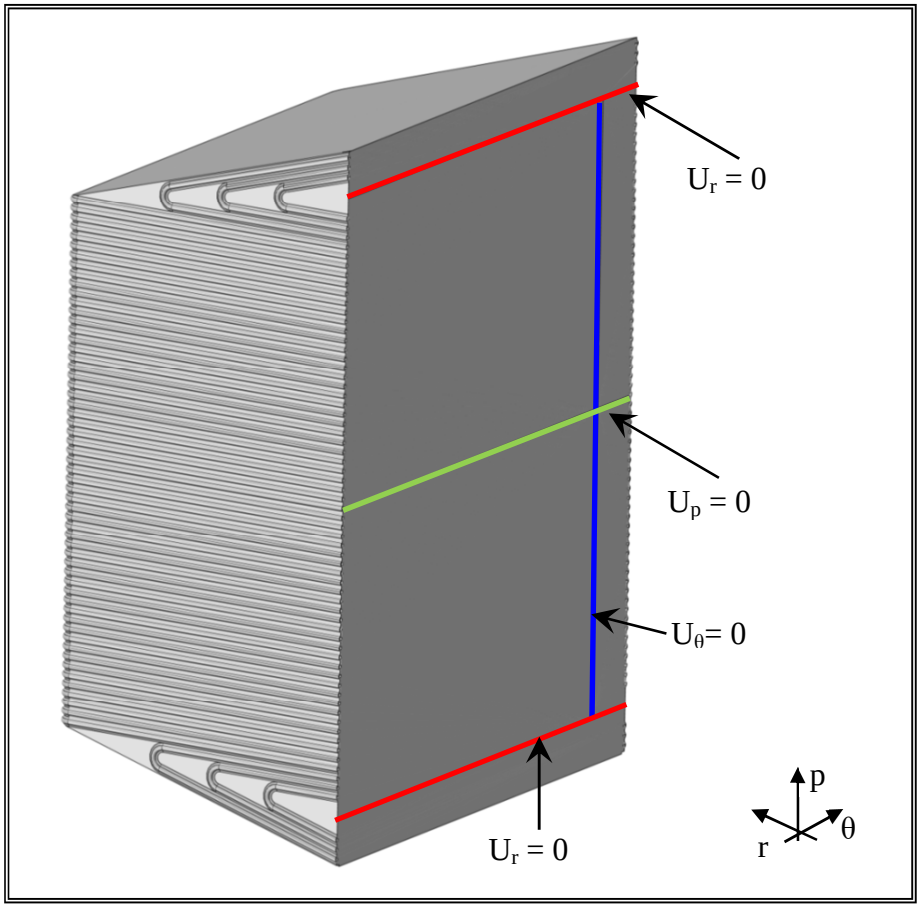


Figure 2-62 - Mechanical boundary conditions.

### 2.5.3 The parametric campaign of analysis

Thermo-mechanical analyses under the abovementioned steady-state conservative OP loading scenario have been performed and results in terms of displacements field have been assessed, taking into account the aforementioned 3D FEM models. In fact, since no detailed assessment of the thermal field has been performed and a uniform thermal level has been considered, the verification of the SDC-IC structural design criteria does not make sense since, in this case, the stress limits values would be excessively under estimated. Therefore, poloidal and radial displacements ($U_p$ and $U_r$ respectively) calculated in each analysis have been compared with values of thermo-mechanical analysis performed at University of Palermo in 2012 [32] and relevant to the DEMO WCLL BB outboard equatorial module designed by CEA. In this analysis, $| U_{r\ Max} |$ = 6.923 mm and $| U_{p\ Max} |$ = 6.559 mm were calculated under the conservative OP scenario. These displacements values, obtained within FW and bottom cap regions respectively, have been adopted as reference values in the SP geometric optimization procedure.

### 2.5.3.1 Results

As to the first step of the SP parametric optimization campaign, geometric configurations from 0 to 5 of those reported in Table 2-22 have been assessed from the thermo-mechanical standpoint under the afore mentioned conservative OP loading scenario.

Concerning Configuration 0, results in terms of total displacement field are shown in Figure 2-63, where maximum $U_r$ and $U_p$ values are highlighted. Moreover, the deformed vs un-deformed geometric configuration has been reported in Figure 2-64. The obtained results indicate that the introduction of a higher number of radial-toroidal SPs is needed in order to limit the radial displacement as well as poloidal-radial SPs should be inserted in order to prevent excessive poloidal displacement.

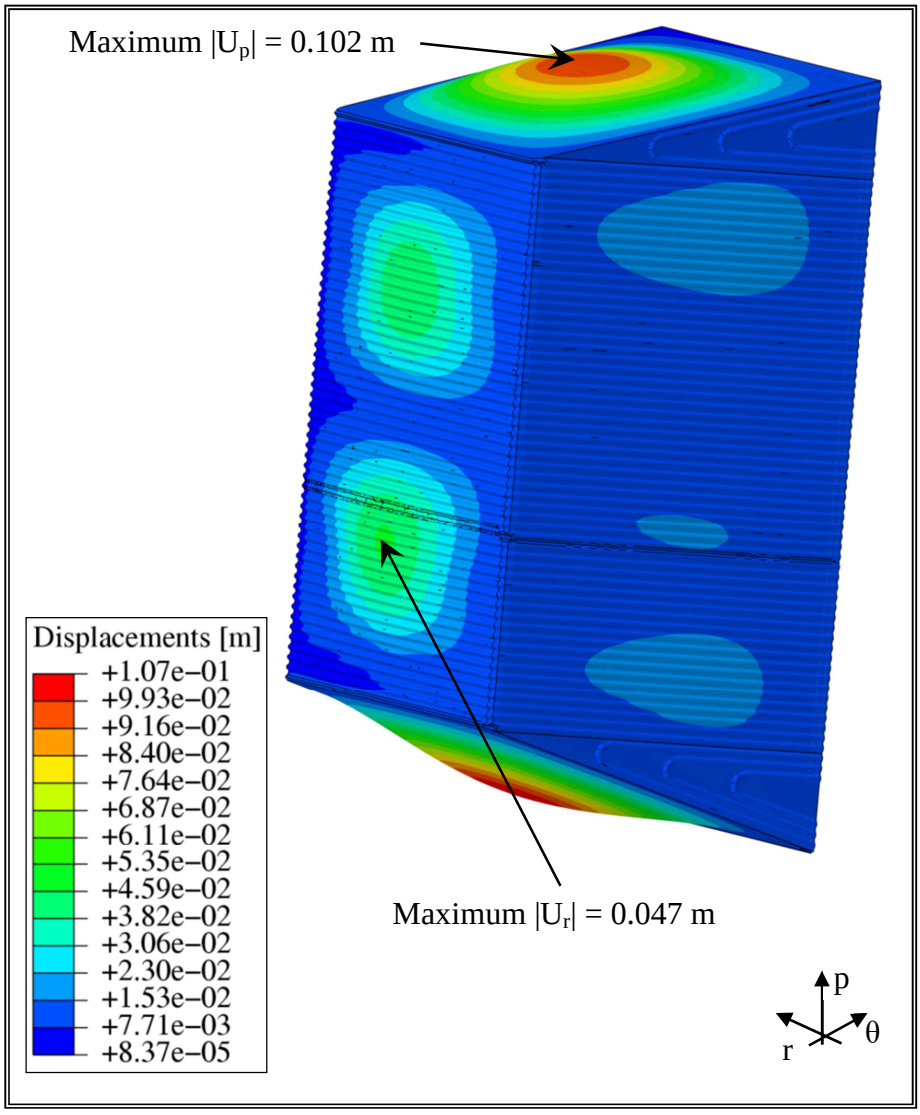


Figure 2-63 - Configuration 0 - Displacement field.

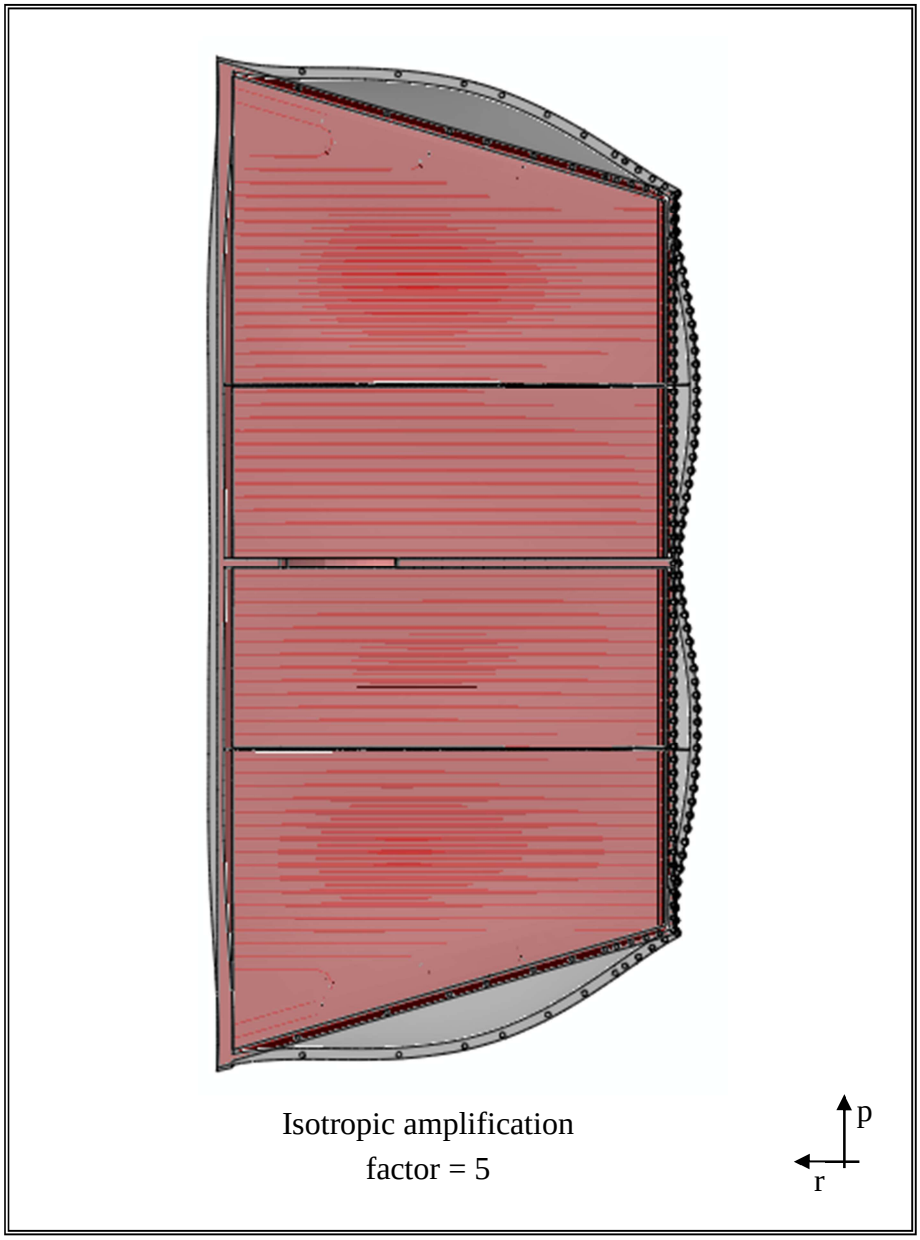


Figure 2-64 - Configuration 0 - Deformed vs un-deformed view.

As to Configuration 1, results in terms of total displacement field are shown in Figure 2-65, where maximum $U_r$ and $U_p$ values are highlighted. Moreover, the deformed vs un-deformed geometric configuration has been reported in Figure 2-66.

The obtained results indicate that the introduction of radial-poloidal SPs strongly limits the poloidal displacements which achieve a maximum value of 0.007 m very close to the reference one, equal to 0.0066 m. Nevertheless, results show that the number and the thickness of the radial-toroidal SPs has to be further optimized in order to limit radial displacements.

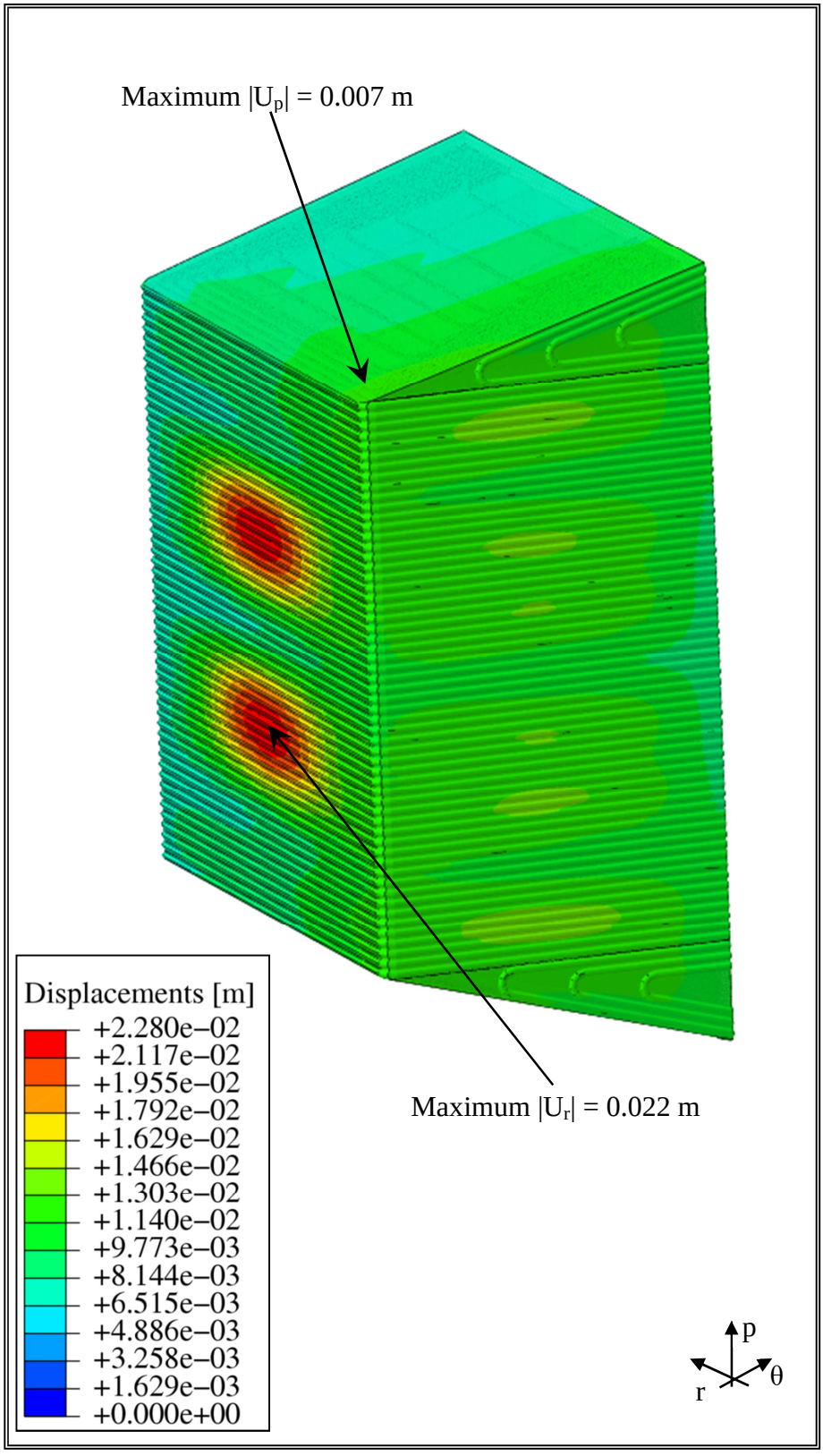


Figure 2-65 - Configuration 1 - Displacement field.

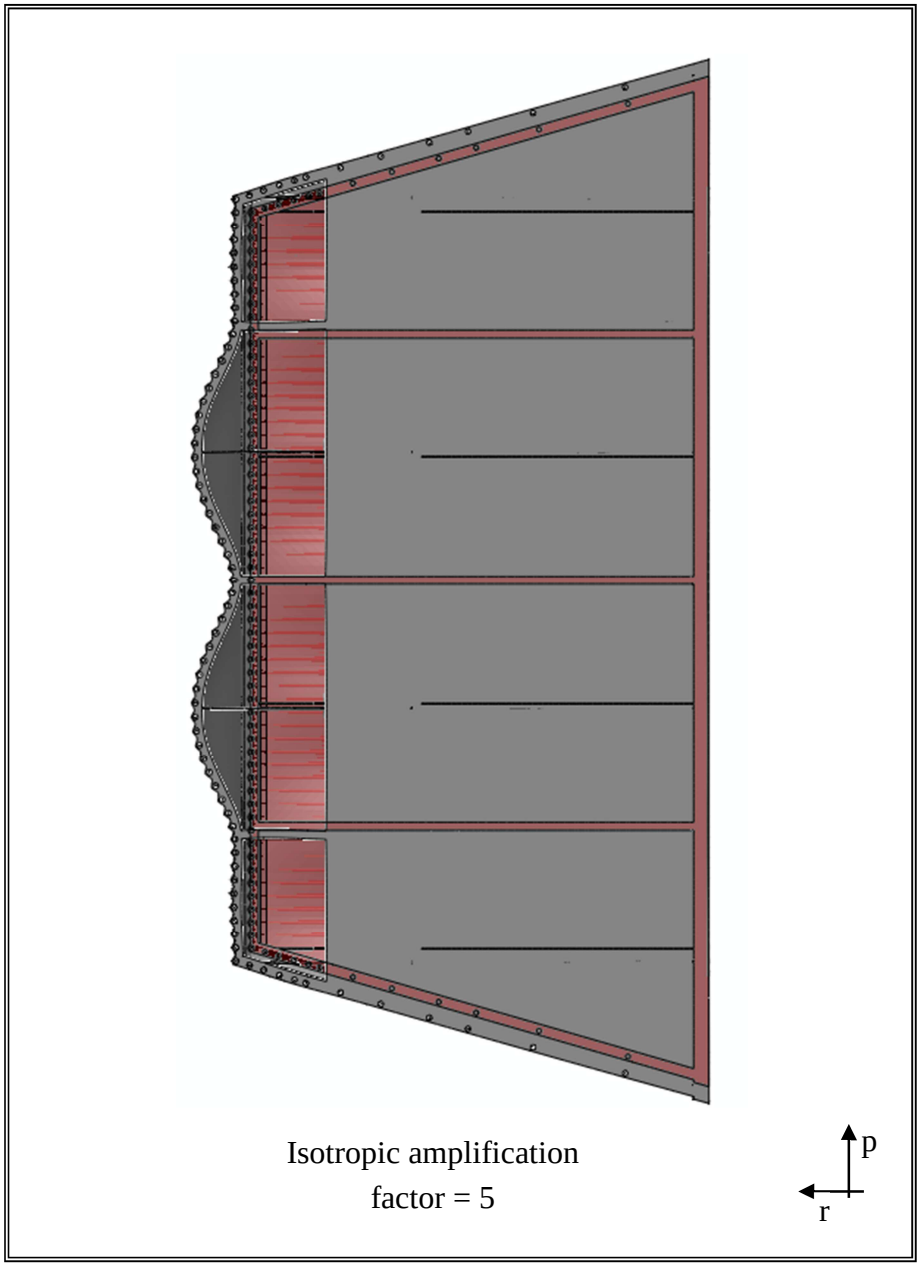


Figure 2-66 - Configuration 1 - Deformed vs un-deformed view.

Regarding Configuration 2, results in terms of total displacement field are shown in Figure 2-67, where maximum $U_r$ and $U_p$ values are highlighted. Moreover, the deformed vs un-deformed geometric configuration has been reported in Figure 2-68.

Results indicate that the increasing of the pierced SPs thickness contributes to reduce maximum radial displacement from 0.022 m obtained in Configuration 1 to 0.016 m, even though it remains still far from the reference obtained value in 2012 analysis, equal to 0.0069 m. Therefore further SP configurations needs to be assessed.

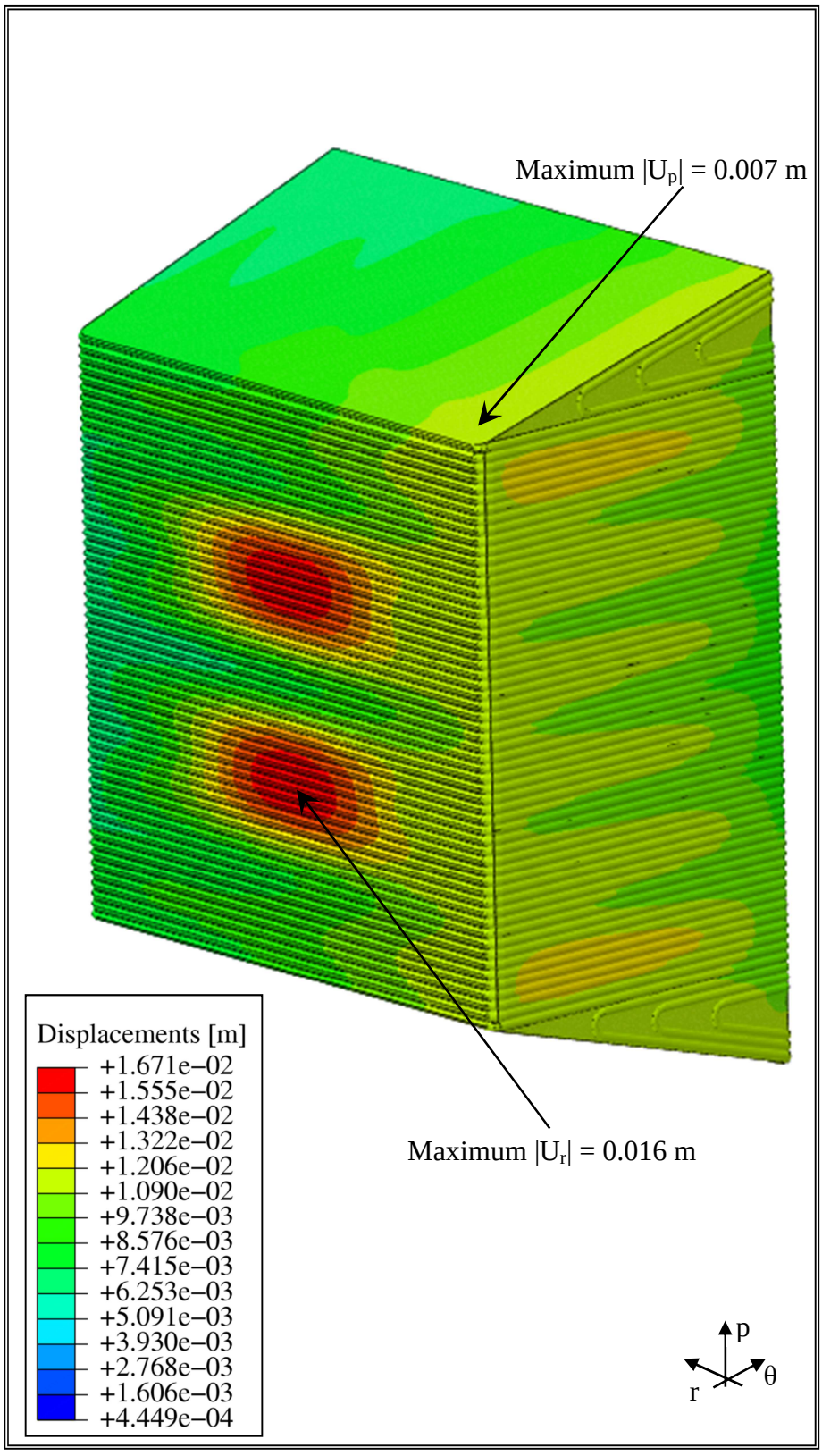


Figure 2-67 - Configuration 2 - Displacement field.

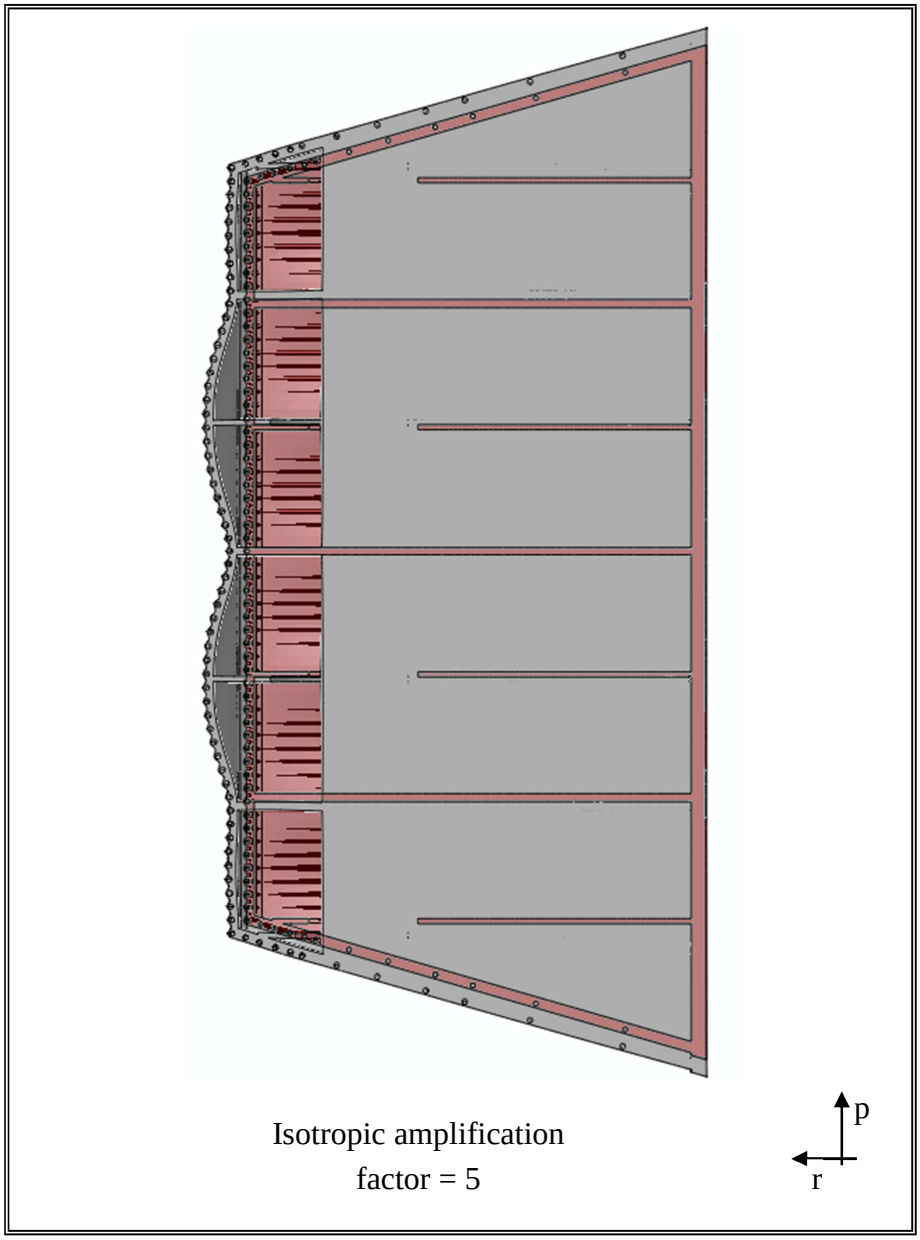


Figure 2-68 - Configuration 2 - Deformed vs un-deformed view.

As to Configuration3, results in terms of total displacement field are shown in Figure 2-69, where maximum $U_r$ and $U_p$ values are highlighted. Moreover, the deformed vs un-deformed geometric configuration has been reported in Figure 2-70.

The obtained results indicate that the effect of the increasing number of the radial-toroidal SPs generate a reduction of the maximum radial displacement down to 0.012 m. This value is the lowest predicted up to this point of the parametric campaign, even though it remains still far from the reference value of 2012 analysis. Therefore further SP configurations needs to be assessed.

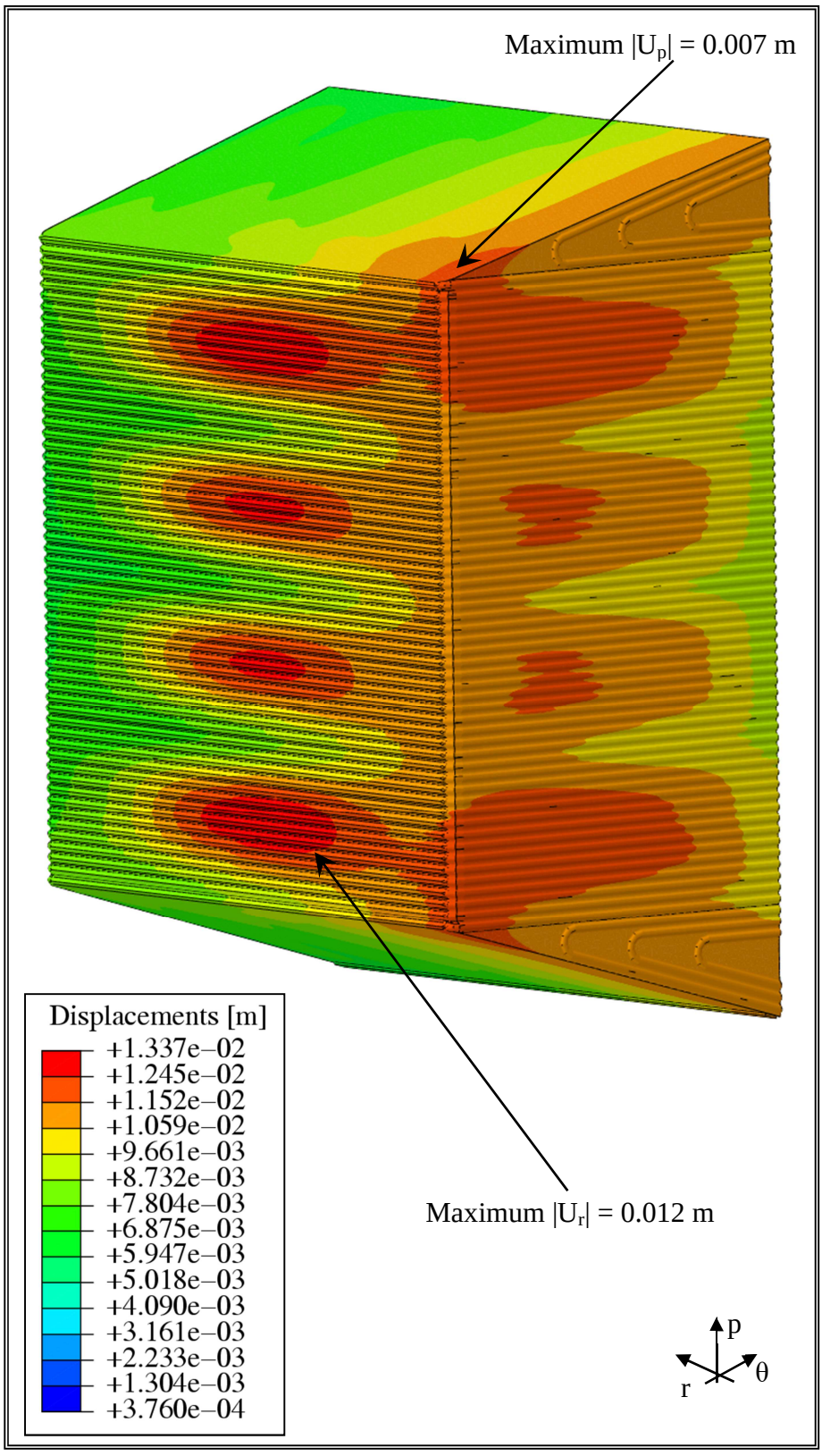


Figure 2-69 - Configuration 3 - Displacement field.

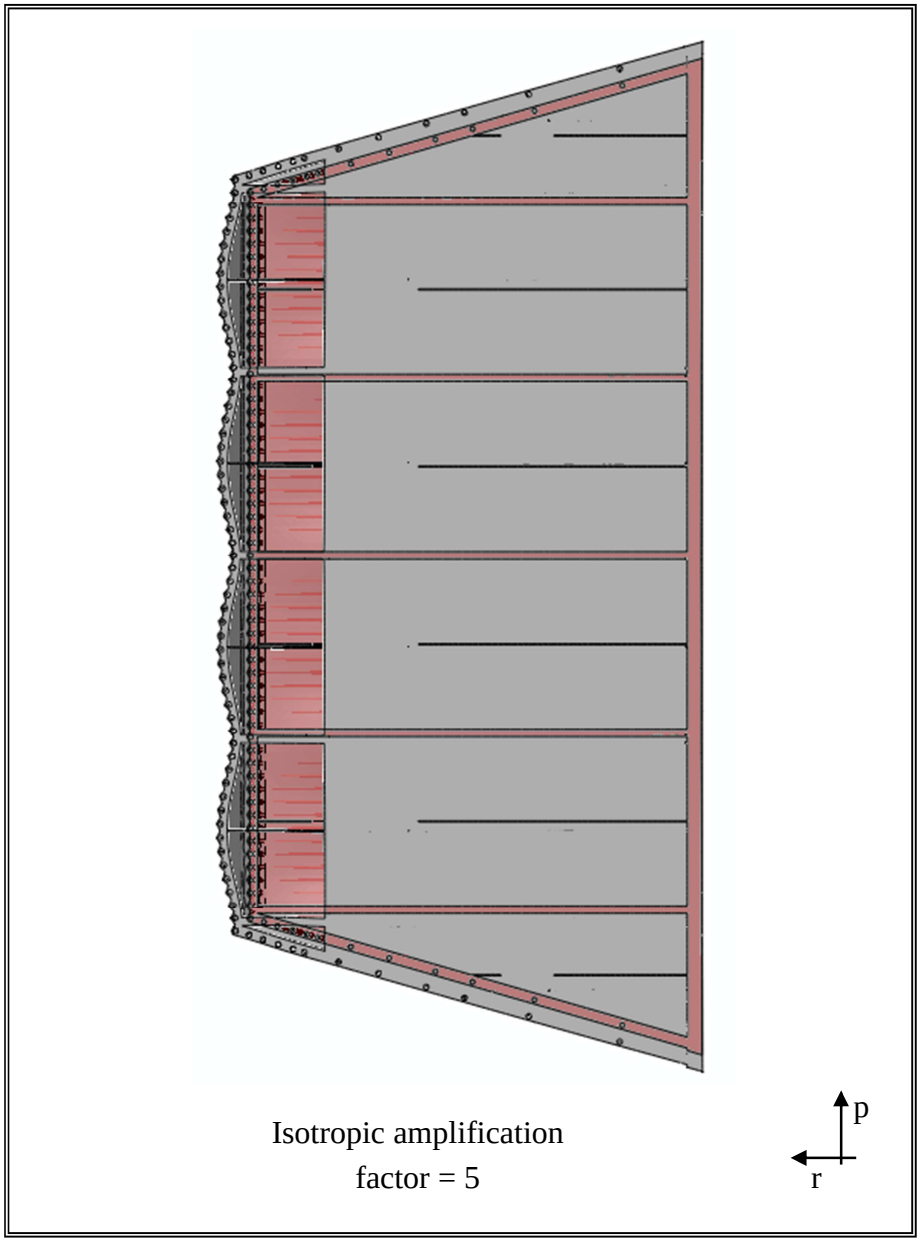


Figure 2-70 - Configuration 3 - Deformed vs un-deformed view.

As regards Configuration 4, results in terms of total displacement field are shown in Figure 2-71, where maximum $U_r$ and $U_p$ values are highlighted. Moreover, the deformed vs un-deformed geometric configuration has been reported in Figure 2-72.

The obtained results indicate that reducing the filled radial-toroidal SP number, even though their thickness has been increased, the maximum radial displacement predicted increases up to 0.023 m. This result leads to the conclusion that the number of filled radial-toroidal SPs may have a strong impact on the SB thermo-mechanical performances, so it is one of the most important parameters that should be further investigated.

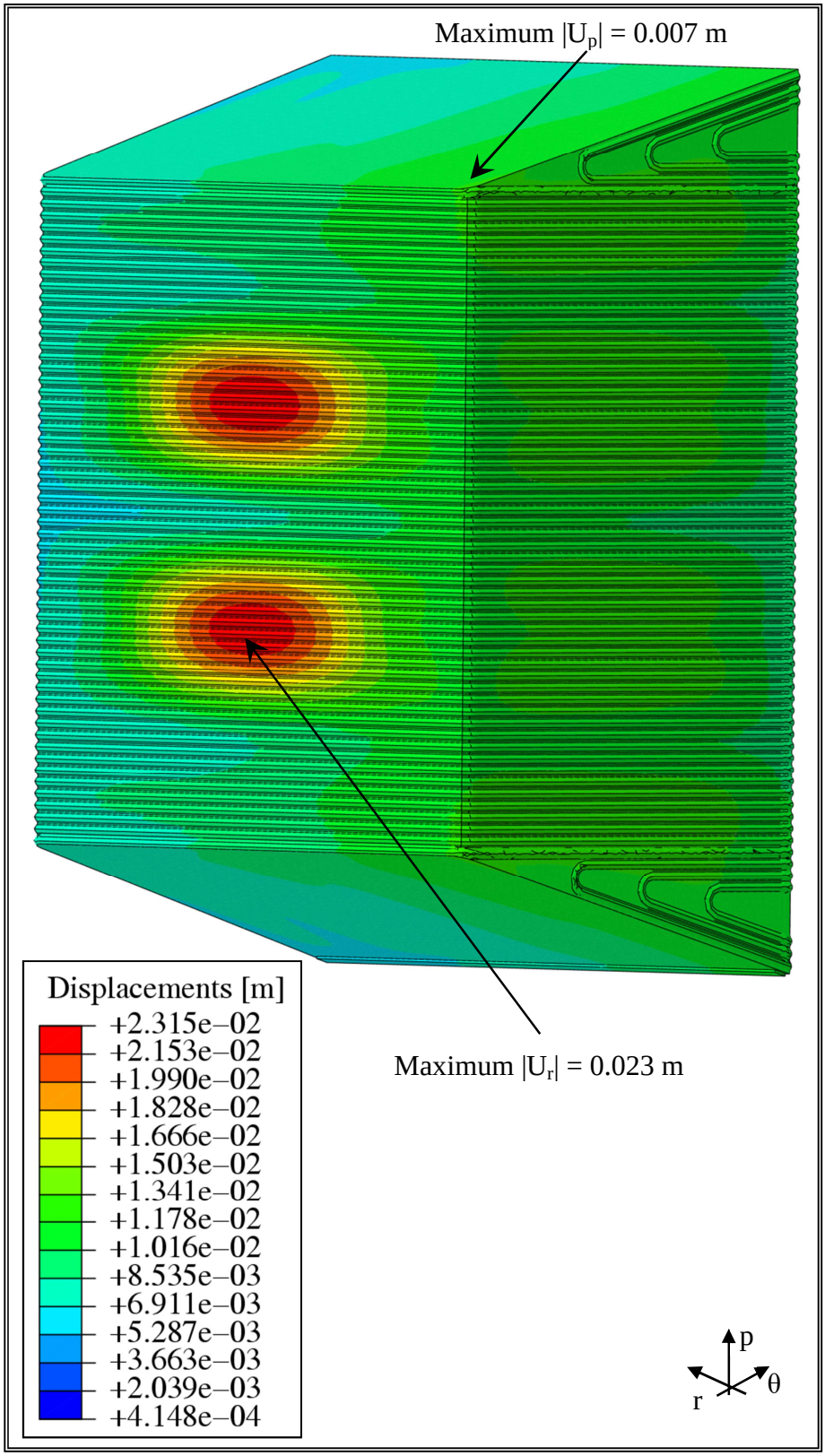


Figure 2-71 - Configuration 4 - Displacement field.

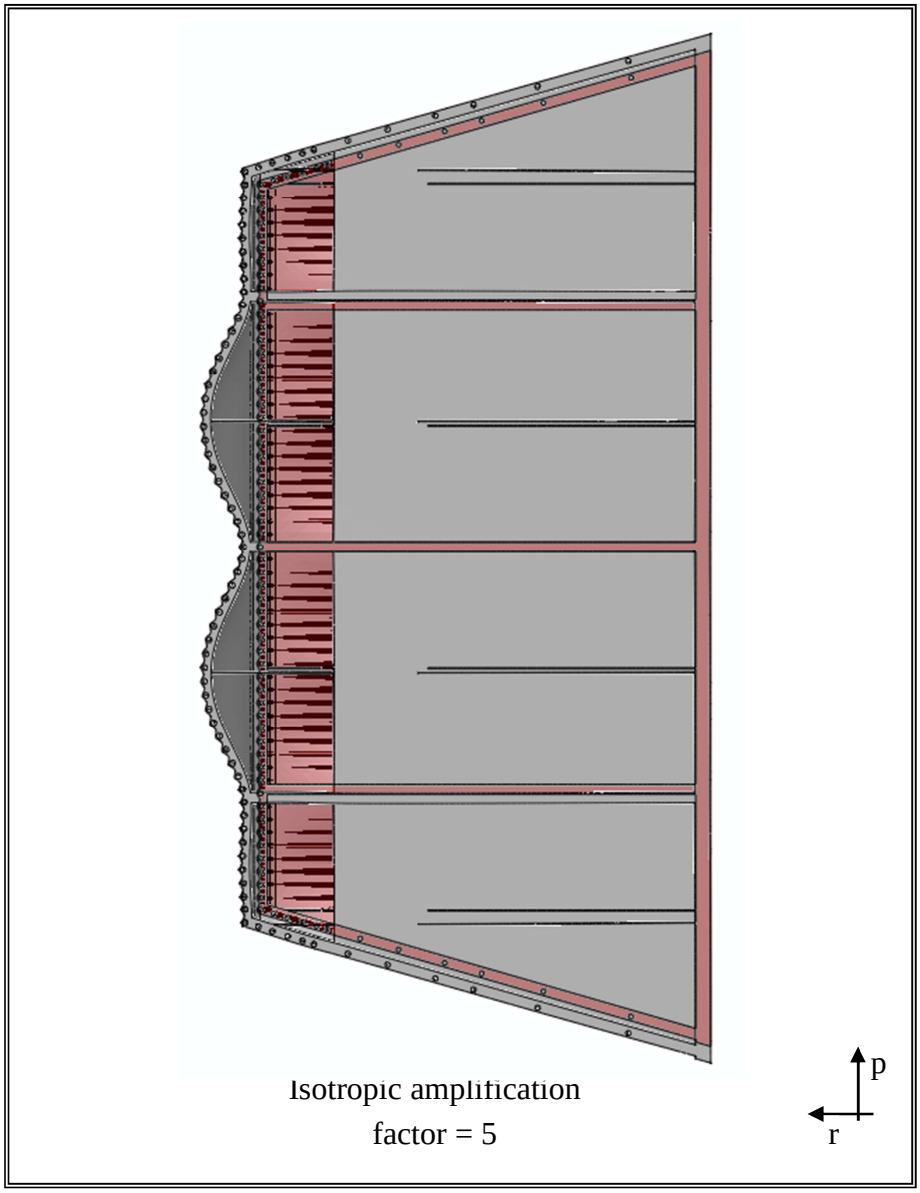


Figure 2-72 - Configuration 4 - Deformed vs un-deformed view.

Concerning Configuration 5, results in terms of total displacement field are shown in Figure 2-73, where maximum $U_r$ and $U_p$ values are highlighted. Moreover, the deformed vs un-deformed geometric configuration has been reported in Figure 2-74. Results of Configuration 5 are not encouraging, since they indicate that also this configuration does not present significant advantages compared with Configuration 3, being the maximum radial displacement equal to 0.021 m.

Results of the 6 assessed configurations in this preliminary step of the SP optimization, in terms of maximum radial and poloidal displacement, are summarized in Table 2-23 where the 2012 reference values are also reported.

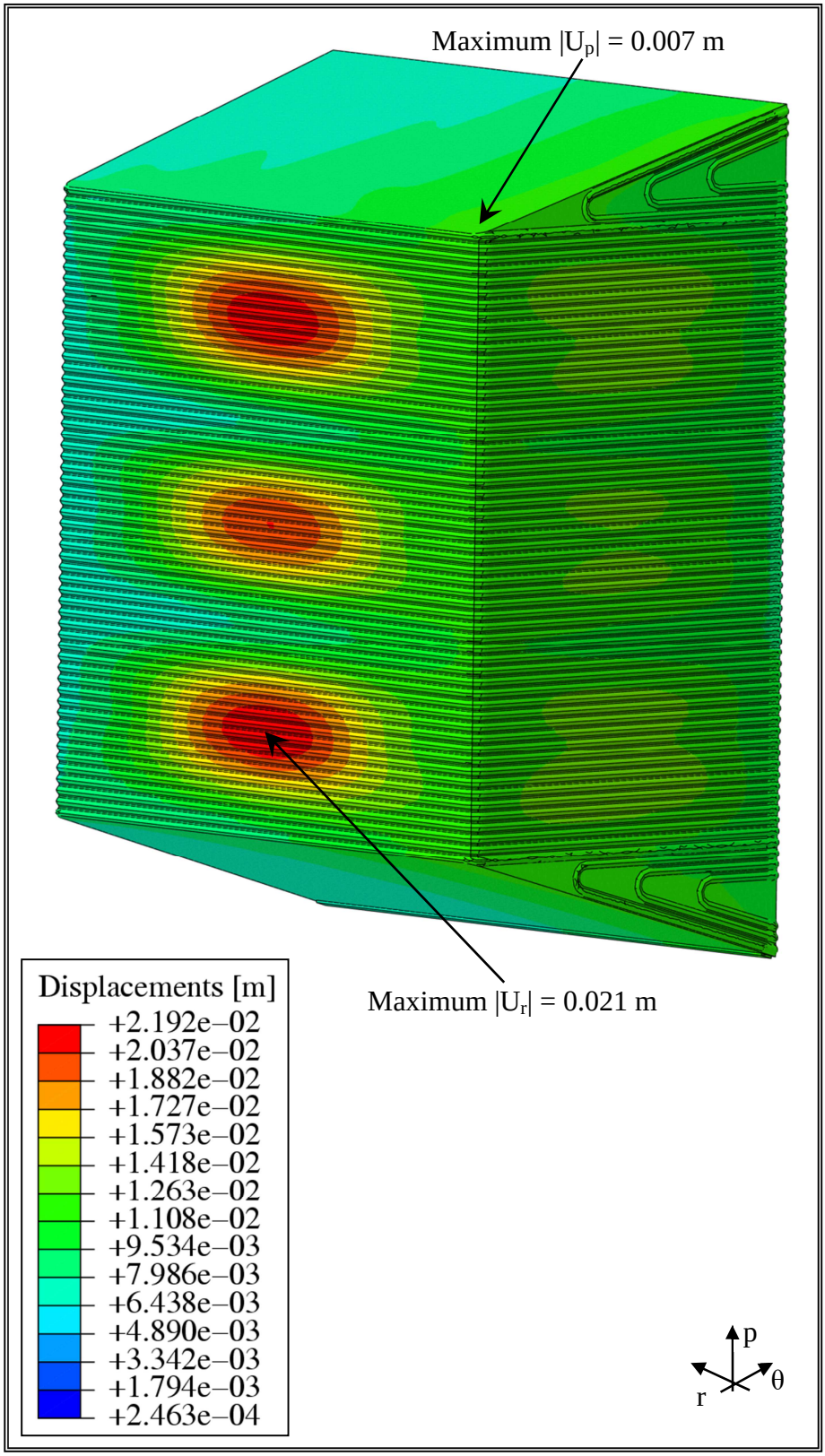


Figure 2-73 - Configuration 5 - Displacement field.

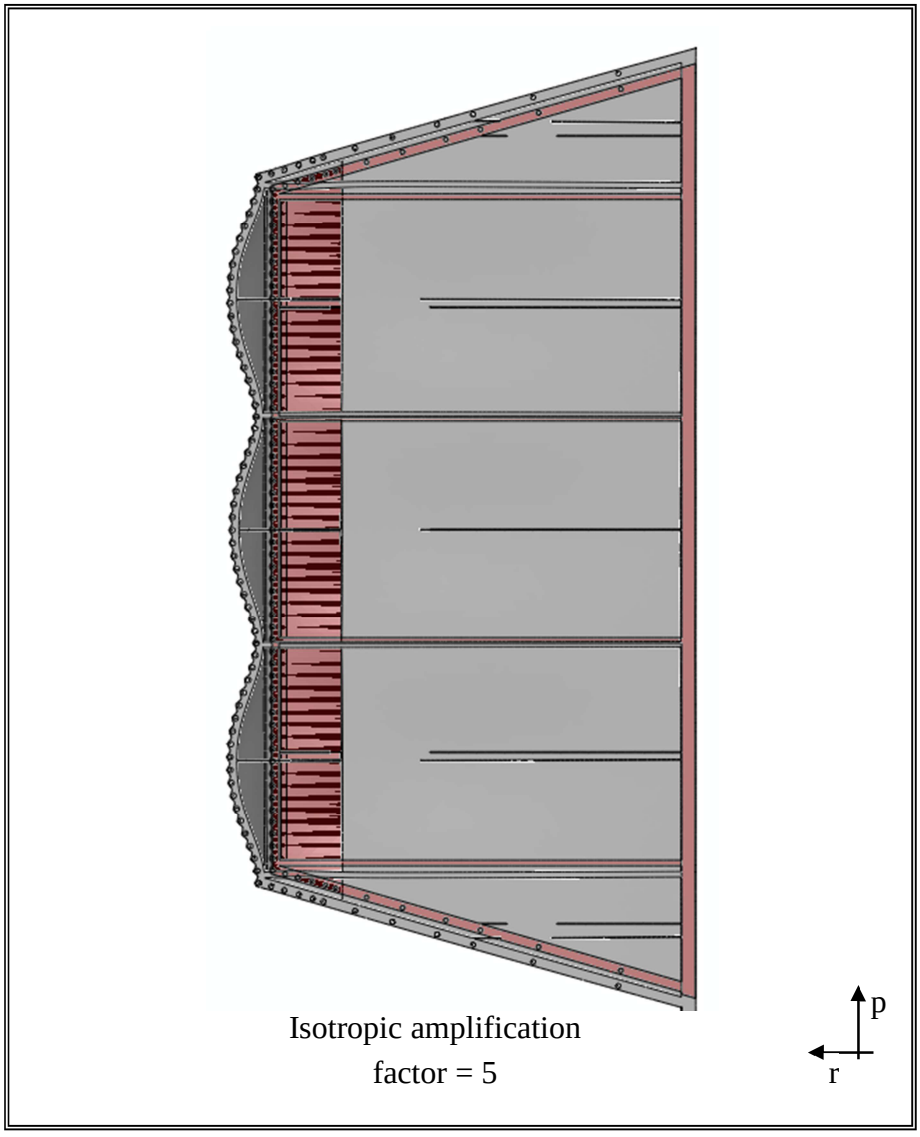


Figure 2-74 - Configuration 5 - Deformed vs un-deformed view.

Table 2-23 - Summary of the preliminary parametric analysis results.

| **Configuration** | **$U_{r\ max}$ [m]** | **$U_{p\ max}$ [m]** |
|---|---|---|
| 2012 analysis | 0.0069 | 0.0066 |
| 0 | 0.047 | 0.102 |
| 1 | 0.022 | 0.007 |
| 2 | 0.016 | 0.007 |
| 3 | 0.012 | 0.007 |
| 4 | 0.023 | 0.007 |
| 5 | 0.021 | 0.007 |

In conclusion of the preliminary campaign of parametric analysis, the obtained results summarized in Table 2-23 have shown that, among all the SP geometric configurations taken into account, the most promising one is Configuration 3, which allows to predict maximum values of both radial and poloidal displacements, equal to 0.012 m and 0.007 m respectively, as closer as possible to the reference ones. For this reason, Configuration 3 has been chosen in order to be further investigated taking into account different geometric modifications aimed to improve its thermo-mechanical performance under steady-state conservative OP loading scenario considered in this study.

The obtained geometric configuration, reported in Table 2-22, have been called as Configuration - Case n, with n ranges from 1 to 4. Furthermore a configuration named Configuration 3 - New Pitch has been also investigated (Table 2-22).

As far as Configuration 3 - Case 1 is concerned, results in terms of total displacement field are shown in Figure 2-75, where maximum $U_r$ and $U_p$ values are highlighted. Moreover, the deformed vs un-deformed geometric configuration has been reported in Figure 2-76. Results of Configuration 3 - Case 1 are not encouraging if compared with Configuration 3 ones, since maximum values of both radial and poloidal displacements are higher.

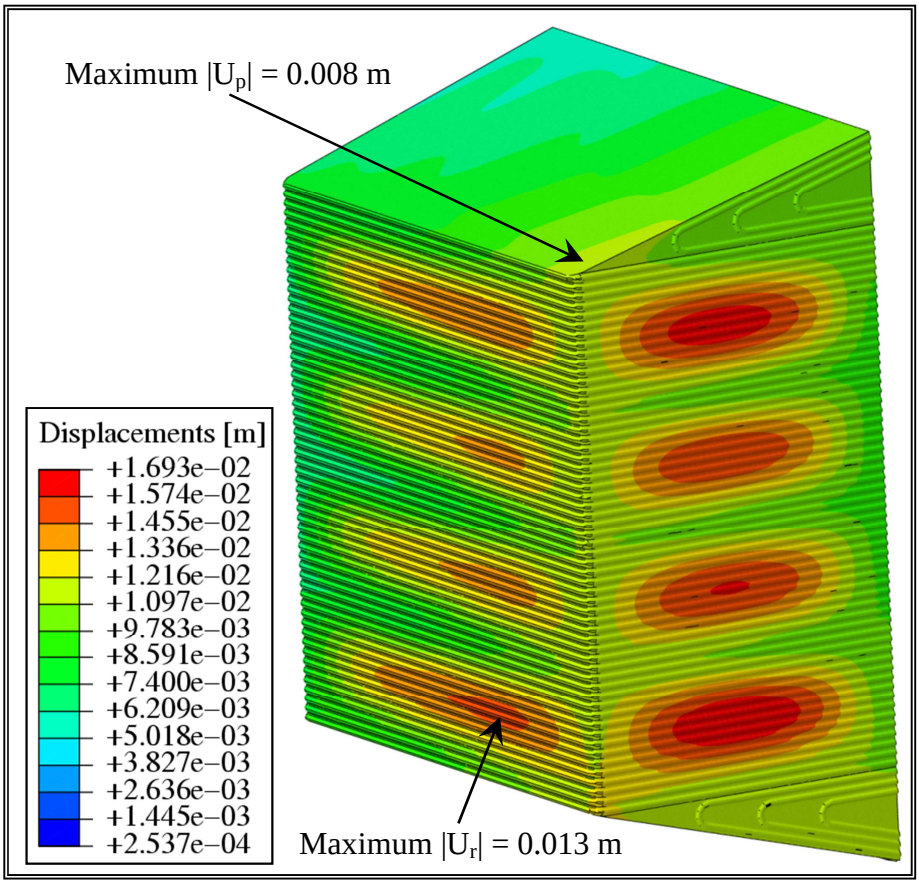


Figure 2-75 - Configuration 3 - Case 1 - Displacement field.

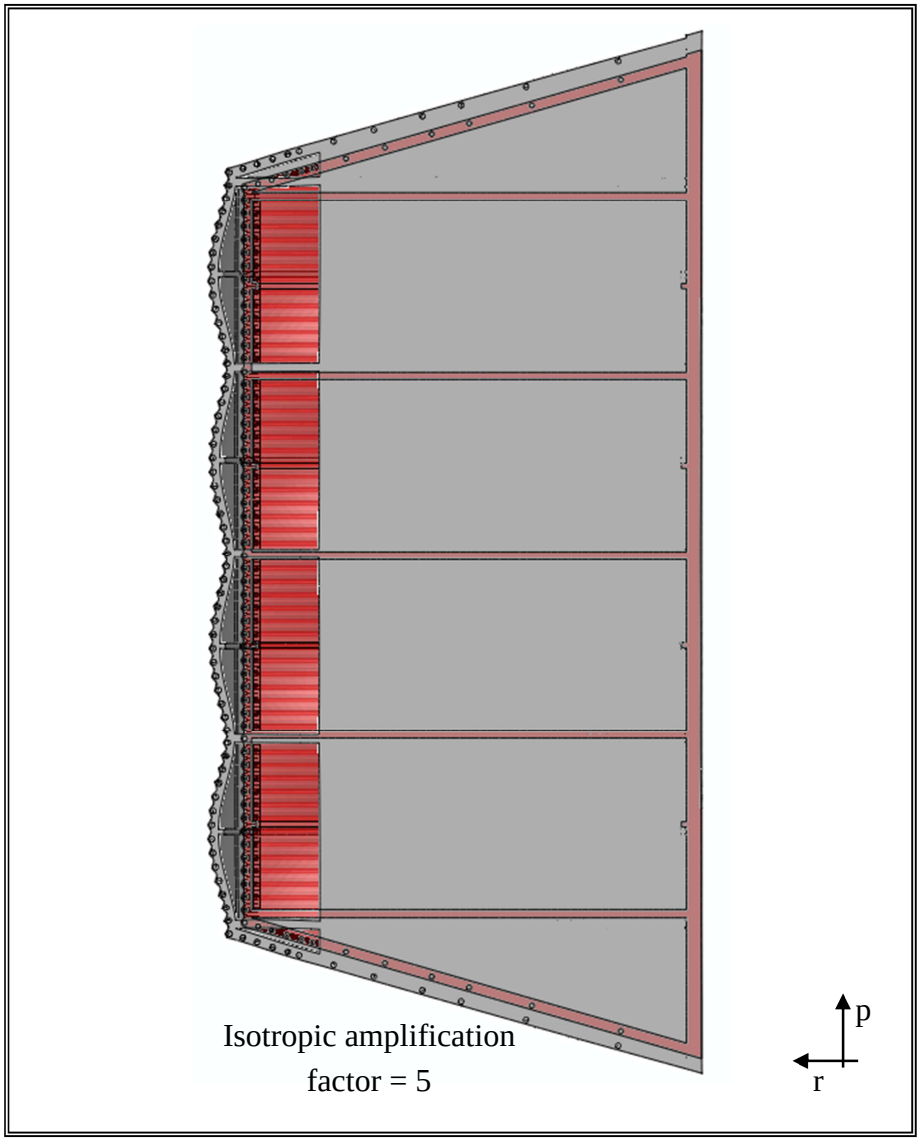


Figure 2-76 - Configuration 3 - Case 1 - Deformed vs un-deformed view.

As to Configuration 3 - Case 2, results in terms of total displacement field are shown in Figure 2-77, where maximum $U_r$ and $U_p$ values are highlighted. Moreover, the deformed vs un-deformed geometric configuration has been reported in Figure 2-78. Results of Configuration 3 - Case 2 are quite similar to those achieved from Configuration 3 - Case 1 analysis, since predicted maximum values of both radial and poloidal displacements remain very similar. For this reason ribs with a section of 0.01 m side have been assumed as the reference ones. Moreover, on the basis of results of cases 1 and 2, it has been decided to investigate further geometric configurations in which the number of the ribs has been increased from 4 to 8 and a set of pierced radial-toroidal SPs has been added to the stiffening grid.

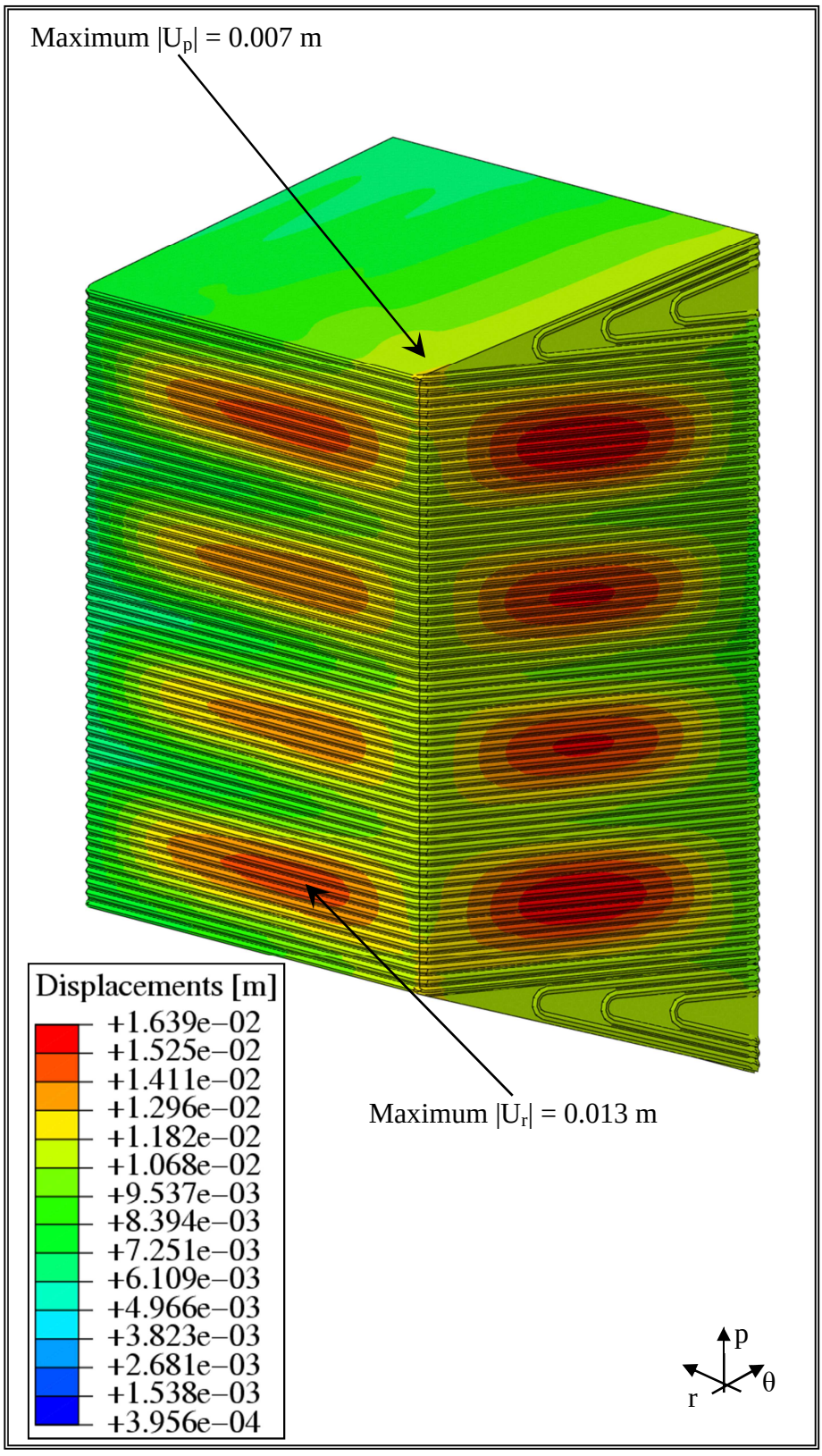


Figure 2-77 - Configuration 3 - Case 2 - Displacement field.

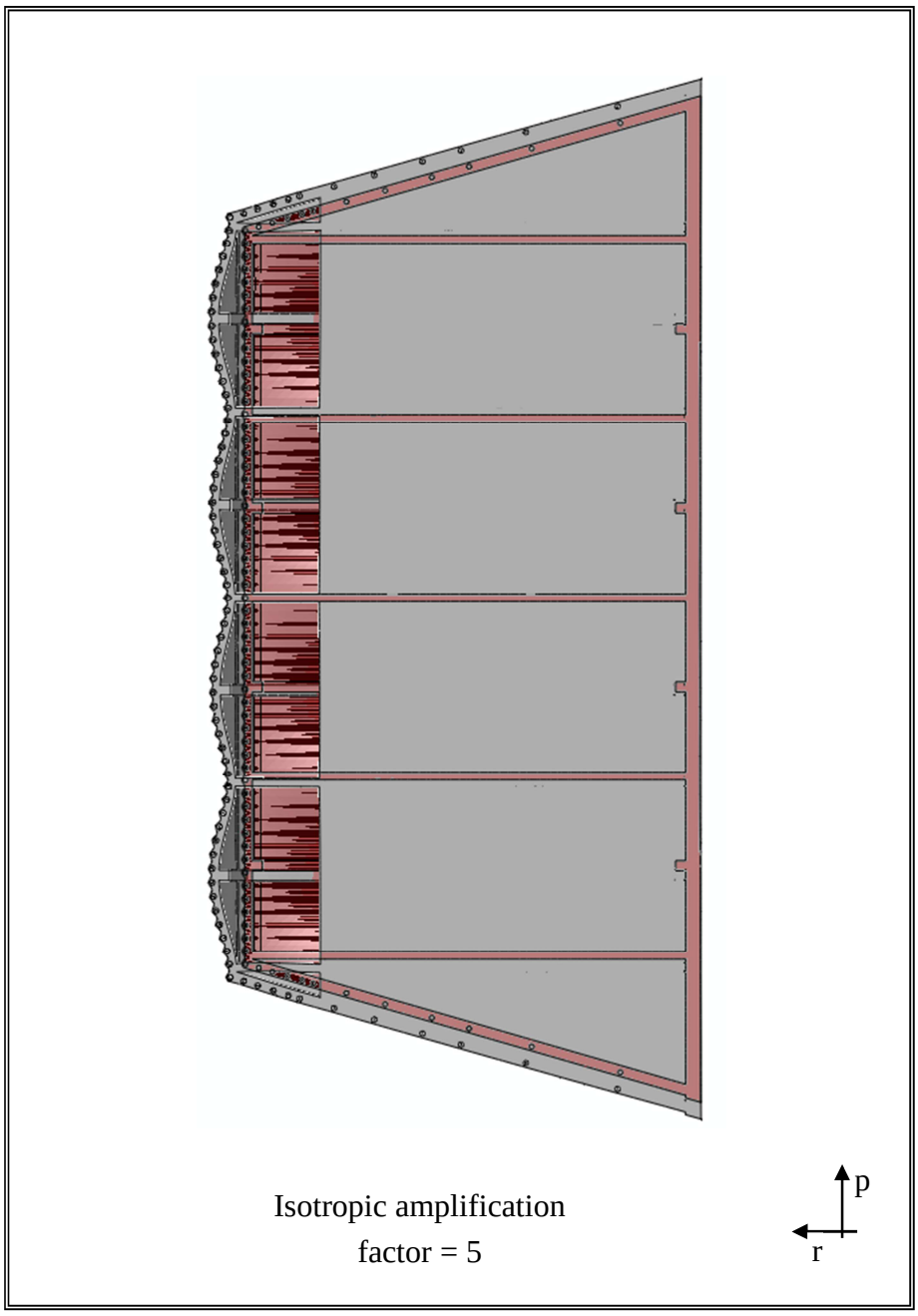


Figure 2-78 - Configuration 3 - Case 2 - Deformed vs un-deformed view.

As far as Configuration 3 - Case 3 is concerned, results in terms of total displacement field are shown in Figure 2-79, where maximum $U_r$ and $U_p$ values are highlighted. Moreover, the deformed vs un-deformed geometric configuration has been reported in Figure 2-80.

Results of Configuration 3 - Case 3 are very similar to those obtained from Configuration 3 assessed in the first step of the parametric campaign of analysis devoted to optimize SP geometric layout.

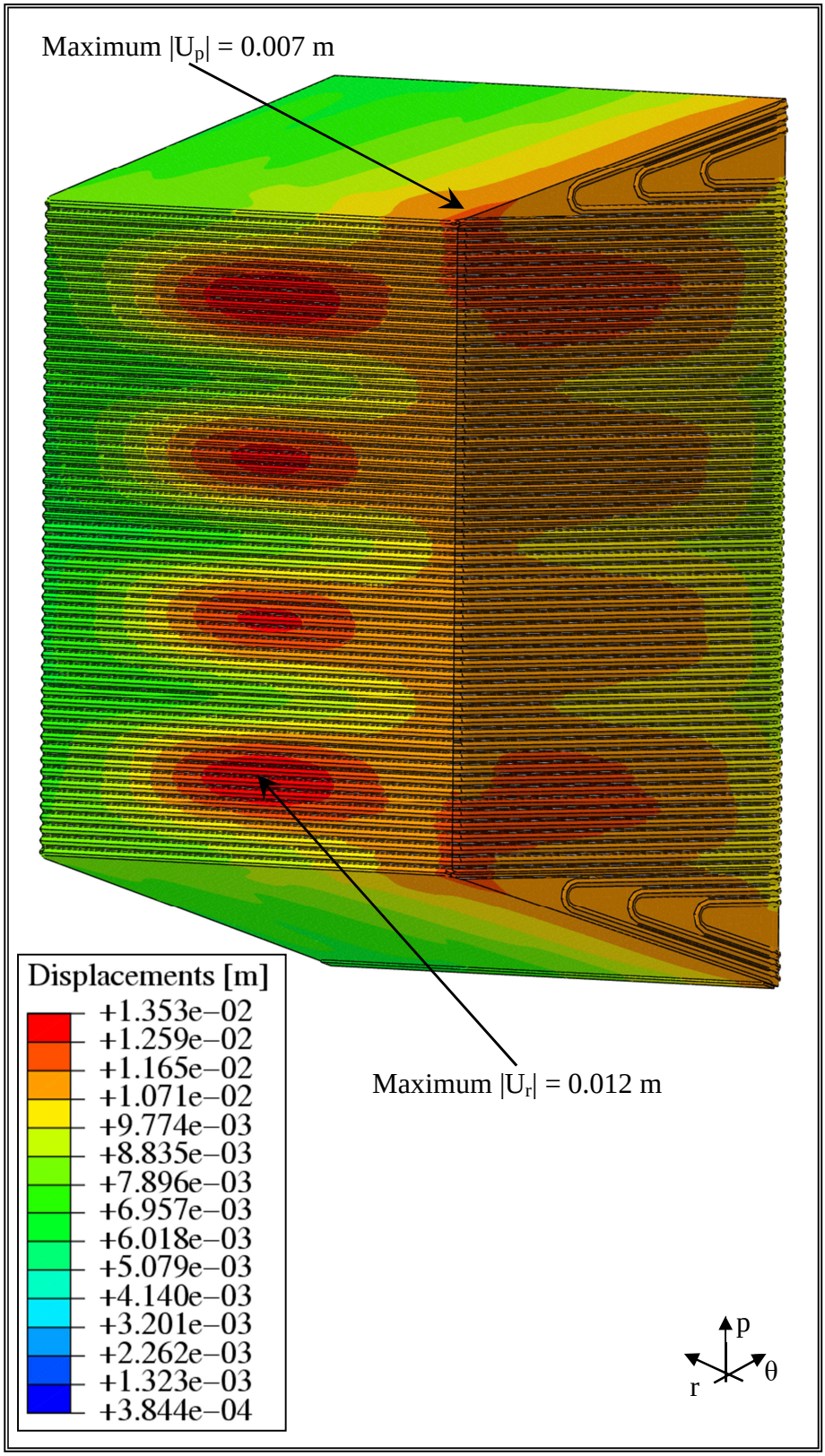


Figure 2-79 - Configuration 3 - Case 3 - Displacement field.

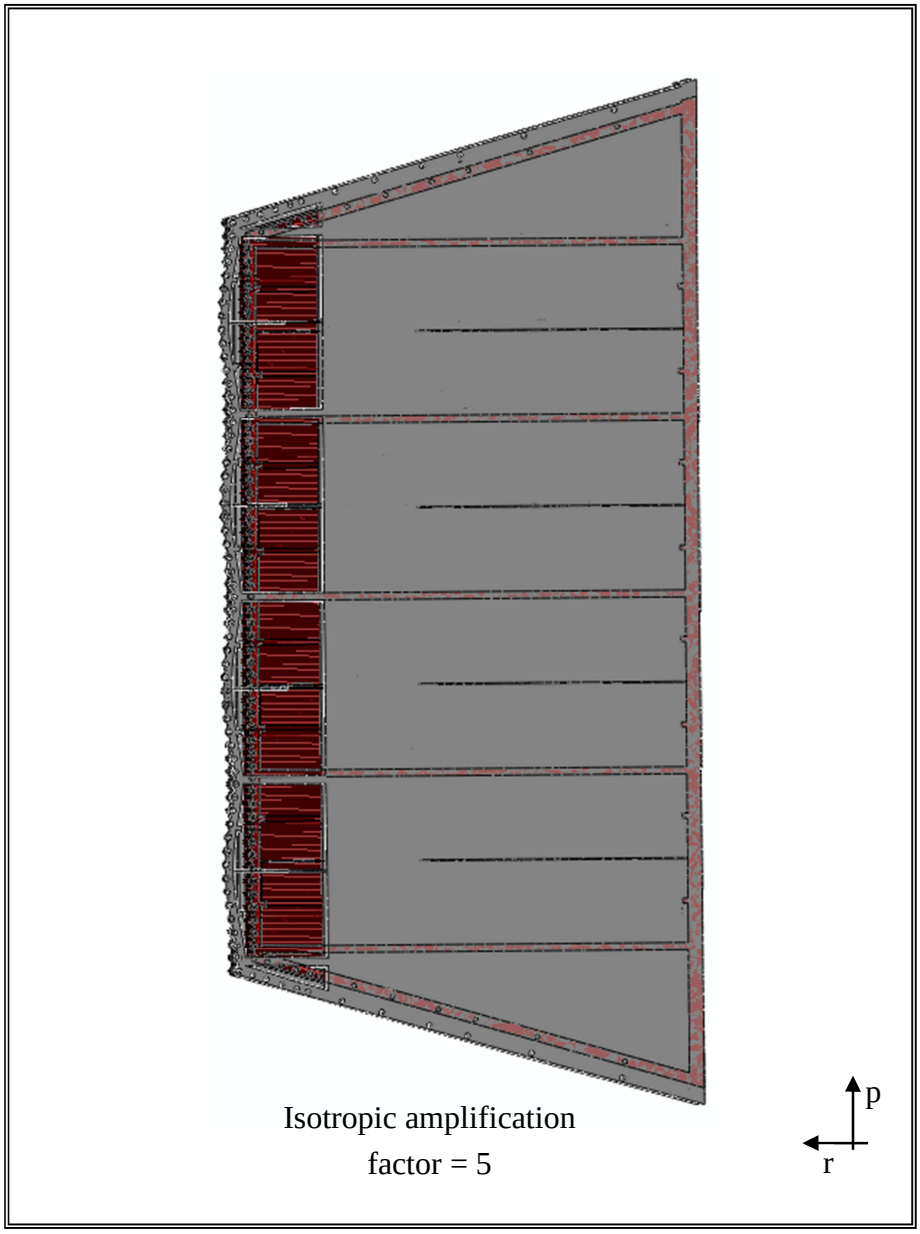


Figure 2-80 - Configuration 3 - Case 3 - Deformed vs un-deformed view.

Concerning Configuration 3 - Case 4, results in terms of total displacement field are shown in Figure 2-81, where maximum $U_r$ and $U_p$ values are highlighted. Moreover, the deformed vs un-deformed geometric configuration has been reported in Figure 2-82.

Results of Configuration 3 - Case 4 are once again very similar to those obtained from Configuration 3, hence the design option foreseeing the ribs and the “reinforced” SPs, considered as potential design option alternative to Configuration 3, has been abandoned. In fact, the 4 different sets of geometric modifications introduced have not been useful to improve the thermo-mechanical performance of the SB.

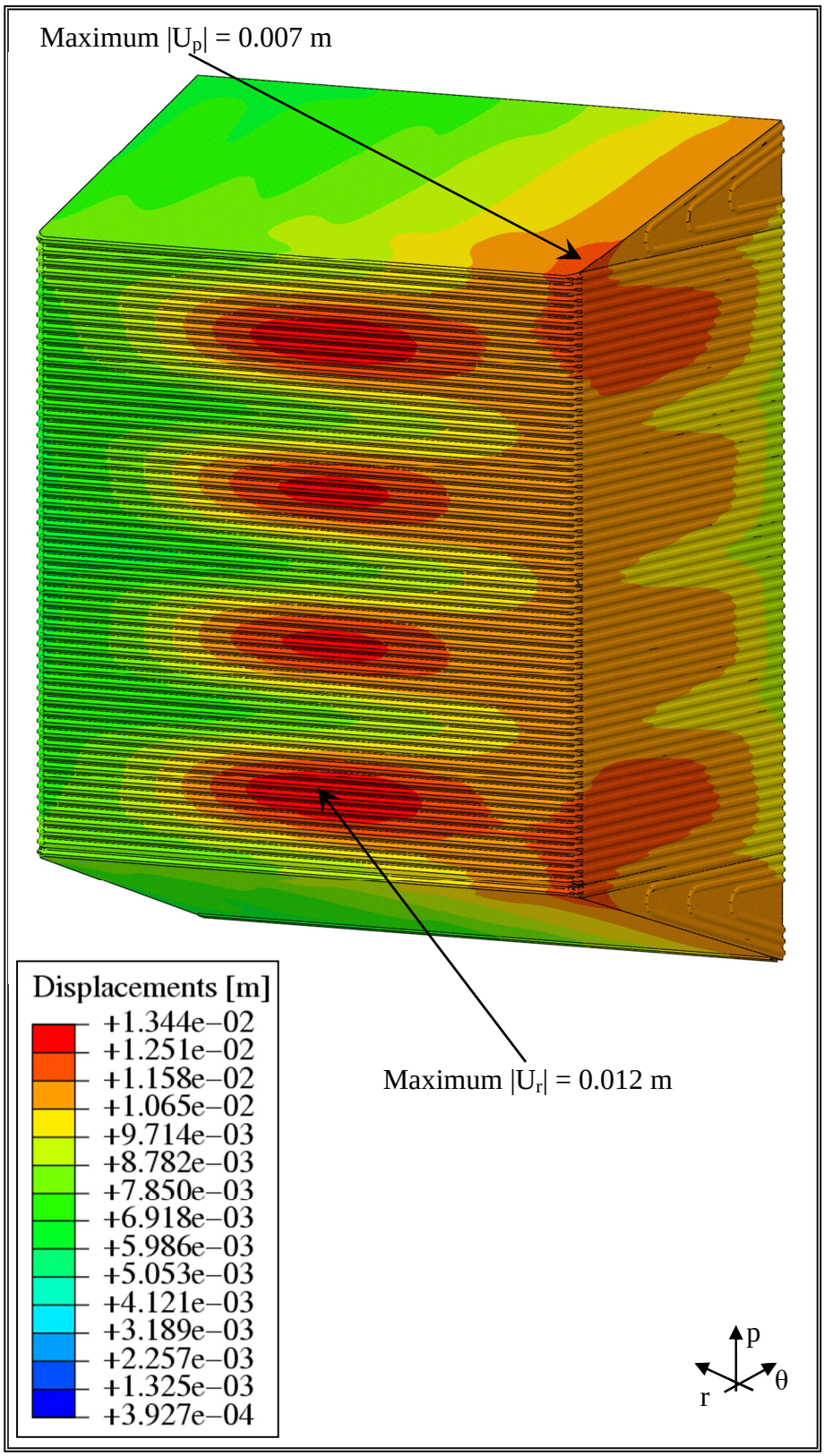


Figure 2-81 - Configuration 3 - Case 4 - Displacement field.

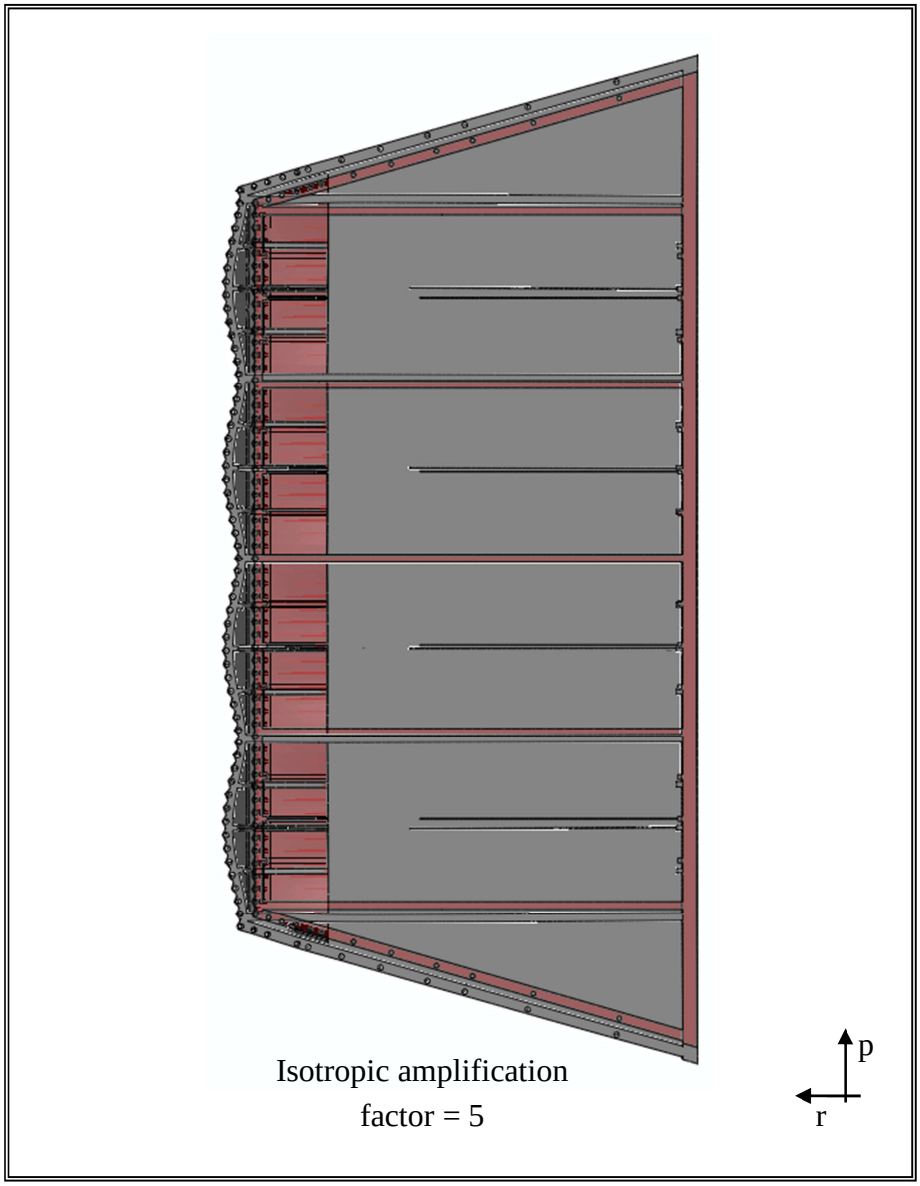


Figure 2-82 - Configuration 3 - Case 4 - Deformed vs un-deformed view.

Hence, Configuration 3 with no modifications has been maintained as the reference one and a further analysis has been performed, aimed at investigating the influence of a SP spatial arrangement variation on the WCLL BB module thermo-mechanical behaviour.

As a first attempt, Configuration 3 with a modified pitch for the radial-toroidal SPs has been investigated under the conservative OP loading scenario. Results in terms of displacement fields are shown in Figure 2-83. Moreover, the deformed vs un-deformed geometric configuration has been reported in Figure 2-84. The obtained results in this further case are encouraging, since the predicted maximum radial displacement decreases from 0.012 m (Configuration 3) down to 0.008 m.

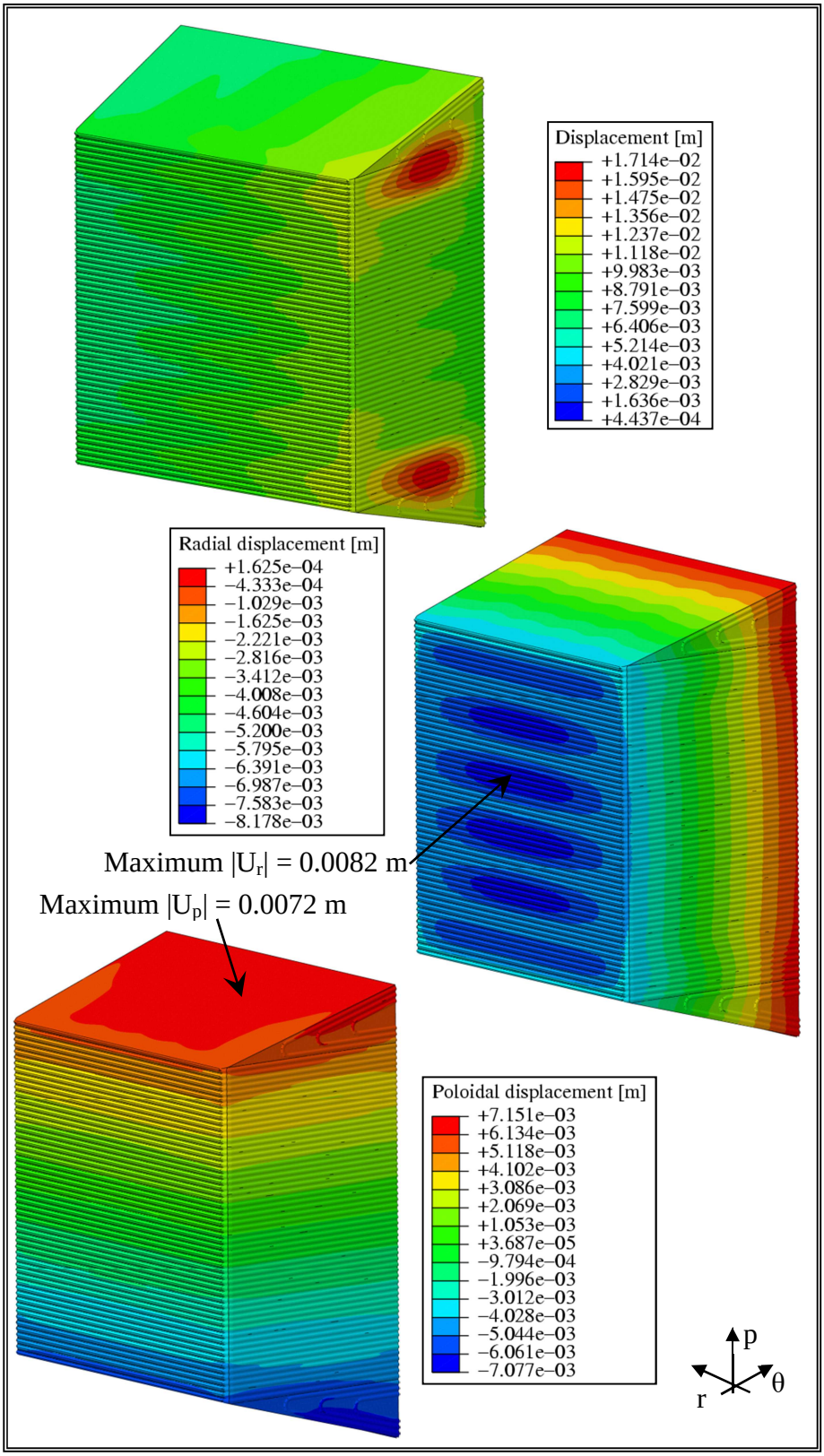


Figure 2-83 - Configuration 3 - Case 4 - Displacement fields.

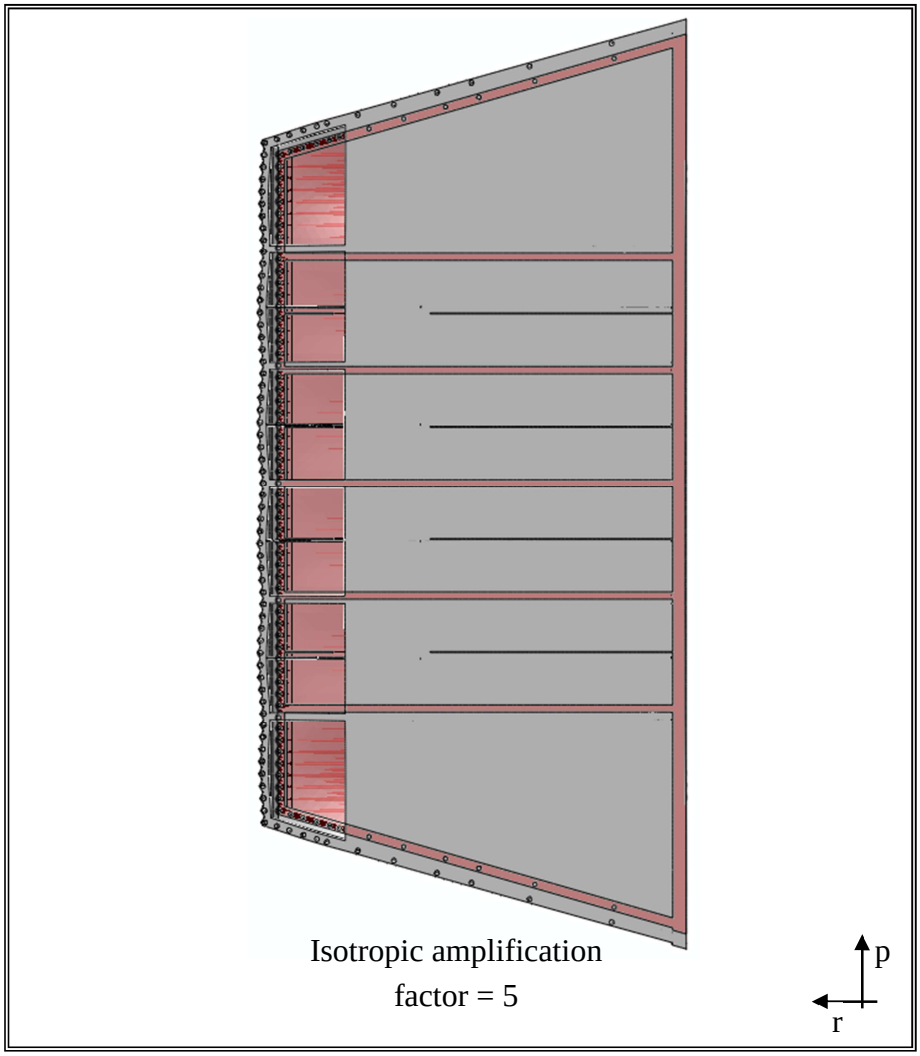


Figure 2-84 - Configuration 3 - Case 4 - Deformed vs un-deformed view.

As a further development of the second step of the parametric campaign of analysis devoted to optimize the SP geometric configuration, the thermo-mechanical behaviour of an additional geometric configuration, named Configuration 6, has been investigated under the steady-state conservative OP scenario. The obtained results in this further case, shown in Figures 2-85 and 2-86, are better than Configuration 3 - new SPs pitch ones, since the maximum value of the radial displacement has been reduced to 0.0071 m. Results of the second step of the SP optimization parametric campaign of analysis have highlighted that the reduction of the radial-toroidal SP poloidal pitch has a positive impact on the module thermo-mechanical performances, leading to a reduction of the radial displacement maximum value, down to ~0.007 m, respect to Configuration 3 of the first step of the parametric study. At the same time, the 5 poloidal-radial SPs adopted ensure the predicted poloidal displacement achieves maximum value close to 0.007 m. These maximum values of radial and poloidal

displacements of Configuration 6 are particularly encouraging, since they are the closest to the reference ones.

For this reason, Configuration 6 represents the best one among those assessed in the two steps of the parametric analysis.

For sake of clearness, maximum values of the radial and poloidal displacements calculated in all the configurations taken into account up to this point have been summarized in Table 2-24, where the reference values have been also reported to make easier the comparison between maximum displacements values calculated in the analysis and the correspondent reference values.

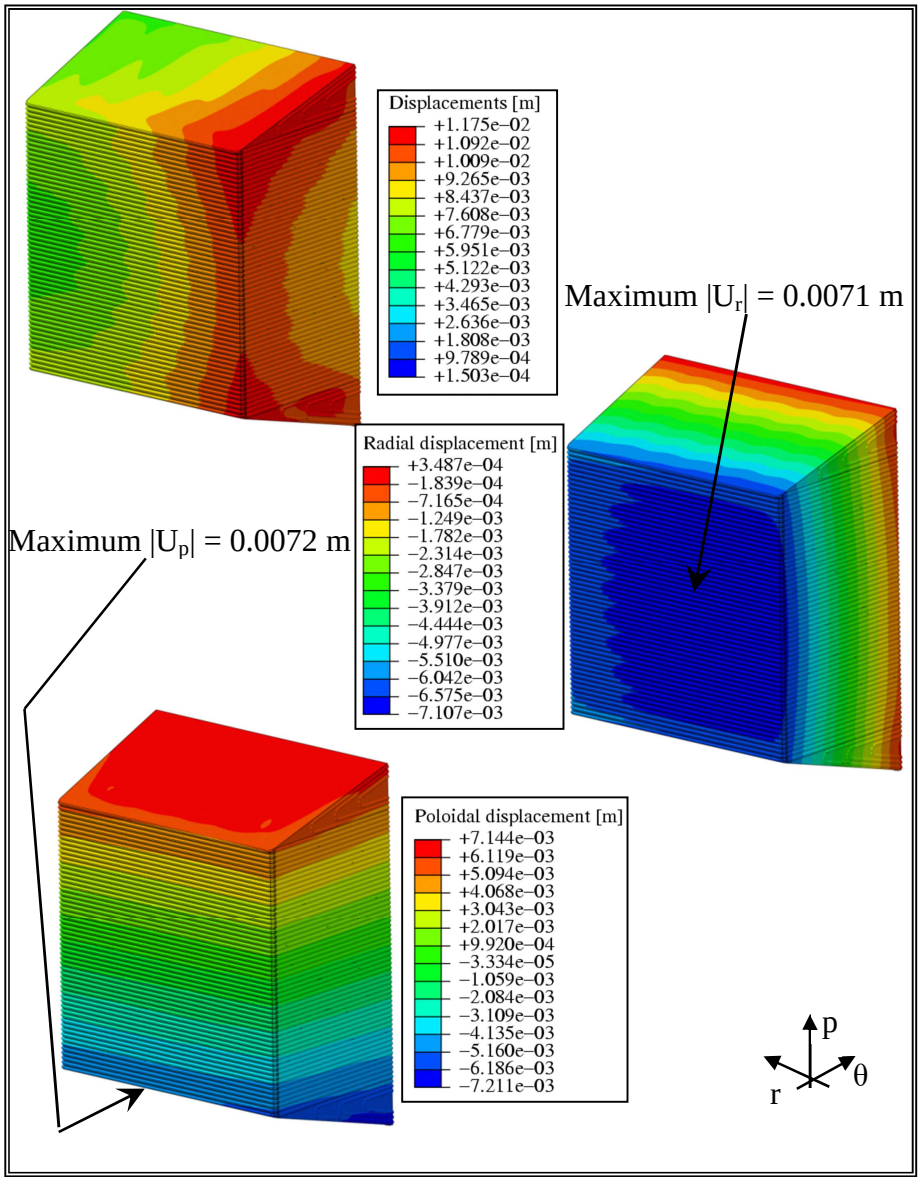


Figure 2-85 - Configuration 6 - Displacement fields.

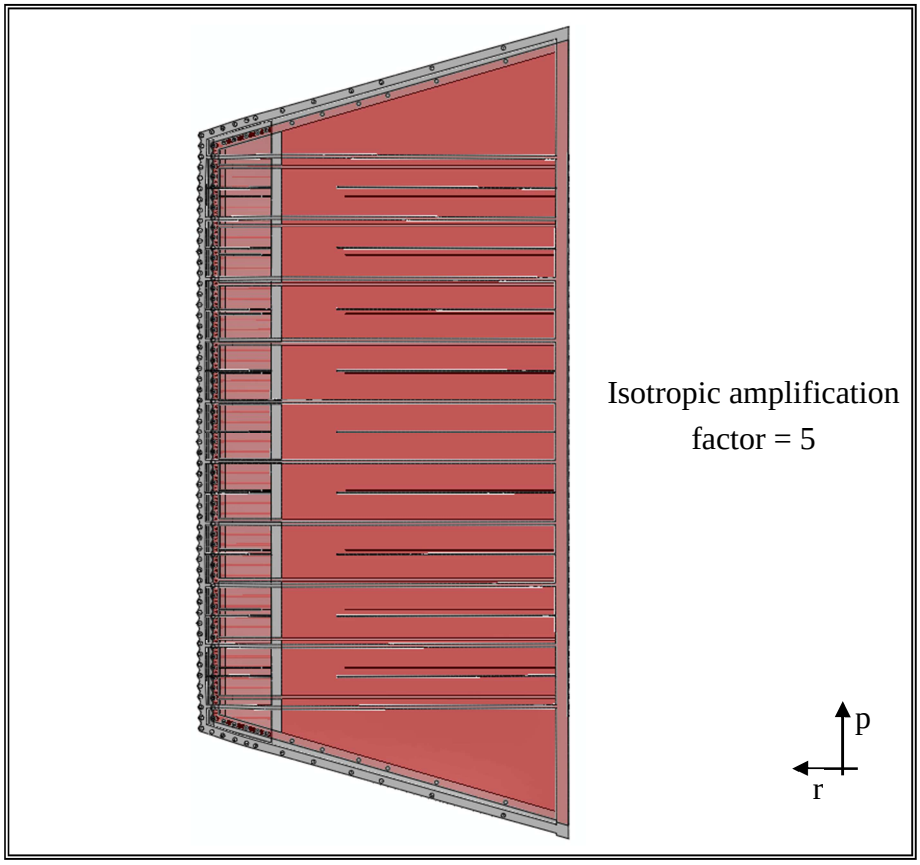


Figure 2-86 - Configuration 6 - Deformed vs un-deformed view.

Table 2-24 - Summary of the obtained results up to the second step of the SP optimization.

| **Configuration** | **$U_{r\ max}$ [m]** | **$U_{p\ max}$ [m]** |
|---|---|---|
| 2012 analysis | 0.0069 | 0.0066 |
| 0 | 0.047 | 0.102 |
| 1 | 0.022 | 0.007 |
| 2 | 0.016 | 0.007 |
| 3 | 0.012 | 0.007 |
| 4 | 0.023 | 0.007 |
| 5 | 0.021 | 0.007 |
| 3 - Case 1 | 0.0132 | 0.0080 |
| 3 - Case 2 | 0.0133 | 0.0071 |
| 3 - Case 3 | 0.0123 | 0.0071 |
| 3 - Case 4 | 0.0122 | 0.0071 |
| 3 - new pitch | 0.0082 | 0.0072 |
| 6 | 0.0071 | 0.0072 |

On the basis of results summarized in Table 2-24, a third step of the SP parametric optimization campaign has been launched in order to refine the SP configuration selected in the Configuration 6. Results of this latter configuration have been the closest to the reference ones. Nevertheless, a further step of the SP optimization procedure has been done in order to possibly improve SP thermo-mechanical performances in terms of displacements. In this third step, two further SP geometric configurations (Configuration 7 and Configuration 8, as reported in Table 2-22), derived from Configuration 6 stiffening grid, have been assessed. The obtained results have shown that Configuration 7 SP spatial arrangement is more promising than Configuration 6, since the calculated maximum value of radial displacement has been reduced from 0.0071 m (Configuration 6) to 0.0069 m as well as the predicted maximum value of the poloidal displacement slightly decreases from 0.0072 m (Configuration 6) down to 0.0071 m. Results relevant to Configuration 7 are shown in Figures 2-87 and 2-88.

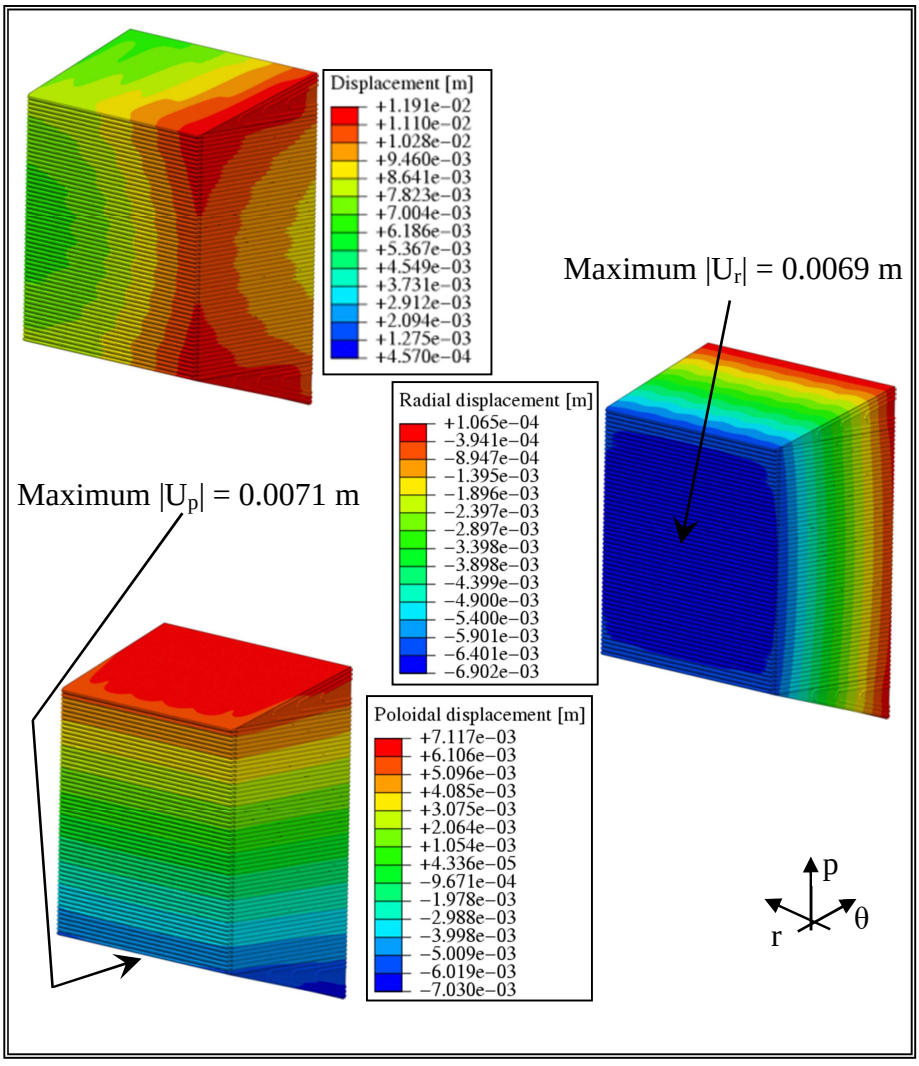


Figure 2-87 - Configuration 7 - Displacement fields.

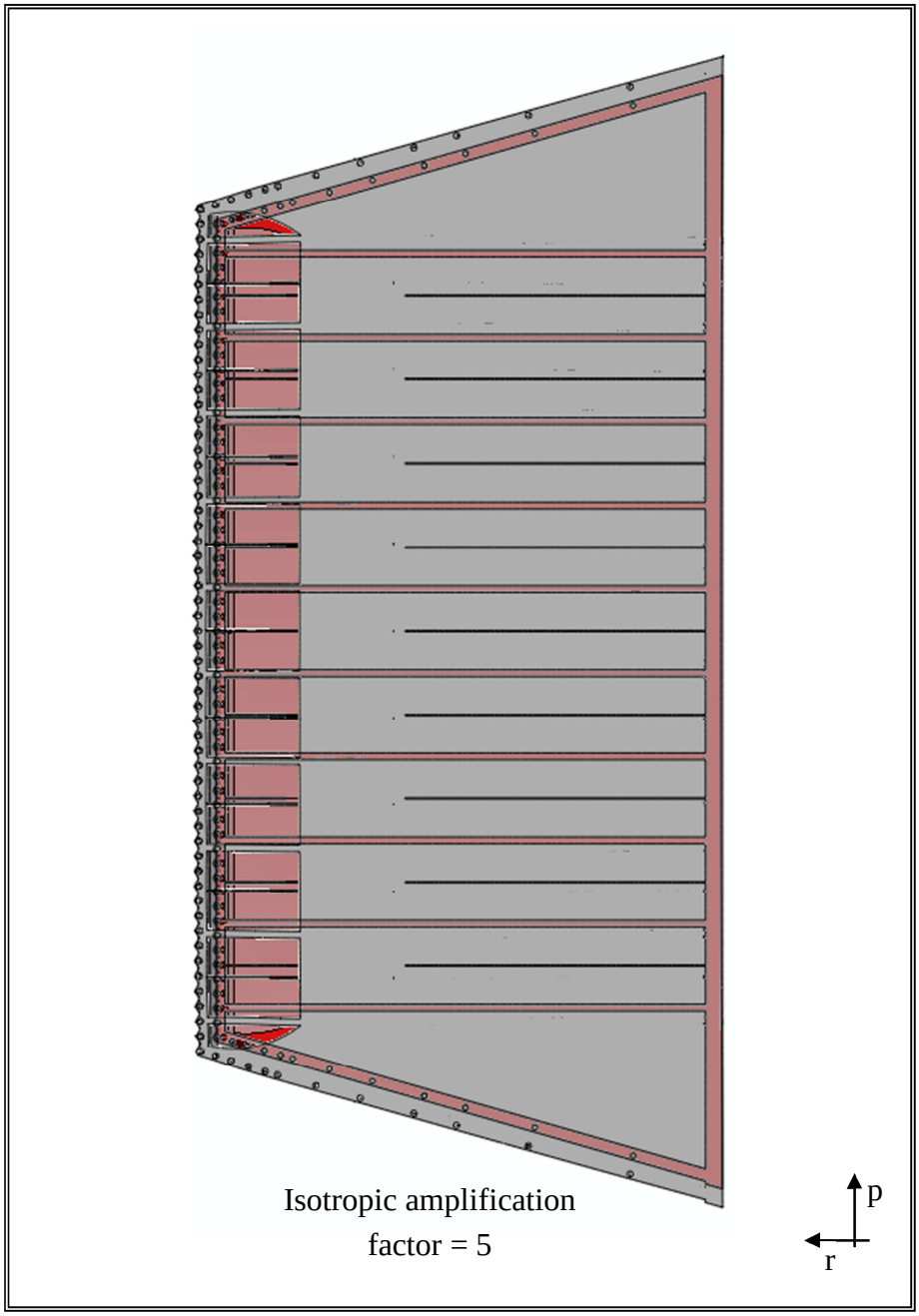


Figure 2-88 - Configuration 7 - Deformed vs un-deformed view.

Regarding Configuration 8, results are shown in Figures 2-89 and 2-90. It has to be observed that, in this case, results in terms of radial and poloidal displacements are the best among those carried out in the whole SP parametric optimization procedure, being the maximum values of both radial and poloidal displacements the most encouraging. In particular, the predicted maximum value of the radial displacement has been equal to 0.0067 m while 0.0066 m has been calculated as to maximum poloidal displacement.

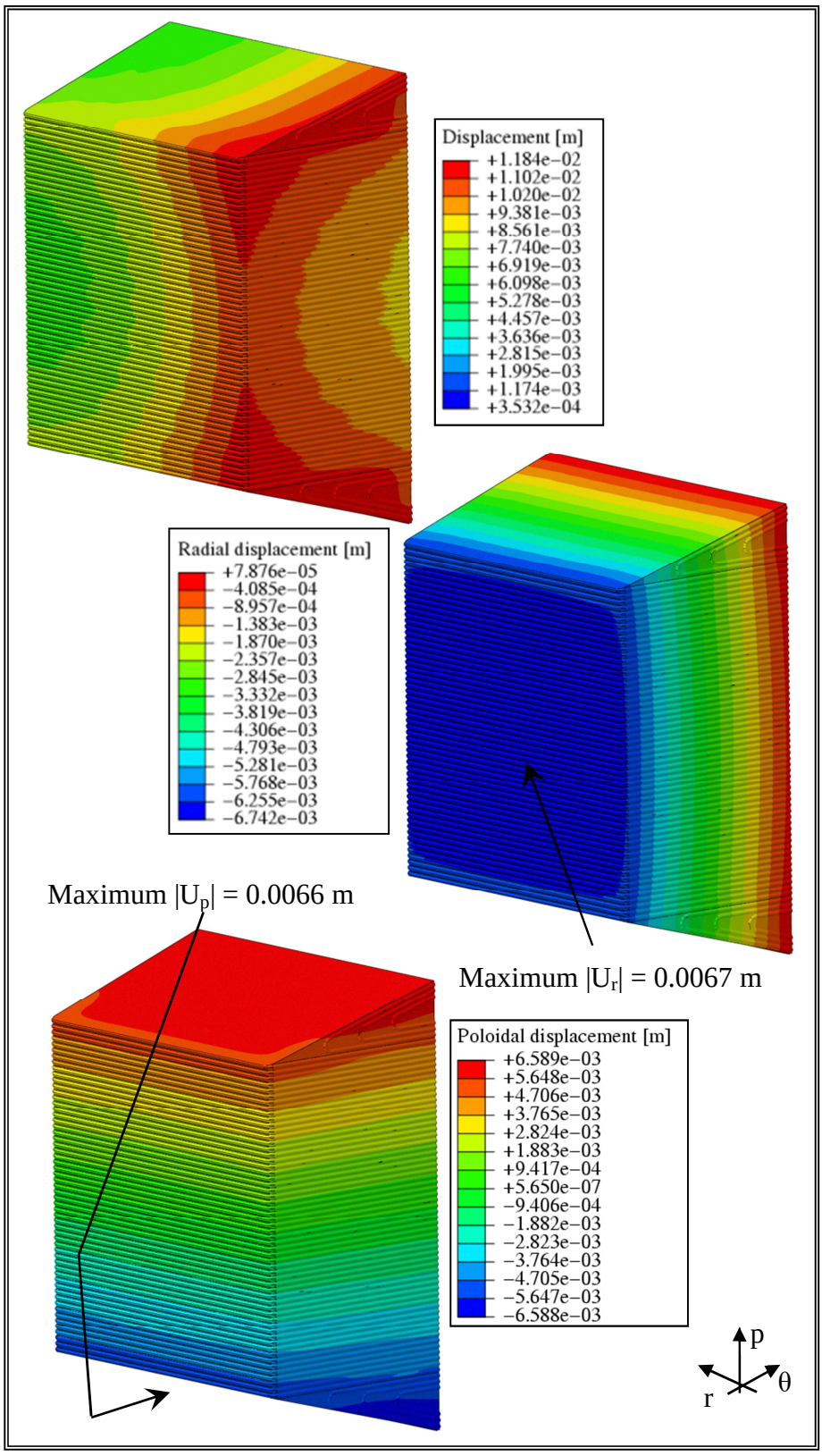


Figure 2-89 - Configuration 8 - Displacement fields.

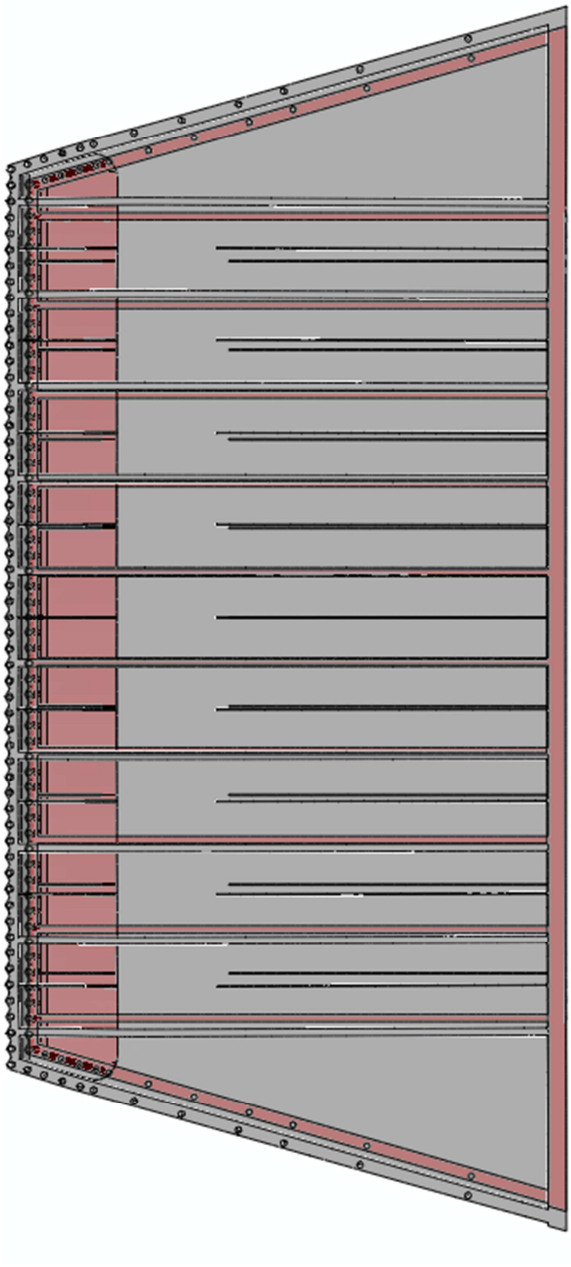

Isotropic amplification
factor = 5

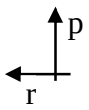


Figure 2-90 - Configuration 8 - Deformed vs un-deformed view.

Finally, results in terms of maximum radial and poloidal displacements during the whole SP parametric optimization campaign have been summarized in Table 2-25, in order to synthetically highlight the thermo-mechanical performances of the different SP geometric configurations taken into account and compare their effect in terms of making the WCLL BB outboard equatorial module SB stiffer.

As it can be observed comparing results of this parametric campaign with SB displacement values carried out in 2012, Configuration 7 and Configuration 8 seem to be the most encouraging for the DEMO WCLL BB design. In fact, maximum displacement values very close to those previously obtained in 2012, adopting a different SP spatial arrangement, have been predicted for these two configurations.

Moreover, the parametric study has shown the necessity to foresee stiffeners along both radial-toroidal and radial-poloidal planes in order to make the SB able to fulfil the loads envisaged for the conservative OP loading scenario.

In fact the initial guess of eliminating the radial-poloidal SPs, in order to strongly reduce the steel amount inside the breeder zone, has been abandoned after the calculation, for these particular SP configurations, of excessively high maximum poloidal displacement due to the pressure exerted by the breeder on the SB wetted surfaces in case of over-pressurization conditions.

Table 2-25 - Final summary of the obtained results.

| **Configuration** | **$U_{r\ max}$ [m]** | **$U_{p\ max}$ [m]** |
|---|---|---|
| 2012 analysis | 0.0069 | 0.0066 |
| 0 | 0.047 | 0.102 |
| 1 | 0.022 | 0.007 |
| 2 | 0.016 | 0.007 |
| 3 | 0.012 | 0.007 |
| 4 | 0.023 | 0.007 |
| 5 | 0.021 | 0.007 |
| 3 - Case 1 | 0.0132 | 0.0080 |
| 3 - Case 2 | 0.0133 | 0.0071 |
| 3 - Case 3 | 0.0123 | 0.0071 |
| 3 - Case 4 | 0.0122 | 0.0071 |
| 3 - new pitch | 0.0082 | 0.0072 |
| 6 | 0.0071 | 0.0072 |
| 7 | 0.0069 | 0.0071 |
| 8 | 0.0067 | 0.0066 |

## 2.6 Summary of the Stiffening Plates design activity

Within the framework of the DEMO R&D activities foreseen by the WPBB of the EUROfusion consortium action, a research campaign has been carried out during the Ph.D. course in order to optimize and design, from the thermo-mechanical point of view, the geometric configuration of the DEMO WCLL outboard breeding blanket equatorial module SPs. In particular, attention has been paid to a SP layout composed of radial-poloidal and radial-toroidal plates, alternative to that proposed by CEA until 2014 and deriving from the ITER TBM research campaign.

The number and the thicknesses of the SPs have been selected as geometric parameters and 3D FEM models of the DEMO WCLL BB outboard equatorial module SB designed by CEA in 2012, properly endowed with several different SP potentially optimized configurations, have been set-up, assuming physically reasonable values for the aforementioned parameters in order to investigate realistic SP configurations.

Thermo-mechanical analysis under the steady-state conservative OP loading scenario have been carried out for each configuration investigated. In order to assess the aptitude of each SP geometric configuration taken into account to make the SB stiffer, avoiding excessive deformation, attention has been focused on radial and poloidal displacement fields arising within SB geometric domain.

Results in terms of SB radial and poloidal displacements have shown that, among all the SP geometric configurations investigated, the most encouraging one is that named Configuration 8, characterized by 10 radial-toroidal 0.012 m thick SPs and 10 radial-poloidal SPs 0.012 m thick. In addition, Configuration 8 includes 9 pierced radial-toroidal SPs 0.002 m thick, each dividing in two equal cells the radial-toroidal region included between two 0.012 m thick SPs. These latter plates does not have structural function, being mainly devoted to address the breeder along the flow path envisaged for it.

For this reason the SP spatial arrangement relevant to Configuration 8 should be taken into account for the new geometric design of the DEMO WCLL BB outboard equatorial module, since it represents the most promising one, in terms of aptitude of making the SB stiffer, among those investigated in the present study.

Nevertheless, in order to attain the preliminary DEMO WCLL BB outboard equatorial module design reported in §1.4, the WCLL BB design team, coordinated by ENEA, has decided to take into account Configuration 7 SPs. This assumption has been justified with the necessity to limit the steel amount inside the breeder zone. In fact, preliminary neutronic analyses [4] [42-44] have shown that an excessive steel amount within breeder zone does not allow to obtain acceptable TBR values. Therefore, considered that obtained results for Configuration 7 and Configuration 8 are quite similar (Tab. 2-25), the adoption of Configuration 7 allows to save one third of steel volume inside the breeder zone having a

positive impact on the TBR prediction without a significant loss under the thermo-mechanical point of view. In fact, being equal the rθ SP number and the thickness (Tab. 2-22), Configuration 7 foresees 5 radial-poloidal SPs 0.016 m thick while Configuration 8 is characterized by 10 radial-poloidal SPs 0.012 m thick.

# Chapter 3

# THERMO-MECHANICAL ANALYSIS OF THE DEMO WATER-COOLED LITHIUM LEAD BREEDING BLANKET OUTBOARD EQUATORIAL MODULE

## 3.1 Introduction

Within the framework of EUROfusion R&D activities an intense research campaign has been carried out during the Ph.D. course in order to investigate the thermo-mechanical performances of the DEMO Water-Cooled Lithium Lead breeding blanket. In particular, attention has been paid to the most recent geometric configuration of the DEMO WCLL BB outboard equatorial module, as designed by WCLL BB project on the basis of the outcomes of the FW and SP geometric optimization activities reported in Chapter 2. In particular, some modifications to the FW geometric configuration selected at the end of the dedicated optimization campaign have been implemented in order to fulfil the manufacturing requirements.

In order to assess the DEMO WCLL BB outboard equatorial module thermo-mechanical behaviour, a realistic 3D geometric model of the whole breeding blanket outboard segment, including all the modules and the Back Supporting Structure, has been considered in order to realistically simulate the thermo-mechanical action of the whole blanket segment on the equatorial module.

The research campaign has been mainly focused on the investigation of the module thermo-mechanical performances under the Normal Operation (Level A) and Over Pressurization (Level D) steady state loading scenarios envisaged for the DEMO WCLL BB.

A theoretical-numerical approach, based on the Finite Element Method, has been followed and the qualified ABAQUS commercial FEM code has been adopted.

The obtained thermo-mechanical results have been assessed in order to verify their

compliance with the design criteria foreseen for the structural material. To this purpose, a stress linearization procedure has been performed along the most critical paths located within the module structure, in order to check the fulfilment of both Level A and Level D rules prescribed by the SDC-IC code.

The assumptions and methodology adopted and the obtained results are herewith reported and critically discussed, highlighting the open issues and suggesting the pertinent modifications to DEMO WCLL BB outboard equatorial module design aimed at the obtaining of the complete fulfilment of the prescribed design criteria.

## 3.2 The design of the WCLL BB outboard equatorial module

The geometric optimization campaign, described in Chapter 2, devoted to attain a FW configuration able to fulfil the prescribed SDC-IC structural design criteria, resulted in the determination of the geometric configuration, called Configuration 4, which was judged to be the most promising among those investigated. Similarly, as to SPs, the geometric configuration named Configuration 8 was found to be the most adapt to reduce, as lower as possible, maximum radial and poloidal displacement within the Segment Box. For these reasons, FW Configuration 4 and SP Configuration 8 were assumed as the reference ones in order to attain an innovative design of the DEMO WCLL BB outboard equatorial module.

Nevertheless, the WCLL BB project team has decided to introduce some modifications in order to meet further neutronic and manufacturing requirements.

In particular, as to FW, the main modification regards the radial steel thickness interposed between the tungsten armour and the cooling channels, indicated with a in the geometric optimization procedure. In order to meet the manufacturing design criteria, it has been increased from the value of 1 mm, found out in the geometric optimization campaign, up to 3 mm.

Furthermore, regarding SPs, Configuration 7 has been chosen for the WCLL BB outboard equatorial module design even though Configuration 8 was considered to be the most promising among those assessed in the geometric optimization campaign (Chapter 2). This change has been necessary in order to avoid the presence of an excessive steel amount inside the breeder zone, which may affect the neutronic performances of the WCLL BB causing, in particular, a remarkable decrease in the Tritium Breeding Ratio. In fact the two SP configurations have the same layout as to radial-toroidal SPs, but Configuration 7 foresees 5 radial-poloidal SPs 0.016 m thick while Configuration 8 is characterized by 10 radial-poloidal SPs 0.012 m thick. Therefore, assuming Configuration 7 instead of Configuration 8 allows to save one third of steel volume inside the breeder zone entailing a certain advantage in terms of TBR and not significantly affecting the SB stiffness.

Moreover, the 2 mm thick pierced radial-toroidal SPs have been replaced with 2 mm thick baffle plates, in order to better address the breeder flow within the module.

On the basis of these considerations, the design of the DEMO WCLL BB outboard equatorial module set-up for the analysis of its thermo-mechanical performances is that depicted in Figures 3-1 and 3-2. It mainly consists of an external Segment Box, composed by the FW directly exposed to the plasma, two Side Walls, a Top Cap (TC) and a Bottom Cap (BC) that close the SB in the upper and lower part and a Back Plate that delimits the module in the radial direction. FW, SWs and caps are cooled by means of square channels in which it flows subcooled water at the pressure of 15.5 MPa (PWR conditions). The SB is reinforced with the SPs, which divides the module in 16 toroidal-radial slices along the poloidal direction, and filled with the liquid metal eutectic alloy of Pb-Li acting as breeder and neutron multiplier. The SB internals are cooled by means of bundles of Double-Walled Tubes where it flows water in PWR conditions. In particular, 21 DWTs are foreseen for each toroidal-radial slice.

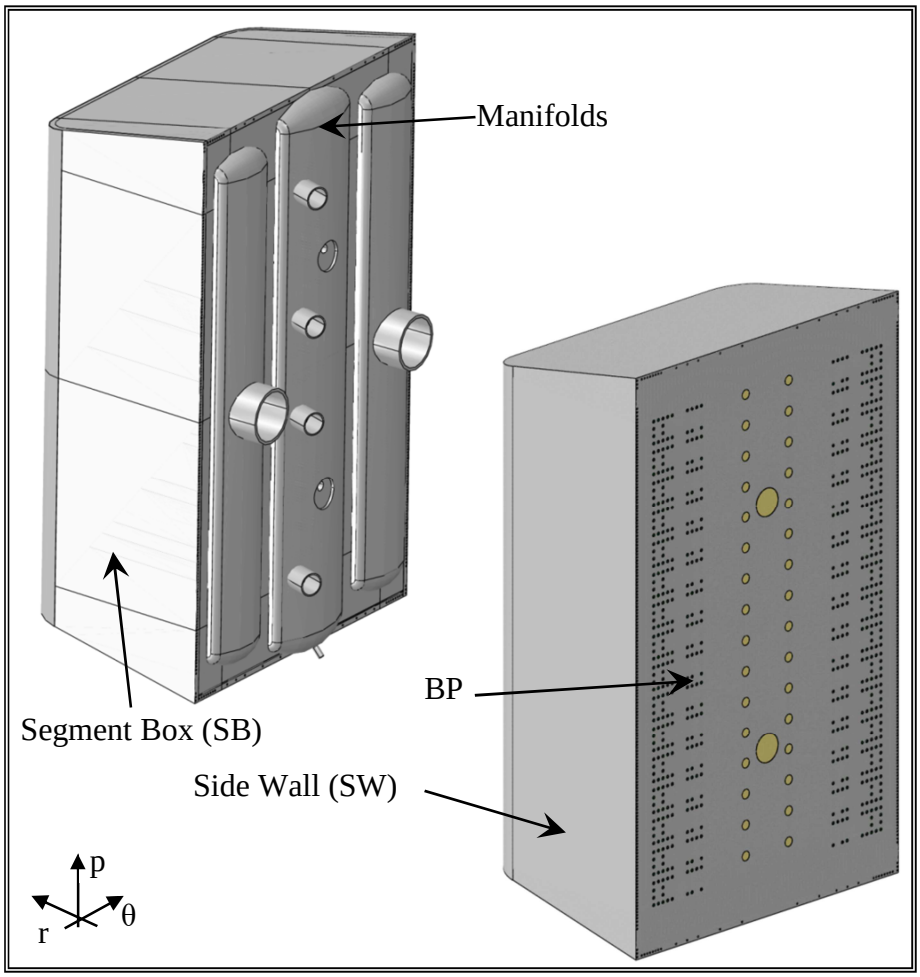


Figure 3-1. The WCLL BB outboard equatorial module - externals.

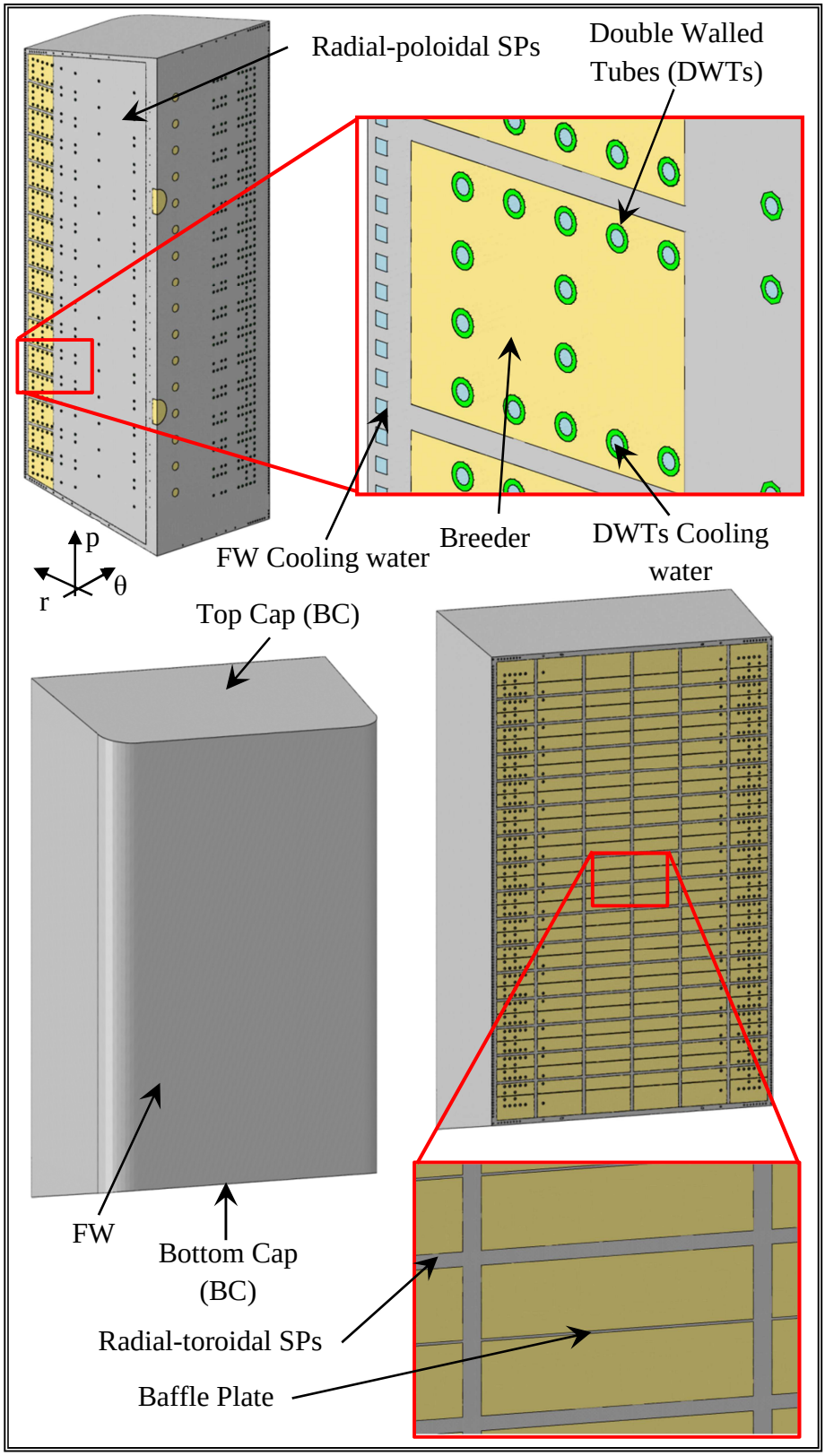


Figure 3-2. The WCLL BB outboard equatorial module - internals.

## 3.3 Thermo-mechanical analysis of the DEMO WCLL BB outboard equatorial module

The research campaign carried out during the Ph.D. course has been focussed on the assessment of the thermo-mechanical behaviour of the WCLL BB outboard equatorial module directly welded to the ribs of the Back-Supporting Structure, purposely lengthened till the back of the module. Moreover, the mechanical effect of the other outboard segment modules has been taken into account by means of the use of "dummy" modules directly tied to the BSS (Fig. 3-3).

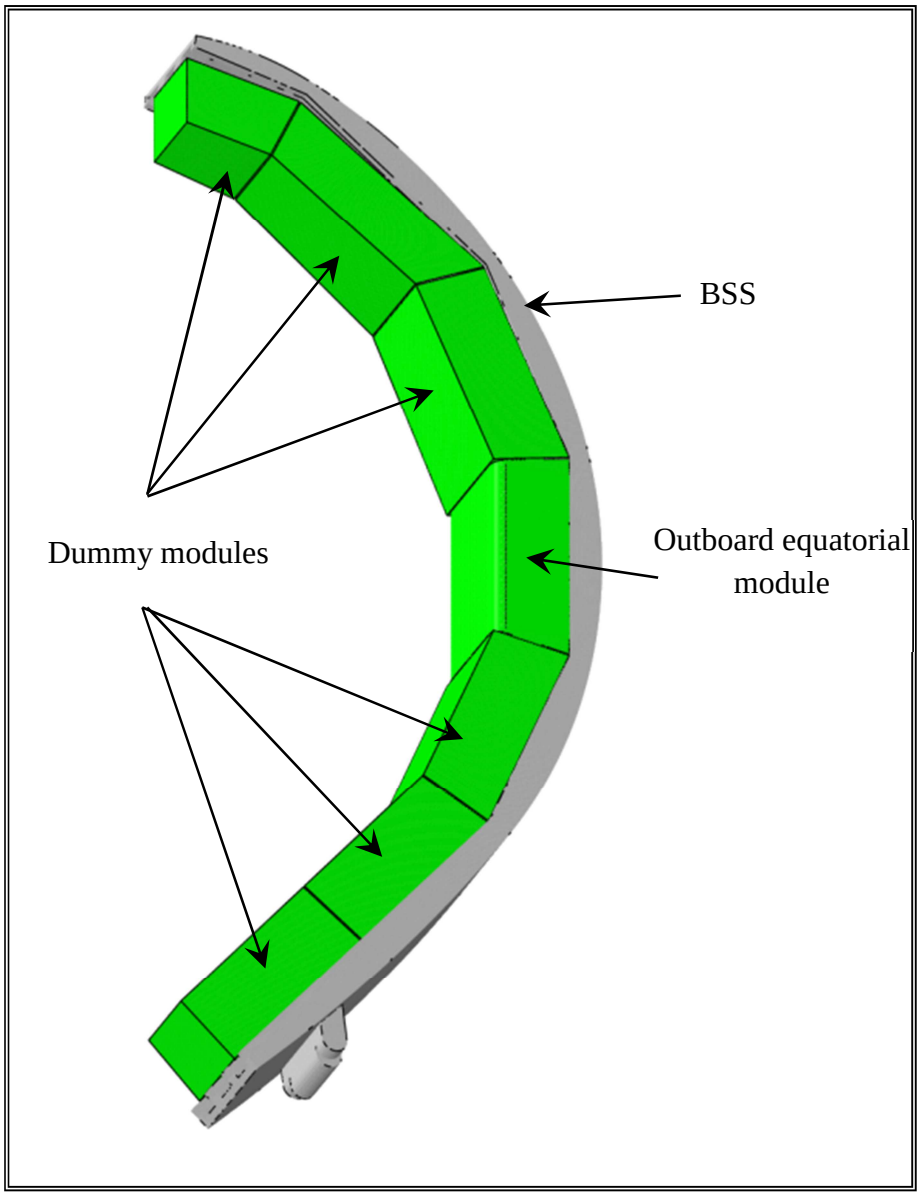


Figure 3-3. The geometric model.

### 3.3.1 The FEM model

In order to perform the thermo-mechanical analysis of the DEMO WCLL BB outboard equatorial module under the selected loading conditions, a detailed 3D FEM model has been set-up. In particular, it reproduces the DEMO WCLL BB outboard equatorial module, including Pb-Li breeder and water coolant flow domain, together with the BSS and the dummy outboard modules.

The FEM model consists in a mesh composed of ~13.6 millions of nodes connected in ~23.2 millions of both linear tetrahedral and hexahedral elements. Some details of the mesh set-up for the equatorial module are reported in Figure 3-4.

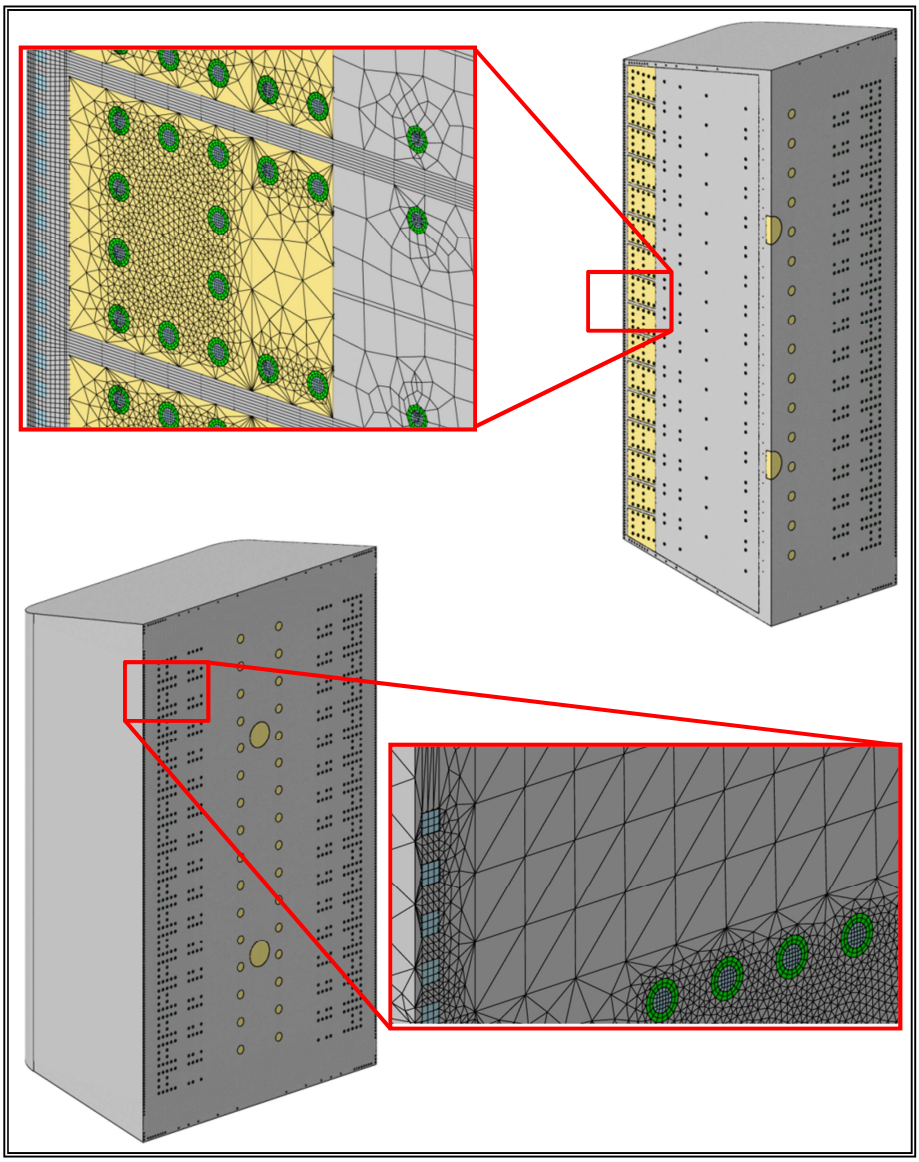

Figure 3-4. Details of the mesh set-up.

### 3.3.1.1 Materials

The whole of SB, SPs and DWTs are made of the reduced activation ferritic martensitic steel EUROFER. A linear elastic model has been adopted for the EUROFER steel, while regarding the thermo-physical properties of both Pb-Li and EUROFER, they have been assumed depending uniquely on temperature. Regarding equatorial module, the 2 mm thick tungsten armour has been properly represented. Thermo-mechanical properties at room temperature (20 °C) have been reported in Table 3-1, while their temperature-dependent behaviours can be deduced from Figures 3-5 - 3-8 [34 - 37] [39] [45] It is remarkable that, with respect to the previously used material data, the updated EUROFER thermo-mechanical properties, reported in [45], have been adopted for these analyses in order to improve the results reliability.

Table 3-1. Materials thermo-mechanical properties at 20 °C.

| Property | EUROFER | Tungsten | Pb-Li | Water at 15.5 MPa |
|---|---|---|---|---|
| $\rho_0$ [kg/m$^3$] | 7744 | 19300 | 10172 | 1005.15 |
| $\lambda_0$ [W/(m·K)] | 28.08 | 174.91 | 7.69 | 0.6055 |
| $c_{p0}$ [J/(kg·K)] | 439.00 | 132.33 | 192.00 | 4138.68 |
| $\alpha_0$ [K$^{-1}$] | $1.03 \cdot 10^{-5}$ | $5.25 \cdot 10^{-6}$ | $1.17 \cdot 10^{-4}$ | - |
| $E_0$ [GPa] | 217 | 408 | - | - |

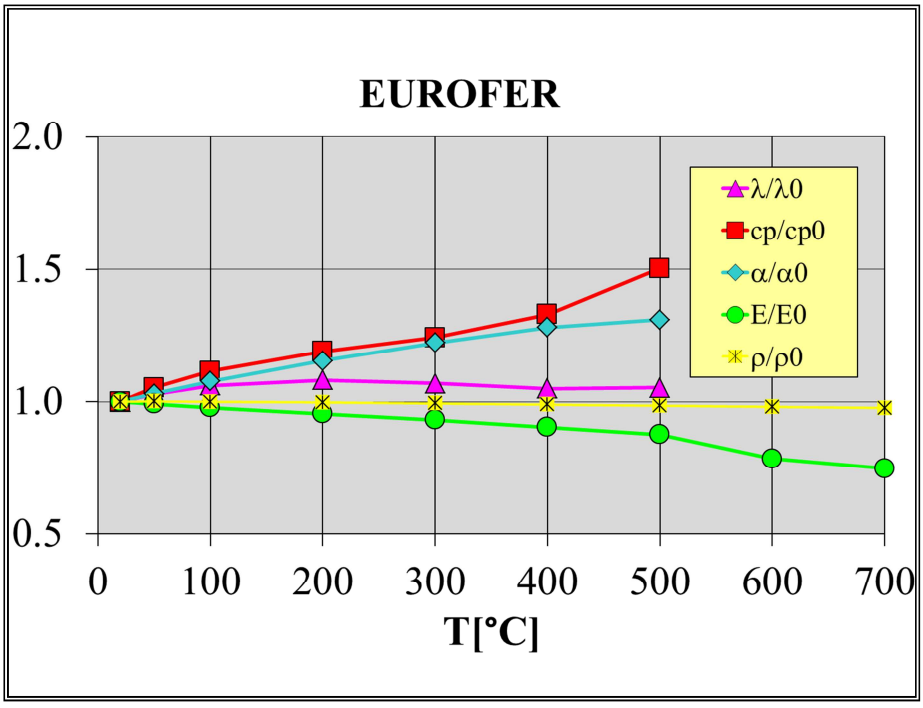


Figure 3-5. EUROFER thermo-mechanical properties vs. temperature.

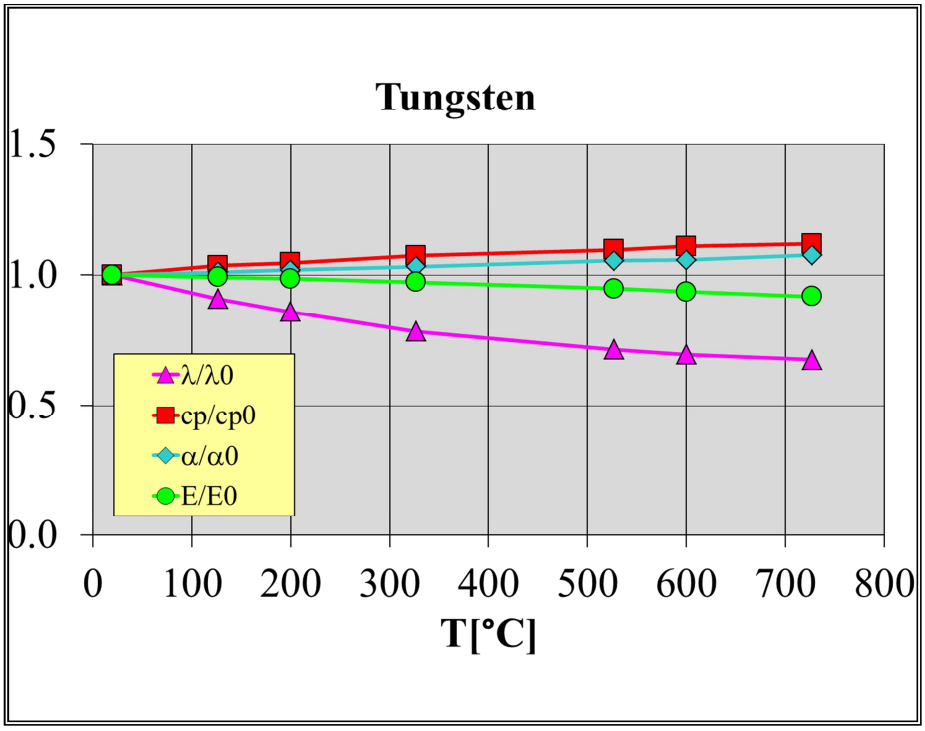


Figure 3-6. Tungsten thermo-mechanical properties vs. temperature.

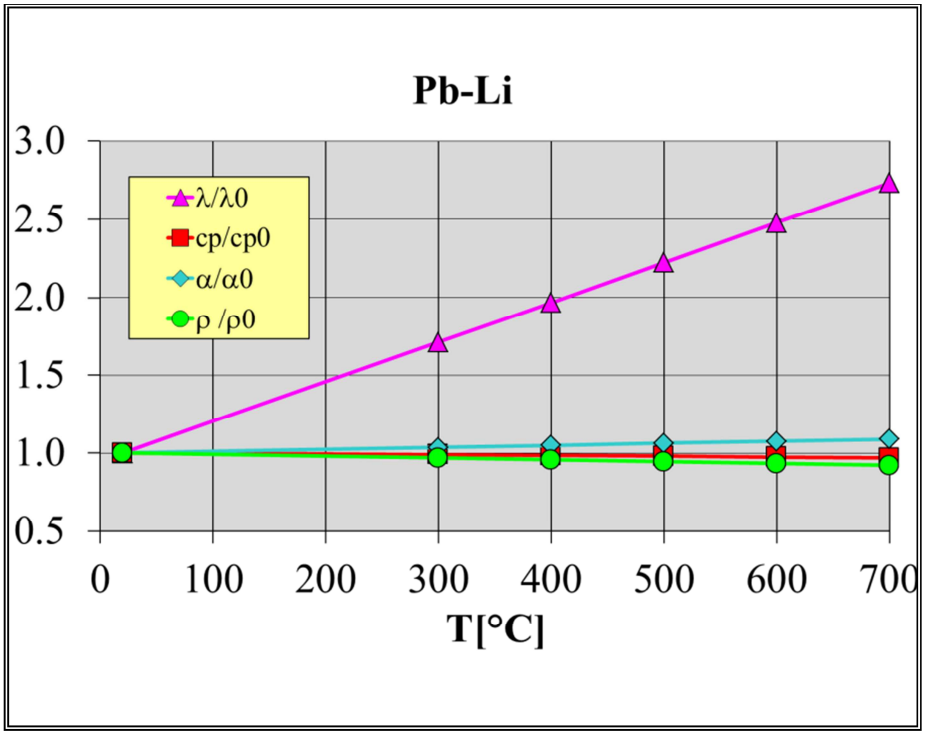


Figure 3-7. Pb-Li thermal properties vs. temperature.

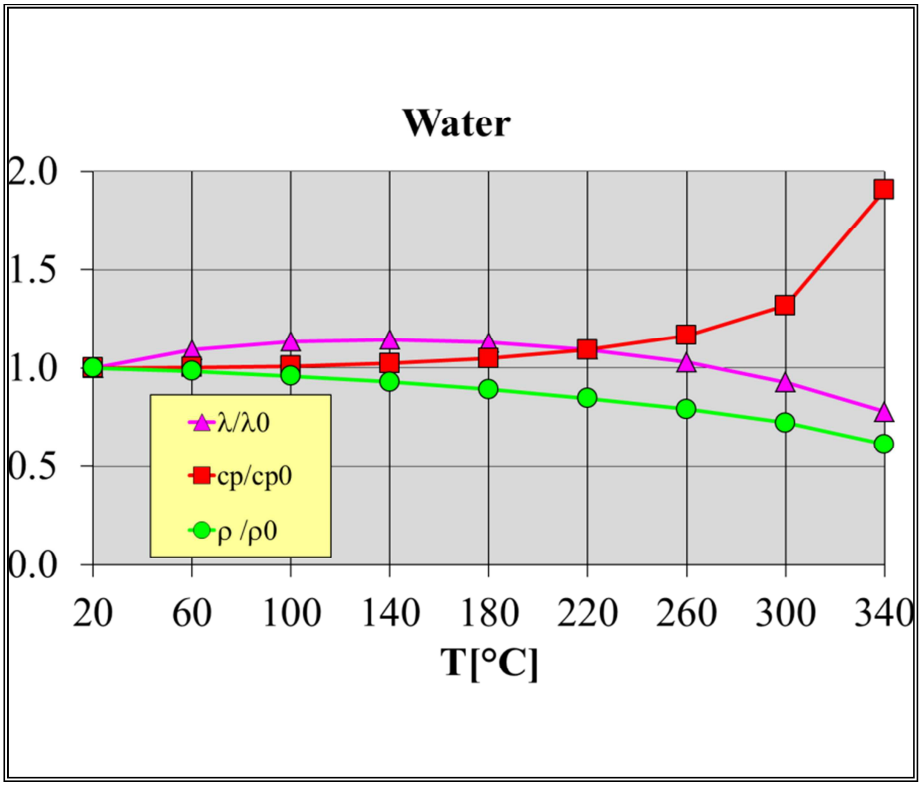


Figure 3-8. Water at 15.5 MPa thermal properties vs. temperature.

### 3.3.1.2 Thermal loads and boundary conditions

The loading conditions relevant to the steady state scenarios of Normal Operation and Over-Pressurization, classified as Level A and Level D, respectively, in the SDC-IC structural design code, have been imposed. In particular, from the thermal point of view, the following loads and boundary conditions have been assumed for both scenarios:

- non-uniform normal heat flux on FW and SW plasma facing surfaces;
- non-uniform volumetric density of nuclear-deposited heat power within structural materials, breeder and coolant;
- forced convective heat transfer within FW-SWs and Cap cooling channels, as well as within breeder DWTs;
- thermal contact model at the breeder-structure interface;
- thermal field imposed to dummy modules and BSS.

Concerning the normal heat flux ($\Phi$) on outboard equatorial module FW and SW plasma facing surfaces, a uniform value ($\Phi_{max}$) has been considered for the FW straight plasma facing surface while a cosine-law dependent heat flux has been imposed onto the SW bend surfaces as indicated in Figure 3-9. Two different values of $\Phi_{max}$ have been assumed equal to 0.5

MW/m² and 1.4 MW/m², hence two thermal scenarios, named Case 1 and Case 2 respectively, have been separately investigated. The non-uniform normal heat flux has been applied to the FW plasma-facing surface by means of a purposely set up FORTRAN routine. The $\Phi_{max}$ value of 0.5 MW/m² corresponds to the reference $\Phi_{max}$ envisaged for the DEMO WCLL BB outboard equatorial module, while the $\Phi_{max}$ value of 1.4 MW/m², coming from the FW optimization campaign, is the maximum normal heat flux that the FW geometric configuration assumed for the module design is able to withstand fulfilling all the thermal-hydraulic and thermo-mechanical design criteria imposed for the FW design procedure, described in Chapter 2.

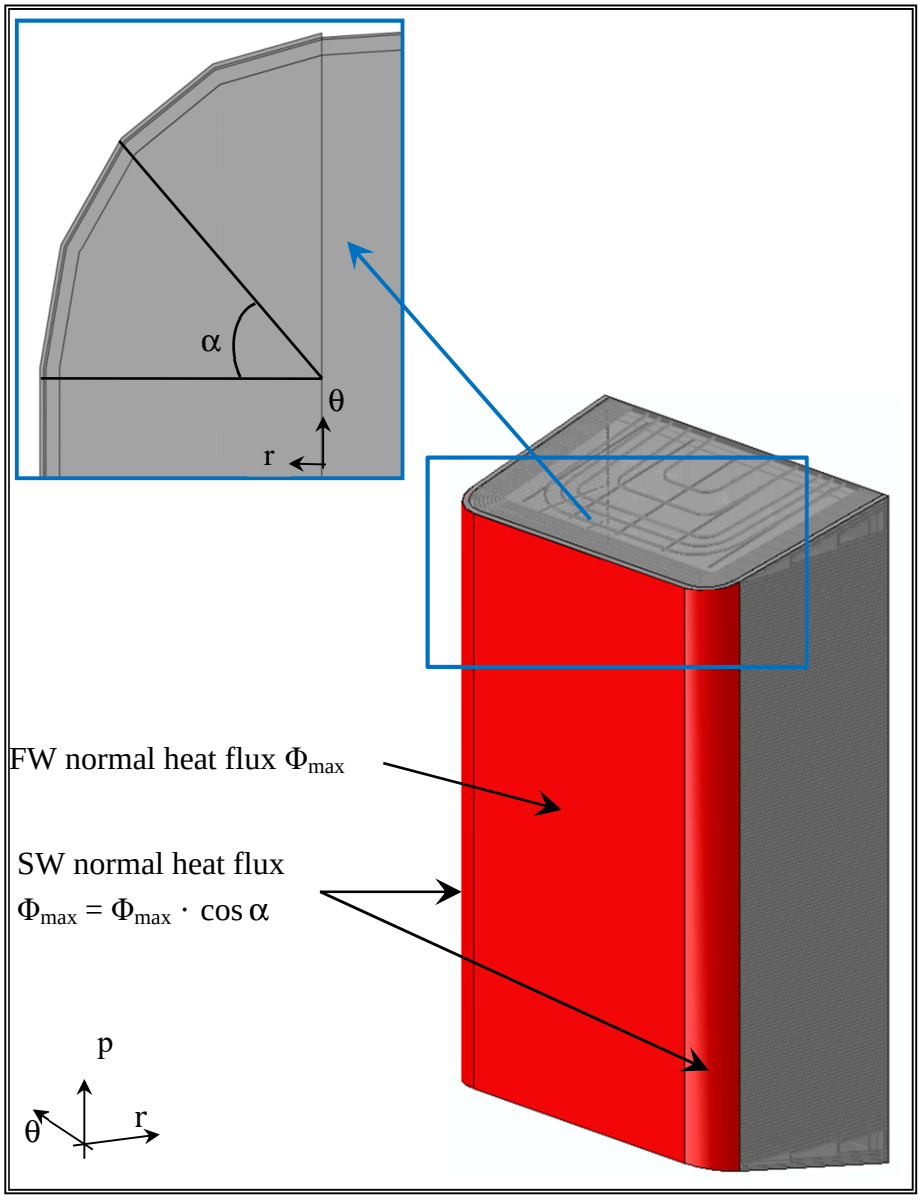


Figure 3-9. The non-uniform normal heat flux.

Regarding the volumetric density of nuclear-deposited heat power within structural materials, breeder and coolant, a non-uniform spatial distribution of heat power volumetric density has been applied to the outboard equatorial module (Fig. 3-10 - 3-12) in order to simulate the deposited nuclear power density taking into account the nuclear heat calculated in [40] and scaled with the DEMO 2015 Neutron Wall Loading.

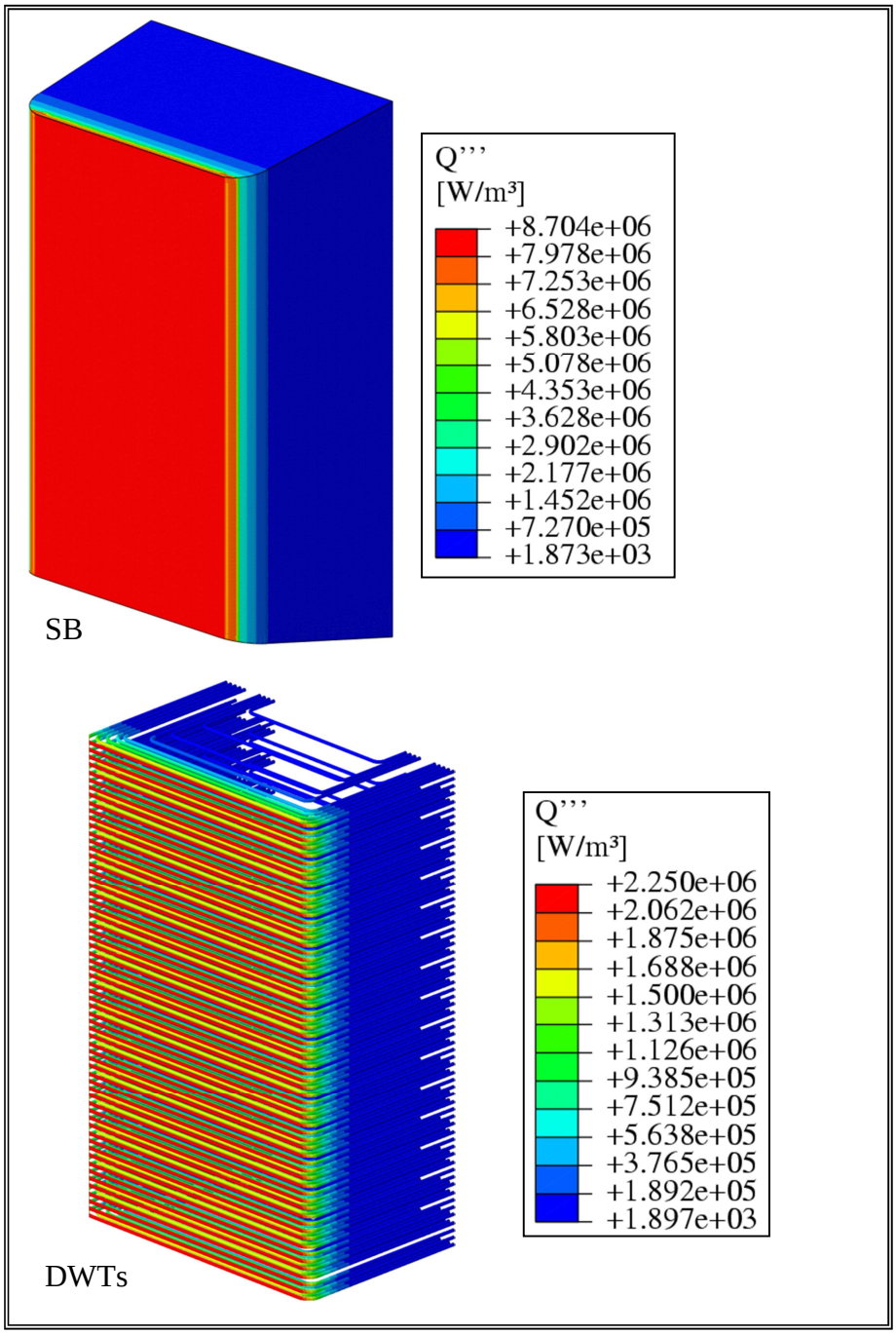


Figure 3-10. The non-uniform volumetric density of nuclear heat power - EUROFER.

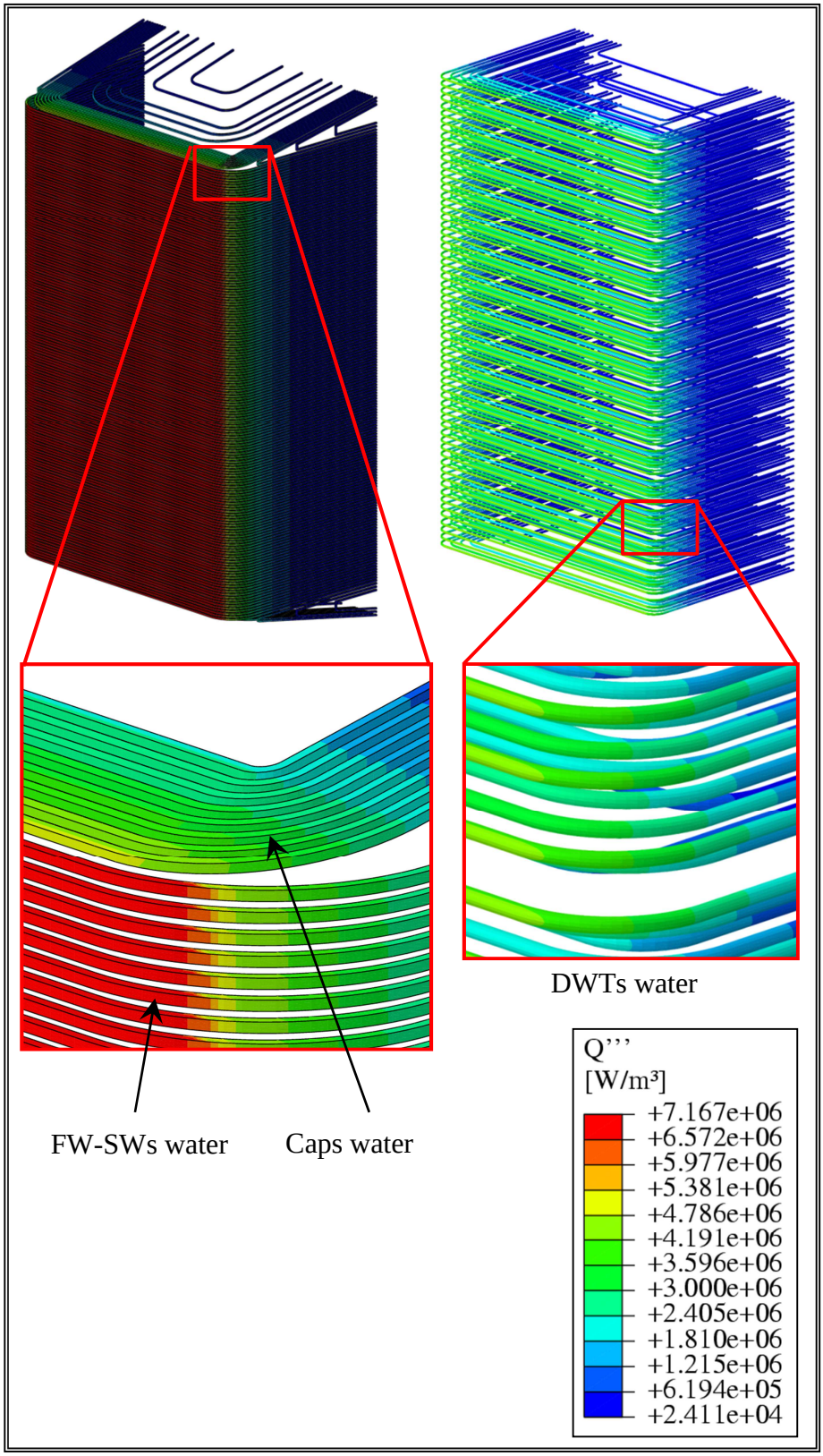


Figure 3-11. The non-uniform volumetric density of nuclear heat power - water.

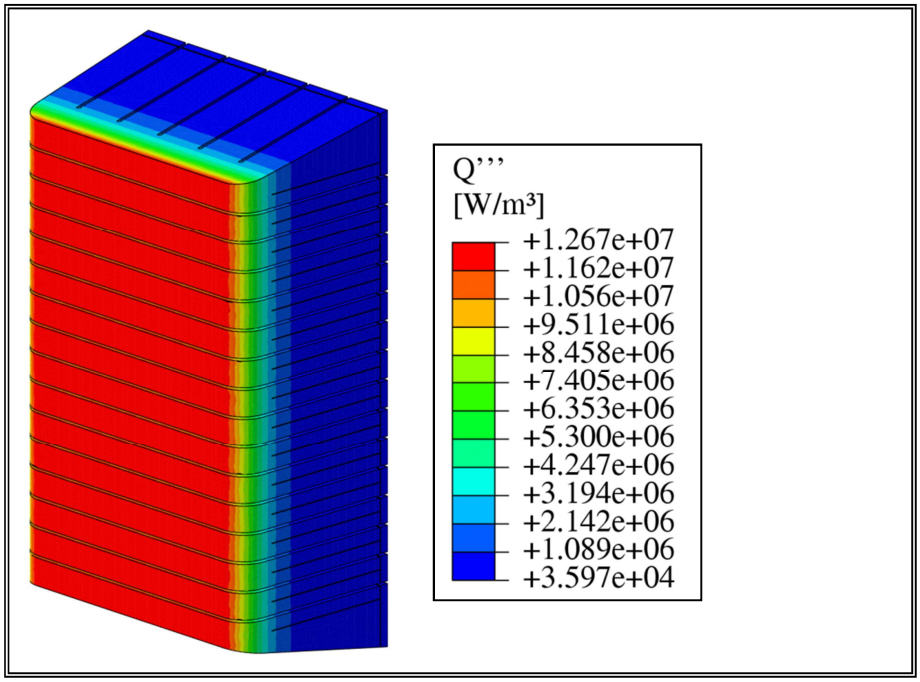


Figure 3-12. The non-uniform volumetric density of nuclear heat power - breeder.

As to forced convective heat transfer between the outboard equatorial module structure and the coolant, it has been simulated modelling convective heat transfer within water flow domain with a simplified FEM approach and adopting a proper thermal contact model between the coolant and the structure wetted walls. As to the FEM simulation of convective heat transfer within water, the so-called "frozen" flow field approach has been adopted. This approach is characterized by the assumption that mass flow rate and heat transfer coefficient values within each channel or tube do not change during the analysis, allowing the calculation, solving by FEM the energy transport equation in the water flow domain, of the spatial distribution of coolant temperature within channels and tubes.

In this particular case, mass flow rates and heat transfer coefficients have been calculated imposing a water temperature increase of 40 °C ($\Delta T_{Design}$) between the inlet and the outlet manifolds. The inlet coolant temperature has been set equal to 285 °C. Concerning the coolant path, regarding Caps and FW-SWs water a counter-current flow scheme has been envisaged while, as to DWT coolant, a flow along a unique direction has been supposed.

Both heat transfer coefficients, calculated adopting the Dittus & Bölter correlation, and mass flow rates needed to ensure the $\Delta T_{Design}$ have been calculated using a purposely set up iterative procedure [46]. In particular, the DWTs and the Cap channels have been divided into different groups on the basis of their minimum radial distance from the FW. A proper mass flow rate and heat transfer coefficient value has been calculated for each of them. Mass flow rate (G) and Heat Transfer Coefficient (HTC) values, computed adopting the aforementioned

iterative procedure, are reported in Table 3-2. It has to be underlined that, since mass flow rate depends on the power to be removed, two different G values for each channel or tube have been calculated on the basis of the thermal case taken into account. Finally, concerning the breeder, no buoyancy effects have been taken into account, assuming the Pb-Li as still. Therefore, pure diffusive heat transfer has been conservatively supposed within the breeder neglecting any forced, buoyancy and or magnetohydrodynamic effect on heat transfer promotion.

Table 3-2. Mass flow rates and heat transfer coefficients.

| **Case 1** | | |
|---|---|---|
| | **G [kg/s]** | **HTC [W/m²°C]** |
| FW channel | 0.0676 | 18801.84 |
| TC channel - Min | 0.0071 | 3083.43 |
| TC channel - Max | 0.0262 | 8793.57 |
| BC channel - Min | 0.0079 | 3375.73 |
| BC channel - Max | 0.0251 | 8509.74 |
| DWT - Min | 0.0046 | 2103.37 |
| DWT - Max | 0.0736 | 19205.32 |
| **Case 2** | | |
| | **G [kg/s]** | **HTC [W/m²°C]** |
| FW channel | 0.1464 | 34877.51 |
| TC channel - Min | 0.0081 | 3436.48 |
| TC channel - Max | 0.0213 | 7475.66 |
| BC channel - Min | 0.0092 | 3803.85 |
| BC channel - Max | 0.0213 | 7475.66 |
| DWT - Min | 0.0046 | 2103.37 |
| DWT - Max | 0.0736 | 19205.32 |

As far as the thermal contact model at the breeder-structure interface is concerned, an ideal thermal contact model, characterized by a thermal conductance amounting to $10^5$ W/m$^2$ °C, has been assumed onto the breeder-SB interaction surfaces as well as between breeder and DWTs outer surfaces. This approach allows to simulate a “perfect” thermal contact among surfaces, neglecting the thermal resistance.

Finally, concerning dummy modules, a non-uniform thermal field linearly depending on the radial distance from the FW has been imposed to them. In particular, temperature values ranging from 500 °C on the FW to 300 °C on the BP have been foreseen. In fact, preliminary analysis has allowed to observe a quite uniform temperature, equal to ~300 °C, within

modules back region while a maximum value of 500 °C is considered as reasonable for the modules plasma facing region. As to BSS, a uniform temperature of 350 °C has been imposed on the basis of similar outcomes coming from preliminary thermal analysis [47].

#### 3.3.1.3 Mechanical loads and boundary conditions

The loading conditions relevant to the steady state scenarios of Normal Operation (NO) and Over-Pressurization (OP), classified as Level A and Level D, respectively, in the SDC-IC structural design code, have been imposed. In particular, from the mechanical point of view, the following loads and boundary conditions have been assumed for both scenarios:

- internal pressure distribution according to the considered loading scenario;
- gravity load;
- non-uniform thermal deformation field;
- radial, toroidal and poloidal restraints.

As far as the internal pressure is concerned, in NO scenario a value of 15.5 MPa has been imposed within each cooling tube or channel since this is the nominal pressure envisaged for the cooling water. Moreover, a pressure of 0.5 MPa has been imposed onto the breeder-wetted surfaces in order to simulate the breeder mechanical action. As far as the OP loading scenario is concerned, a pressure of 18.6 MPa, equal to the coolant pressure increased by 20% as indicated in [28], has been imposed onto all wetted surfaces in order to take into account a coolant leak (small in-box LOCA accident) inside the Segment Box.

The weight force has been taken into account properly imposing a gravity load to the whole model.

As to dummy modules, the presence of the breeder has been simulated by imposing an equivalent density, calculated under the assumption that the percentages of steel, water and breeder inside each module are equal to that calculated for the equatorial module and it does not change for the others.

The non-uniform thermal deformation field, arising as consequence of the temperature distribution and the expansion tensor, has been imposed to the equatorial outboard module according to the thermal case taken into account.

Both the WCLL BB outboard equatorial module and the 6 dummy modules have been considered directly welded to the BSS ribs. In order to reproduce the mechanical effect of the outboard segment attachment system to the Vacuum Vessel, the displacements of some sets of nodes have been prevented in both NO and OP loading scenarios. In particular, the displacement along the radial direction has been forbidden to nodes highlighted in blue in Figure 3-13, the toroidal ones to nodes highlighted in red, while radial and poloidal displacements have been prevented to nodes highlighted in yellow.

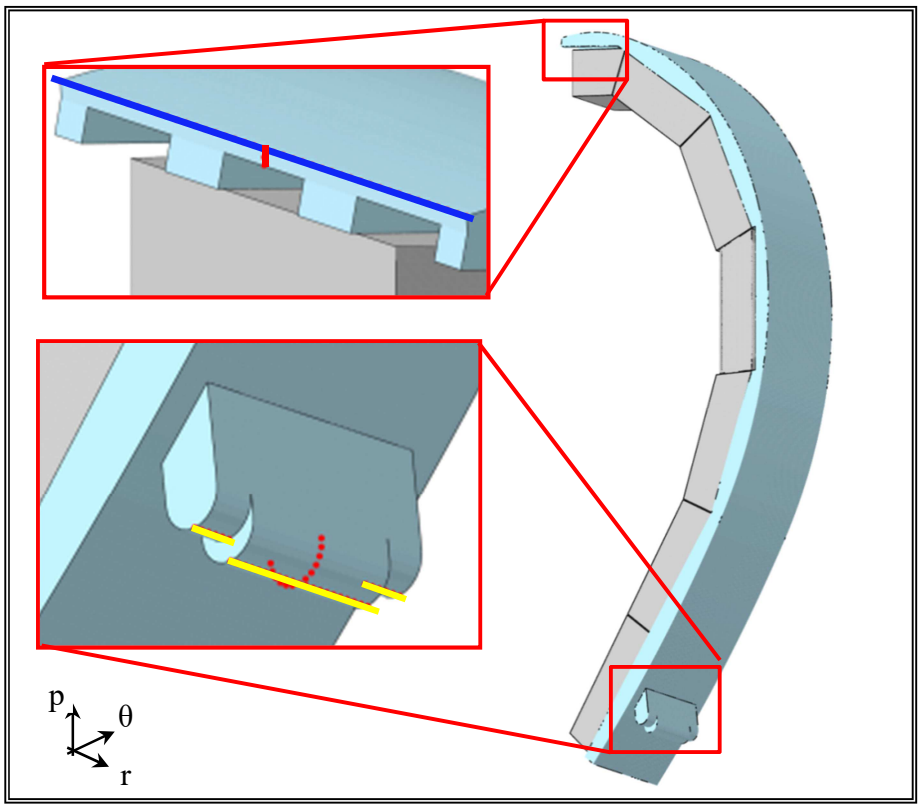


Figure 3-13. Mechanical constraints.

### 3.3.2 Results

Un-coupled steady state analysis have been run in order to assess the thermo-mechanical behaviour of the WCLL BB outboard equatorial module under the selected NO and OP loading scenarios. A stress linearization procedure has been properly carried out in order to verify that the limit design values foreseen for the structural material and the structural design criteria prescribed by the SDC-IC are successfully met. From the thermal point of view, results regarding Case 1 are depicted in Figures 3-14 - 3-17 while thermal fields concerning Case 2 are shown in Figures 3-18 - 3-21. Lastly, in Table 3-3 the thermal power removed in each actively cooled component are reported and, moreover, in Figure 3-22 the Case 2 / Case 1 temperature ratio for the SB is shown. As far as the structural material is concerned, results have shown that temperature values remain below the EUROFER maximum allowable value of 550 °C except in Case 2, where the temperature reaches the maximum value of 582 °C in poorly cooled very restricted areas located near the Cap bend region. Concerning the SB, the hottest parts are located at the interface between baffle plate extremities and breeder, probably due to the fact the breeder circulation has not been modelled. Regarding the breeder, temperature achieves maximum values in the poorly cooled region located in the front region

of the Breeder Zone. Moreover, breeder-structure interface temperature is predicted to be lower than 300 °C nearby the DWT inlet region, suggesting the potential concern of local breeder solidification, while it is predicted to be higher than 480 °C mainly nearby the baffle plates, indicating the potential enhancement of corrosion issues. Finally, the thermal field calculated for the coolant has shown that, regarding water flowing into SW-FW and Cap channels, the maximum temperatures are reached in correspondence of the bend regions of the channels, as a consequence of the counter-current flow. The minimum coolant margin against saturation is predicted in Case 2 and it amounts to 5.6 °C. Regarding the BZ tubes, water flowing into the bundles of DWTs located in the boundary slices (along poloidal direction) experiences temperature values higher respect to that reached in the coolant of the DWTs situated in the inner slices probably due to the not optimized DWT layout in these cells, having a geometric configuration different from the others since they are closed by Caps and by the SW triangular region. As far as Case 1 mechanical results are concerned, the Von Mises equivalent stress fields relevant to NO and OP loading scenarios are shown in Figures 3-23 and 3-24 respectively. It has to be noted that the highest stress values are predicted at the FW-Cap interface probably due to the sharp edge connecting the two components. As to displacement field, results regarding NO and OP scenarios are depicted in Figures 3-25 and 3-26 respectively. As it can be observed, BSS radial and poloidal displacements strongly depend on the set of mechanical restraints imposed for the analysis. This necessarily affects the outboard equatorial module displacement fields, which reach high maximum values. The same remarks can be done for Case 2 mechanical results, reported in Figures 3-27 - 3-28 (Von Mises stress) and 3-29 - 3-30 (displacement fields). Finally, a stress linearization procedure has been carried out along some significant paths of the SB in order to verify whether the Level A and Level D design criteria are fulfilled. In particular, paths lying on the toroidal mid-plane have taken into account for FW, Cap and BP (Fig. 3-31), while paths lying on different poloidal and radial planes have been considered for the SPs (Fig. 3-32). Results are reported in Tables 3-4 - 3-11. Mechanical results relevant to NO scenario have shown, for both Case 1 and Case 2, that the most critical areas are those related to paths located within the SPs and near the Cap, where the criterion against immediate plastic flow localization is not fulfilled. This is probably due to the resistance exerted by vertical SPs against the thermal expansion of horizontal SPs and vice versa, as well as to the compression exerted by BP and Caps, due to their lower poloidal thermal expansion with respect to FW, for paths located near the Cap. Concerning the OP loading scenario, paths located near the Cap continue to do not satisfy all design criteria, especially in Case 2 where the high temperatures reached on the FW cause the failure also for creep damage. On the other hand, less SP paths fail to fulfil the criteria, probably due to the effect of the higher pressure imposed on the internal SB surfaces. All paths located within the BP successfully fulfil all safety criteria in all loading scenarios investigated.

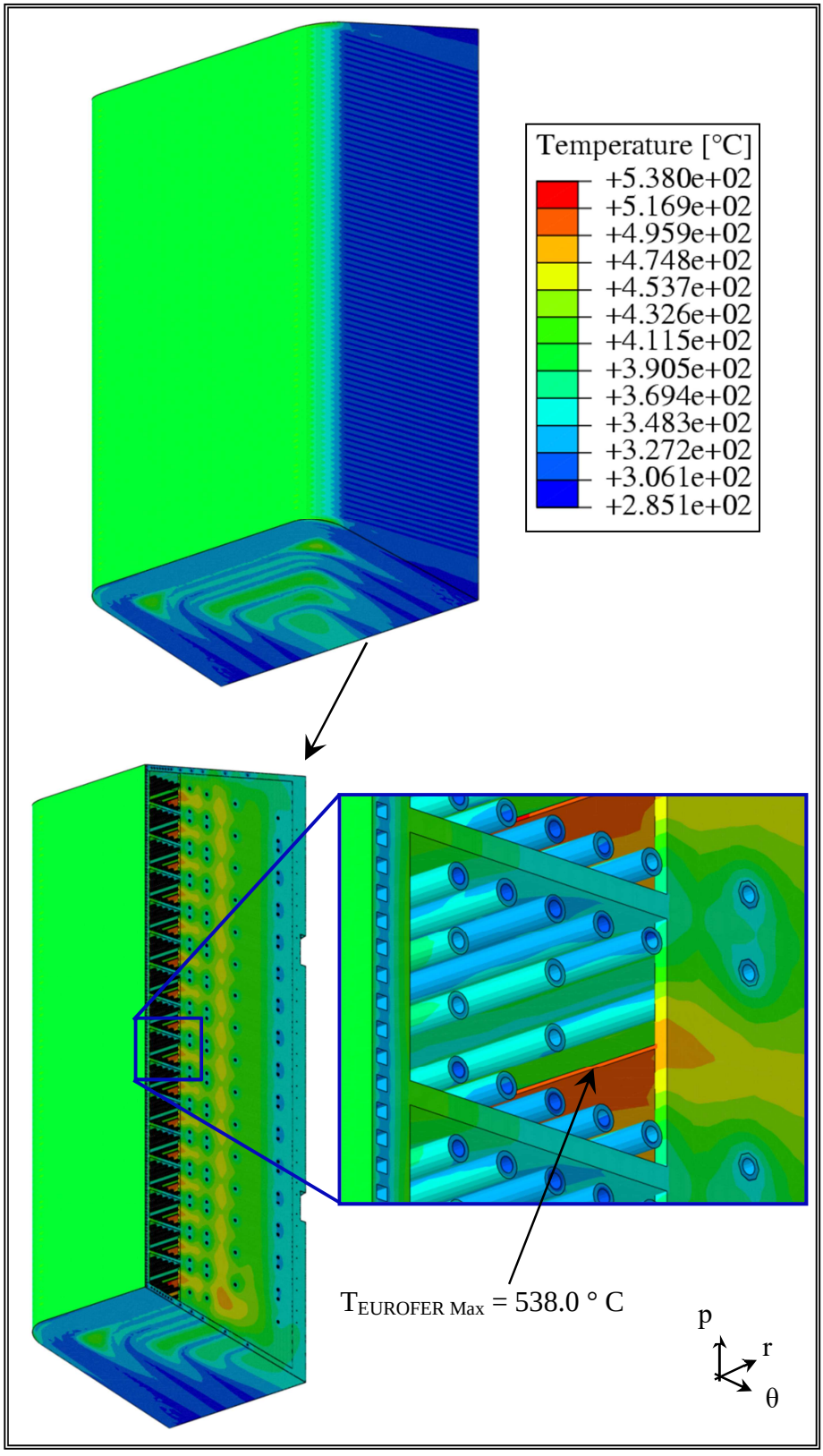


Figure 3-14. Case 1 - Thermal results - Segment Box.

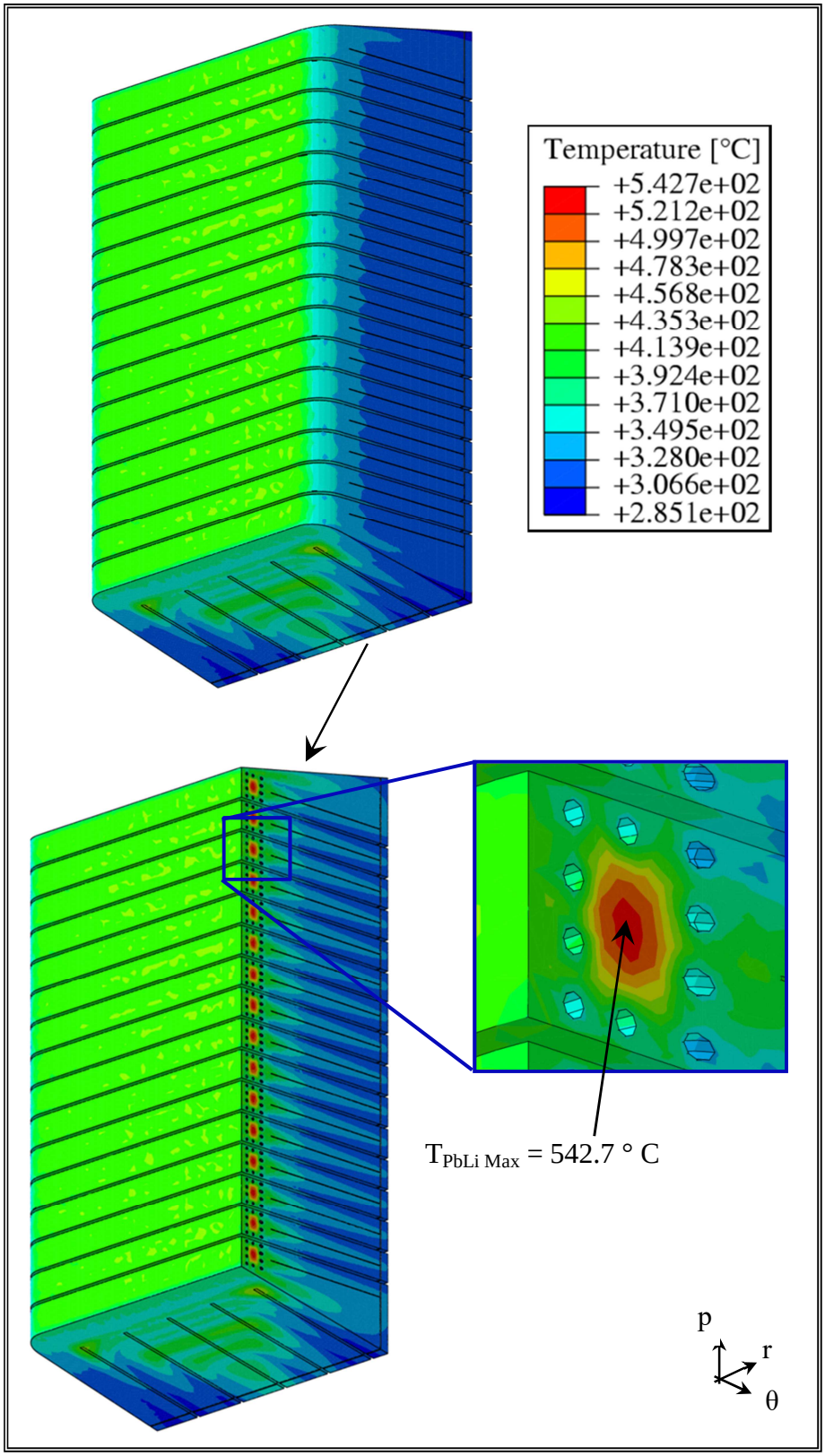


Figure 3-15. Case 1 - Thermal results - Breeder.

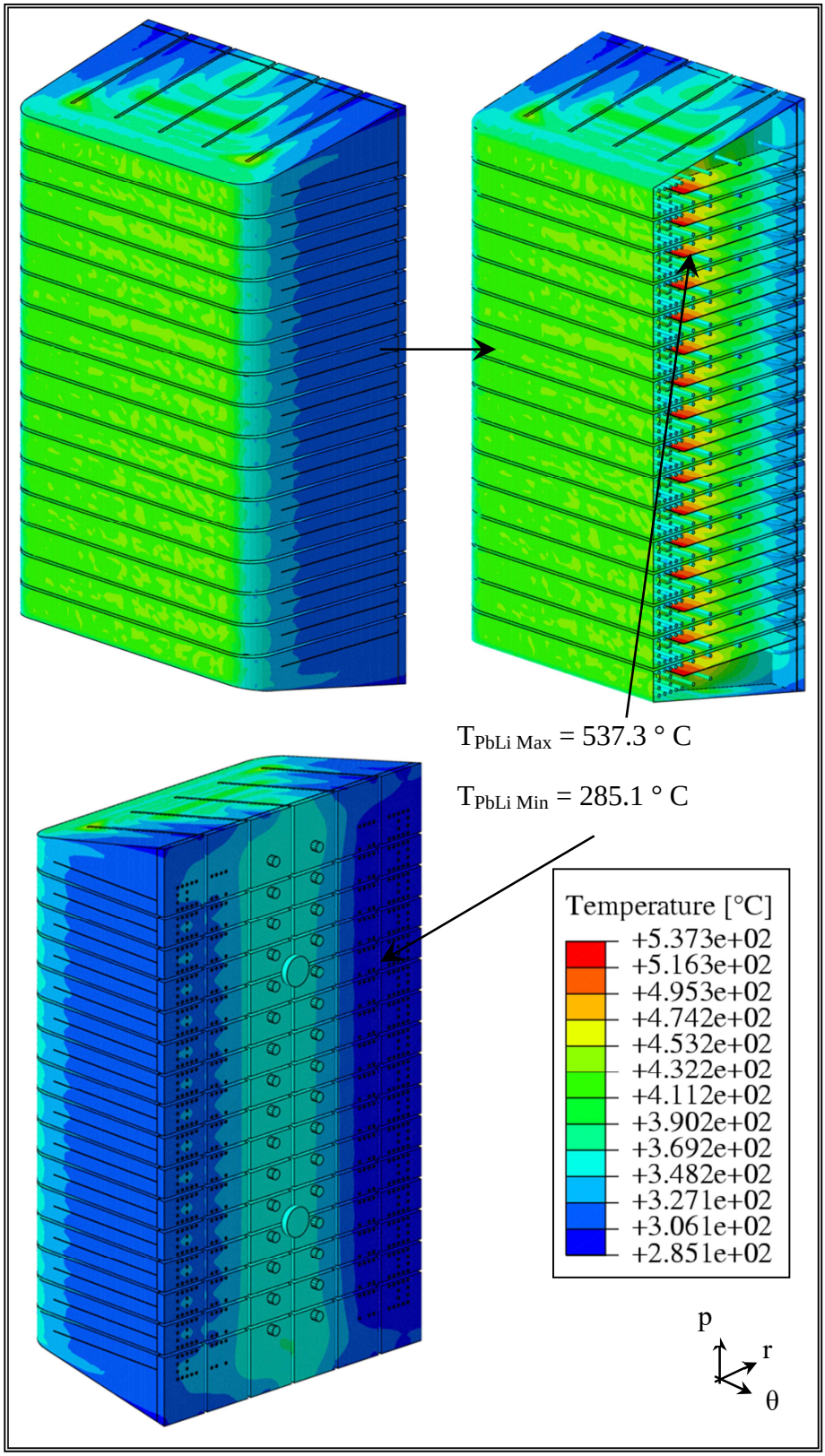


Figure 3-16. Case 1 - Thermal results - Breeder-structure interface.

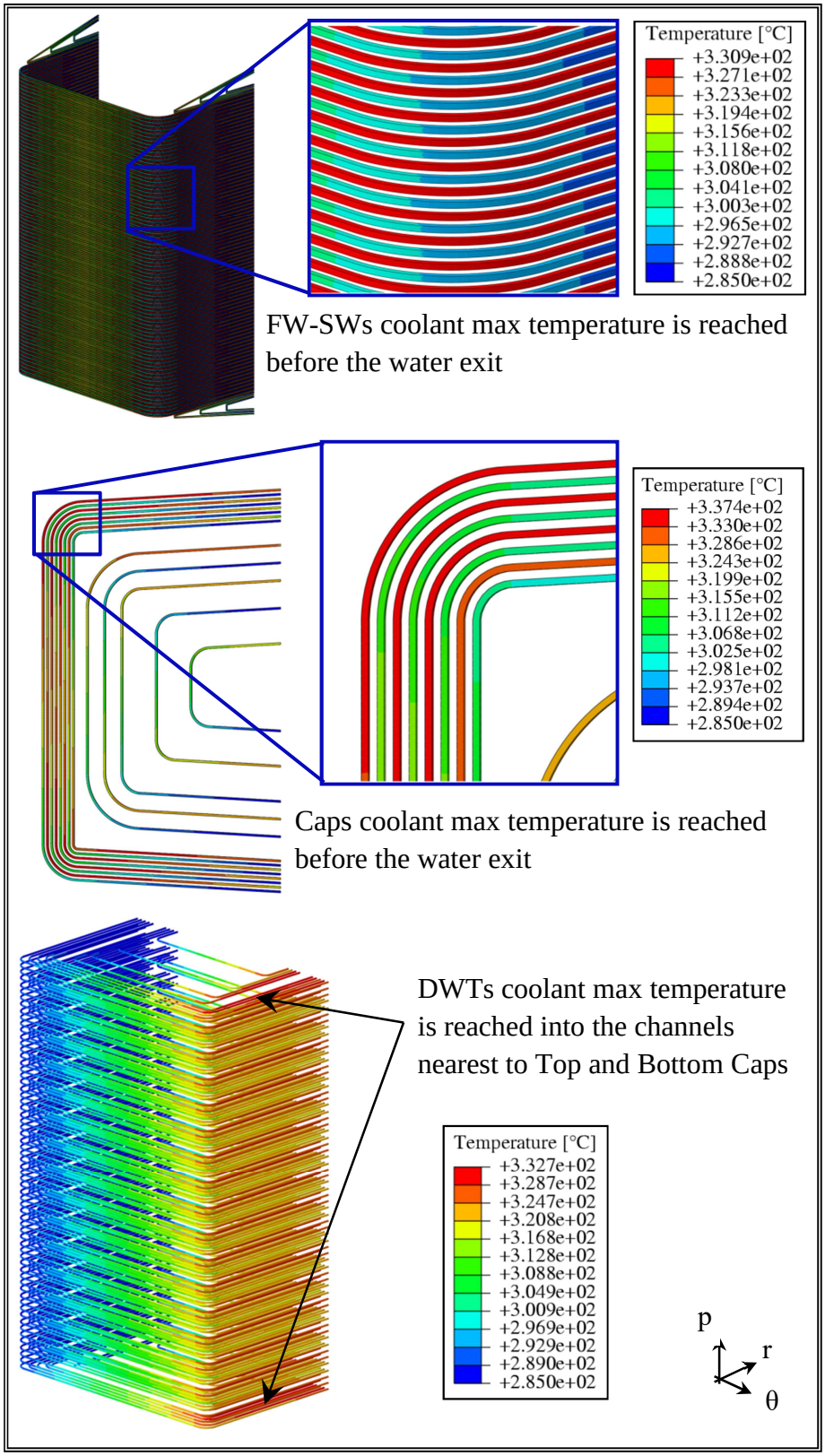


Figure 3-17. Case 1 - Thermal results - Cooling water.

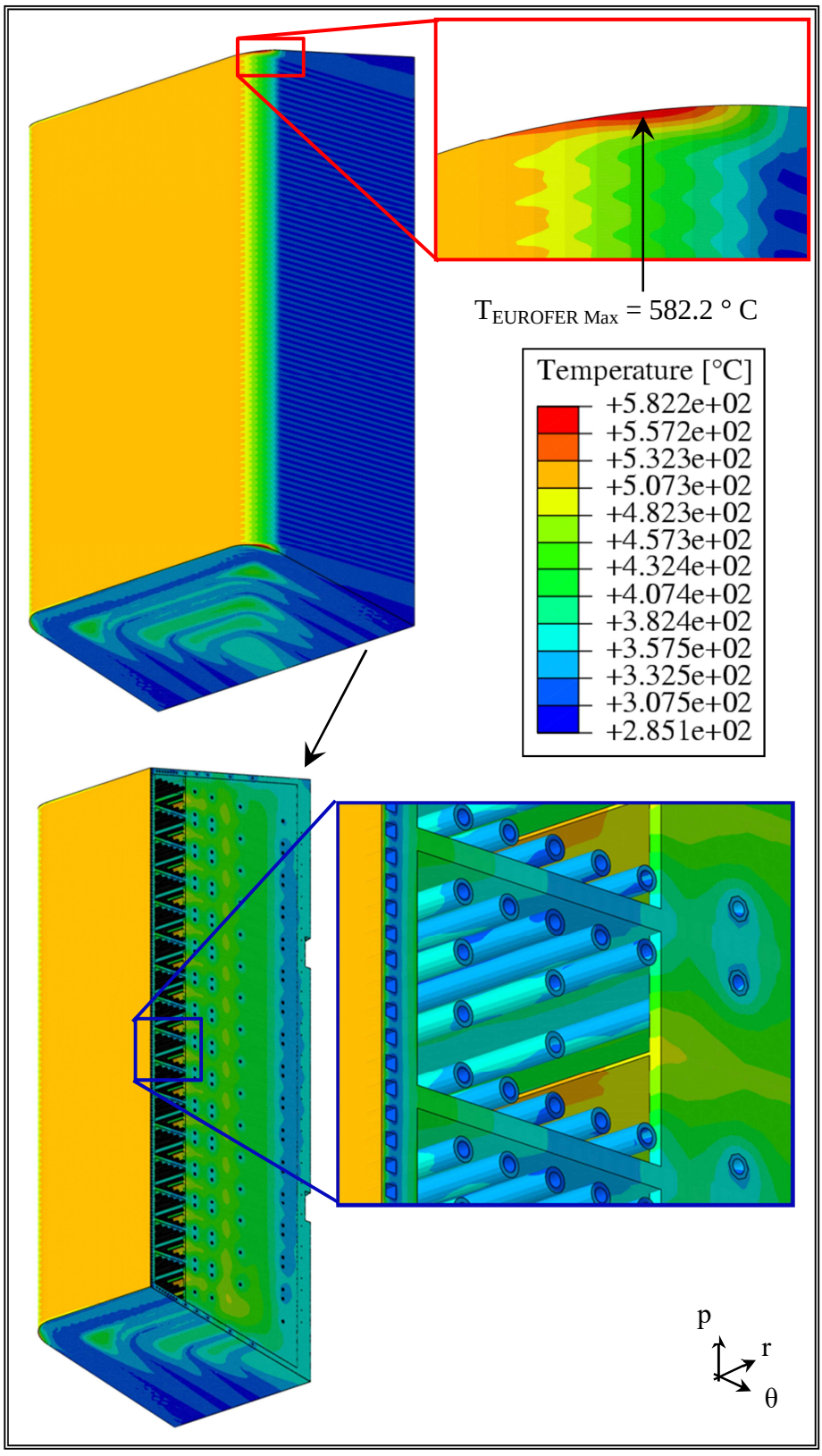


Figure 3-18. Case 2 - Thermal results - Segment Box.

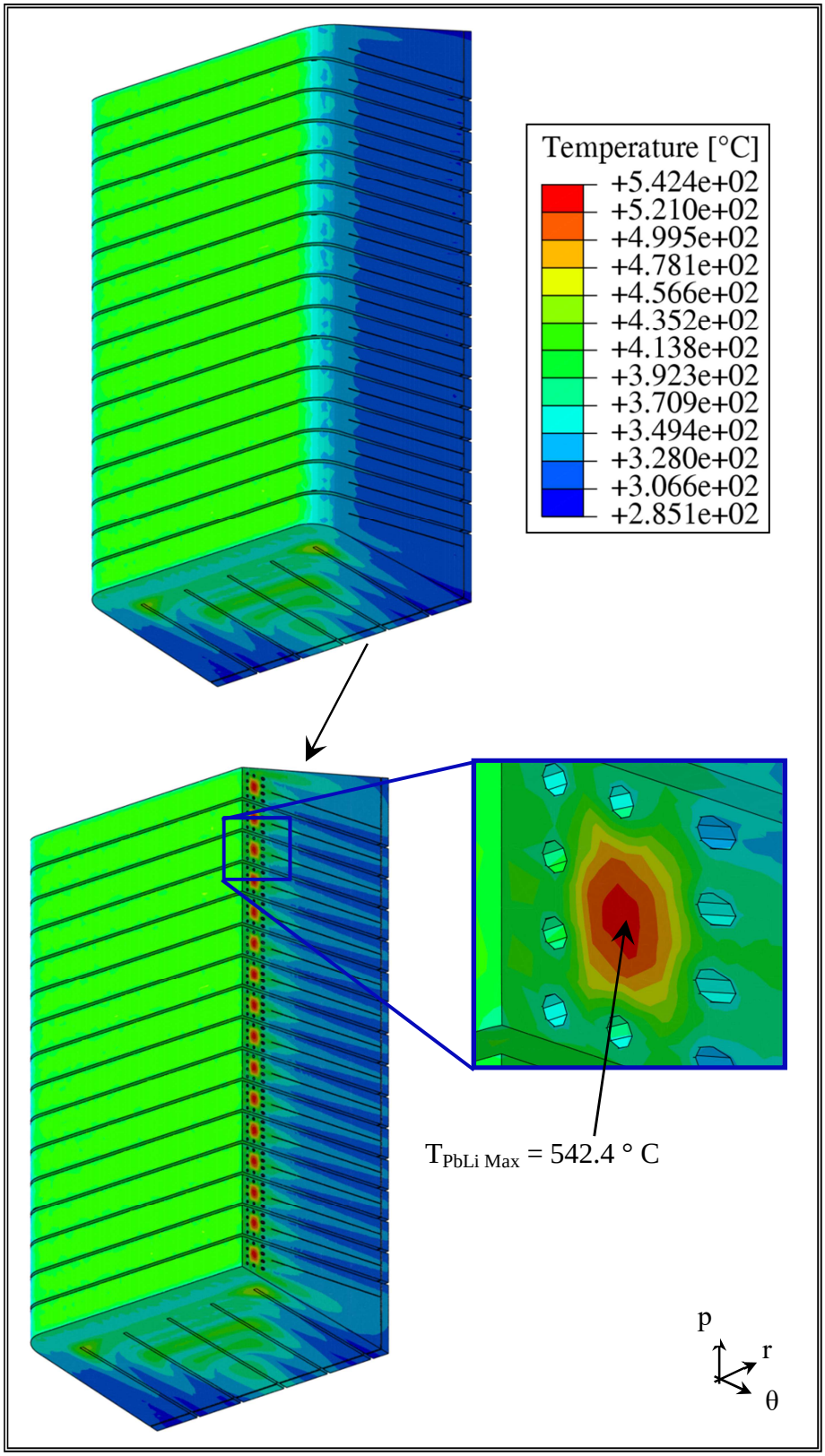


Figure 3-19. Case 2 - Thermal results - Breeder.

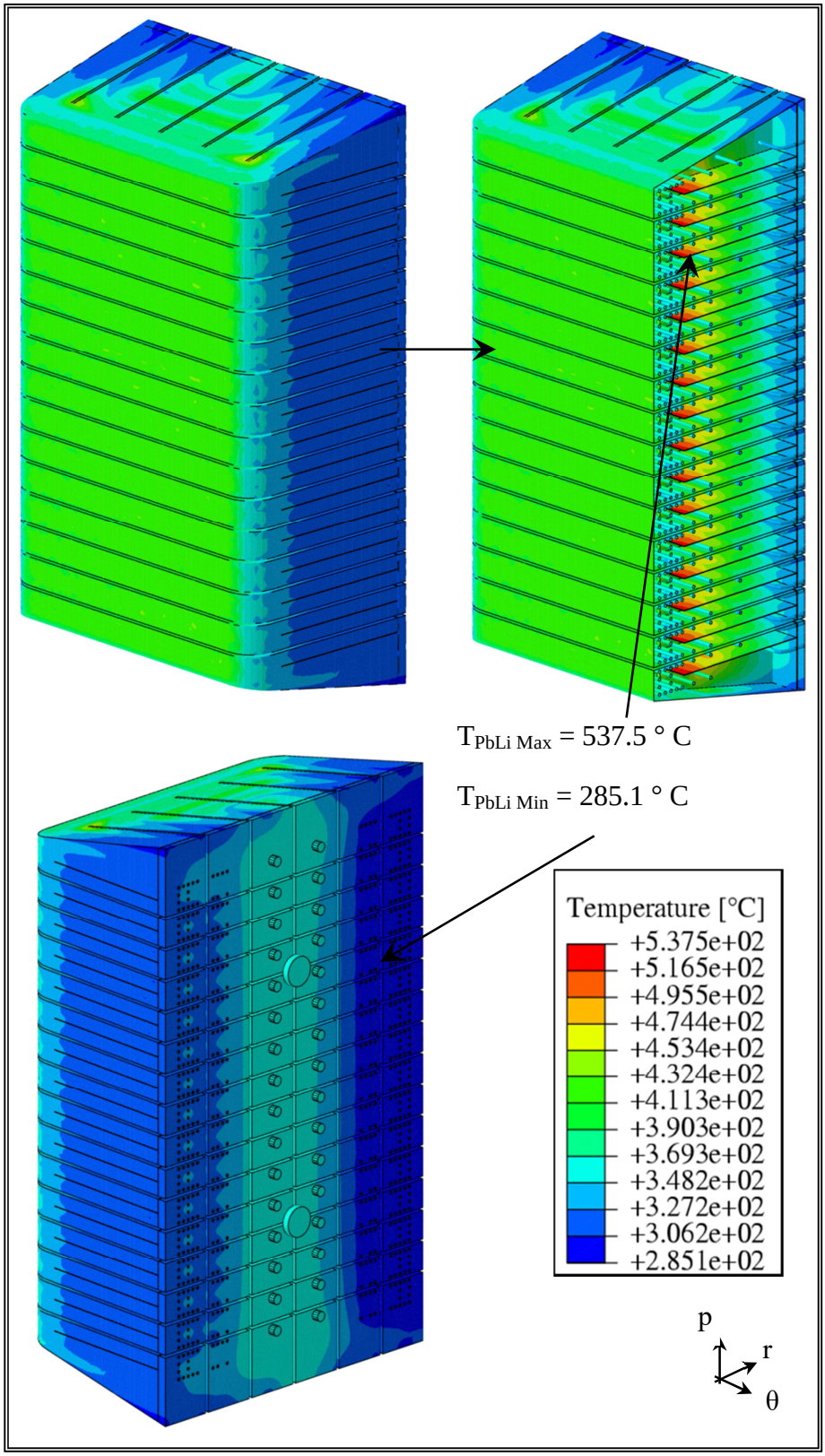


Figure 3-20. Case 2 - Thermal results - Breeder-structure interface.

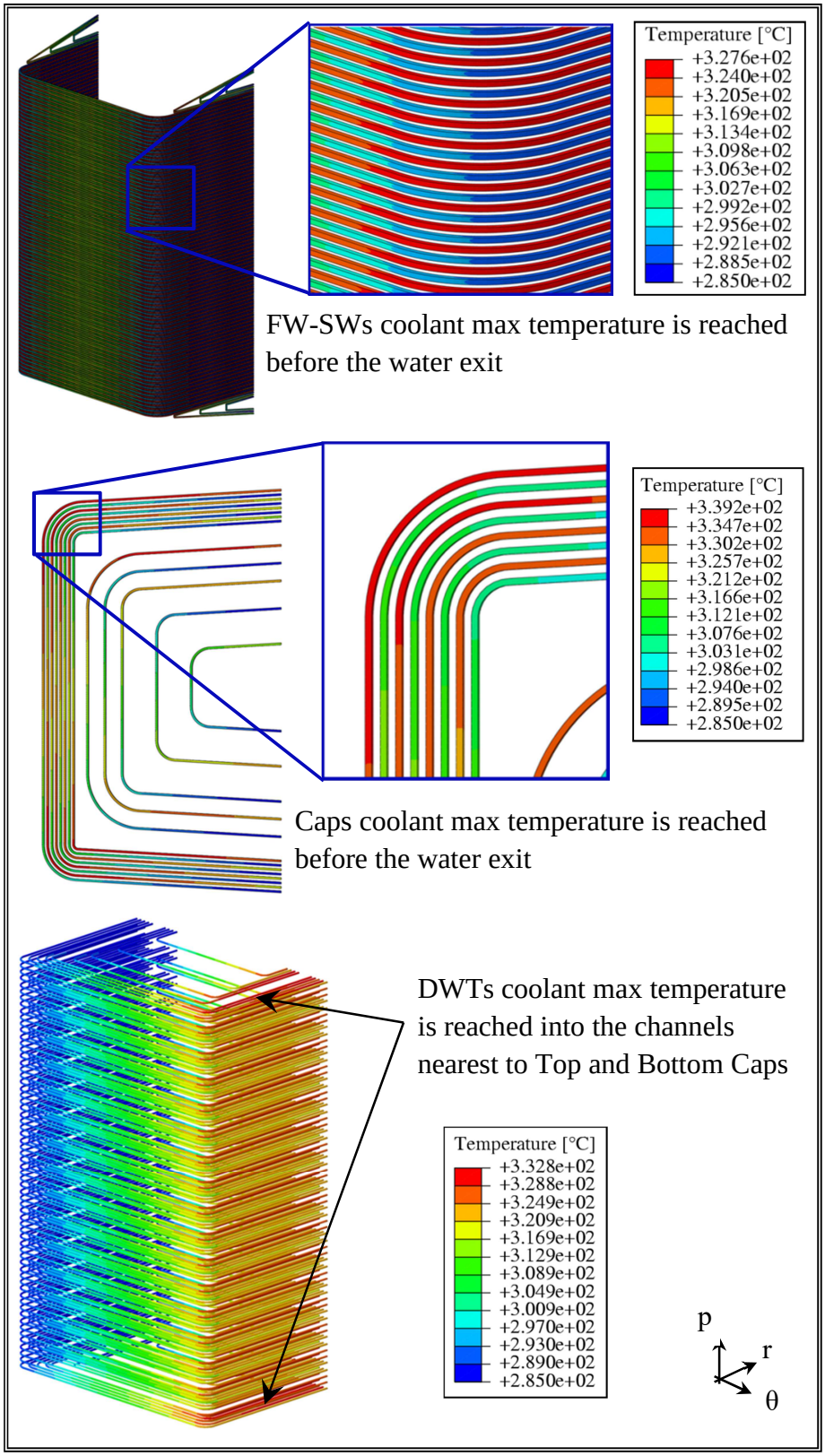


Figure 3-21. Case 2 - Thermal results - Cooling water.

Table 3-3. Mass flow rates and heat transfer coefficients.

| **Case 1** | | | |
|---|---|---|---|
| **Component** | **G [kg/s]** | **Q [W]** | **Q [%]** |
| Top Cap | 0.217 | $4.334 \cdot 10^4$ | 0.76 |
| Bottom Cap | 0.217 | $4.491 \cdot 10^4$ | 0.79 |
| DWTs - BZ | 14.093 | $3.161 \cdot 10^6$ | 55.38 |
| FW-SWs | 11.027 | $2.458 \cdot 10^6$ | 43.07 |
| Total | 25.554 | $5.707 \cdot 10^6$ | 100.00 |
| **Case 2** | | | |
| **Component** | **G [kg/s]** | **Q [W]** | **Q [%]** |
| Top Cap | 0.209 | $4.277 \cdot 10^4$ | 0.50 |
| Bottom Cap | 0.213 | $4.445 \cdot 10^4$ | 0.52 |
| DWTs - BZ | 14.093 | $3.148 \cdot 10^6$ | 36.73 |
| FW-SWs | 23.867 | $5.334 \cdot 10^6$ | 62.25 |
| Total | 38.382 | $8.569 \cdot 10^6$ | 100.00 |

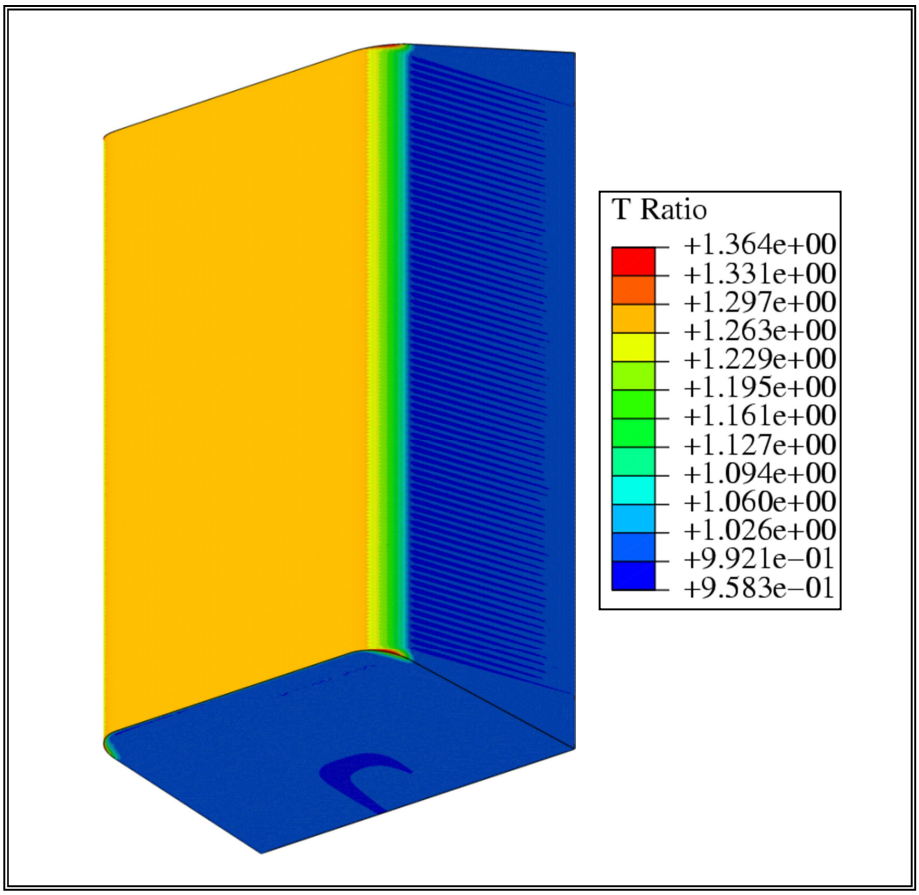


Figure 3-22. SB - Case 2over Case 1 temperature ratio.

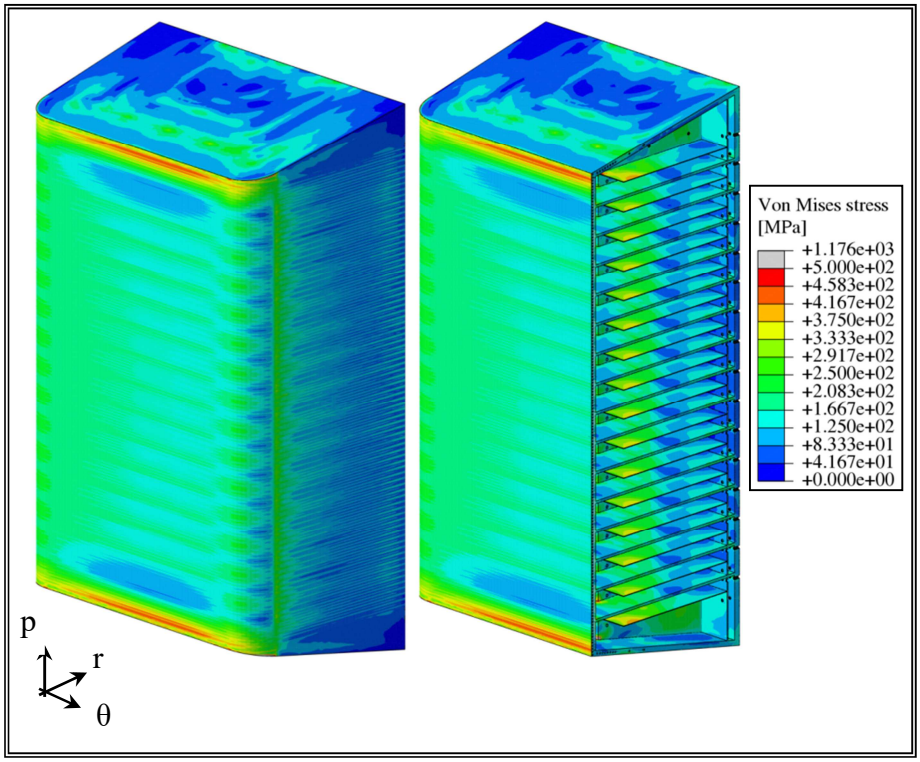


Figure 3-23. Case 1 - Von Mises equivalent stress field - NO scenario.

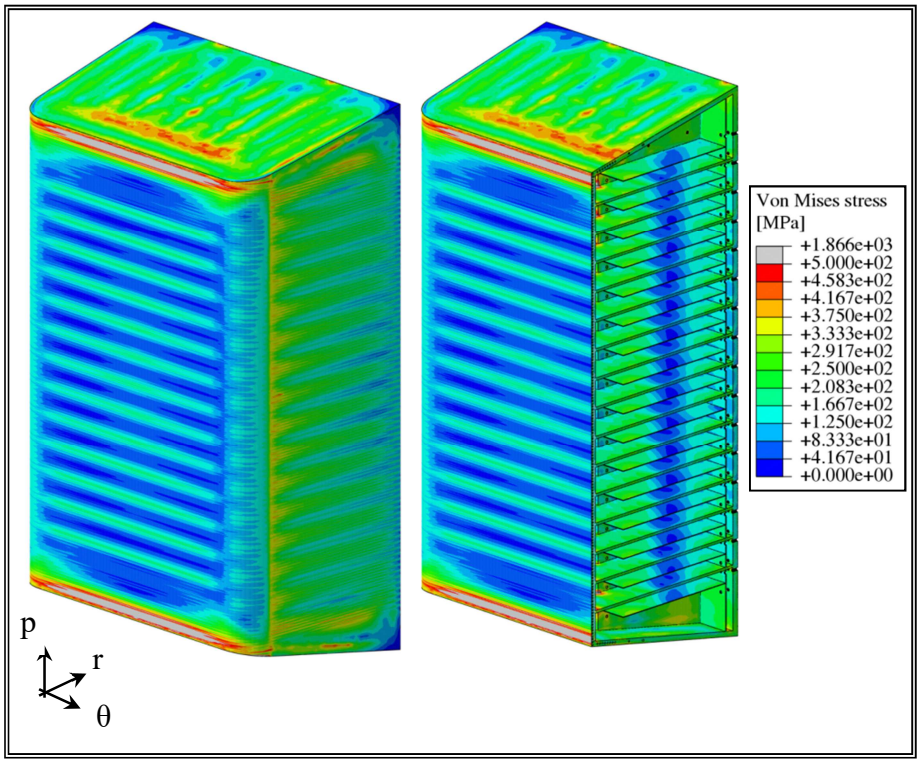


Figure 3-24. Case 1 - Von Mises equivalent stress field - OP scenario.

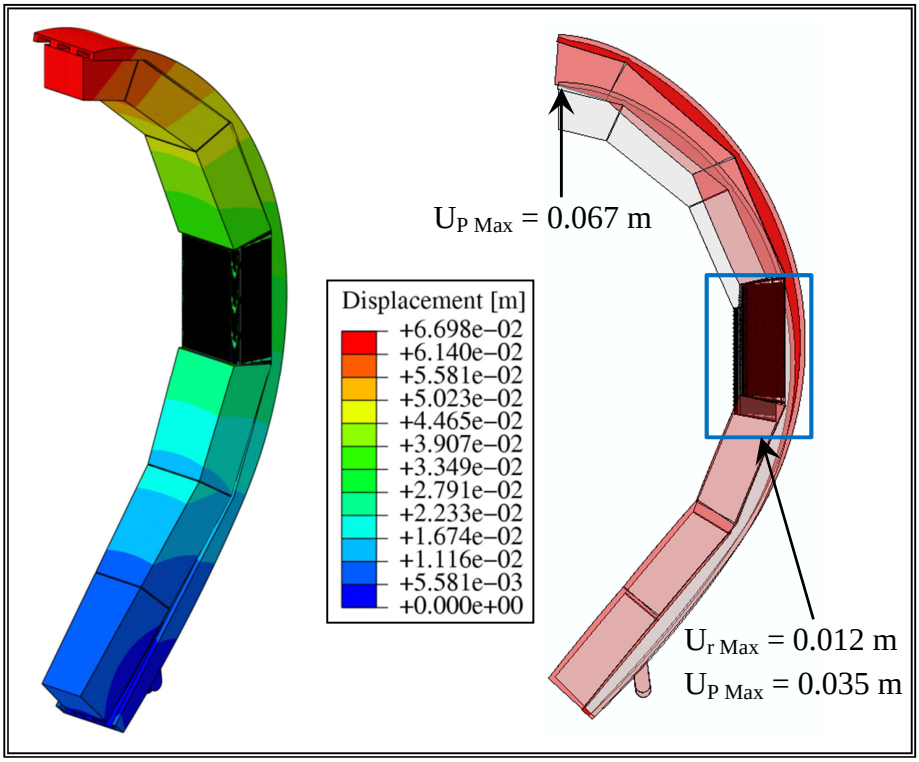


Figure 3-25. Case 1 - Displacement fields - NO scenario.

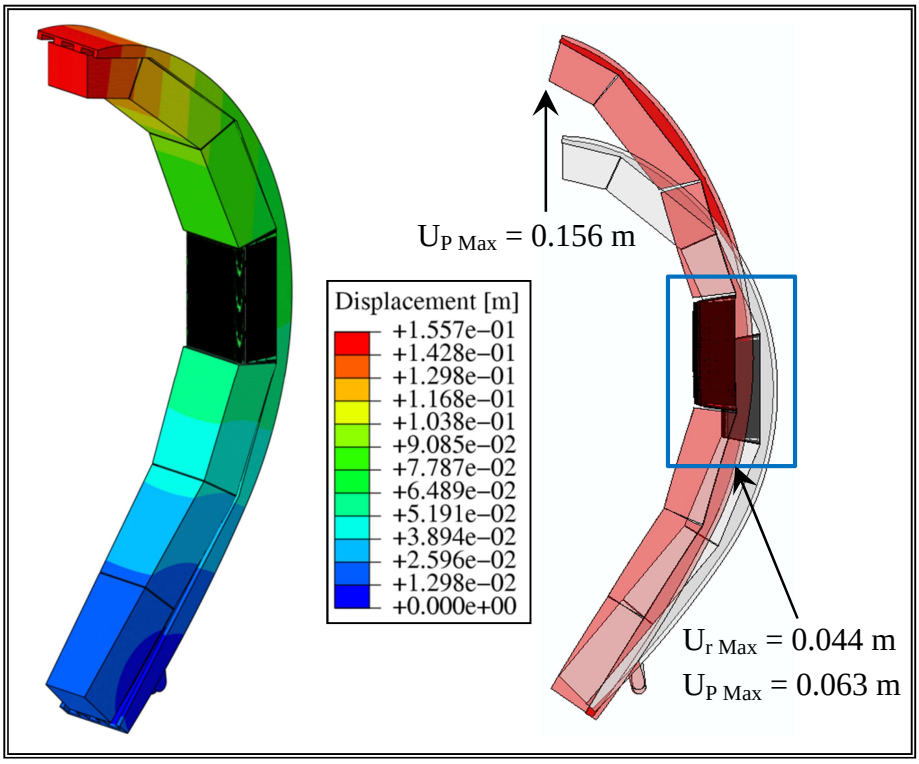


Figure 3-26. Case 1 - Displacement fields - OP scenario.

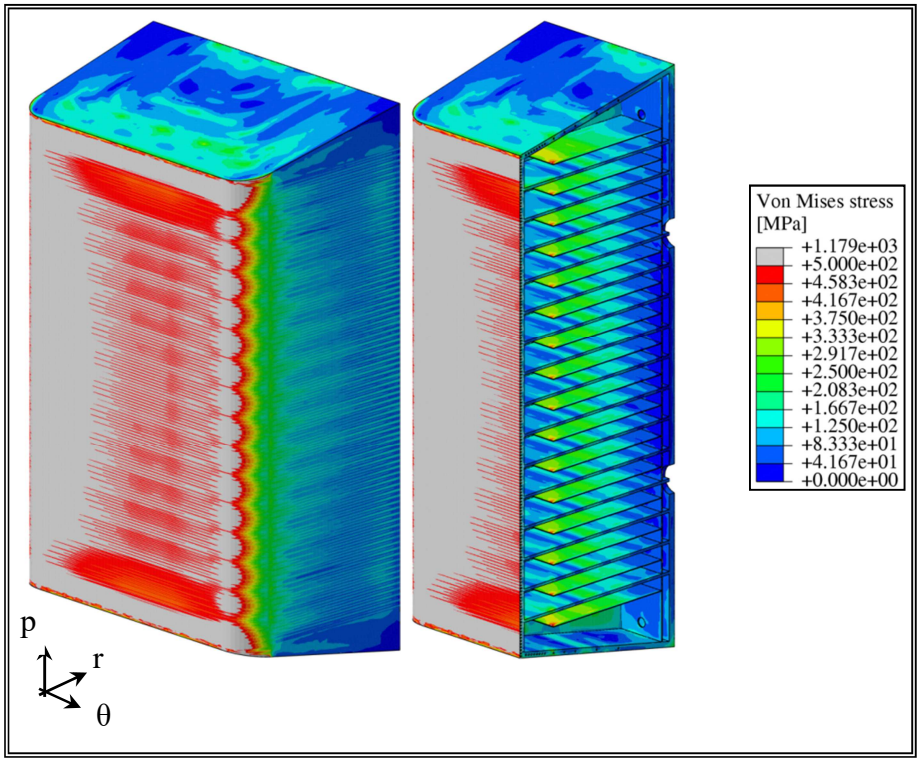


Figure 3-27. Case 2 - Von Mises equivalent stress field - NO scenario.

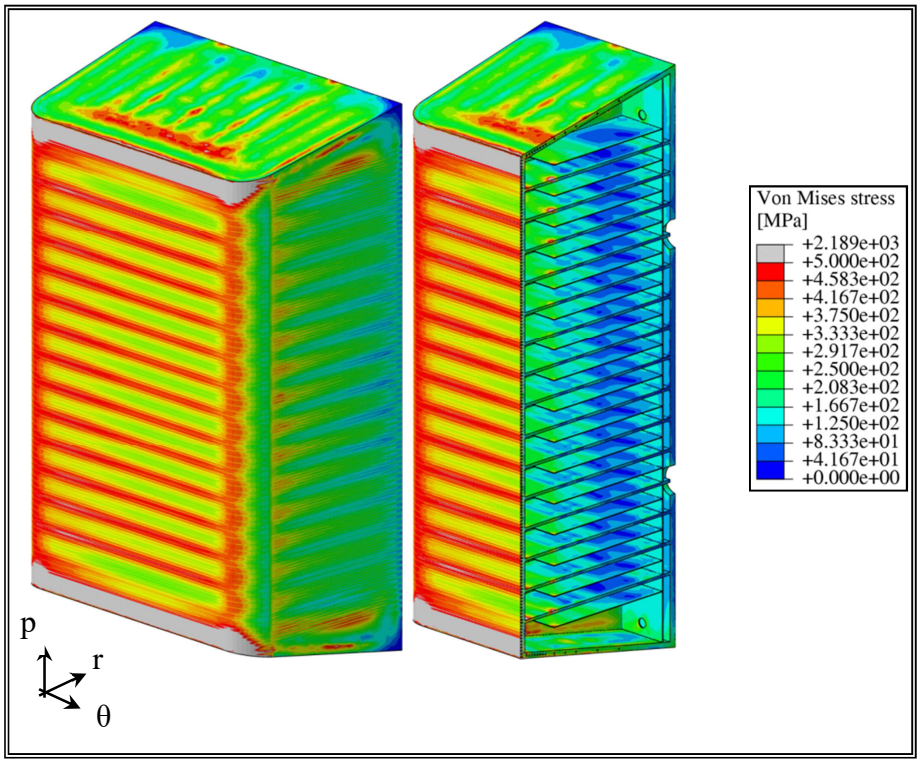


Figure 3-28. Case 2 - Von Mises equivalent stress field - OP scenario.

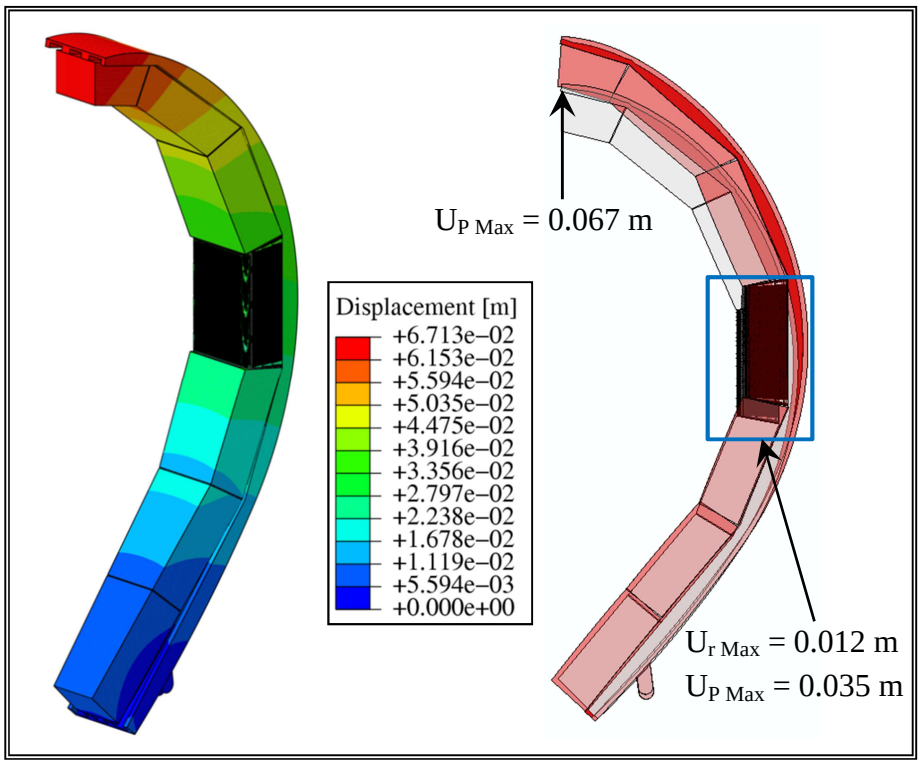


Figure 3-29. Case 2 - Displacement fields - NO scenario.

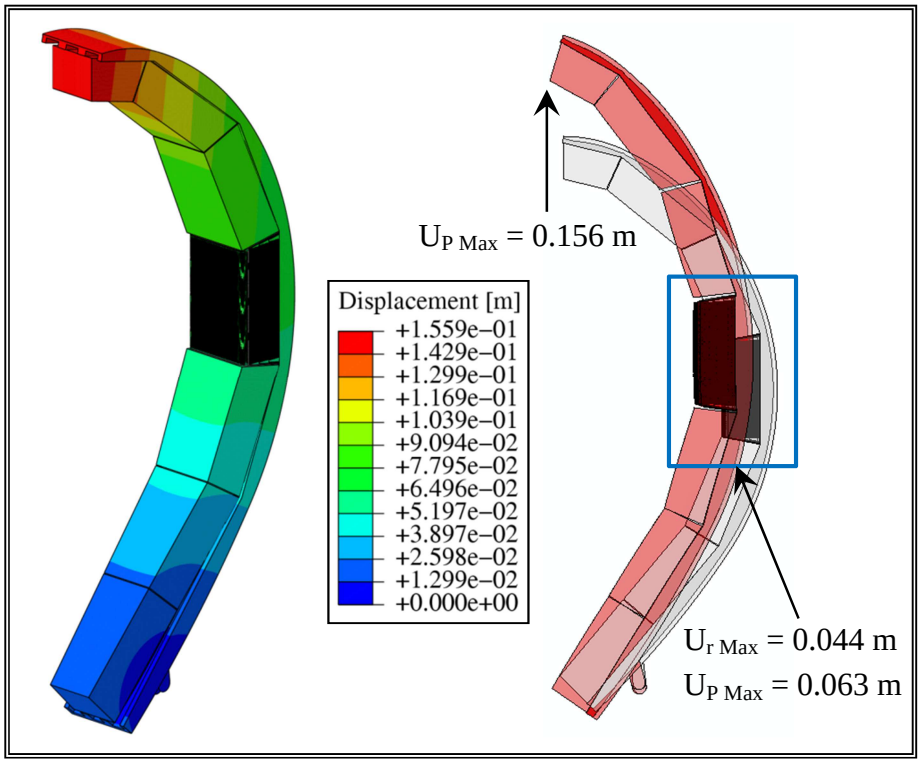


Figure 3-30. Case 2 - Displacement fields - OP scenario.

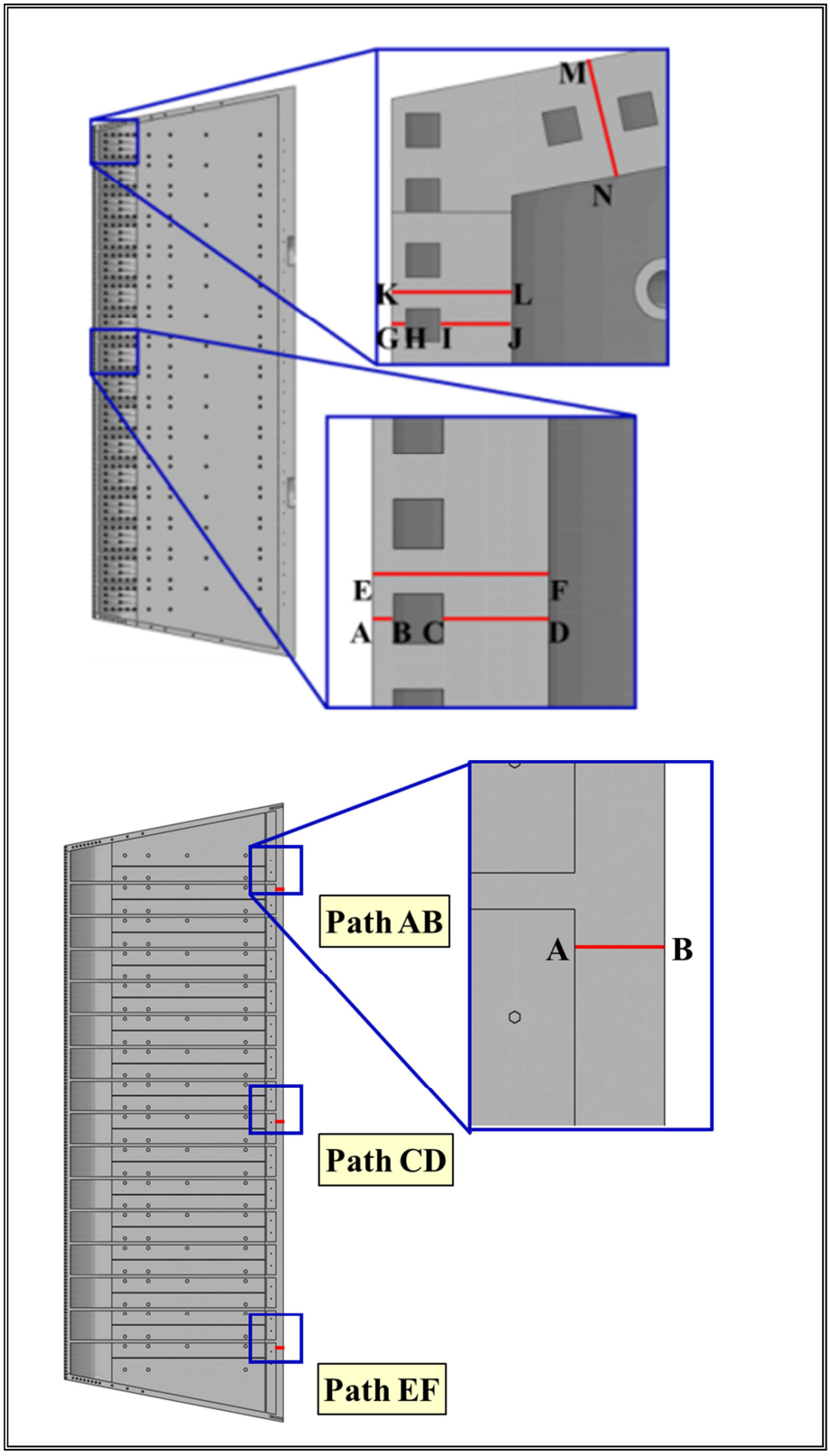


Figure 3-31. FW-SW and BP paths at toroidal mid-plane.

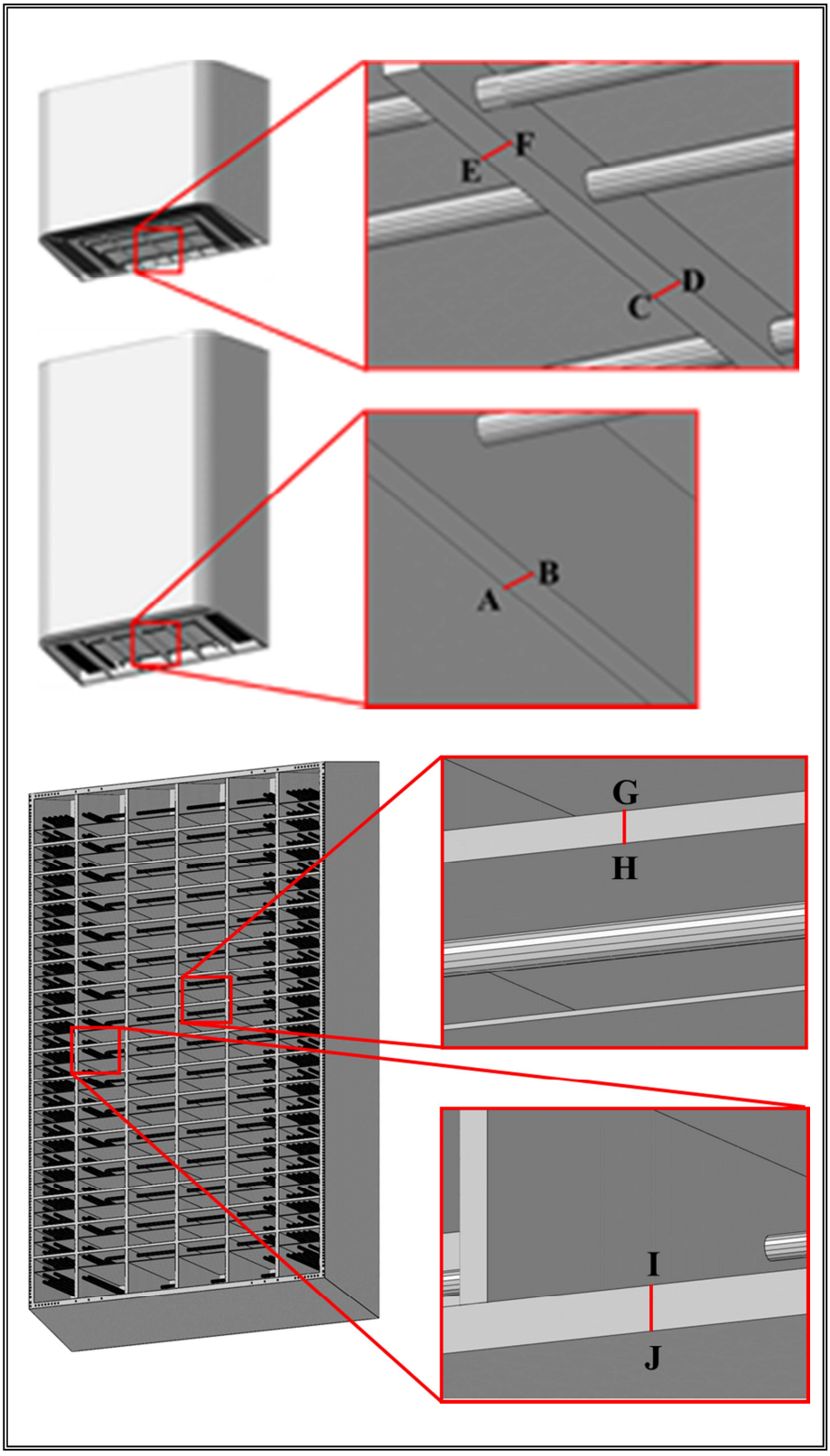


Figure 3-32. Paths located within SPs.

Table 3-4 - SDC-IC criteria - Case 1 - paths located within FW.

| **Case 1** | | | | | | |
|---|---|---|---|---|---|---|
| | **Stress linearization path** | | | | | |
| | **AB** | **CD** | **EF** | **GH** | **IJ** | **KL** |
| $T_{Max-Path}$ [°C] | 408.9 | 423.9 | 421.1 | 407.7 | 404.2 | 412.3 |
| **Level A criteria** | | | | | | |
| $P_m/S_m$ | 0.117 | 0.059 | 0.024 | 0.074 | 0.094 | 0.036 |
| $(P_m+P_b)/K_{eff}\ S_m$ | 0.099 | 0.057 | 0.074 | 0.070 | 0.077 | 0.095 |
| $P_m/S_t$ | - | - | - | - | - | - |
| $(P_m+P_b/K)/S_t$ | - | - | - | - | - | - |
| $(P_m+Q_m)/S_e$ | 0.633 | 0.901 | 0.683 | 2.030 | 0.521 | 0.375 |
| **Level D criteria** | | | | | | |
| $P_m/\sigma_{lim}$ | 0.503 | 0.505 | 0.413 | 0.676 | 1.200 | 0.495 |
| $(P_m+P_b)/K_{eff}\ \sigma_{lim}$ | 0.349 | 0.372 | 0.440 | 0.616 | 1.350 | 0.994 |
| $W_t[1.35\ (P_m+P_b/K)]$ | - | - | - | - | - | - |
| $(P_m+Q_m)/2\cdot S_e$ | 0.433 | 0.303 | 0.475 | 1.690 | 1.370 | 0.531 |

Table 3-5 - SDC-IC criteria - Case 1 - path located within Cap.

| **Case 1** | | | | | | |
|---|---|---|---|---|---|---|
| | **Stress linearization path** | | | | | |
| | **MN** | | | | | |
| $T_{Max-Path}$ [°C] | 379.1 | | | | | |
| **Level A criteria** | | | | | | |
| $P_m/S_m$ | 0.033 | | | | | |
| $(P_m+P_b)/K_{eff}\ S_m$ | 0.039 | | | | | |
| $P_m/S_t$ | - | | | | | |
| $(P_m+P_b/K)/S_t$ | - | | | | | |
| $(P_m+Q_m)/S_e$ | 0.332 | | | | | |
| **Level D criteria** | | | | | | |
| $P_m/\sigma_{lim}$ | 0.343 | | | | | |
| $(P_m+P_b)/K_{eff}\ \sigma_{lim}$ | 0.725 | | | | | |
| $W_t[1.35\ (P_m+P_b/K)]$ | - | | | | | |
| $(P_m+Q_m)/2\cdot S_e$ | 0.316 | | | | | |

Table 3-6 - SDC-IC criteria - Case 1 - paths located within SPs.

| Case 1 | | | | | | |
|---|---|---|---|---|---|---|
| | Stress linearization path | | | | | |
| | AB | CD | EF | GH | IJ | |
| $T_{Max\text{-}Path}$ [°C] | 411.7 | 456.3 | 426.5 | 466.9 | 363.4 | |
| **Level A criteria** | | | | | | |
| $P_m/S_m$ | 0.052 | 0.046 | 0.033 | 0.024 | 0.028 | |
| $(P_m+P_b)/K_{eff}\ S_m$ | 0.035 | 0.034 | 0.022 | 0.017 | 0.020 | |
| $P_m/S_t$ | - | 0.035 | - | 0.019 | - | |
| $(P_m+P_b/K)/S_t$ | - | 0.035 | - | 0.019 | - | |
| $(P_m+Q_m)/S_e$ | 1.490 | 1.680 | 1.130 | 1.590 | 1.640 | |
| **Level D criteria** | | | | | | |
| $P_m/\sigma_{lim}$ | 0.714 | 0.858 | 0.664 | 0.366 | 0.446 | |
| $(P_m+P_b)/K_{eff}\ \sigma_{lim}$ | 0.477 | 0.574 | 0.444 | 0.245 | 0.298 | |
| $W_t[1.35\ (P_m+P_b/K)]$ | - | 36.10 | - | ~ 0 | - | |
| $(P_m+Q_m)/2\cdot S_e$ | 1.020 | 0.269 | 0.225 | 0.561 | 0.969 | |

Table 3-7 - SDC-IC criteria - Case 1 - path located within BP.

| Case 1 | | | | | | |
|---|---|---|---|---|---|---|
| | Stress linearization path | | | | | |
| | AB | CD | EF | | | |
| $T_{Max\text{-}Path}$ [°C] | 353.7 | 342.4 | 345.9 | | | |
| **Level A criteria** | | | | | | |
| $P_m/S_m$ | 0.010 | 0.010 | 0.076 | | | |
| $(P_m+P_b)/K_{eff}\ S_m$ | 0.008 | 0.011 | 0.053 | | | |
| $P_m/S_t$ | - | - | - | | | |
| $(P_m+P_b/K)/S_t$ | - | - | - | | | |
| $(P_m+Q_m)/S_e$ | 0.176 | 0.062 | 0.285 | | | |
| **Level D criteria** | | | | | | |
| $P_m/\sigma_{lim}$ | 0.296 | 0.130 | 0.174 | | | |
| $(P_m+P_b)/K_{eff}\ \sigma_{lim}$ | 0.207 | 0.119 | 0.170 | | | |
| $W_t[1.35\ (P_m+P_b/K)]$ | - | - | - | | | |
| $(P_m+Q_m)/2\cdot S_e$ | 0.227 | 0.123 | 0.227 | | | |

Table 3-8 - SDC-IC criteria - Case 2 - paths located within FW.

| **Case 2** | | | | | | |
|---|---|---|---|---|---|---|
| | **Stress linearization path** | | | | | |
| | **AB** | **CD** | **EF** | **GH** | **IJ** | **KL** |
| $T_{Max\text{-}Path}$ [°C] | 521.5 | 415.9 | 527.3 | 520.6 | 397.3 | 527.1 |
| **Level A criteria** | | | | | | |
| $P_m/S_m$ | 0.140 | 0.059 | 0.029 | 0.090 | 0.093 | 0.044 |
| $(P_m+P_b)/K_{eff}\ S_m$ | 0.119 | 0.057 | 0.090 | 0.084 | 0.077 | 0.012 |
| $P_m/S_t$ | 0.139 | - | 0.029 | 0.089 | - | 0.045 |
| $(P_m+P_b/K)/S_t$ | 0.170 | - | 0.115 | 0.116 | - | 0.148 |
| $(P_m+Q_m)/S_e$ | 2.350 | 0.565 | 0.791 | 3.640 | 0.526 | 0.423 |
| **Level D criteria** | | | | | | |
| $P_m/\sigma_{lim}$ | 0.612 | 0.502 | 0.510 | 0.832 | 1.190 | 0.616 |
| 0.428 | 0.428 | 0.369 | 0.546 | 0.748 | 1.340 | 1.240 |
| $W_t[1.35\ (P_m+P_b/K)]$ | 4.230 | - | 96.70 | 2.470 | - | $\sim 10^9$ |
| $(P_m+Q_m)/2\cdot S_e$ | | | | | | |

Table 3-9 - SDC-IC criteria - Case 2 - path located within Cap.

| **Case 2** | | | | | | |
|---|---|---|---|---|---|---|
| | **Stress linearization path** | | | | | |
| | **MN** | | | | | |
| $T_{Max\text{-}Path}$ [°C] | 376.6 | | | | | |
| **Level A criteria** | | | | | | |
| $P_m/S_m$ | 0.033 | | | | | |
| $(P_m+P_b)/K_{eff}\ S_m$ | 0.039 | | | | | |
| $P_m/S_t$ | - | | | | | |
| $(P_m+P_b/K)/S_t$ | - | | | | | |
| $(P_m+Q_m)/S_e$ | 0.494 | | | | | |
| **Level D criteria** | | | | | | |
| $P_m/\sigma_{lim}$ | 0.342 | | | | | |
| $(P_m+P_b)/K_{eff}\ \sigma_{lim}$ | 0.72 | | | | | |
| $W_t[1.35\ (P_m+P_b/K)]$ | - | | | | | |
| $(P_m+Q_m)/2\cdot S_e$ | 0.340 | | | | | |

Table 3-10 - SDC-IC criteria - Case 2 - paths located within SPs.

| Case 2 | | | | | | |
|---|---|---|---|---|---|---|
| | Stress linearization path | | | | | |
| | **AB** | **CD** | **EF** | **GH** | **IJ** | |
| $T_{Max\text{-}Path}$ [°C] | 410.4 | 456.3 | 426.5 | 466.9 | 363.4 | |
| **Level A criteria** | | | | | | |
| $P_m/S_m$ | 0.052 | 0.046 | 0.033 | 0.024 | 0.028 | |
| $(P_m+P_b)/K_{eff}\ S_m$ | 0.035 | 0.031 | 0.022 | 0.017 | 0.020 | |
| $P_m/S_t$ | - | 0.035 | - | 0.019 | - | |
| $(P_m+P_b/K)/S_t$ | - | 0.035 | - | 0.019 | | |
| $(P_m+Q_m)/S_e$ | 1.456 | 1.656 | 1.113 | 1.583 | 1.567 | |
| **Level D criteria** | | | | | | |
| $P_m/\sigma_{lim}$ | 0.713 | 0.859 | 0.664 | 0.366 | 0.446 | |
| $(P_m+P_b)/K_{eff}\ \sigma_{lim}$ | 0.476 | 0.574 | 0.444 | 0.245 | 0.298 | |
| $W_t[1.35\ (P_m+P_b/K)]$ | - | 36.30 | - | ~ 0 | - | |
| $(P_m+Q_m)/2\cdot S_e$ | 1.01 | 0.275 | 0.232 | 0.558 | 0.942 | |

Table 3-11 - SDC-IC criteria - Case 2 - path located within BP.

| Case 2 | | | | | | |
|---|---|---|---|---|---|---|
| | Stress linearization path | | | | | |
| | **AB** | **CD** | **EF** | | | |
| $T_{Max\text{-}Path}$ [°C] | 353.7 | 342.4 | 345.9 | | | |
| **Level A criteria** | | | | | | |
| $P_m/S_m$ | 0.010 | 0.010 | 0.076 | | | |
| $(P_m+P_b)/K_{eff}\ S_m$ | 0.008 | 0.011 | 0.053 | | | |
| $P_m/S_t$ | - | - | - | | | |
| $(P_m+P_b/K)/S_t$ | - | - | - | | | |
| $(P_m+Q_m)/S_e$ | 0.171 | 0.061 | 0.286 | | | |
| **Level D criteria** | | | | | | |
| $P_m/\sigma_{lim}$ | 0.297 | 0.132 | 0.179 | | | |
| $(P_m+P_b)/K_{eff}\ \sigma_{lim}$ | 0.207 | 0.119 | 0.173 | | | |
| $W_t[1.35\ (P_m+P_b/K)]$ | - | - | - | | | |
| $(P_m+Q_m)/2\cdot S_e$ | 0.277 | 0.124 | | | | |

## 3.4 Conclusion

A research campaign, fully developed in the framework of the EUROfusion consortium WPBB action, has been carried out within the framework of the Ph.D. course in order to investigate the thermo-mechanical performances of the DEMO WCLL BB outboard equatorial module, opportunely connected to the BSS, under both NO and OP steady state loading scenarios. In this study, the whole WCLL BB outboard segment has been modelled in order to reproduce, as more realistically as possible, the effect of the entire BSS and the other modules on the equatorial one.

For each scenario, two load cases have been investigated differing as far as the heat flux on the FW-SW plasma facing surface is concerned. In particular, values of $\Phi_{max}$ = 0.5 MW/m² and $\Phi_{max}$ = 1.4 MW/m² have been considered.

From the thermal point of view, the obtained results in case of $\Phi_{max}$ = 0.5 MW/m² show that an acceptable temperature distribution is reached within structure, breeder and coolant domains, while in case of $\Phi_{max}$ = 1.4 MW/m² hotspots are predicted in a poorly cooled restricted area located in the bottom and top corners of FW.

These results allow to conclude that, in order to avoid the hotspots insurgence in case of FW-SW maximum heat flux, the layout of the module cooling scheme in the FW corners region should be slightly modified.

From the mechanical point of view, the obtained results in both cases show that a revision of the SP geometric configuration has to be performed in order to limit the secondary stress insurgence, by possibly changing their thickness and number as partially suggested at the end of the SP geometric optimization (Chapter 2). This could have a certain impact on the module TBR, hence the best compromise between the module breeding performances and the design criteria fulfilment has to be found in the following steps of the WCLL BB design activities. To this purpose a multi-physical approach might be followed in order to simultaneously optimize the module from both neutronic and structural standpoints, allowing the achievement of a SP grid geometry which ensures an acceptable TBR value and a satisfying structural behaviour in terms of SDC-IC design criteria fulfilment.

Another remarkable result of this study is that concerning the FW top and bottom corner regions, which should be reinforced as well in order to avoid their design criteria failure due to immediate plastic flow localization.

In particular, in order to ensure the fulfilment of the SDC-IC design criteria in the FW corner regions, an alternative approach may be represented by making thinner the Caps and the BP. In fact, considering the margin in the design criteria fulfilment for Caps and BP and observing that the FW-SW seems to be caught in the grips of these components, if they were thinner a probable reduction in the FW-SW stress amounting, especially within corner regions, may be expected with a simultaneous increasing of the BP and Cap stress values. In

this case, the best compromise should be obtained so that BP and Cap design criteria continue to be satisfied, even if with a lower margin, and stress amount within FW corner regions significantly decreases ensuring the SDC-IC rules fulfilment also in this region.

Lastly, the displacement fields clearly show that results are influenced by the boundary conditions assumed in order to simulate the BSS connection to the VV. Therefore a refinement of the FEM model adopted, more realistically simulating the BSS-VV attachment system, is necessary in order to improve the results reliability. To this purpose, a realistic design of the attachments should be provided by the WCLL BB project team in a next future so that it could be implemented in the FEM model allowing a more detailed assessment of the DEMO WCLL BB outboard equatorial module thermo-mechanical performances.

# Conclusion

The research activity performed during the Ph.D. course in *"Energia e Tecnologie dell'Informazione - curriculum fisica tecnica e ingegneria nucleare (XXIX ciclo)" ("Energy and Information Technologies - nuclear engineering and applied physics curriculum, 29$^{th}$ cycle")*, held at the University of Palermo, has been carried out within the framework of the R&D activities connected to the development of the European DEMO, funded by the European research programme Horizon 2020 and promoted by the EUROfusion consortium with the purposely foreseen WPBB. The University of Palermo is deeply involved in the R&D activities promoted by EUROfusion, being indicated by ENEA as linked third part to the consortium. Therefore, the research activities performed during the above mentioned Ph.D. course, developed in this international context, have regarded the conceptual design and the numerical thermo-mechanical analysis of the DEMO WCLL BB, focussing attention on the outboard equatorial module.

In particular, in the first phase of the research activity, the design of the First Wall (FW) and of the Stiffening Plates (SPs) of the DEMO WCLL BB outboard equatorial module has been performed, in order to attain proper geometric configurations of these two components aimed at the contribution of the development of a preliminary module conceptual design. To this purpose, specific parametric campaigns of thermo-mechanical analyses have been launched assuming the main geometric features of the two components as parameters and selecting, for each of them, reasonable ranges of values.

As to FW, the geometric optimization has been performed in accordance with both the thermal-hydraulic requirements and the SDC-IC structural design criteria, in order to find geometric configurations able to totally fulfil the prescribed requirements maximizing the heat flux that they can safely withstand. In total, 5929 different FW configurations have been investigated under both nominal and accidental steady-state loading conditions, for a total of 154154 thermal analysis run. The parametric study, totally automated by purposely set-up script files, has allowed to select 4 configurations, among those assessed, able to meet all the imposed requirements withstanding a maximum heat flux equal to 2.0 MW/m$^2$ on the FW facing plasma surface. These selected configurations have been further assessed by means of more realistic models, allowing to select one configuration as the most promising one.

Concerning SPs, their geometric optimization has been performed adopting a parametric approach and considering the thermo-mechanical effect, under steady-state accidental loading conditions, of the potentially optimized SP geometric configurations considered on the old design of the Segment Box previously released by CEA. To this purpose, the Segment Box displacement fields have been assessed for each SP configuration taken into account and, at the end of the parametric analyses, a promising SP geometric configuration has been selected.

On the basis of the outcomes, a preliminary conceptual design of the DEMO WCLL BB outboard equatorial module has been set-up. In order to attain this design, the WCLL BB project team does not have exactly adopted the FW and SP geometric configurations selected at the end of the dedicated optimization campaigns, since supplementary neutronic and manufacturing issues, not previously considered, have had to be addressed. Therefore, the FW and SP geometric configurations selected at the end of the above mentioned dedicated parametric studies have been slightly modified in order to match the new requirements.

In the second phase of the research activity, performed during the Ph.D. course, the so designed WCLL breeding blanket outboard equatorial module has been assessed, from the thermo-mechanical standpoint, under nominal and accidental steady-state loading scenario foreseeing, for each scenario, two thermal cases differing each other for the maximum FW heat flux assumed. To this purpose, a proper 3D FEM model of the whole DEMO WCLL breeding blanket outboard segment, including all the modules and the Back Supporting Structure, has been set-up in order to assess, as more realistically as possible, the thermo-mechanical behaviour of the equatorial module.

The obtained thermal results, in terms of maximum temperature achieved within the structural material, have shown that, when a maximum heat flux of 1.4 $MW/m^2$ on the FW externals is assumed, the maximum EUROFER allowable temperature of 550 °C is overcome in a poorly cooled restricted area located nearby the FW-Cap corner region. This leads to the conclusion that, from the thermal standpoint, the cooling channel layout should be slightly modified in this region in order to avoid these hotspots.

The obtained mechanical results have shown that the predicted thermo-mechanical behaviour is influenced by the connection strategy of the Back Supporting Structure (BSS) to the Vacuum Vessel (VV), so a more accurate design of an attachment system should be addressed by the WCLL BB project team so that it could be implemented in the FEM model.

Moreover, considering the SDC-IC structural design criteria verification, a revision of the SPs has to be performed in order to limit their secondary stress, by possibly changing their thickness and number as suggested during the SP optimization parametric campaign, in order to ensure the total fulfilment of the prescribed criteria. To this purpose a feedback from the neutronic calculations, aimed at the calculation of the module TBR, may be expected, possibly adopting a multi-physical approach in order to take into account both neutronic and structural aspects.

Furthermore, the First Wall top and bottom corner regions should be reinforced in order to avoid their failure in SDC-IC criteria verification due to immediate plastic flow localization. In addition an alternative approach, consisting in making thinner the Caps and the BP, may be followed. In fact, observing that the FW-SW seems to be caught in the grips of BP and Cap, if they were thinner a probable reduction in the FW-SW stress amounting, especially within corner regions, may be expected with a simultaneous increasing of the BP and Cap stress values. In this case, the best compromise should be obtained so that BP and Cap design criteria continue to be satisfied, even if with a lower margin, and stress amount within FW corner regions significantly decreases ensuring the SDC-IC rules fulfilment also in this component.

In conclusion, as a further development of this work, the above said design modifications and a realistic design of the BSS-VV attachment system should be provided in the next future by the WCLL BB project team allowing to more realistically assess, under the selected loading scenarios, the thermo-mechanical performances of the updated WCLL BB outboard equatorial module design with the aim of verifying the SDC-IC criteria fulfilment or, alternatively, suggesting further design modifications.

# Appendix 1

# THE EUROFUSION CONSORTIUM AND THE WPBB

## A.1 Introduction

In order to take an overview of the international framework in which the research activity performed during the Ph.D. course has been developed, some details about the EUROfusion consortium organization are given in this Appendix. Some information about the WPBB are given as well, in order to better clarify the organizational chart of the BB R&D activities.

## A.2 The EUROfusion consortium

In order to promote and coordinate the R&D activities on DEMO funded by European Commission through the research programme Horizon 2020, the EUROfusion consortium has been created thanks to the joint effort of European laboratories, universities, research centres and industries. In particular, 29 members, representing 26 European Union member states plus Switzerland, signed, in 2014, the agreement of the EUROfusion consortium. In addition about 100 Third Parties, which are mainly Universities followed by laboratories and industries, contribute to the research activities through the Consortium members. Among these Third Parties, the University of Palermo is involved in the EUROfusion consortium being indicated by ENEA, which is one of the 29 consortium members. EUROfusion collaborates with Fusion for Energy (F4E) and intensively supports the ITER International Organization. EUROfusion funds fusion research activities in accordance with the Roadmap to the realisation of fusion energy. The Roadmap outlines the most efficient way to realise fusion electricity by 2050. It is the result of an analysis of the European Fusion Programme undertaken in 2012 by the Research laboratories within EUROfusion's predecessor agreement, the European Fusion Development Agreement, EFDA [48]. In this context, the organizational arrangement of the DEMO conceptual design work in EUROfusion is rather

unconventional and different from what is done in other projects [2]. The plant design and physics integration are coordinated centrally whereas the design and R&D of individual systems is executed in geographically-distributed WPs - projects in their own rights [2]. The necessary horizontal integration between various WPs is ensured by the project leaders and the central team. Below, a brief summary of activities conducted in the distributed WPs is provided listing the projects in alphabetical order [2].

*Breeding blanket (WPBB)*

Four design options have been progressed utilising He, water, and Pb-Li as coolants and a solid or Pb-Li breeder/multiplier. The main design drivers include tritium self-sufficiency, thermal-hydraulic efficiency and structural feasibility to withstand the most severe loading conditions due to accidental conditions and disruptions. For the FW design, three architectural options have been proposed: a thermal-hydraulically and mechanically integrated option, a thermal-hydraulically decoupled one, and an option enabling the replacement of selected sections of the FW. The adoption of these different options will depend on the loads acting locally on the FW surface.

*Balance of plant (WPBoP)*

The primary objective of this project is to develop a feasible and integrated conceptual design for the primary heat transfer system and Balance of Plant (BoP) systems that meets the overall DEMO plant requirements and the system requirements for the in-vessel components, interfacing with the BoP.

*Diagnostics and control (WPDC)*

The main objective of the diagnostics and control project is to develop a conceptual design of a control system that ensures machine operation in compliance with nuclear safety requirements, avoids machine damage, and achieves high plant availability and an optimized fusion performance.

*Divertor (WPDIV)*

In the divertor project, engineering work focusses on: (i) the design of the divertor cassette body, considering a number of variant layouts; and (ii) the development of a number of candidate divertor target concepts including fabrication trials and high-heat flux tests. Currently, seven different divertor target concepts are being developed for water-cooled plasma-facing targets and one for helium-cooling.

*Heating and current drive (WPHCD)*

Feasible technology options for neutral beams injection, electron cyclotron heating and ion cyclotron heating systems for DEMO are being explored in order to design the systems devoted to heat the plasma in the DEMO start-up phase.

*Magnets (WPMAG)*

The magnets project has been considering basic coil and winding pack layouts, fabrication methods, and possibilities for using high temperature superconductors. Most of the work to date has concentrated on the design of the TF conductors and coils. Three options for the TF winding pack were proposed, encompassing a broad technological domain ranging from ITER-like concepts to more technologically challenging ones.

*Materials (WPMAT)*

Work has continued to consolidate a material database and material processing trials have been performed to improve the performance of key structural material candidates for in-vessel components. A major part of the advanced steel program is dedicated to the extension or shift of the operating temperature window of EUROFER-type steels.

*Remote maintenance (WPRM)*

Technical work is progressing in the definition and development of the Remote Maintenance (RM) system, including a comprehensive requirements capture exercise, in-vessel and ex-vessel maintenance equipment concept and strategy development, and the development of service joining techniques. A complete set of system requirements for the RM system has been developed.

*Safety and environment (WPSAE)*

From the very beginning of DEMO conceptual design, safety and environmental (S&E) considerations are at the heart of the project due to their social relevance. The favourable characteristics of fusion power in terms of low accident potential, good operational safety and minimal environmental impact provide a potential for excellent S&E performance. But to fully realise this potential the design must incorporate safety provisions to minimize hazards and to ameliorate the consequences of any abnormal operation or system failure. In the EU DEMO project a safety approach has been adopted based on principles such as Defence in Depth, and with a view to the possible requirements that may arise from licensing by a European nuclear regulator.

*Tritium fuelling and vacuum (WPTFV)*

One important milestone achieved in early 2015 was the establishment of a novel architecture of the inner fuel cycle to avoid an excessively large tritium inventory in the system that would result from a simple scale-up of the ITER technologies for pumping and isotope separation. The large inventory would result in long deuterium-tritium cycle times and a correspondingly slow-acting control characteristic of the whole fuel cycle. This is because a novel concept is being proposed now, which replaces batch processes by continuous processes wherever possible.

*Early neutron source (WPENS)*

Finally, although not directly connected to the DEMO project, in order to finalize the DEMO design and licensing an appropriate neutron source is proposed to characterise the materials to be used. Work has started in 2015 in strong coordination with F4E and building on the knowledge acquired with the IFMIF/EVEDA project. Both F4E and EUROfusion have agreed the selected configuration for the Early Neutron Source (ENS) is the IFMIF-DONES (DEMO Oriented Neutron Source) approach, based on a IFMIF-type neutron source with reduced specifications. The primary objectives of WPENS are to: (i) perform the engineering design of the plant with a focus on design integration to enable start of the ENS construction around 2020; (ii) develop the engineering design of all systems which are not on the critical path but have interfaces to the systems described in (i); (iii) support the R&D activities required to finalize the engineering design of the IFMIF-DONES plant.

The above mentioned projects are coordinated through a reactor integration project at level of EUROfusion Programme Management Unit, in Garching.

## A.3 The Breeding Blanket project in EUROfusion

Major requirements of the DEMO plant are the production of the tritium necessary to sustain the thermonuclear reaction and the delivery of several hundreds of MW of electrical power in net around 2050. In order to accomplish these tasks, the BB is the key component using the neutron of the fusion reaction to produce tritium (reaction with Li) and converting the energy of neutron, particles and photons coming out from both the burning plasma and the nuclear reactions with breeder in thermal energy suitable for power generation systems [4]. In order to perform and coordinate R&D activities devoted to the BB design the WPBB has been properly foreseen by the EUROfusion consortium, playing a pivotal role within the framework of the whole DEMO design. The BB requires large external auxiliary systems to perform its functions, namely the Primary Heat Transfer System, the Power Generation System and the Tritium Extraction System. For these reasons the selection of the type of blanket is a strategical choice that strongly constraints the whole DEMO plant design [4]. Even if the present DEMO configuration is setting specific requirements to the blanket design, the breeding blanket development can refer to a very long tradition of studies. In EU, Japan, USA and Russia, large blanket studies have been conducted since the 80-teens years in international and national programmes; more recently other countries (China, Korea and India) have joined the fusion community participating to ITER construction and to the development of own Roadmaps for the DEMO and commercial power plant [4]. Furthermore, all these countries are participating to the Test Blanket Programme, where six blanket prototypes (the so called Test Blanket Modules) will be tested in 3 Equatorial Ports of ITER;

the programme aims to gain operational information on the behaviour of blanket mock-ups, materials, processes and technologies in the integrated fusion environment offered by ITER [4]. The major goal of the WPBB is to complete the design at conceptual level of the BB systems compatible with the DEMO requirements and interfaces. It is currently assumed that after 2020 one or two plant concepts will be selected for starting an engineering phase that should lead to a constructive design of a fusion power plant in the time foreseen by the Fusion Roadmap. The WPBB programme in 2014–2020 has as main milestones: (i) a consolidated design of the candidate blankets at the end of the 2017 and (ii) a final conceptual design of these systems at the end of 2019. The design work is supported by a relatively large R&D programme to consolidate the knowledge of the proposed technologies, to assess feasibility, maturity and costs [4]. Following the recommendations of the Roadmap, investigations on 4 blanket concepts have been included in the WPBB programme. The WPBB is organized in 9 Work Areas (WAs); the first 4 areas are related to the work of design teams dedicated to the development of one of the considered blanket design, the other 4 WAs are cross technologies used by several blanket concepts (like Pb-Li systems, tritium extraction and control, blanket manufacturing and FW design and performances). The 9$^{th}$ area refers to the group in KIT supporting the Project Leader in Technical Coordination, Project Management, System Engineering and Configuration (Tab. A-1). Seven Research Units (RUs) are involved in the WPBB activities, namely KIT (that has the coordination role), ENEA, CVR (IPP.CR), CIEMAT, CEA, CCFE, Wigner RCP (HAS) [4]. In Table A-1, underlined represents the RU having coordination role in the WA.

Table A-1. Working Areas in the WPBB.

| WA | WA description | RUs involved |
|---|---|---|
| 1 | HCPB BB design and ceramic breeder development | KIT, CIEMAT, HAS |
| 2 | HCLL BB design | CEA, IPP.CR, HAS |
| 3 | WCLL BB design and water cooling technology development | ENEA |
| 4 | DCLL BB design and flow channel insert development | CIEMAT, IPP.CR, KIT |
| 5 | Pb-Li technology development | ENEA, KIT, CIEMAT, IPP.CR |
| 6 | Tritium technology development | KIT, ENEA, CIEMAT, CCFE |
| 7 | BB manufacturing | CEA, KIT, IPP.CR |
| 8 | FW/limiter design | CCFE, KIT, IPP.CR |
| 9 | Supporting group | CEA, KIT |

# References


[1] C. Bachmann et alii, *Initial DEMO tokamak design configuration studies*, Fusion Engineering and Design 98-99, pp. 1423-1426, 2015.

[2] G. Federici et alii, *Overview of the design approach and prioritization of R&D activities towards an EU DEMO*, Fusion Engineering and Design 109-111, pp. 1464-1474, 2016.

[3] G. Federici et alii, *Overview of EU DEMO design and R&D activities*, Fusion Engineering and Design 89, pp. 882-889, 2014.

[4] L.V. Boccaccini at alii, *Objectives and status of EUROfusion DEMO blanket studies*, Fusion Engineering and Design, http://dx.doi.org/10.1016/j.fusengdes.2015.12.054, 2016.

[5] F. Hernandez et alii, *Fluid dynamic and thermal analyses of a HCPB TBM Breeder Unit mock-up*, Fusion Engineering and Design, 86, pp. 2278-2281, 2011.

[6] F. Hernandez et alii, *Thermo-mechanical analyses and assessment with respect to the design codes and standards of the HCPB-TBM Breeder Unit*, Fusion Engineering and Design, 87, pp. 1111-1117, 2012.

[7] F. Hernandez et alii, *Set-up of a pre-test mock-up experiment in preparation for the HCPB BreederUnit mock-up experimental campaign*, Fusion Engineering and Design, 88, pp. 2378-2383, 2013.

[8] G. Zhou et alii, *Preliminary structural analysis of the new HCPB blanket for EU DEMO reactor*, International Journal of Hydrogen Energy, 41, pp. 7053-7058, 2016.

[9] G. Zhou et alii, *Preliminary steady state and transient thermal analysis of the new HCPB blanket for EU DEMO reactor*, International Journal of Hydrogen Energy, 41, pp. 7047-7052, 2016.

[10] G. Aiello et alii, *Thermo-hydraulical and thermo-mechanical analysis of the HCLL-TBM breeding unit*, Fusion Engineering and Design, 83, pp. 1227-1231, 2008.

[11] G. Aiello et alii, *A new cooling scheme for the HCLL TBM, Fusion Engineering and Design*, 84, pp. 390-393, 2009.

[12] G. Aiello et alii, *Transient thermo-hydraulical/thermo-mechanical analysis of the*

*HCLL-TBM for ITER*, Fusion Engineering and Design, 85, pp. 1565-1572, 2010.

[13] G. Aiello et alii, *HCLL TBM design status and development*, Fusion Engineering and Design, 86, pp. 2129-2134, 2011.

[14] G. Aiello et alii, *Development of the Helium Cooled Lithium Lead blanket for DEMO*, Fusion Engineering and Design, 89, pp. 1444-1450, 2014.

[15] J. Aubert et alii, *Status on DEMO Helium Cooled Lithium Lead breeding blanket thermo-mechanical analyses*, Fusion Engineering and Design, 109-111, pp. 991-995, 2016.

[16] J-C. Jaboulay et alii, *Comparison over the nuclear analysis of the HCLL blanket for the European DEMO*, Fusion Engineering and Design, 109-111, pp. 365-370, 2016.

[17] J. Aubert et alii, *Thermo-mechanical analyses and ways of optimization of the helium cooled DEMO First Wall under RCC-MRx rules*, Fusion Engineering and Design, http://dx.doi.org/10.1016/j.fusengdes.2016.12.040, 2016.

[18] M. A. Fütterer et alii, *Design development and manufacturing sequence of the European water-cooled Pb-17Li test blanket module*, Fusion Engineering and Design, 39-40, pp. 851-858, 1998.

[19] M. A. Fütterer et alii, *Further improvements of the water-cooled Pb–17Li blanket*, Fusion Engineering and Design, 58-59, pp. 523-527, 2001.

[20] Y. Poitevin et alii, *Status of the design and performances of the WCLL test blanket module for ITER-FEAT*, Fusion Engineering and Design, 61-62, pp. 431-437, 2002.

[21] J.Aubert et alii, *Development of the water cooled lithium lead blanket for DEMO*, Fusion Engineering and Design, 89, pp. 1386-1391, 2014.

[22] J.Aubert et alii, *Optimization of the first wall for the DEMO water cooled lithium lead blanket*, Fusion Engineering and Design, 98-99, pp. 1206-1210, 2015.

[23] P. Norajitra, et alii, *Conceptual design of the dual-coolant blanket in the frame of the EU power plant conceptual study*, Fusion Engineering and Design, 69, 669-673, 2003.

[24] D. Rapisarda et alii, *Conceptual Design of the EU-DEMO Dual Coolant Lithium Lead Equatorial Module*, IEEE Transactions on plasma science, Vol. 44 n. 9, pp. 1603-1612, 2016.

[25] I. Palermo et alii, *Neutronic analyses of the preliminary design of a DCLL blanket for theEUROfusion DEMO power plant*, Fusion Engineering and Design, 109-111, pp. 13-19, 2016.

[26] H. S. Carslaw, J. C. Jaeger, *Conduction of Heat in Solids*, 2nd Ed., Oxford University Press, London (GREAT BRITAIN), (1959).

[27] S. P. Timoshenko, J. N. Goodier, Theory of Elasticity, McGraw-Hill, New York, (USA), (1970).

[28] *ITER structural design criteria for in-vessel components (SDC-IC)* code, G 74 MA 8 01-05-28 W 0.2, 2012.

[29] A. Li Puma et alii, *Potential and limits of water cooled divertor concepts in view of their use for DEMO*, CEA report SERMA/LPEC/RT/12-5272, pp. 17-20, 2012.

[30] A.F. Tavassoli et alii, *Materials design for reduced activation martensitic steel type EUROFER*, Journal of Nuclear Materials, 329-333, pp. 257-262, 2004.

[31] G. Aiello et alii, *Assessment of design limits and criteria requirements for EUROFER structures in TBM components*, Journal of Nuclear Materials, 414, pp. 53-68, 2011.

[32] P.A. Di Maio at alii, *Thermo-mechanical analysis of DEMO Water-Cooled Lithium Lead (WCLL) breeding blanket*, Report of the research activity of the consulting contract EFDA WP12-DAS02-Task03, 2013.

[33] F. Tavassoli, *Fusion Demo Interim Structural Design Criteria (DISDC)/Appendix A Material Design Limit Data/A3.S18E Eurofer Steel*, EFDA TASK TW4-TTMS-005-D01. CEA Report DMN/DIR/NT/2004-02/A, 2004.

[34] Goodfellow, *Metals, Alloys, Compounds, Ceramics, Polymers, Composites*, Catalogue 1993/94.

[35] Frank P. Incropera, David P. Dewitt, *Fundamentals of Heat and Mass Transfer*, Second Edition,1985.

[36] Ivica Smid et alii, *Material and Design considerations for the Carbon Armored ITER Divertor*, July 1993.

[37] *ITER Documentation Series No 29*, IAEA, Vienna 1991. Blanket, Shield Design and Material Data Base.

[38] J. Aubert at alii, *Presentation for the Final Review Meeting*, EFDA-WP13-DAS-02-Task10, 2013

[39] *Reference Material data for the HCLL TBS*, compiled by J-F. Salavy following exchanges with F4E on input data for TG01, TBM-CA document D2-2009.002 V1.0, 2009.

[40] A. Li Puma and WCLL/HCLL team, *Specifications on loading conditions for WCLL/HCLL blanket design*, WP12-DAS-02-T03 - WP12-DAS-02-T04.

[41] P. Chiovaro et alii, *Analysis of the thermo-mechanical behaviour of the DEMO Water-Cooled Lithium Lead breeding blanket module under normal operation steady state conditions*, Fusion Engineering and Design, 98-99, pp. 1737-1740, 2015.

[42] U. Fischer et alii, *Neutronic analyses and tools development efforts in the EuropeanDEMO programme*, Fusion Engineering and Design, 89, pp. 1880-1884, 2014.

[43] U. Fischer et alii, *Neutronic requirements for a DEMO fusion power plant*, Fusion Engineering and Design, 98-99, pp. 2134-2137, 2015.

[44] U. Fischer et alii, *Neutronic performance issues of the breeding blanket options for theEuropean DEMO fusion power plant*, Fusion Engineering and Design, 109-111, pp. 1458-1463, 2016.

[45] *Material Property Handbook pilot project on EUROFER97 (MTA EK, KIT)* - IDM Ref. EFDA_D_2MRP77, 24/02/2016.

[46] P.A. Di Maio et alii, *Analysis of the thermo-mechanical behaviour of the DEMO Water-Cooled Lithium Lead breeding blanket module under normal operation steady state conditions*, Fusion Engineering and Design, 98–99, pp. 1737–1740, 2015.

[47] P.A. Di Maio, et alii, *Optimization of the breeder zone cooling tubes of the DEMO Water-Cooled Lithium Lead breeding blanket*, Fusion Engineering and Design, http://dx.doi.org/10.1016/j.fusengdes.2016.03.021F, 2016.

[48] https://www.euro-fusion.org/eurofusion/